Étude Thermodynamique et par Spectrométrie de Masse du Comportement de Poudres de Carbure de Silicium (SiC) à Haute Température

G. Honstein

INSTITUT POLYTECHNIQUE DE GRENOBLE

N° attribué par la bibliothèque
|__|__|__|__|__|__|__|__|__|__|

T H E S E

pour obtenir le grade de

DOCTEUR DE L'INSTITUTE POLYTECHNIQUE DE GRENOBLE

Spécialité : « Matériaux Mécanique Génie Civil Electrochimie»

préparée au laboratoire : Science et Ingénierie des Matériaux et Procédés (SIMAP)

dans le cadre de l'Ecole Doctorale
« *Ingénierie-Matériaux Mécanique Energétique Environnement Procédés Production (I-MEP2)*»

présentée et soutenue publiquement

par

Gabriele HONSTEIN

le 23 octobre 2009

Thermodynamic and Mass Spectrometric Study of the Behaviour of Silicon Carbide (SiC) Powders at High Temperature

Étude Thermodynamique et par Spectrométrie de Masse du Comportement de Poudres de Carbure de Silicium (SiC) à Haute Température

_____

Directeur de thèse :
Christian CHATILLON

Codirecteur de thèse :
Francis BAILLET

_____

JURY

M. Thierry DUFFAR	**Président**
M. Francis TEYSSANDIER	**Rapporteur**
M. Jean Claude VIALA	**Rapporteur**
M. Christian CHATILLON	**Directeur de thèse**
M. Francis BAILLET	**Codirecteur de thèse**
M. Jaques ROGEZ	**Examinateur**
M. Christophe AUGIER	**Invité**

Preface

The present manuscript contains two volumes:

- The first volume is written in english and is a conventional PhD manuscript with bibliographic review, thermodynamic calculations, description of experiments and their results following by a conclusion from the experimental results and a general conclusion of the work.
- The second volume, demanded from the Polytechnic Institute of Grenoble – France, is written in french and is a brief summary of the first volume.

Acknowledgments

I wish to express my deep gratitude to my advisors, Christian Chatillon and Françis Baillet, for their encouragement and support during these years. Thanks to their help and motivation, our discussions and ideas, this study could progress. I have appreciated a lot to work with them and I appreciate even more the persons behind the professional "shell".

I wish to thank Thierry Duffar for the honor to accept to be the president of my PhD graduation jury, despite his injury. I am very grateful to Francis Theyssandier and Jean Claude Viala to be the PhD manuscript examiner and for their unexpected great examination reports. In the same way I wish to express my gratitude to Jaques Roges for participation as examiner at my PhD graduation.

I wish to express my gratitude to my industrial supervisors, Christophe Augier, Anthony Briot and Matteo Scalabrino, who, despite their charged agendas, always did anything possible to help the study to progress, be it with helpful information, discussion or with simple questions.

In addition I am greatly indebted to Francine Roussel-Dherbey and Frédéric Charlot for the excellent SEM/FEG images, which provide the undeniable prove for the study conclusions. I am indebted in the same way to Michel Mermoux for a great many of performed Raman Spectrometric analyses and to César Steil and Marc Henault for the same number of grain size measurements.

I wish to thank the whole SIMAP personal. I have appreciated a lot the human environment in this laboratory.

I thank a lot my parents, my sister and my brother for their constant moral and material support.

I am very grateful to my daughter, Meya, born in June 2008, for her patience during the long days and nights of writing.

The last, but not least, Lamine, there are no words to express my gratitude for your support and patience. It was really hard sometimes, but we made it!

Contents

Introduction

The Silicon Carbide (SiC) is a high performance ceramic with a number of interesting properties: it is very resistant to high temperatures and to corrosive medias, it has a high thermal conductivity and low temperature expanding coefficient, its hardness is near to diamond's. Some of these properties are very positive for the use of this material but because of them it is difficult to make pure SiC bulk bodies.
Depending on the application there are different possibilities of manufactoring. Almost all of them include a final sintering step. Generally, sintering includes material transport via liquid phase, gaseous phase and diffusion in the solid phase or they acts all together depending on the sintering conditions. The first one demands very high temperatures in the case of pure SiC, finally the real melting point of SiC is even not found yet. The most probable way for the material transport seems to be via gaseous phase that is already considered for the fabrication of porous SiC bodies, so called "recrystallized SiC". Besides, single SiC crystals have been elaborated via gaseous transport from SiC powder acting as a source.
In the very beginning the aim of this work was to obtain informations about the phenomenon of "vaporization/recrystallization" processes of SiC. Finally due to discovering of a large number of processes working all at the same time just before, during and after the so called recrystallization the decision was taken to study the evaporation behavior of different compositions of SiC and silica powders and investigate their impact on the following condensation behavior.
The analysis of the evaporation behavior during heat treatments was performed via in situ measurements of the partial pressures of the different samples applying mass spectrometric method coupled with either so called effusion cells or capillary tubing. The investigations on the recrystallization behavior were made on the obtained samples after the high temperature (or temperature range) vaporization runs and partial pressure or flow measurements. The scanning electron microscope (SEM) and field emission gun microscopes (FEG) were used to image the obtained connections between the SiC grains, Raman spectroscopy was used to characterize structural changes. Also grain size measurement was used to visualize the elimination of a grain size fraction and the general size jump towards higher diameters. More particular aim was to observe the growth of the crystals, the elimination of a grain size fraction, probably the smallest ones, and/or the creation of "necks" between crystals.
The analysis of the evaporation behaviour during heat treatments is performed by in situ measurements of either the vapour pressures or the vapour flows using mass spectrometry to identify the nature of the vapours. Using High Temperature Mass Spectrometry that is the coupling of a mass spectrometer with a Knudsen effusion cell, the real vapour pressures can be monitored associated to very small mass losses. Using the coupling of a quadrupole mass spectrometer with a capillary sampling allows the measurements of permanent gas flows—in this case the carbon monoxide—with higher mass losses. The aim is to identify

different sequences in the oxygen departure when monitoring oxygen containing molecules as SiO(g) and CO(g).
As the only mass spectrometric measurements cannot be quantitatively interpreted, a preliminary thermodynamic study of the vaporisation processes occurring in the Si-C and Si-C-O systems was performed in order to give a framework for the understanding of the main reactions which are occurring in relation to the flow of matter that is lost by the powders. This thermodynamic study has been also amplified by the calculation of matter flow exchanges with exhaust gases or impurities—especially oxygen—in order to simulate plus or minus the matter flows occurring in the experiments or in industrial furnaces.
The final step was to detect the moment, the environment and the main reactions which lead to grain growth in relation with silica or oxygen content as well as to propose some quantification of the main parameters that define the best conditions for the grain growth.

1 Bibliographic survey

1.1 Silicon carbide: structure, applications and manufacturing

Silicon carbide is known as a chemical compound for approximately 200 years but it was discovered as a natural product in meteorites and volcanic sediments only in 1905 by Moissan (Moissanit is the name for natural SiC). Before it was observed as a secondary reactions product in aluminum melts. SiC belongs to the group of non-oxide ceramic materials. Its industrial manufacturing in large quantities is made by since 1891 known Acheson-process using petrol coke and quartz-sand. Main industrial production technologies of SiC can be summarized as:

- Building from the elements:
  $\mathrm{Si(s)} + \mathrm{C(s)} \rightarrow \mathrm{SiC(s)}$ $1500 < T < 1650°\mathrm{C}.$
- Acheson-Process:
  $\mathrm{SiO_2(s)} + 3\mathrm{C(s)} \rightarrow \mathrm{SiC(s)} + 2\mathrm{CO(g)}$ $1600 < T < 2500°\mathrm{C}.$
- Precipitation from the gaseous phase:
  $2\mathrm{SiO_2(s)} + \mathrm{C_2H_6(g)} \rightarrow 2\mathrm{SiC(s)} + 2\mathrm{H_2O(g)} + \mathrm{H_2(g)}$ $600 < T < 1400°\mathrm{C}.$
- Pyrolisis of Si-organic compositions:
  Polycarbosilane $1300 < T < 1500°\mathrm{C}.$

The Acheson-process made SiC accessible for a large number of applications in the cutting, grinding and refractory industries. With development of Lely-process (1955), which is a crystal growth process, and modified Lely-process, which is a seeded sublimation growth process, SiC for electronic applications could be produced in large quantities and its semiconductor characteristics could be widely exploited. Contrarily to SiC polycrystals from Acheson-synthesis one obtains very pure SiC monocrystals from modified Lely-synthesis, mainly used for wafer manufacturing.

1.1.1 The structure of Silicon carbide

SiC is the only one known solid compound in the Si-C system. The bond is made by sp^3-hybridization. The s-orbitals of the outer shells of Si and C have two electrons in the normal state. By energy supply one electron from the s-orbital jumps in the incomplete p-orbital [1]. Following all the paths of the outer shell are simply occupied and there are four single electrons for the valency bond. Every Si-atom is surrounded by four C-atoms that are placed to form of a tetrahedron; the same follows for each C-atom that is surrounded by a tetrahedron of Si-atoms (see fig. 1.1). The covalent part of the bond is 88% and the free binding energy is $75 \pm 16\,\mathrm{kJ/mol}$ [2]. This high value for the binding energy is due to the sp^3-hybridization and is the reason for the high temperature resistance and hardness of the

SiC materials.
The layers of atoms build by interconnected tetrahedrons can be stacked differently, from which results the large number of different SiC-polytypes. They can be roughly divided in α-SiC with hexagonal or rhombohedral structure and β-SiC with cubic structure.
α-SiC is known as a stable high temperature modification and has a wurzit structure. At this moment more than 140 polytypes are identified but most important are the hexagonal 2H, 4H and 6H and the rhombic 15R-type.
β-SiC has diamond or zincblende structure and is formed already at low temperatures. It was already observed occurring at 525°C from Si and C elements in a melt of zinc and aluminum [3].
It is frequently assumed that β-SiC transforms into α-SiC at 2100°C [1] and that at this temperature the transition runs slow but at 2300°C it is spontaneous [4]. Heat of formation and equilibrium data indicate that β-SiC is more stable up to 1700°C. But the adopted thermodynamic functions suggest that this is the case for all temperatures, the stability difference being small [5]. For the calculations in this work we applied the data for α-SiC.

1.1.2 Manufacturing of bulk SiC bodies

Depending on the application one can find different appropriate SiC material qualities. Generally for the applications at low temperatures with low mechanical performances (manufacturing of whet discs or heat converters) low temperature processing modes can be used

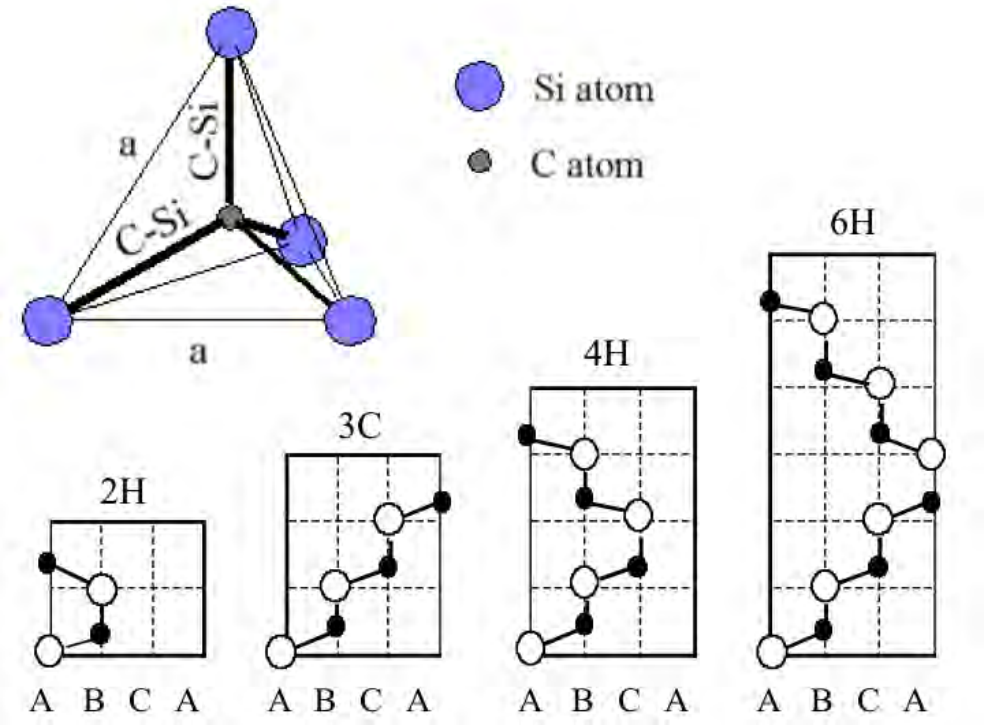

Figure 1.1: Structure of SiC: Tetragonal bonding of C and Si atoms (a = 3,08 Å, C-Si = 1,89 Å) and most common SiC polytypes resulting from different stacking of Si-C tetrahedrons.

like “ceramic” bond with addition of clay. For the high temperature stability pure and porous SiC parts can be obtained by so called recrystallization (sintering above 2000°C, approx. 20% porosity). Mechanically strong parts can be made by reaction sintering with Si-excess (SiSiC or RBSC), sintering (SSiC) or hot pressing (HPSiC) [6].
Some manufacturing methods of bulk bodies are similar to those of the traditional ceramics. Most processes can be divided in

- raw components mixing,
- shaping
- and firing/sintering step.

Further processing methods for layer deposition from the gaseous phase are known.
Most important is the firing/sintering step, during which the consolidation of the parts is obtained. One can classify reaction bond, liquid phase sintered and solid phase sintered SiC.
For reaction bond SiC a preform is made from Si- and C-powders or SiC- and C-powders. In the first case by heating of such a preform above the Si-melting temperature Si and C react to produce SiC and build a porous structure. In the second case one obtains a SiC structure by bringing the preform in contact to liquid or gaseous silicon. It reacts with C and build secondary SiC on the primary SiC grains.
Liquid phase sintering takes place with ceramic additives. For production of refractory materials 10 – 20% refractory clay is added to give the ceramic mixture necessary properties for the shaping. During the firing step formed mullite and glass become the binding phase between the SiC particles.
Solid phase sintered SiC bodies are consolidated at 1900 – 2200°C under vacuum or in Nitrogen or Argon atmospheres with pressures below 1 bar. The consolidation takes place via solid phase reaction of boron and carbon, added as sintering aids, with SiC. The recrystallized SiC (RSiC) is a special case, because the consolidation is performed without sintering aids. The mass transport takes place via gaseous phase due to reaction of SiC with its SiO_2 native layer.
For all of described SiC manufacturing methods material transport via vapors can play an important role. The main difficulty is to decrease the SiC composition evolution due to material loss, mainly Si, at high temperatures and prevent carbon precipitation.

1.2 SiC vaporization behavior and mass spectrometry

SiC is a silicon based compound. Silicon is known to be stable to the oxidation media because of the formed SiO_2 scale on its surface, which build a barrier to further oxidation. The SiC behaves in the same way. This is one of the reasons for its high resistance to corrosive attacks.
SiC powders have always SiO_2 as impurity. The amount of the SiO_2 content is dependent on the surface of the SiC powder, generally same volumes of smaller grains present larger surface and following are richer in SiO_2 as coarse SiC powders.

1.2.1 Binary compound SiC

The investigations on the constitution of the silicon-carbon system are difficult because of necessity to apply very high temperatures. The only compound found in the Si-C is SiC. A review of experimental data was made by R. W. Olesinski and G. J. Abbaschian in 1984 [7]. They found the data from R.T. Dollof [8] most reliable with T eutectic at 1677 ± 5 K and composition of $0,75 \pm 0,5$ at% C. Peritectic T is reported at 2818 ± 40 K with SiC and a liquid of 27 at% C.

New measurements of carbon solubility in liquid silicon made by H. Kleykamp and G. Schumacher [9] established higher values for transformation temperatures and lower carbon solubility as reported in [7]. They found a degenerate eutectic at 1686 K with 0,02 at% C and they observed peritectically melt Si-C at 3100 K with 13 at% C.

J. Gröbner et al. [10] pointed out that the values reported by R.T. Dollof [8] disagree with all other experimental found data which all agree with the value of 3100 K for the peritectic transformation. Furthermore eutectic reaction, $T^{eut} = T_{Si}^{fus} - 0,9 \pm 0,7$ K, reported by H. Kleykamp et al. [9] as very close to Si melting temperature is accepted. The solubility of carbon at eutectic temperature was found very small.

Phase diagram calculated by SGTE in 2004 [11] is based on the assessment of J. Gröbner et al. [10]. They optimized the peritectic at 3096,5 K. This agree with most of the experimental data. The phase diagram of Si-C (fig. 1.2) shows three different results. The value (b) corresponds at best to SGTE calculations for the peritectic temperature and carbon solubility is set to 17,3%.

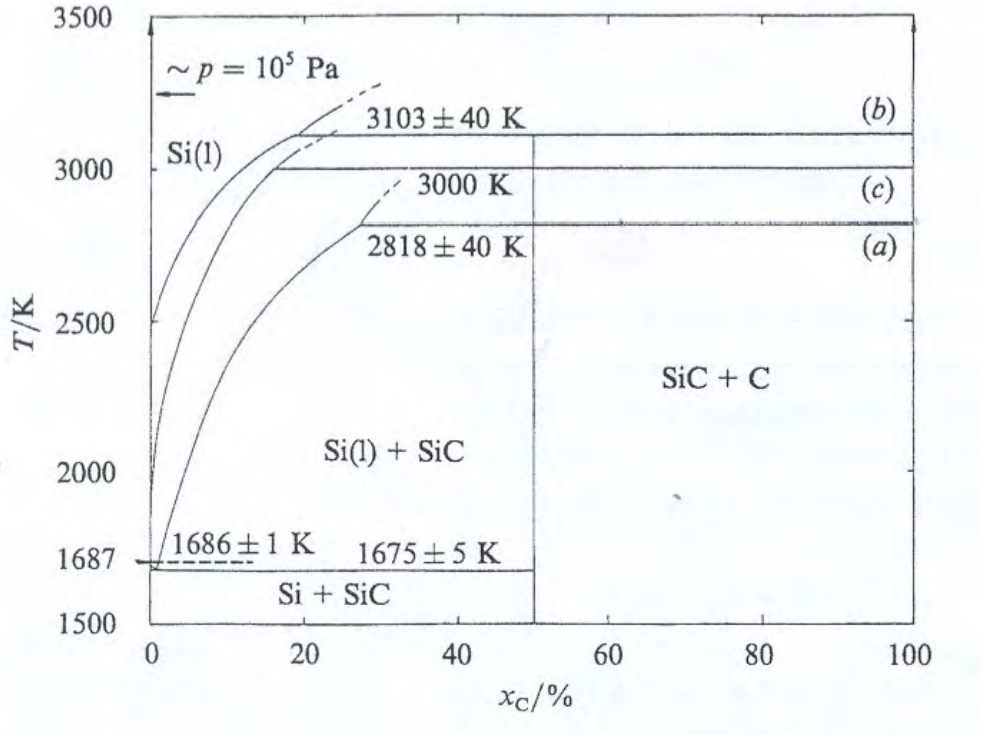

Figure 1.2: Phase diagram of Si-C system as proposed by (a) R.T. Dollof [8], (b) R.I. Scace and G.A. Slack [12] and (c) calculated by L. Kaufman [13].

Complimentary F. Durand and J.C. Duby [14] made a review concerning carbon solubility at eutectic temperature in solid and liquid silicon and proposed for $T = 1687\,\mathrm{K}$ as the eutectic temperature a solubility of 0,0009% in solid and 0,0261% in liquid Si. The lower solubility values were also proposed by P. Rocabois et al. [15] after measurements of silicon activity along the liquidus performed by high temperature mass spectrometry.
The extend of SiC as single phase was investigated by D.P. Birnie III et al. [16]. They determined using X-Ray diffraction, bulk density measurements and chemical analysis the concentrations for simple point defects. They found that equilibrium antisite defect concentration at 2400°C is below 0,2%. They admitted that this result is controversial to earlier proposed diffusion model which requires at least 1% of silicon antisite defects [17]. Their conclusion is that the silicon carbide lattice is nearly stoichiometric with an accuracy of 0,1%.
A number of publications is made for investigations of vapors and partial pressures in the Si-C system. Pure substances Si and C have already a large variety of gaseous molecules under vaporization conditions. For carbon vaporization these are in decreasing pressure order: C_3, C, C_2, C_5, C_4 until C_7 reported by M.G. Inghram et al. [18]. Silicon forms by vaporization Si, $Si_2 - Si_7$ gaseous molecules reported also in [18].
Species with very low partial pressures could be firstly detected employing the mass spectrometric technique coupled with Knudsen cells which was first applied to Si-C system by J. Drowart. He made a large number of investigations on gaseous species. His investigations on Si-C [19, 20] have shown the plenitude of composed gaseous molecules formed during vaporization. Before the measurements with a mass spectrometer one could only measure the total pressure of gases above a condensed phase and vapor composition, which always showed a ratio of $Si/C > 1$.
Different gaseous molecules were observed and investigated during mass spectrometric studies of Si(s), C(s), SiC(s), Si-SiC(s) and SiC-C(s) performed by different authors (species listed in JANAF tables [5] are bold):

- Si(s):
  - R.E. Honig et al. (cited in [18]) sampling via Langmuir vaporization in BeO cell at $1450 - 1650\,\mathrm{K}$:
    Si, **Si_2**, **Si_3**, $Si_4 - Si_7$
  - C. Chatillon [21] and P. Rocabois et al. [22]) sampling by Knudsen vaporization in vitreous carbon cell:
    Si, **Si_2**, **Si_3**, $Si_4 - Si_7$
  - R.W. Schmude et al. [23, 24, 25, 26, 27] added to mass spectrometric determinations quantum chemistry calculations of the geometry of Si-polymers: **Si**, **Si_2**, **Si_3**, $Si_4 - Si_6$
- C(s):
  - M.G. Inghram et al. [18] sampling by Knudsen vaporization in Ta and W cells at $1800 - 2700\,\mathrm{K}$:
    C_3, **C**, C_2, C_5, C_4

- Si-C system:
  - J. Drowart et al. [19, 20, 18, 28] sampling by Knudsen vaporization in graphite cells at $1700 - 2320\,\mathrm{K}$:
    Si, $\mathbf{Si_2}$, $\mathbf{Si_3}$, $\mathbf{SiC_2}$, $\mathbf{Si_2C}$, **SiC**, Si_2C_2, Si_2C_3, Si_3C
  - R.W. Schmude et al. [29] sampling by Knudsen effusion in graphite cells at $1700 - 1750\,\mathrm{K}$ and :
    $\mathbf{SiC_2}$, $\mathbf{Si_2C}$, Si_2C_2, Si_3C and Si-polymers
  - P. Rocabois et al. [22] sampling by Knudsen effusion in graphite cells at $1500 - 2000\,\mathrm{K}$:
    Si, $\mathbf{Si_2}$, $\mathbf{Si_2C}$, $\mathbf{Si_3}$, $\mathbf{SiC_2}$, $Si_4 - Si_7$, Si_2C_2, Si_3C, Si_4C, Si_3C_2

The only species which partial pressure exceed 1% of the gaseous phase total pressure, like $Si - Si_3$, $C - C_3$, SiC_2, Si_2C and SiC, were considered for the calculation performed in the present study.
R.W. Schmude et al. [29] calculated the relative stability of the Si_xC_y polymer molecules by quantum chemistry. Then, applying the harmonic-oscillator rigid-rotor approximation they could improve entropy values calculated previously for these molecules in the work of Rocabois et al. [22].
The "Knudsen-effusion mass spectrometric study of the group 14 atomic clusters" from G. Meloni et al. [23] gathers works on C-, Si-, Ge- and Sn-polymers sometimes considered as clusters. For Si-polymers, work of P. Rocabois et al. [22] is not cited, the authors give references of their own works on Si_2 to Si_6. In these original works, quantum chemistry calculations have been performed in order to propose the most stable structure or alternately two structures the stability of which is similar.
Free (Langmuir) vaporization studies performed by R.G. Behrens et al. [30] show a decrease of partial pressures when the SiC surface build a C layer by Si excess loss, contrarily to stable pressures expected for the diphasic SiC-C. This is rather attributed to surface adsorbed species content decrease due to material loss and not to Si and C diffusion in a C surface layer. Furthermore in the same paper the authors ascertain the difficulty of the system to attain equilibrium partial pressures and attributed this fact to low evaporation coefficients (α), which was already mentioned by S.G. Davis et al. [31]. R.G. Behrens determined α at $2350\,\mathrm{K}$ to be $1,5 \cdot 10^{-3}$ for Si(g) and $8,2 \cdot 10^{-3}$ for SiC_2. Conversely P. Rocabois et al. [15] determined evaporation coefficients using different Knudsen cells geometry in a multiple cell experiment. The evaporation coeff of the Si, Si_2C and SiC_2 species were found to be the same and equal to $(5 \pm 2) \cdot 10^{-3}$ at $2150\,\mathrm{K}$.

1.2.2 Ternary system Si-C-O

The ternary Si-C-O diagram is of large interest for all who work with SiC for the reason of the unavoidable silicon oxide presence due to silicon oxidation exposed to oxygen containing atmospheres. Furthermore the production of silicon is often performed by formation of SiC as intermediate phase from SiO_2 and carbon.
Before use of complex equilibrium calculation softwares, obtaining the partial pressures in equilibrium with different solid or liquid phases sets required to solve a set of independent reactions and to apply the phase rule. A. Ghosh and G.R. St.Pierre [32] present the phase

diagram of Si-C-O under one atmosphere at 1700 K (fig. 1.3). Since the studies performed by A. Ghosh and G.R. St. Pierre [32] from 1969 no new ternary phase diagram was proposed.

There is no known ternary compounds in the Si-C-O system, but only some amorphous phases obtained generally by deposition processes.

From a structural point of view R. Pampuch et al. [33] observed the formation of an intermediate ternary Si-O-C phase. This phase was formed during isothermal oxidation of SiC for 5 hours between 675 and 1425 K and at 1775 K in a flow of oxygen (1 bar). The weight of each specimen before and after etching by HF was monitored. The HF treatment was done to remove SiO_2. Obtained samples were examined with XPS, ESCA, IR spectra and SEM. Photoelectron spectroscopy has shown bonds O-Si-C as an intermediate oxidation state. The proposed formula of this phase is $Si_2O_2C_2$. This phase disappears for higher oxidation level.

L. Porte and A. Sartre [34] performed XPS measurements on the Nicalon fiber. References were graphitic C and single crystal SiC. After the analysis of the rough surface the samples were exposed to Ar^+ bombardment to remove approx. 100 nm and to analyze the bulk material. The surface was found to be enriched in oxygen and depleted in silicon. Peaks

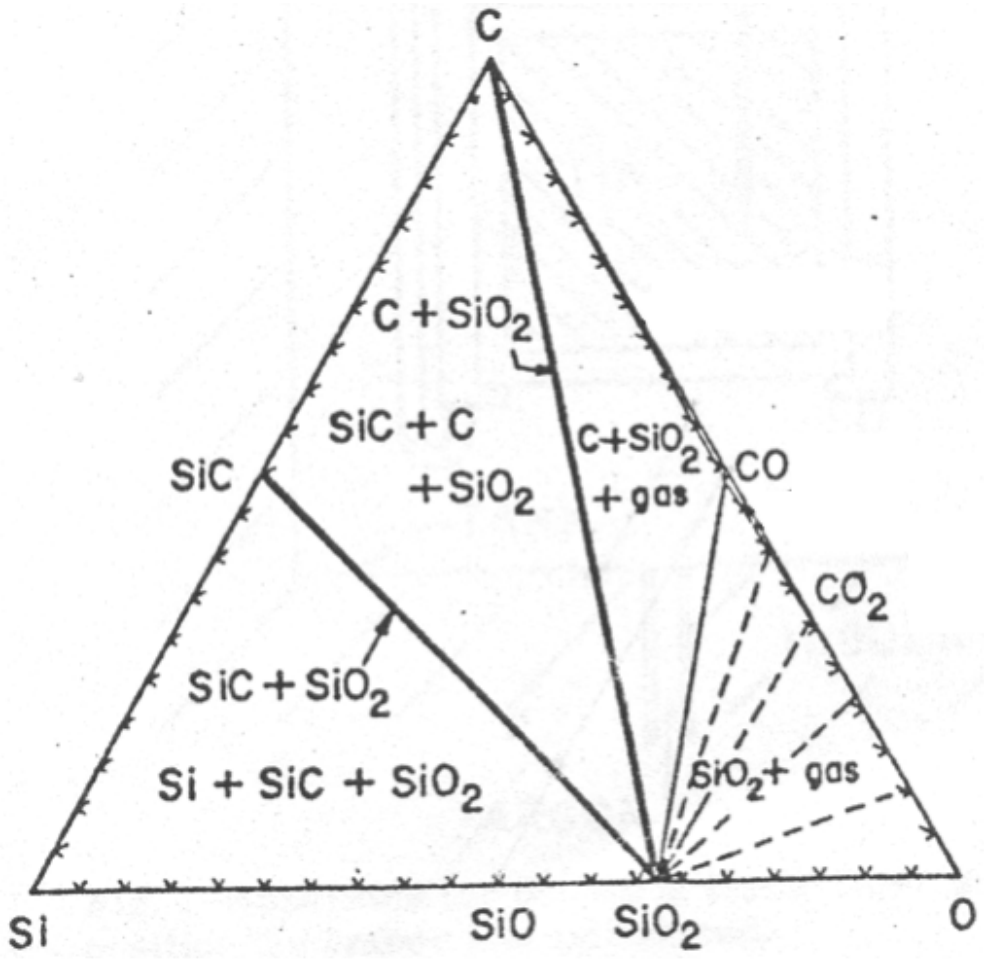

Figure 1.3: Ternary Si-C-O diagram proposed by A. Ghosh and G.R. St. Pierre [32]

of binding energies reveal three C and three Si bonds: Si-C, Si-O and one peak coming from a new bond. Because SiO_x bonds have never been observed, the authors proposed an oxycarbide SiO_xC_y. However the SiC compound remains the more important compound in the Nicalon fiber. The total elemental composition is calculated and corresponds to the chemical analysis of the fiber.
M. Nagamori, J.-A. Boivin and A. Claveau [35] performed the study of thermodynamic stability of Nicalon fiber. Nicalon is an amorphous solid with variable compositions as $SiC_\alpha O_\beta$, according to different studies, where α and β refer to the respective atomic ratios C/Si and O/Si in the oxycarbide. These compositions exist with precipitates of SiO_2 , C etc... $Si_5C_6O_2$ is the mean composition formula proposed for an amorphous solid solution. S.M. Johnson et al. [36] measured SiO(g) pressures over Nicalon to be lower than for the same molecule over pure amorphous SiO(am) by Knudsen cell mass spectrometry. From these pressure data M. Nagamori et al. [35] used the postulated main decomposition reaction:

$$SiC_\alpha O_\beta(\text{am}) = \frac{1}{2}((1+\alpha-\beta)\text{SiC(s,s)} + \frac{1}{2}(-1+\alpha+\beta)\text{CO(g)} + \frac{1}{2}(1-\alpha+\beta)\text{SiO(g)},$$

where SiC is considered as dissolved in the amorphous phase. Because the ratio CO/SiO calculated from available α and β values (CO/SiO = 11) are different from the one found experimentally (= 2) by S.M. Johnson et al. [36], M. Nagamori et al. [35] concluded that the CO(g) measured pressure was in error because permanent gases are usually difficult to measure [19]. So they use the only SiO(g) partial pressure to evaluate the stability of the amorphous phase. Different assumptions were used:

- Estimates of the heat capacity by interpolation between SiC, Si and C.
- Applying Neumann-Kopp addivity rule (heat capacity estimate) from amorphous SiO_2 and Si(s).
- Estimates of the standard entropy (from the same above compounds as reference).
- Ideal activity of SiC in the amorphous mixtures.

According to experimental mass spectrometric works of P. Rocabois et al. [37, 38] the low partial pressures observed over SiO(am) and Black Glass amorphous compounds are directly related to vaporization kinetics. The results from experiments with different ratios of effusion orifices cross sections to cell cross sections show clearly partial pressures decrease with increasing orifice sizes. Moreover, Rocabois et al. [37, 38] have determined evaporation coefficients, with high accuracy using multiple cell device, which characterize clearly kinetics of vaporization. Determined values are very low: $\alpha(\text{SiO}) \approx 10^{-2}$ and $\alpha(\text{CO}) \approx 10^{-3}$ to 10^{-4}. Consequently, in effusion cells, the partial pressures can be measured with a factor 5 to 10 lower than equilibrium vaporization of mixtures Si-SiC-SiO_2 or SiC-SiO_2-C. For these last three-phases mixtures P. Rocabois et al. [37, 38] determined evaporation coefficients too. These works concluded definitely that vapor pressure measurements with any flow method (effusion, transport, transpiration method, etc...) cannot give equilibrium pressures.
Main consequence of such kinetic limitations on the vaporization is, that partial pressures are always under-evaluated. Using such experimental values in any thermodynamic cycle leads inevitably to negative free energy of formation and consequently the authors proposed

stable amorphous compounds. In such a context M. Nagamori et al. [35] could produce predominant diagrams that cannot be significant for any thermodynamic condition.
Most recent published work to this subject is from T. Vargas et al. [39]. SiCO-like amorphous material structures are presented which are constituted by nano-domains with special graphene (basal graphite planes) walls. Chemical analysis of these SiCO mixture-phases are performed in order to locate them in a ternary phase diagram. Calorimetric measurements referred to SiO_2, SiC and graphite show negative enthalpies of formation, which becomes more pronounced with C enrichment. The stability of the different chemical bonds Si-C or Si-O around the same carbon, as well as the nano-domains structure can explain the apparent stability of these mixture-phases against re-crystallization at high temperature.
As a conclusion, no well characterized ternary compounds are known in the Si-C-O system.
Vapor pressures studies performed by different authors in the ternary Si-C-O system agree that main gaseous species are SiO(g) and CO(g). These two species take more than 99% of the gaseous phase. P. Rocabois et al. [38] and N.S. Jacobson et al. [40] performed studies on vaporization behavior of pseudo-binary SiC-SiO_2 mixtures using High Temperature Mass Spectrometer with Knudsen Cells. They report that

$$2\mathrm{SiO_2(s)} + \mathrm{SiC(s)} \leftrightarrow 3\mathrm{SiO(g)} + \mathrm{CO(g)}$$

is the main reaction between the two condensed components. Furthermore they have shown that pseudo-binary mixtures behave as an azeotropic section. Any composition point in the ternary Si-C-O system will evolve with time to the pseudo-binary composition as a result of vaporization losses. This behavior remains until temperatures of 1700 K.
N.S. Jacobson et al. [41] measured the ratios of SiO/CO using Thermogravimetric Analysis (TGA) and HTMS with Knudsen effusion cells. They found values within 2 to 1 and decreasing partial pressures with time. For the three-phases mixture SiC-SiO_2-C, P. Rocabois et al. [38] determined very low evaporation coefficients: $\alpha_{SiO} = 5,4 \times 10^{-4}$ and $\alpha_{CO} = 5,8 \times 10^{-6}$, which show that the decrease relative to the equilibrium pressures is much more pronounced for CO(g).
Summarizing, different authors have seen experimentally that in the ternary system Si-C-O the evaporation does not attain equilibrium partial pressures. Measured vapor pressures are always smaller than calculated. Determined evaporation coefficients $\lll 1$ confirm this fact. The remaining question concerns the ratio SiO(g)/CO(g) < 3 even during experimental congruent vaporization of SiC-SiO_2. This behavior can still not be explained nowadays.

1.3 Vaporization of Silicon Carbide in oxidative environments

The behavior of silicon carbide under corrosive attack in oxygen containing atmospheres at high temperatures got a big interest with the view on the spacial use. For this reason a large number of publications is attended to oxidation of Si and SiC.
Generally two mechanisms of Si, SiC and any silicon containing compound oxidation are known:

- *Passive oxidation* is called so because of building of a SiO_2 layer on SiC surface exposed to oxidation atmosphere/flow, which makes the surface resistant, i.e. passive, to further direct oxidative attack. Oxidation then proceeds by O diffusion in the scale.

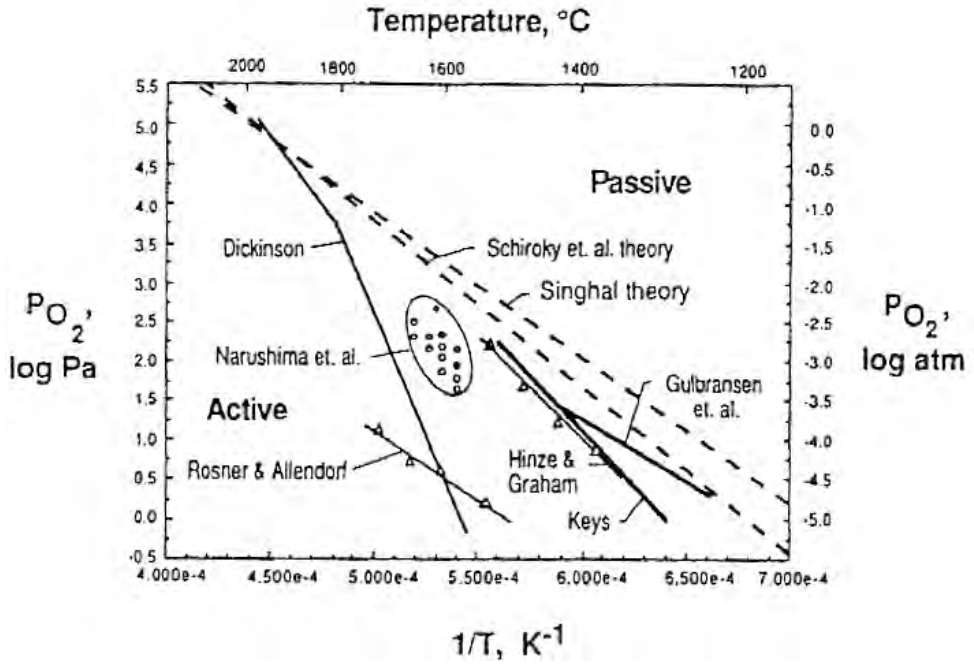

Figure 1.4: Literature data for the active-to-passive oxidation transition for SiC collected by W.L. Vaughn et al. [42].

As long as the scale is compact the oxidation is slow. This behavior of Si/SiC is reported for high oxygen partial pressures. The reaction is:

$$SiC(s) + 3/2O_2(g) \rightarrow SiO_2(s) + CO(g)$$

- *Active oxidation* is called so because SiC is oxidized actively this time, without any protective layer building. At low oxygen partial pressures only volatile silicon and carbon mono-oxides are formed according to reaction:

$$SiC(s) + O_2(g) \rightarrow SiO(g) + CO(g)$$

In this case SiC surface remains bare, open for any further reactions at the surface.

1.3.1 Experimental observations

Most of experiments were performed concerning the transition of active-to-passive domains. W.L. Vaughn and H.G. Maahs [42] summarized in 1990 the works made then on the active-to-passive transition. Figure 1.4 shows the result of their literature research.
The variations in the collected transition data are due to different materials used as samples (Hot-pressed SiC, sintered SiC etc.) and to the use of wide range of gas pressures, flow rates and oxidizing gas mixtures. Characteristic for the passive oxidation is a net mass increase. Sintered α-SiC samples were tested applying low-pressure, flowing air in high temperature (1700°C) DTA-TGA(differential thermal analysis-thermal gravimetric analysis) apparatus.

One suggestion made by J.W. Hinze and H.C. Graham [43] is that the transition partial pressure is determined and controlled by the CO(g) out-flow from the SiC surface. Further data collected from the literature by W.L. Vaughn et al. [42] and own experiments have shown that for given partial pressure in an increasing flow rate the transition temperature moves towards higher temperatures (see fig. 1.4).

T. Narushima et al. [44] investigated oxidation behavior of chemically vapor-deposited(CVD) SiC under CO/CO_2 flows. They measured the mass loss with thermogravimetric method (TGA) (1 bar) in the temperature range 1823 and 1923 K. They found a linear rate law for mass loss:

$$M = k_{CO \cdot CO_2} \cdot t \tag{1.1}$$

with M mass loss, t oxidation time and $k_{CO \cdot CO_2}$ the mass loss rate. The results are displayed in fig. 1.5. The dashed line represents the $(p^b_{CO_2}/p^b_{CO})^*$ at which the mass loss rate was maximal. At $p^b_{CO_2}/p^b_{CO}$ below this value a formation of carbon layer was observed on the CVD-SiC surface and above this value SiO_2 (cristobalite) was observed on the surface.

E.J. Opila and R.E. Hann Jr. [45] investigated some more complicated case of CVD SiC oxidation. They measured the mass change also by TGA at 1 bar pressure in 1 : 1 gas mixture of $H_2O : O_2$ flowing at 4,4 cm/s in temperature range $1472 - 1673$ K. E.J. Opila et al. [45] found paralinear oxidation behavior of CVD SiC and observed volatilization of the silica layer by silanols ($Si(OH)_4$, $Si(OH)_2 \ldots$) under conditions of their study.

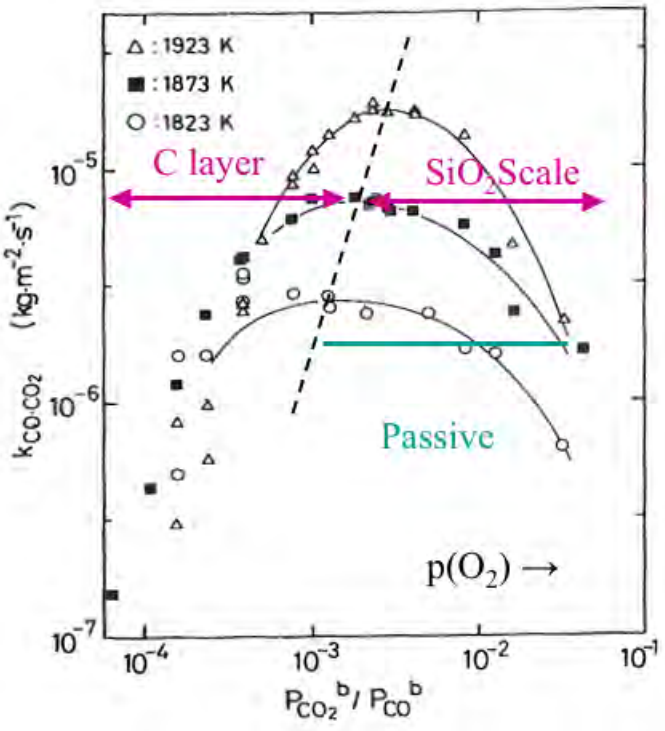

Figure 1.5: Relationship between $k_{CO \cdot CO_2}$ and $p^b_{CO_2}/p^b_{CO}$/ from [44].

1.3.2 High temperature mechanisms in passive oxidation domain

In the passive oxidation domain of SiC at high temperature several phenomena are reported. The most important effect is the formation of SiO_2 layer which decreases significantly the vaporization of SiC.
W. Bremen et al. [46] investigated the SiO_2 layer thickness on pyrolytically deposited β-SiC. A continuous coating SiO_2 (β-cristobalite) layer was formed under various CO-CO_2 atmospheres at $1273 - 1673\,K$. The growth rate of this layer was found to be controlled only by the oxygen diffusion rate through β-cristobalite.
Z. Zheng et al. [47, 48] investigated the oxidation of single 4H SiC crystals in dry oxygen in the temperature range of 1473 to 1773 K and 10^{-3} to 1 atm oxygen partial pressures. They found that at $T < 1573\,K$ the O_2 permeation in amorphous SiO_2 is the oxidation controlling factor and at higher temperature it is rather the O diffusion in cristobalite. Furthermore the carbonaceous diffusion does not control the oxidation rate ($D_C >> D_O$). The permeation flow is higher than diffusion flow. Following at high temperatures the scale growth is cut down because of the oxidation regime change.
K.L. Luthra [49] has made investigations on the oxidation rates of SiC comparing to Si, which is much higher. Mixed diffusion, inward of O_2 and outward of CO, through the silica scale are proposed as oxidation rate controlling factors. Furthermore the interface reactions interfere with the diffusion processes and bubbles can be formed.
N.S. Jacobson [50] summarized in his paper the parabolic oxidation rate constants of different SiC materials with silica scales for isothermal oxidation. At high temperatures the SiO_2 scale melting, scale volatility and reactions with the substrate become further limiting factors to the already mentioned above. Volatility diagrams were established as a function of the "internal" oxygen partial pressure at the interface substrate/scale using melting of the silica or vaporization gas pressure (1 bar as arbitrary criterion at interface) as stability criteria.

1.3.3 Theoretical analysis of the active to passive transition

A number of publications treat theoretically the transition from active to passive oxidation of SiC. N.S. Jacobson [50] summarize transition works as:

- based on volatility diagrams. For instance mass balance for oxygen: $p(O_2) = 1/2p(SiO)$ at the interface Si/SiO_2 for pure silicon;
- adding mass transport considerations. For instance J.W. Hinze et al. [43] use congruent vaporization as the main reaction to determine the transition ($p(SiO)/p(CO) = 3/1$). E.A. Gulbransen et al. [51] using C. Wagner theory [52] introduce diffusion coefficients in the molecular flow regime to balance CO output and O_2 input flow: the authors do some simplifications choosing only one main species as the product of oxidation:

$$SiC(s) + 3/2O_2(g) = CO(g) + SiO_2(s) \tag{1.2}$$

Among different authors, the ratio Si/C (stoichiometry of SiC) = 1 is never clearly used to solve the vaporization at transition, when taking into account of the whole gas phase. Moreover, only one main reaction is postulated.
Experiments performed by B. Schneider et al. [53] with TGA of a SiC square plate submitted to a parallel gas flow at low pressure (100 to 800 Pa) within the $1300 - 1700°C$

range. The gas flow is a mixture of Ar and O_2 at relatively high velocity i.e. 10 to 60 m/s. Mass loss is observed at constant velocity which increases with oxygen pressure, go to a maximum, then decreases. The maximum is attributed to the active to passive oxidation transition. Post experimental analysis revealed a silica surface layer although TGA shows a mass loss. In the higher range ($1600 - 1700°C$) the maximum as well as the silica layer is not observed. This is probably due to insufficient oxygen flow (total pressure too low) as we calculated in this work for the limit SiC-C. Theoretical considerations use thermodynamics of vaporization associated to the surface of SiC or the interface SiC-SiO_2 plus or minus associated to the incident oxygen potential with or without a boundary layer (diffusion in the gas phase). The authors try to determine the main gaseous species that explains the mass loss. Their conclusion is that the main species is SiO(g). The assumption of active oxidation due to the CO/SiO ratio or the mass balance for departure of C and Si with ratio 1 is never used as a criteria for active oxidation. The transition fixed at the maximum is not proved by theoretical considerations.
The approach of K.G. Nickel et al. [54] is to perform thermodynamic calculations in a configuration that can be related to some particular experimental or practical situations. Thermodynamics needs temperature and constant total pressure as well as a particular number of initial moles of each component or constituants. In case of corrosion the authors calculate under $p = 1$ bar, $T =$ constant, and for fixed ratio $SiC : H_2 : H_2O$. Two limits are calculated: Si-SiC and SiC-C in different atmospheres. These thermodynamic calculations give the different partial pressures in equilibrium, and consequently different gas compositions.
For corrosion applications, it is then necessary to use a flow relation in order to calculate the corrosion rate (moles of SiC taken away, or thickness of SiC corroded).

- First case is sweeping out slowly the saturated gas in which the Si-C vapors are vaporized, using the Marriott law, $pV = nRT$, and a constant laminar flow rate. This gives the maximum corrosion rate in an isothermal furnace. Practically this corresponds to a transpiration experiment.

- Second case is to sweep out gases formed at the surface by a high flow rate gas-reactive or not, or the equilibrium vaporisation under vacuum. The maximum vaporization rate is calculated by the Hertz-Knudsen equation which is the maximum vaporization flow. In case of reactive impinging gas the second condition is that the surface reactions are rapid, i.e. at equilibrium. A first thermodynamic calculation gives the gases in equilibrium, then the Knudsen flows are calculated.

In both cases, the authors [54] calculated first the different condensed phases that are formed. When SiO_2 or C are formed, calculations fixed the two extreme conditions. Then within these conditions the oxidation is active—SiC compound is the only condensed phase in equilibrium—and corrosion rates are calculated. Taking into consideration of condensed phases formed at the surface improves the understanding of corrosion mechanisms, as well as looking at the composition of the vapors since the authors observe that under active oxidation there exists a balance between Si number of atoms and C number of atoms in the gas phase i.e. Si/C ratio close to 1. Figure 1.6 shows a result for corrosion rate of SiC by H_2-H_2O flow.
But yet, the matter balance at the surface is neither taken into account as a necessary condition for active oxidation. These calculations simulate "externally" the whole phenomenon,

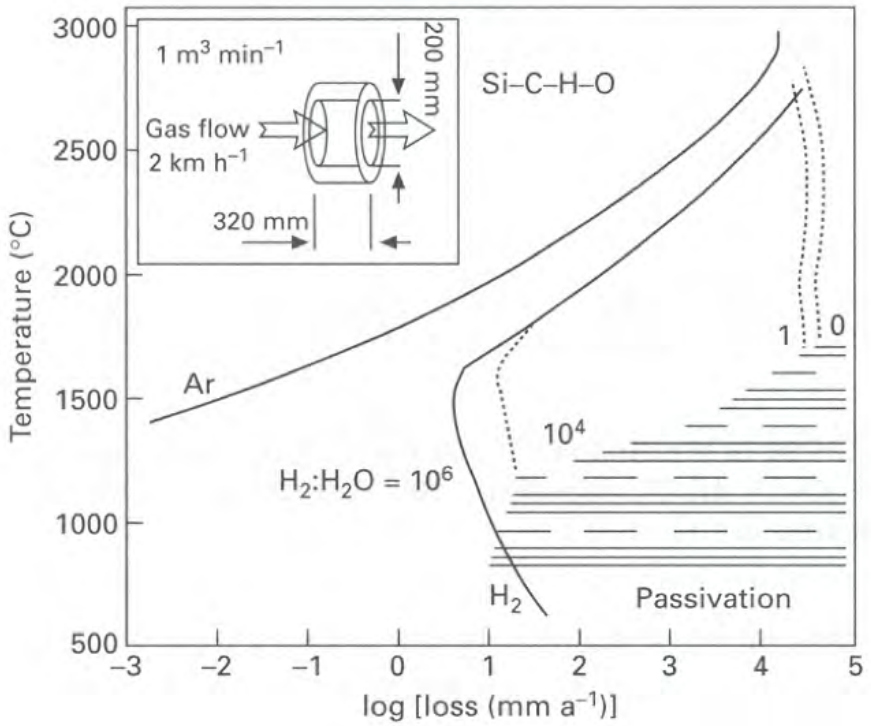

Figure 1.6: Predicted SiC losses in different environments for the model situation described by inset drawing according to [54]. This is the only author who suggested a transition zone and not a line.

but neither consider that the SiC surface controls the whole phenomenon by imposing the Si/C vaporization ratio = 1 corresponding to the integrity of the SiC stoichiometric compound.

M. Balat et al. [55] calculated the transition (input flow pressure versus the inverse of temperature) for SiC in a laminar flow of neutral gases loaded either with O_2(g) or O(g) produced by a plasma source. The theory of C. Wagner [52] was used in conjunction with thermodynamics of the vaporization of SiC (active vaporization) or SiC+SiO_2 (passive oxidation). Thermodynamics was used to choose the main reaction (equilibrium constants) occurring in the two domains. Experiments were performed with a special flow apparatus in the $1653 - 1948$ K range and for pressures in the 200 to 2100 Pa range. The SiC surface was analyzed after experiments either by mass gain and XRD for thick SiO_2 layers or Auger Electron Spectroscopy for thin layers (eg. pollution of the surface).

Experiments performed with O_2(g) show a transition at slightly lower temperature for a constant oxygen pressure (in the gas flow) which means that the passive oxidation occurs more rapidly than attended. But yet the difference can be attributed to experimental uncertainty, especially temperature measurement of the SiC surface (the authors [55] indicate ± 50 to 60 K). Experiments with atomic O(g) show the reverse, and the difference is also in the same temperature range. Note that the presence of the plasma in the gas flow can change the real temperature of the surface even if the authors [55] measured this temperature just before starting the oxidation on a temperature plateau during a certain time.

R.S. Sickafoose Jr. and D.W. Readley [56] analyzed by TGA either powders of β-SiC or compacts that have been first passived at air. Passivation at air at 900°C shows that the porosity of the compacts does not change significantly. Thermodynamic calculations are used to determine the different partial pressures either for SiC+oxygen or SiO_2+oxygen in a closed vessel. These simplifying assumptions impose the matter flow balance for SiO_2 departure (congruent vaporization in the pseudobinary SiC-SiO_2) and for active oxidation with H_2/H_2O when SiO_2 has disappeared. Gas diffusion in pores (Wagner theory [52]) is then used to calculate the purification time (SiO_2 departure) when using H_2/H_2O gas flow. As a conclusion, previsions and thermodynamic calculations coupled with diffusion are in rather good agreement with experimental determinations. However, the difference observed with O_2(g) and O(g) could be attributed either to gas-surface kinetics for impinging flows or to retarded built up of the SiO_2(s) layer for nucleation.

1.4 Miscellaneous

1.4.1 Some features issued from sintering processes

Literature information coming from the studies of SiC sintering process is a priori not available for the present study because vaporization is usually not considered important in this process. Moreover, these studies are generally focussed on the role of additives and the formation of intermediate liquid phases that are the way to warranty dissolution and re-precipitation processes. Thus, in the present study silica—native or added—could have an influence in the dissolution of SiC or C, although no serious studies have been undertaken to evaluate the reciprocal solubilities. In the framework of sintering with a liquid phase, a preceding study of S. Baud et al. has been undertaken using thermodynamics [57] and mass spectrometry [58, 59] in order to evaluate the influence of vaporization processes when sintering with oxide mixtures (Al_2O_3 – Y_2O_3). The main result was the quantification of losses by vaporization and consequently the growth of pores due to large erosion flow values. Among sintering studies, we retain the works of J. Kriegesmann and coworkers [60, 61, 62, 63] who take into account on the gas phase in the consolidation process of pure SiC in view of the so called re-crystallisation. These works are summarized in [63]. The authors summarize the shrinkage mechanisms during firing of SiC powders (sintering of the recristallized-SiC or R-SiC) with no special additives. So to insure sintering and densification, bimodal distribution of powders is used and high temperatures (> 2000°C) are applied. With larger original grains higher temperature is necessary for densification. Lack of shrinking implies only microscopic observations of the growth process. From these observations, the evaporation-condensation process is analyzed. No shrinking is observed for SiC doped C or pure SiC. In the consolidation process SiO_2 native layer is invoked that is associated to different reactions,

- as

$$2SiO_2(s) \leftrightarrow 2SiO(g) + O_2(g) \tag{1.3}$$

$$SiC(s) + SiO(g) \leftrightarrow 2Si(g) + CO(g) \tag{1.4}$$

that leads to the overall reaction,

$$2SiC(s) + 2SiO_2(s) \leftrightarrow 4Si(g) + 2CO(g). \tag{1.5}$$

The authors eliminate the last reaction on the basis that Si(g) is not stable against SiO(g).

- Or

$$SiC(s) + 2SiO_2(s) \leftrightarrow 3SiO(g) + CO(g). \tag{1.6}$$

that is assumed to start at the SiC/SiO_2 interface for local pressure more than 1 bar.

The last reaction going from left to right is sublimation of the material, and the reversal is condensation. So, if condensation is desired (going to the left), it is necessary to find a source of vapors.
The microscopic observation of terrasses with triangular or hexagonal shapes let the authors assume that the transport of gases is focussed on lattice defects (dislocations). In fact as studied by G.M Rosenblatt [64] with As or III-V (GaAs related) compounds the evaporation also groves the crystals into the same shape since preferential growth or erosion occurs at kinks after surface diffusion on the terrasses and diffusion along the edges of the terrasses. Such mechanism has been calculated to explain rather high values of the evaporation coefficient, within $0{,}3-1$ [65]. Sinks or pyramids are observed with different helicoidal stairs, a typical shape for 2-dimensional growth or erosion.
The microscopic observations of growth must be related necessarily to a mass transport from a source. With a bimodal distribution, the smaller grains "feed" the coarse ones because their partial pressures must be higher due to surface tension effects. Effectively the authors observed that the small grains usually disappear and pores are created in place of.

In firing experiments (1 hour isotherm), one is presented at figure 1.7, the authors show that no shrinkage was observed till $1850-1880°C$ (domain I) , then a very small but detectable shrinkage ($\approx 1.2\%$) is observed at 1960°C (domain II) then a very slight swelling up to 2150°C (domain III). The authors attribute these effects to "overfiring". The microscopic

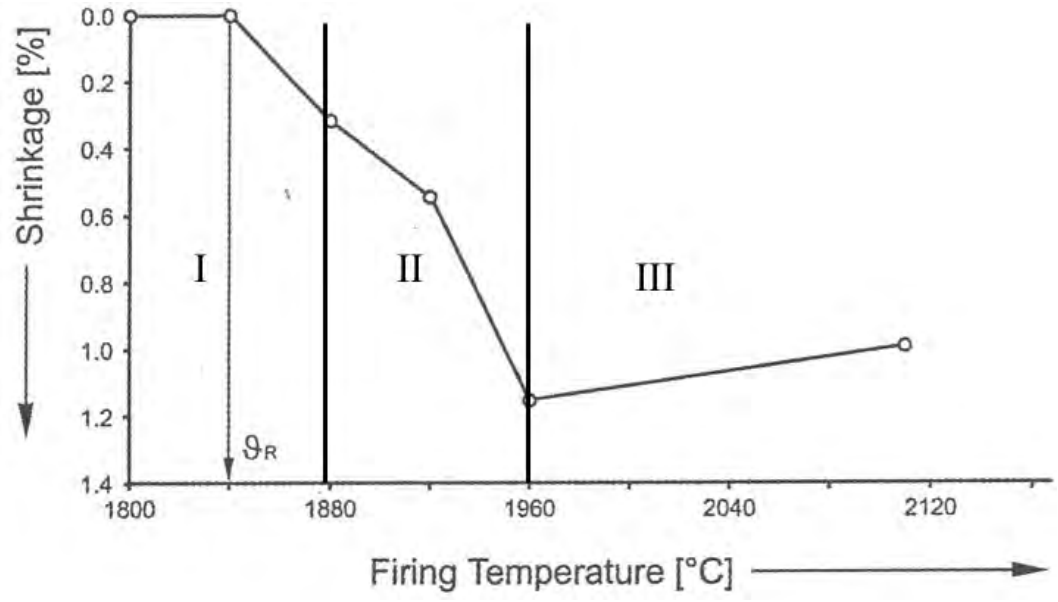

Figure 1.7: Shrinkage of a SiC sample during firing experiment from [63].

observations show the elimination of small grains at the end of the domain I, and BET surface measurements show a constant decrease of the specific surface in domain I, then very small variations for domains II and III. The decrease of the specific surface is then directly associated to the small grain consumption. Due to the lack of direct observation of vapours, the mass loss of the samples is mainly attributed by the authors to SiO(g) vaporization and erosion of SiO_2. The total mass loss is obtained practically at the end of domain I, and attributed to silica total loss. In the present experiments it corresponds also to the disappearance of small grains and beginning of shrinkage.
The authors conclude that:

- Consolidation (end of re-crystallisation) corresponds to the end of the evaporation-condensation process in relation with SiO_2 departure (1720°C in their reactor).
- Small grains fraction is the source of vapors.
- Lattice defects are sinks for vapors and growth start at these sites to build "necks"
- The evaporation-condensation process is a sintering phenomenon which cannot reach its final stage
- With increasing size of coarser grains smaller densification after SiO_2 departure are achieved.
- Grain growth when "overfiring" would be due to diffusion process, meanwhile the preferential Si(g) vaporization create swelling by gas pressure in closed pores.

From thermodynamics, the invoked main reactions have no real signification since in the stoechiometric domain of SiC the partial pressures can vary considerably, and at least 7 to 10 gaseous species as tabulated in thermodynamic tables build up the vapour phase. Following a complete thermodynamic analysis of the experimental conditions have to be performed to understand the transport processes and prove or invalidate the retained main reactions.
W.D. Kingery et al. [66] made investigations on the initial stages of sintering. They subdivide them into different modes in view of mass transport: viscous flow, plastic flow, evaporation-condensation, surface diffusion and volume diffusion. Plastic flow and volume diffusion being very low in the case of sintering of two spheres in contact are finally not considered for the explicit study. The authors performed a calculation of rates from models and experimental determination of different sintering modes. The case of NaCl spheres is shown as example for characteristic "necks" formation between the single grains for evaporation-condensation as mass transport mode. The different vapor pressures above different surface curvatures maintain gas flow and following mass transfer between the grains (positive curvature) and their contact points (negative curvature).
W.F. Knippenberg [67] studied the growth of SiC crystals and their polymorphism. He found that the structure and chemical composition of obtained SiC crystals are directly related to the growth conditions—heating procedure, phase transitions, impurities. He observed appreciable surface diffusion above 2000°C and that cubic SiC transforms into hexagonal SiC by surface diffusion. Figure 1.8 sketches found relation between the temperature and the obtained SiC structure. Furthermore, it shows the influence of equilibrated Si/C ratio in the corresponding gaseous phase when hexagonal structures are desired.

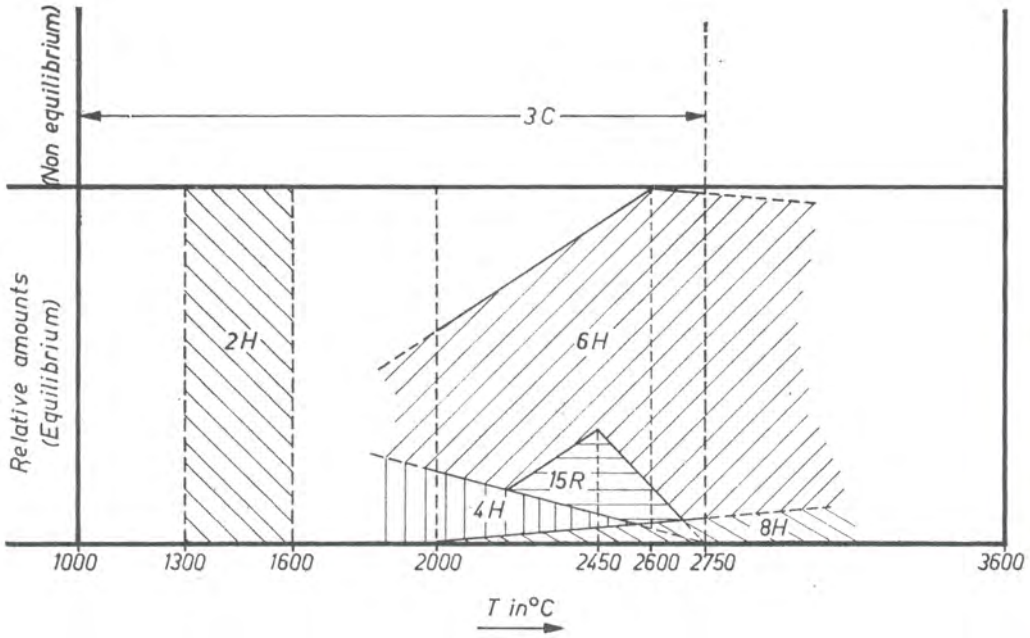

Figure 1.8: Relation between SiC structure and temperature of occurrence. The relative amounts of the different hexagonal structures are shown. The equilibrated Si/C ratio in the vapor will result in hexagonal structures at corresponding temperature. Cubic structure is obtained when this ratio is not equilibrated in the temperature range until 2750°C. [67]

1.4.2 SiC Surface and SiC-SiO_2 interfaces

The surface structure and composition of SiC after oxidation was studied applying different characterization devices by authors.
Auger electron spectroscopy (AES) and scanning AES, scanning electron microscope (SEM), low-energy electron diffraction (LEED) and X-ray photoelectron spectroscopy(XPS) were used by J.M. Powers et al. [68] to analyze oxidized surface of single-crystal α-SiC. Oxidation was performed at low pressure ($1 \cdot 10^{-8}$ Torr (Ultra High Vacuum) or at 1 atm. From 300 to 833 K the oxide layer was present like a suboxide "SiO" or Si-O-Si bonds at the surface. From 833 to 1100 K, SiO(g) vaporized and the surface precipitation of C(graphite) was observed. When thick layers were obtained at high temperatures ($933 - 1373$ K) the surface was composed from only SiO_2 and no C-precipitation at the surface was observed.
S. Hara et al. [69] analyzed the content of β-SiC(001) surface in O, Si and C by AES. The surface structure reconstruction from a silicon-rich surface to a carbon-rich surface when oxidized under $1 \cdot 10^{-7}$ Torr O_2 pressure at 1050°C was analyzed by LEED. The authors [69]—contrarily to earlier results from literature [68]—discuss the fact that the C-terminated surface is in fact a sp^3 structure and not a sp^2 graphite structure. This etching method is proposed for the preparation of clean SiC surfaces with C atoms at the surface.
The SiO_2/SiC interface was analyzed with AES by R. Bejoan et al. [70]. CVD β-SiC was oxidized at $1300 - 1360$°C during 10 min in 1 atm O_2(g). The formed thick silica layer (1600 Å) was analyzed using AES with erosion profile as well as secondary ion mass spectrometry (SIMS) to confirm the AES observations. A 400 Å interface with Si-O-C bonds was observed and a precipitate of carbon near the interface only. The nature of observed carbon was not determined.

1.4.3 Silicon metallurgy and thermodynamics

During the production of Si in industrial furnaces SiC occurs as intermediate phase. A thermodynamic approach by calculations of equilibria was performed by several authors.
Determination of thermodynamic data for silicon compounds has been for long time the basic work for thermodynamic analysis of the silicon production in industrial arc-furnaces. The different analysis has been summarized by T. Rosenqvist [71].
I.V. Ryabchikov [72] made a thermodynamic analysis using the three variables—total pressure, temperature and the ratio SiO/CO in the gaseous phase—showing the stability domains of SiC and Si. This kind of analysis has been recently performed again by F. Danes et al. [73] and shows that the theoretical transition region $2000 - 2100$ K for production of silicon from SiC (+ SiO_2) is –(i) at 0,367 bar and 2011 K when no external pressure is applied, –(ii) and temperature can be moved up by increasing the total pressure applied to the system in order to increase the Si/SiO_2 production yield. The main difficulty when making such thermodynamic analysis is that the calculations are performed at constant temperature and pressure, but there is no way to control the ratio SiO/CO in a real furnace. So, any "global" thermodynamic analysis cannot explain the whole industrial production, which is performed with temperature, pressure and composition gradients.
N. Nagamori et al. [74] argued in a long thermodynamic presentation of the so-called "predominance diagrams" that the only explanation by the existence of a SiO(s,l) phase—a new phase proposed earlier by O. Kubachewski and C.B. Alcock [75]—was sufficient to explain industrial production of Silicon. Improvements could be done by using double

reactors in which carburization and reducing would be performed in two different stages. T. Rosenqvist and J.Kr. Tuset [76] in a comment to the N. Nagamori paper [74] explained, that the production is in fact not only relevant from thermodynamics, but from exchange of matter in the industrial furnaces, which are in fact open systems working as "countercurrent reactors". Moreover, the production of silicon would be in fact relevant of kinetics that fixes the ratio SiO/CO. N. Nagamori et al. reply [77] to these observations by the publication of new data set for the SiO phase.

F. Danes et al. [78] propose to increase the production yield (final Si/initial SiO_2) by recycling part of the gas phase produced by the condensed phase. Taking into account of the matter flow coupled with equilibrium calculations G. Eriksson and K. Hack [79] propose a simulation of the metallurgical grade silicon production in an arc-furnace with 4 stages. More recently, P. Rocabois et al. [38] and N.S. Jacobson and E.J. Opila [40] have shown that the pseudobinary SiO_2-SiC is in fact—considering the only two main gaseous species SiO(g) and CO(g)—a pseudo-azeotropic line for which the total pressure (SiO+CO) is lower than in the two adjacent triphasic Si-SiO_2-SiC and SiO_2-SiC-C domains. This minimum of total pressure pertains till about $2000 - 2100\,K$ depending on the choice of thermodynamic data. Above the CO(g) pressure becomes more important than SiO(g) pressure and silicon can nucleate as an independent phase by producing more CO(g) in the vapour phase, or when removing CO(g) as it occurs in metallurgical open furnaces. The main interest of all these thermodynamic analysis is to evidence a change of the vaporization behaviour of the mixtures SiO_2-SiC before and after this transition. At lower temperatures the vaporization is pseudo-congruent and SiO_2 is preferentially eliminated by vaporization till a pure SiC residue is produced (see [38]), meanwhile at higher temperatures metallic silicon can be produced in presence of SiO_2-SiC mixtures, even with liquid silica.

In earlier experiments using Knudsen cells K.-G. Günther [80] observed that the vaporization of Si-SiO_2 mixtures or of the available so called "amorphous SiO" compound depend on the effusion orifice section that shows the importance of kinetic limitations. A value of $4{\cdot}10^{-3}$ for the evaporation coefficient of SiO(g) was determined. P. Rocabois et al. [37] using the multiple cell method coupled with a mass spectrometer vaporized altogether mixtures of Si+SiO_2 and SiO(amorphous) and by direct comparison determined the evaporation coefficient of commercial SiO(amorphous) as well as of different mixtures Si-SiO_2 powders of different compositions. Using the determined evaporation coefficients, P. Rocabois et al. [37] calculated the equilibrium pressures in the effusion cells that showed that there are no differences in theoretical equilibrium pressures between these mixtures and the amorphous SiO(s, am). Their conclusion was that SiO(s, am) is in fact an intimate mixture of Si and SiO_2 tetrahedrons or nanodomains and this interpretation is consistent with structural observations (see [37]). S.I. Shornikov et al. [81] summarize the works on evaporation coefficients of SiO(g) and Si_2O_2(g) from different condensed phases altogether with their own determinations [82].

Further, P. Rocabois et al. [38] showed also by mass spectrometry that the vaporization of the triphasic Si-SiO_2-SiC and SiO_2-SiC-C mixtures is kinetically limited, i.e. "hindered" (english term) or "retarded" (american term) vaporization occurred. The effect on pressures (or matter flows) is more pronounced for CO(g) than for SiO(g). So the above transition from azeotropic to non-azeotropic vaporization is moved towards higher temperatures. Indeed, in industrial furnaces temperature is within $2400 - 2600\,K$. For the pseudo-binary section SiO_2-SiC N.S. Jacobson [83] observed by mass spectrometry a vaporization process which can be also called "non-equilibrium" since the congruent ratio is not observed but

yet the composition of the samples remains in the pseudobinary section.
As a conclusion, and as proposed by T. Rosenqvist and J.Kr. Tuset [76], the vaporisation of SiO_2-SiC and C mixtures is relevant from kinetics even at high temperature meanwhile thermodynamics remains a guide for the dominant tendencies in composition evolutions when matter is lost by vaporization. Thermodynamic evaluation of these losses will be always over-evaluated when compared to the real state in furnaces. A better understanding of the mechanisms that lead to low values of the evaporation coefficients would improve our knowledge of the behaviour of this system during metallurgical treatments in high temperature furnaces.

1.5 Conclusion

The SiC vaporization in reality occurs firstly always as SiC-SiO_2 mixture vaporization because of the native SiO_2 layer which builds always on the SiC-air interface at room temperature. The same can occur in the vacuum because of the gas atmosphere in the first stages of pumping or in the first stages of heat treatment which liberate oxidizing species from the sample surroundings. The oxygen partial pressures are always in the passive oxidation range. This behavior of SiC material can be influenced by the treatment, for instance different modes of milling, wet or dry. The Si-C connections are broken during this treatment and the terminating surface layer is determining the oxidation behavior: it is evident that a C-terminating surface is less susceptible to oxidation than Si-terminating surface layer, which reacts directly with air oxygen.
It was observed experimentally that the native silica layer transforms by heating from amorphous to cristobalite.
The transition of the oxidation mode from passive to active was observed experimentally. Different authors have used different materials in their studies and / or different experimental parameters which led to non-coherent results with each other. The main question to ask is if this transition “line” is in reality rather a domain of certain width. The results from reported studies are giving a “line”, but they considered neither the stoechiometric expansion of SiC nor the surface potentials.
The role of oxygen and carbon in the re-crystallization of SiC described with evaporation-condensation model is not completely clear. One is evident, the SiC surface must be locally free from any kind of precipitation to build a neck. The presence of oxygen in form of SiO_2 is following necessary to maintain this surface bare with active oxidation. But there is an absolute temperature limit at approx. 2000 K above which the presence of SiO_2 in the SiC samples leads to Si precipitation. Carbon presence in re-crystallization samples is generally considered as not favorable.

2 Theoretical approach to the vaporization phenomena of Si-C and Si-C-O systems

In this chapter we will describe the performed theoretical approach to the complex vaporization phenomena in Si-C binary system and also in Si-C-O ternary system. The manufacturing of SiC based ceramics must be often performed at high temperatures, so vaporization occurs and interferes in the process. These interferences can have as positive, desirable, influence on the manufacturing process as negative. For example material transport via the gaseous phase in the parts, that leads to the bonding reactions, and out of the parts, that leads to the aging of kiln furniture. Obtaining more informations on the gaseous phase behavior during the manufacturing process would help to improve the quality of the produced material as well as to prevent fast aging of the kiln furniture.
SiC ceramics, because of their refractory properties, gain also more and more importance for high temperature applications. Also here it is important to know its evaporation behavior to know their limits or improvement possibilities.
We took in our observation also the Si-C-O ternary system because it is important to know the vaporization phenomena of the mixture of SiC with SiO_2. The SiO_2 is almost always present on the open surfaces of silicon based materials, which include SiC.

2.1 Binary Si-C system

2.2 Vaporization in the Si-C binary system

Vaporization of pure SiC, the stoichiometric domain of which is known to be very restricted and till now not strictly determined is braced by two two-phases domains Si-SiC et SiC-C. The gaseous phase contains atomic Si and C and a number of molecules which were studied using High Temperature Mass Spectrometer (HTMS) [19, 20, 15, 22]. The most important gaseous species are Si, Si_2, Si_3, Si_2C, SiC_2, C, C_3, C_5. They are included in the thermochemical tables JANAF [5]. The minor gaseous species are $Si_{4\,\mathrm{to}\,8}$, C_2 and carbides SiC, Si_2C_2, Si_2C_3, Si_3C_2 Si_3C, Si_4C. The vapor pressures can be calculated by choice of elementary reactions as followings:

$$\mathrm{Si(s\ or\ l)} = \mathrm{Si(g)} \qquad \text{with} \qquad K_p = \frac{p(\mathrm{Si})}{a(\mathrm{Si})} \tag{2.1}$$

$$2\mathrm{Si(s\ or\ l)} = \mathrm{Si_2(g)} \qquad \text{with} \qquad K_p = \frac{p(\mathrm{Si_2})}{a^2(\mathrm{Si})} \tag{2.2}$$

$$\mathrm{Si(s\ or\ l)} + \mathrm{SiC(s)} = \mathrm{Si_2C(g)} \qquad \text{with} \qquad K_p = \frac{p(\mathrm{Si_2C})}{a(\mathrm{Si}) \cdot a(\mathrm{SiC})} \tag{2.3}$$

$$\mathrm{SiC(s)} + \mathrm{C(s)} = \mathrm{SiC_2(g)} \qquad \text{with} \qquad K_p = \frac{p(\mathrm{SiC_2})}{a(\mathrm{SiC}) \cdot a(\mathrm{C})} \tag{2.4}$$

The activities of pure solids are equal 1 by definition and same for liquid Si, as we do not know the thermodynamics of the liquid phase and the solubility of carbon remains small. Indeed Rocabois et al. [15] have shown by Mass Spectrometry that the activity of Si along of the liquidus line is near unity in the presently concerning temperature region up to ≈ 2200 K.
We have calculated the partial pressures of the main vapor species in the two diphasic domains SiC-C and Si-SiC. Figure 2.1 is the result of these calculations for the SiC with silicon excess. The behavior of the vapor pressures in this diphasic system can be plotted as generally known in thermodynamics by $\log p = \frac{\mathrm{A}}{T} + \mathrm{B}$. Coefficients A and B are listed in the table 2.1.
Same as for the SiC with Si excess we made for the SiC rich in carbon. Results of the calculation are shown in figure 2.2 and coefficients A and B of the plot according to $\log p = \frac{\mathrm{A}}{T} + \mathrm{B}$ are also listed in table 2.1.

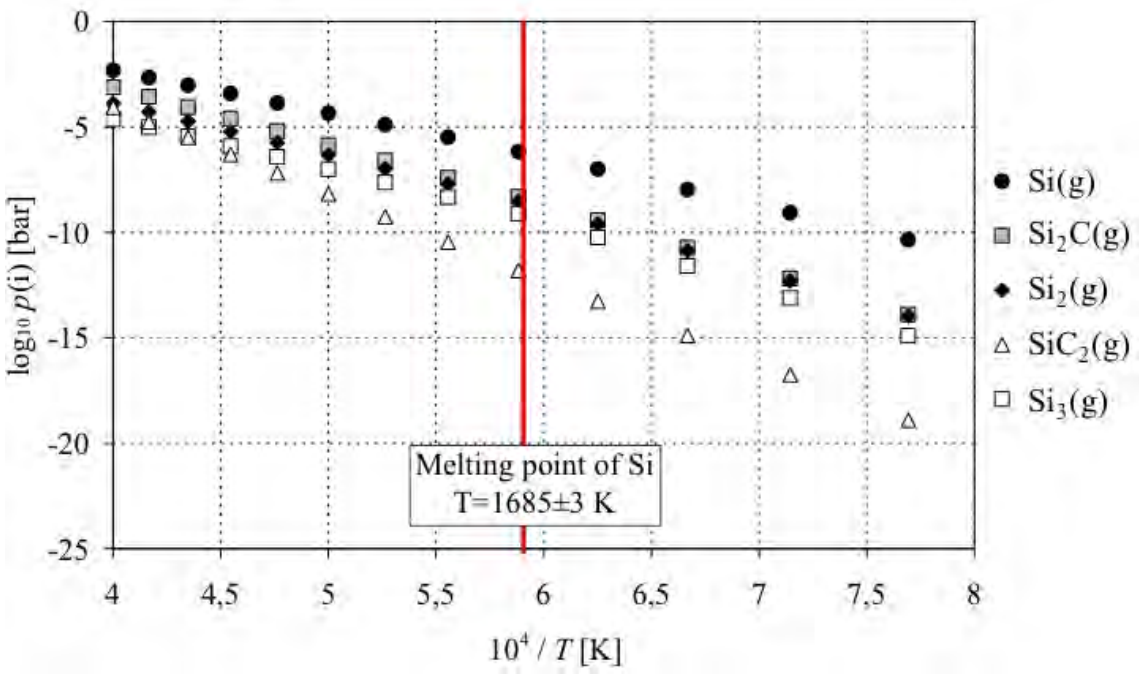

Figure 2.1: Vapor pressures above the SiC with excess of Si calculated from JANAF tables [5].

Table 2.1: The coefficients A, B for the decimal logarithmic plot of the partial pressures of the two SiC diphasic domains as a function of the inverse of temperature, $\log p = \mathrm{A}\frac{10^4}{T} + \mathrm{B}$ with p in bar and T in Kelvin. For the first diphasic domain the slope changes because of Si melting at 1685 K.

Compound	**A**		**B**	
Si-SiC	$T < 1685\,\mathrm{K}$	$T > 1685\,\mathrm{K}$	$T < 1685\,\mathrm{K}$	$T > 1685\,\mathrm{K}$
Si	-2,324	-2,0454	7,5216	5,8679
Si_2	-3,0236	-2,466	9,2994	5,9901
Si_3	-3,2246	-2,3825	9,9017	4,9038
Si_2C	-3,0861	-2,7719	9,8495	7,9854
SiC_2	-3,9054	-4,1208	11,149	12, 429
SiC-C				
SiC	-4,0906		10,143	
Si	-2,6852		7,8516	
Si_2	-3,7459		9,9589	
SiC_2	-3,5069		10,569	
Si_2C	-3,4263		10,039	
C	-3,7471		8,2154	
C_3	-4,1558		10,377	

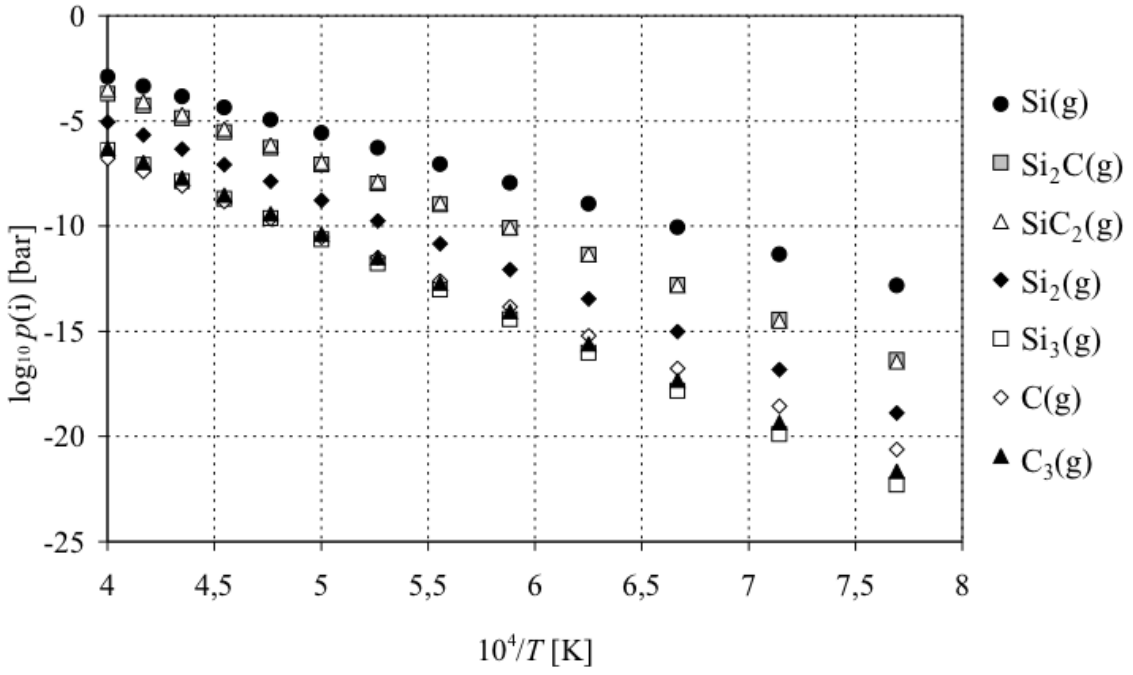

Figure 2.2: Vapor pressures above the SiC pure with excess of C calculated from JANAF tables [5]. p(SiC) is not quoted because its pressure is very low.

2.3 Evaporation flows in the binary Si-C

Using the plots of partial pressures in equilibrium with a composition of interest we are able now to obtain the composition of the gaseous phase and compare it to the composition of the condensed phase. Following equations were used to calculate the composition of the gaseous phase applying the perfect gas law:

$$\frac{N(\mathrm{Si})\ RT}{V} = p(\mathrm{Si}) + 2p(\mathrm{Si_2}) + 3p(\mathrm{Si_3}) + p(\mathrm{SiC_2}) + 2p(\mathrm{Si_2C}) + p(\mathrm{SiC}) \quad (2.5)$$

$$\frac{N(\mathrm{C})\ RT}{V} = 2p(\mathrm{SiC_2}) + p(\mathrm{Si_2C}) + p(\mathrm{C}) + 3p(\mathrm{C_3}) + p(\mathrm{SiC}) \quad (2.6)$$

and the next to obtain the molar fraction of the vapor:

$$X(\mathrm{Si}) = \frac{N(\mathrm{Si})}{N(\mathrm{Si}) + N(\mathrm{C})} \quad (2.7)$$

$$X(\mathrm{C}) = \frac{N(\mathrm{C})}{N(\mathrm{Si}) + N(\mathrm{C})} \quad (2.8)$$

The ratio $\frac{X(\mathrm{Si})}{X(\mathrm{C})} = \frac{N(\mathrm{Si})}{N(\mathrm{C})}$ is displayed in figure 2.3 with full black symbols for the two systems rich in Si and rich in C. It shows that the gaseous phase contains always more Si than C even if the condensed phase is rich in carbon.
In the case of SiC vaporization under neutral gas atmosphere the mass loss will be proportional to $N(i)$ multiplied by the carrier gas flow rate. The original SiC compound will lose excess of Si and will turn into SiC+C: a carbon residue will form. This behavior was already

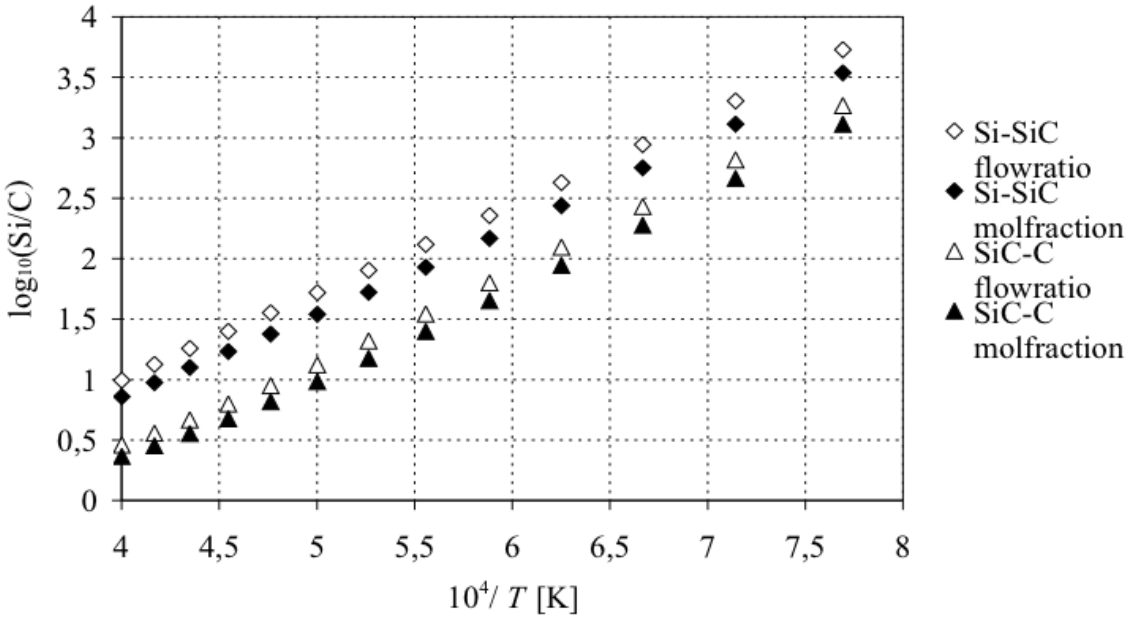

Figure 2.3: Decimal logarithm of ratio $\frac{X(\mathrm{Si})}{X(\mathrm{C})} = \frac{N(\mathrm{Si})}{N(\mathrm{C})}$ for SiC rich in Si and for SiC rich in C compared to the molecular flow composition $\phi(\mathrm{Si})/\phi(\mathrm{C})$.

frequently observed by numerous researchers who worked on this system. The residue looks rapidly as graphite easy to identify with X-Ray Diffraction methods [30].
In the case of vaporization under molecular vacuum it is the composition of the vaporization flow or Knudsen flow that counts rather than vapor pressure. During the mass spectrometric experiments using the effusion cells we observe the Knudsen flows.
The relations 2.9 and 2.10 are used to calculate the atomic flow per unity of time for a surface S.

$$\phi(\mathrm{Si}) = \frac{S}{\sqrt{2\pi RT}}\left[\frac{p(\mathrm{Si})}{\sqrt{M_{\mathrm{Si}}}} + \frac{2p(\mathrm{Si_2})}{\sqrt{2M_{\mathrm{Si}}}} + \cdots + \frac{2p(\mathrm{Si_2C})}{\sqrt{2M_{\mathrm{Si}}+M_{\mathrm{C}}}}\cdots\right] \tag{2.9}$$

$$\phi(\mathrm{C}) = \frac{S}{\sqrt{2\pi RT}}\left[\frac{p(\mathrm{Si_2C})}{\sqrt{2M_{\mathrm{Si}}+M_{\mathrm{C}}}} + \frac{2p(\mathrm{SiC_2})}{\sqrt{M_{\mathrm{Si}}+2M_{\mathrm{C}}}}\cdots\right] \tag{2.10}$$

Then, it is the ratio $\frac{\phi(\mathrm{Si})}{\phi(\mathrm{C})}$ that must be compared to the composition ratio $\frac{X(\mathrm{Si})}{X(\mathrm{C})}$ of the solid phase. The presence of the molar masses in these expressions leads to slightly different composition ratios compared to those calculated for neutral gas atmospheres, e.g. Argon (see Fig. 2.3 white symbols). During the spectrometric measurements we have to pay attention on this difference due to vacuum evaporation processes.

2.4 Vaporization of the SiC compound

The aim concerning the SiC compound behavior is to know what happens between the two diphasic domains. The components Si and C are in the SiC solid solution (s, s) in equilibrium with the SiC compound:

$$\mathrm{SiC} = \mathrm{Si_{SiC}(s,\ s)} + \mathrm{C_{SiC}(s,\ s)} \qquad \text{with} \qquad K_p(T) = \frac{a(\mathrm{Si})\,a(\mathrm{C})}{a(\mathrm{SiC})} \tag{2.11}$$

The equilibrium constant will be calculated from the standard free enthalpies listed in the JANAF tables [5]. Using this we obtain:

$$\Delta_{\mathrm{r}}G^{\circ}(T) = -RT\ln K_p \tag{2.12}$$

Per definition in the standard state, the activity of the pure components or a compound in a pure phase is equal to unity. For the equilibrium state in SiC with excess of Si, $a(\mathrm{Si}) = 1$, we obtain the minimum of the activity of carbon and reversely if we have a SiC rich in carbon. The isothermal evolution of the activities in the SiC stoichiometric domain is displayed on fig. 2.4 *, by enlarging this domain. This kind of representation allows to understand how the partial pressures of the different vapor species vary in this domain connecting the two diphasic domains by starting with equilibria of the form:

$$\mathrm{Si_{SiC}(s,s)} = \mathrm{Si(g)} \tag{2.13}$$

$$\mathrm{Si_{SiC}(s,s)} + \mathrm{SiC} = \mathrm{Si_2C(g)} \tag{2.14}$$

We are able now to calculate the partial pressures of the different gaseous molecules for

*As the true SiC stoichiometric composition domain is unknown, we have drawn the activities as straight lines; but according to the nature of the existing defects a S-form connecting lines would result more or less curved.

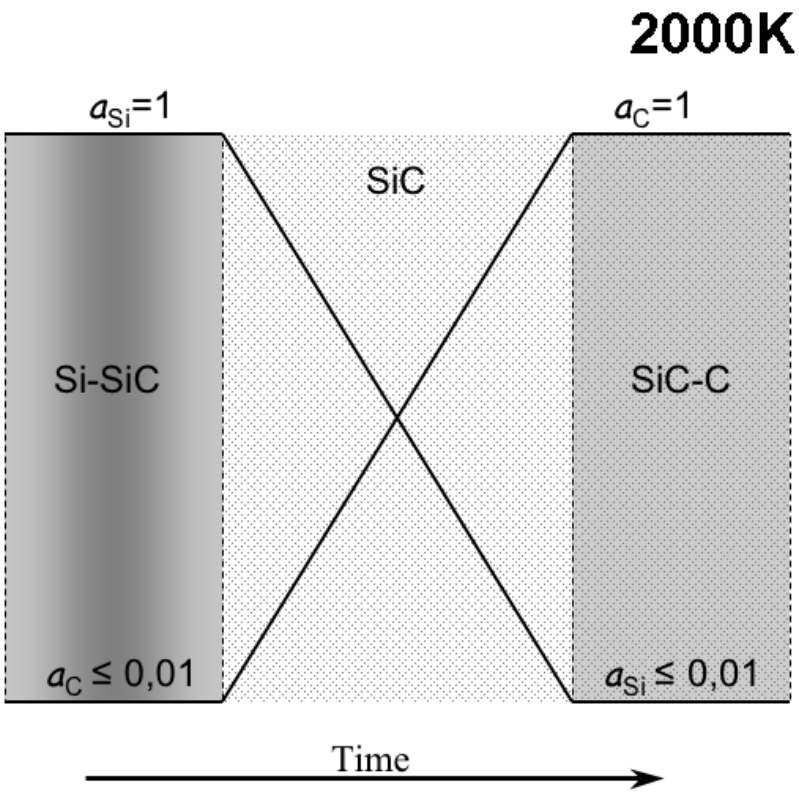

Figure 2.4: Isothermal evolution of the activities of Si and C components in the stoichiometric domain of SiC, displayed by enlarging intentionally this domain.

each (unknown) composition included in the stoichiometric SiC domain. It is evident that they are located on the connecting lines of the two diphasic domains that brackets the SiC stoichiometric region (see footnote $*$).
The modification in the partial pressures is due to that of the condensed phase composition caused by the material vaporization. Figure 2.5 displays the above reasoning. The partial pressure values are located between the calculated extrema. They correspond to the straight lines which connect the partial pressure values in the diphasic domains Si-SiC to SiC-C.

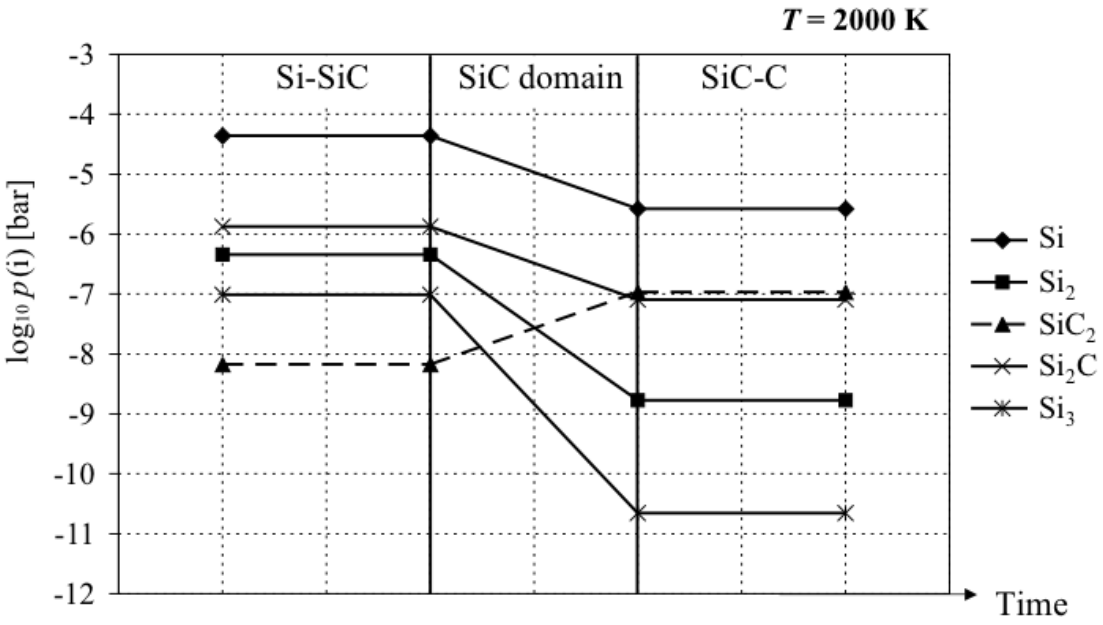

Figure 2.5: Isothermal evolution of the partial pressures above SiC at 2000 K due to the change of condensed phase composition by material loss under vaporization conditions. (The stoichiometric domain of SiC has been intentionally enlarged.)

2.5 Evolution of the SiC composition

The stoichiometric composition of the SiC solid phase will change because of the evaporation flows. We calculated first the silicon and carbon flows per surface unit as a function of temperature. They are displayed on the figure 2.6.
If we assume that:

- For a composition saturated with Si, the C evaporated flow can come only from SiC, so we can consider this flow equal to the SiC erosion.

  This kind of reasoning based on the only C matter flow may seem wrong because it seems that we underestimate the erosion of SiC, as we already know that the Si flow is always superior and causes a deposition of carbon in form of graphite. In fact graphite cannot be deposited as long as we are vaporizing the diphasic Si-SiC that is in the domain rich in Si. So the escaping gaseous carbon (via $Si_2C(g)$ and $SiC_2(g)$) is the only one that causes the erosion of SiC and the Si(g) excess flow comes from free Si.

- For a composition saturated with C, the Si evaporated flow must be equal to the SiC erosion. Indeed, the composition rich in C will be enriched in C because escaping Si excess comparing to C, will cause a C residue on the surface corresponding to the main vaporization reaction:

$$\mathrm{SiC} = \mathrm{Si(g)} \uparrow + \mathrm{C} \downarrow$$

.

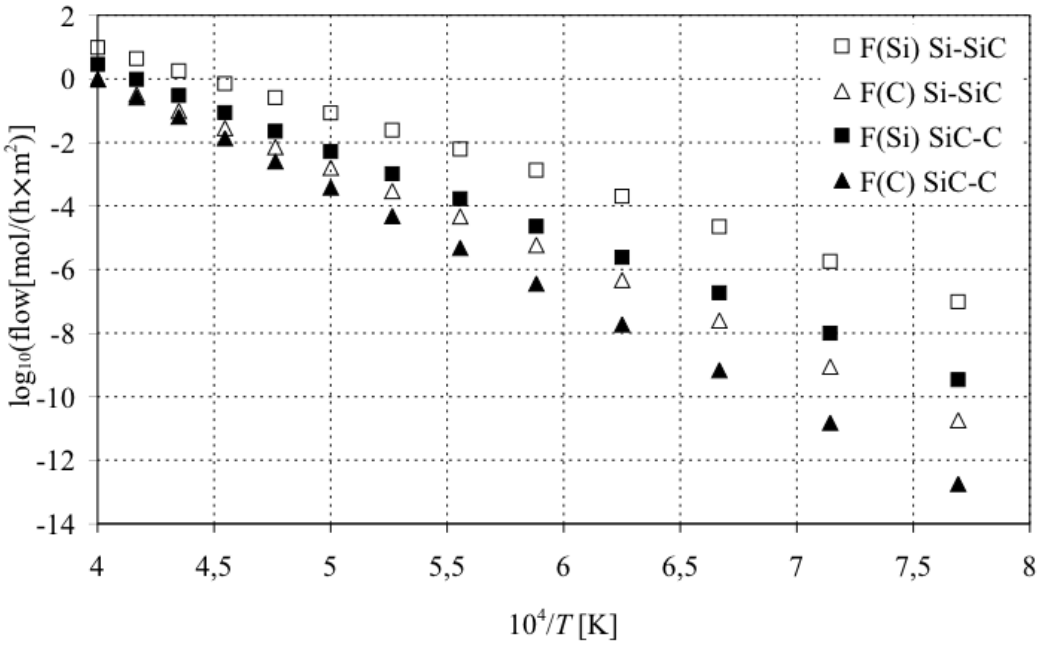

Figure 2.6: The evaporated Si-flow and C-flow from SiC per surface unity ($1\,m^2$) as a function of temperature for the two compound limits, Si-SiC and SiC-C, calculated from the equilibrium partial pressures.

We have calculated the erosion of SiC as a layer thickness, i.e. in micrometers per hour (μm/h) as displayed in the figure 2.7 for the vaporization process under neutral gas.
The above proposed explanations allow to calculate time that is necessary for a Si–SiC (limit of the diphasic) to turn into SiC–C if we would know the composition range of the stoichiometric domain of SiC. Two values, about 1% and $\leqslant 0,1\%$, have been published [17, 16]. We represented this time as a function of temperature considering arbitrarily 0,1% of change of stoechiometry as reported in [16], i.e. $Si_{0,5}C_{0,5}$ into $Si_{0,499}C_{0,501}$. In this case, in an arbitrarily chosen volume of the SiC phase, 0,1% of the SiC molecules turns into C(s) by Si lost under equilibrium vaporization conditions. Figure 2.8 shows this "time of stoichiometric change" for a vaporizing layer with 1 and 10 μm SiC thickness. The calculations were performed with average Si- and C-flows between Si-rich and C-rich SiC. It becomes visible that the "time of existence" of the pure SiC as a single phase under equilibrium vaporization conditions becomes very restricted when increasing temperature. For example at 1400 K we need approximately 80 s, at 1500 K only ca. 7 s and at 1600 K less than 1 s to turn 0,1% of SiC molecules in 1 μm thick layer into C.
These calculations are based on the simple assumption that the vaporization phenomena are not limited by bulk diffusion of Si in SiC as well as in the neutral gas flow. If so carbon will appear sooner at the surface. Muehlhoff et al. [84] have observed differently terminated faces of SiC under high vacuum in XPS and AES. Between 900 and 1300 K they found both, Si-terminated and C-terminated faces, covered with a graphite layer. Only above 1300 K the massive graphitization of both surfaces is attributed to Si(g) vaporization from SiC surfaces, which corresponds to the present assumptions. With XPS and AES the observations are limited on one or two atomic layers, our calculations for 1 μm correspond to 10000 atomic layers. For lower temperatures the diffusion is predominant and the carbon-rich structures appear generally earlier than predicted.

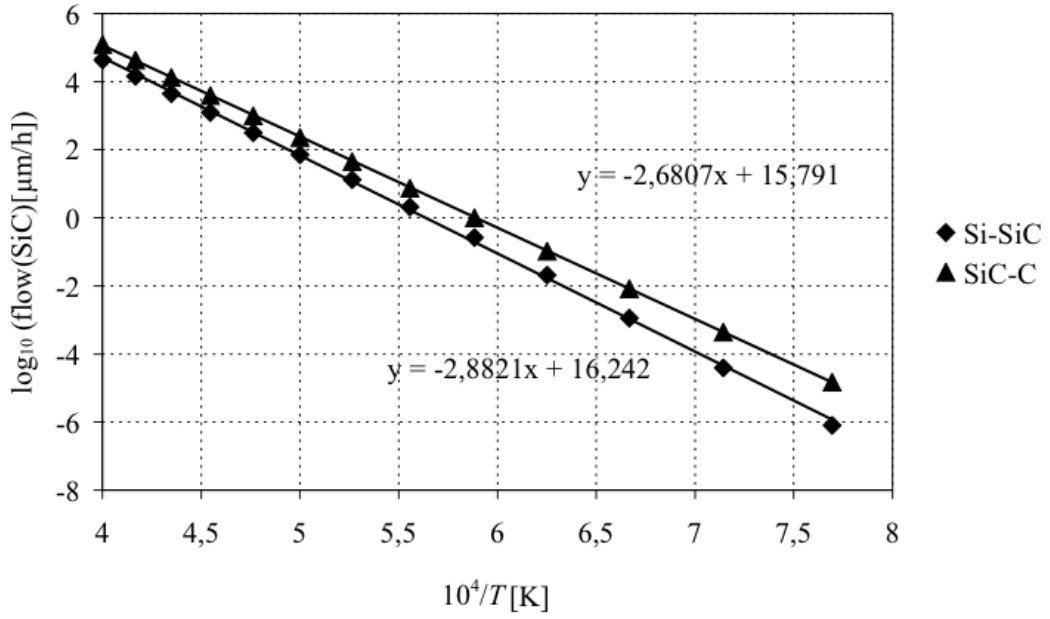

Figure 2.7: The erosion rate of SiC as a layer in μm/h as a function of the inverse of temperature for the two compound limits calculated from the equilibrium partial pressures in a neutral gas.

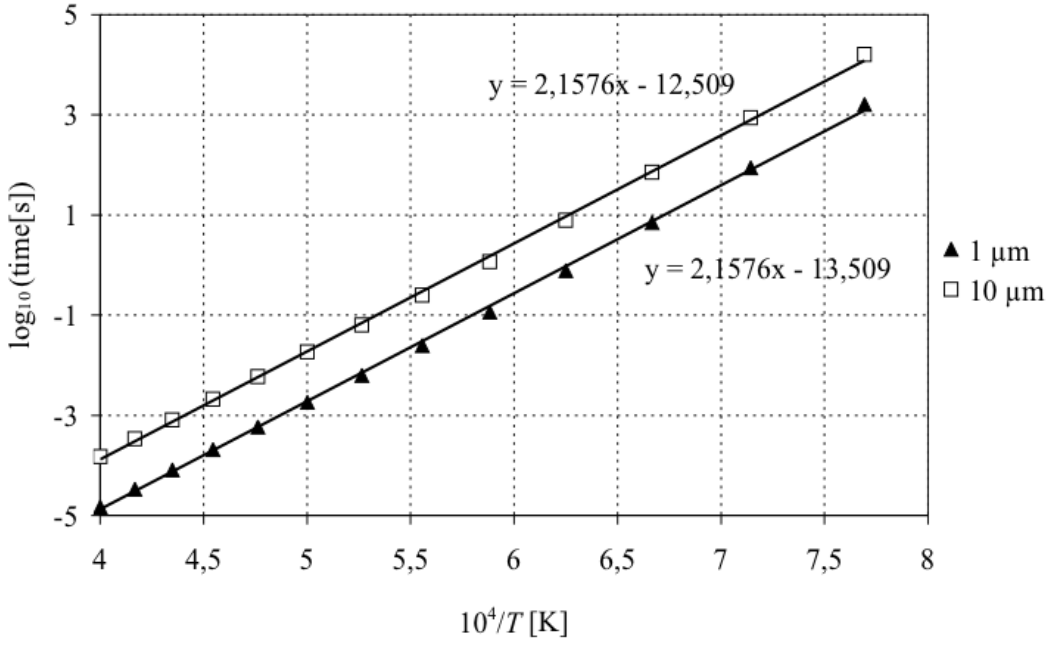

Figure 2.8: Vaporization time necessary to turn a $Si_{0,5}C_{0,5}$ compound into a $Si_{0,499}C_{0,501}$ due to matter loss via vaporization in a neutral carrier gas as a function of the inverse of temperature. The calculation was performed using average Si- and C-flows from Si-SiC and SiC-C.

2.6 Ternary Si-O-C system

The SiC, like other Si compounds, builds under oxidative conditions, at air for example, a SiO_2 protective layer. So we can consider that SiC is always present rather as a ternary Si-C-O compound than pure SiC. We saw in the preceding chapter that, because of its restricted stoichiometric domain, SiC is relatively difficult to be obtained in stoichiometric pure state and it will be either rich in Si or in C. The same is true for the ternary compound, we have to take a look on the vaporization behavior of the so called pseudo-binary compound SiO_2-SiC and on the mixtures of SiO_2 with Si rich or C rich SiC to complete the study.

2.6.1 Vaporization in the ternary compound Si-C-O

Figure 2.9 presents the ternary Si-C-O system at $T = 1700\,\mathrm{K}$ and $1\,\mathrm{bar}$ external applied pressure. The section of interest for our investigation is the connecting line between SiC and SiO_2, which is also known as a pseudo-binary section. Because we consider Si and C rich compositions, the compositions near this line are also included. Following we have to look on a band of compositions near this line.
The main vaporization reaction in the pseudobinary section, like already reported by Rocabois et al. [38], is

$$\mathrm{SiC(s)} + 2\mathrm{SiO_2(s)} = 3\mathrm{SiO(g)} + \mathrm{CO(s)} \qquad \text{with} \tag{2.15}$$

$$K_p(T) = \frac{p^3(\mathrm{SiO})\,p(\mathrm{CO})}{a(\mathrm{SiC})\,a^2(\mathrm{SiO_2})} \tag{2.16}$$

Looking at figure 2.9 and on equation 2.15 we see that the composition of the gaseous phase above the SiC-SiO_2 compositions range will contain SiO and CO gases as the main components. The presence of SiO_2 makes also possible the simultaneous reactions to produce CO_2 which is also usual to find.
We calculated the equilibrium partial pressures of different gaseous molecules characteristic for every condensed mixture of compounds SiC and SiO_2 included in their near-stoichiometric domain. Figures 2.10 and 2.11 show the logarithmic plots of these partial pressures as a function of the inverse of temperature respectively for Si rich and C rich compositions, i.e. three-phases Si-SiO_2-SiC and SiO_2-SiC-C domains respectively.
To determine partial pressures of SiO for the compounds rich in Si we used relation 2.17. From known $K_p(T)$ of the main vaporization reaction 2.16 we obtain the partial pressure of CO. Other gases characteristic for SiC rich in Si have the same values as already calculated and described for adjacent binary Si-C system in section 2.2 on the page 25.
For the compounds rich in C equation 2.19 was used to obtain the partial pressure of CO and proceeded further like for the Si rich compounds.

$$\mathrm{SiO_2(s)} + \mathrm{Si(s\ or\ l)} = 2\mathrm{SiO(g)} \qquad \text{with} \tag{2.17}$$

$$K_p(T) = \frac{p^2(\mathrm{SiO})}{a(\mathrm{Si})\,a(\mathrm{SiO_2})} \tag{2.18}$$

$$\mathrm{SiO_2} + 3\mathrm{C(s)} = 2\mathrm{CO(g)} + \mathrm{SiC(s)} \qquad \text{with} \tag{2.19}$$

$$K_p(T) = \frac{p^2(\mathrm{CO})}{a^3(\mathrm{C})\,a(\mathrm{SiO_2})} \tag{2.20}$$

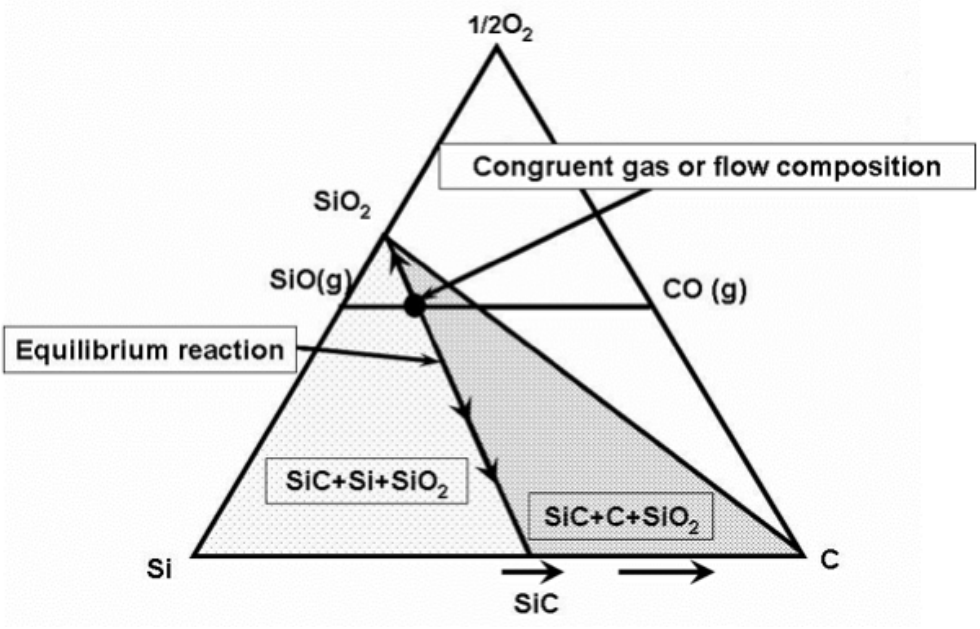

Figure 2.9: Isothermal cross section of the ternary diagram of Si-O-C at least up to 1700 K.

Figure 2.12 shows the partial pressures in the case of congruent vaporization of SiC and SiO_2 according to the relation 2.15. Here we used the condition from the Gibbs-Konovalow theorem [85] that for a fixed SiC/SiO_2 composition the pressure will be an extremum for a system which has an indifferent (azeotropic or congruent) state. So for the congruent composition of the pseudo-binary SiC-SiO_2 the total pressure must be:

$$p_{tot} = p(\mathrm{SiO}) + p(\mathrm{CO}). \tag{2.21}$$

Using 2.16:

$$p_{tot} = p(\mathrm{SiO}) + \frac{K_p}{p^3(\mathrm{SiO})} \tag{2.22}$$

And finally:

$$\frac{\mathrm{d}p_{tot}}{\mathrm{d}p(\mathrm{SiO})} = 1 - 3\frac{K_p}{p^4(\mathrm{SiO})} \tag{2.23}$$

with an extremum for

$$p(\mathrm{SiO}) = 3p(\mathrm{CO}) \tag{2.24}$$

Using this condition with (2.16) we obtain the azeotropic equilibrium partial pressures of SiO and CO for all compositions of SiO_2 and SiC located in the pseudo-binary section (SiO_2 and SiC connecting line) in the ternary Si-O-C diagram shown in figure 2.9.
When we consider vaporization of material under Knudsen conditions, i.e. vacuum, we have to look at the flow of different species rather than at their partial pressures. This means that the partial pressure ratio at the congruent state will be different as showed before. For congruent flow conditions we must consider:

$$\phi(\mathrm{SiO}) = 3\phi(\mathrm{CO}) \tag{2.25}$$

and using the Knudsen relation for flows:

$$p(\mathrm{SiO}) = 3\sqrt{\frac{M(\mathrm{SiO})}{M(\mathrm{CO})}}\, p(\mathrm{CO}) = 3,76\; p(\mathrm{CO}) \tag{2.26}$$

This relation shows that in the case of vaporization under vacuum the pressure ratio of SiO and CO is higher (= 3, 76) than for that under neutral gas atmosphere (= 3) for example Argon.
It is also possible to calculate the partial pressures of minor (compared to SiO and CO) gaseous species using different equilibria:

$$\mathrm{SiO_2 + Si(g)} = \mathrm{2SiO(g)} \qquad \text{with} \tag{2.27}$$

$$K_p = \frac{p^2(\mathrm{SiO})}{a(\mathrm{SiO_2}) \cdot p(\mathrm{Si})} \tag{2.28}$$

$$\mathrm{2Si(g)} = \mathrm{Si_2(g)} \qquad \text{with} \tag{2.29}$$

$$K_p = \frac{p(\mathrm{Si_2})}{p^2(\mathrm{Si})} \tag{2.30}$$

$$\mathrm{Si(g) + SiC(s)} = \mathrm{Si_2C(g)} \qquad \text{with} \tag{2.31}$$

$$K_p = \frac{p(\mathrm{Si_2C})}{p(\mathrm{Si}) \cdot a(\mathrm{SiC})} \tag{2.32}$$

$$\mathrm{3SiC(s) + CO(g)} = \mathrm{2SiC_2(g) + SiO(g)} \qquad \text{with} \tag{2.33}$$

$$K_p = \frac{p^2(\mathrm{SiC_2}) \cdot p(\mathrm{SiO})}{a^3(\mathrm{SiC}) \cdot p(\mathrm{CO})} \tag{2.34}$$

To obtain the partial pressure of CO_2 we considered the equation 2.36 for the congruent and Si rich compositions and equation 2.35 for the C rich composition.

$$\mathrm{SiO_2(s) + 2\,C(s)} = \mathrm{SiC(s) + CO_2(g)} \tag{2.35}$$

$$\mathrm{SiO_2(s) + SiC(s)} = \mathrm{Si(g) + CO_2(g)} \tag{2.36}$$

Table 2.2 lists the coefficients A and B for the decimal logarithmic plots as a function of the inverse of temperature for the different compositions domains analyzed above.

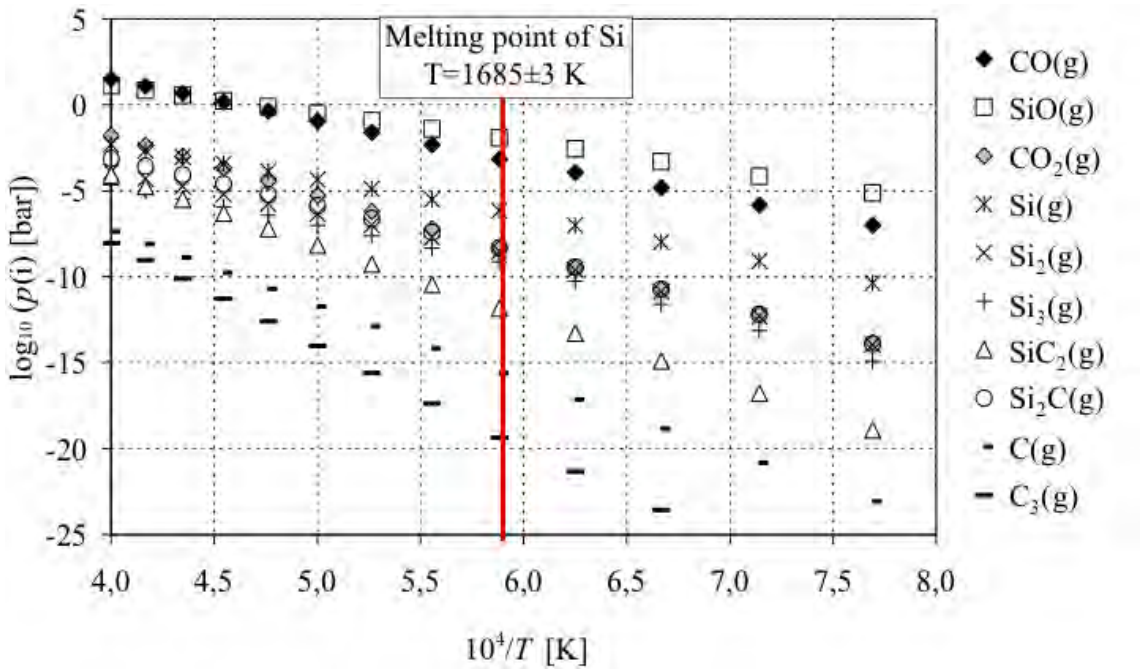

Figure 2.10: Decimal logarithmic plot of partial pressures in equilibrium with three-phases domain SiC-SiO_2-Si as a function of the inverse of temperature [K]. After melting point of Si at $T = 1685\,\mathrm{K}$ the slope of the curves changes.

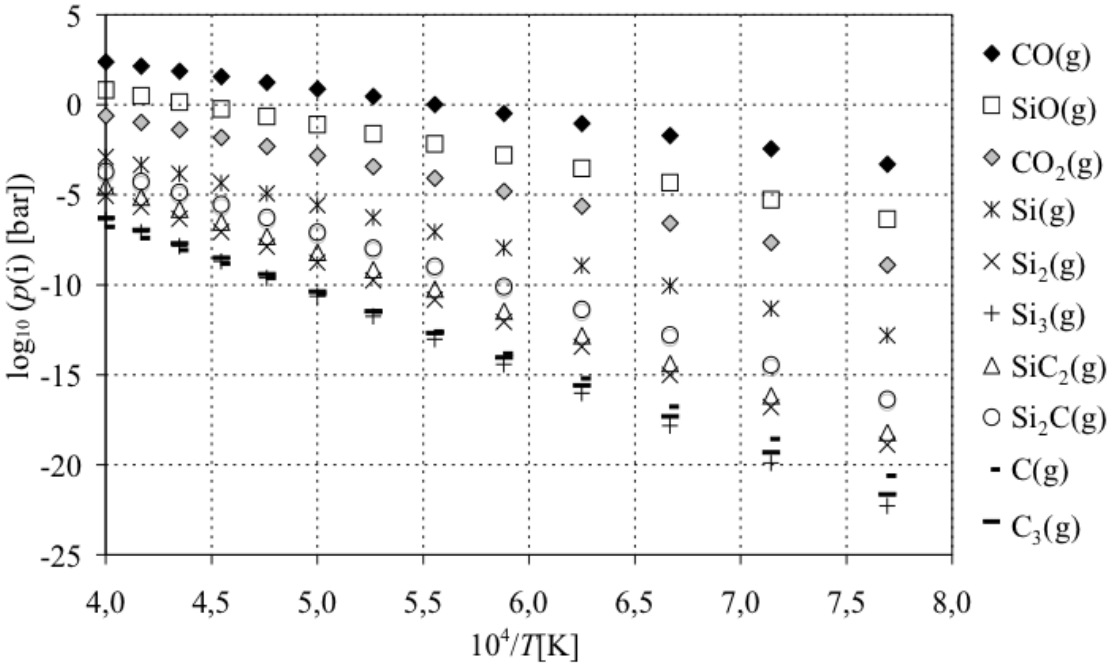

Figure 2.11: Decimal logarithmic plot of partial pressures in equilibrium with the three-phases domain SiC-SiO_2-C as a function of the inverse of temperature.

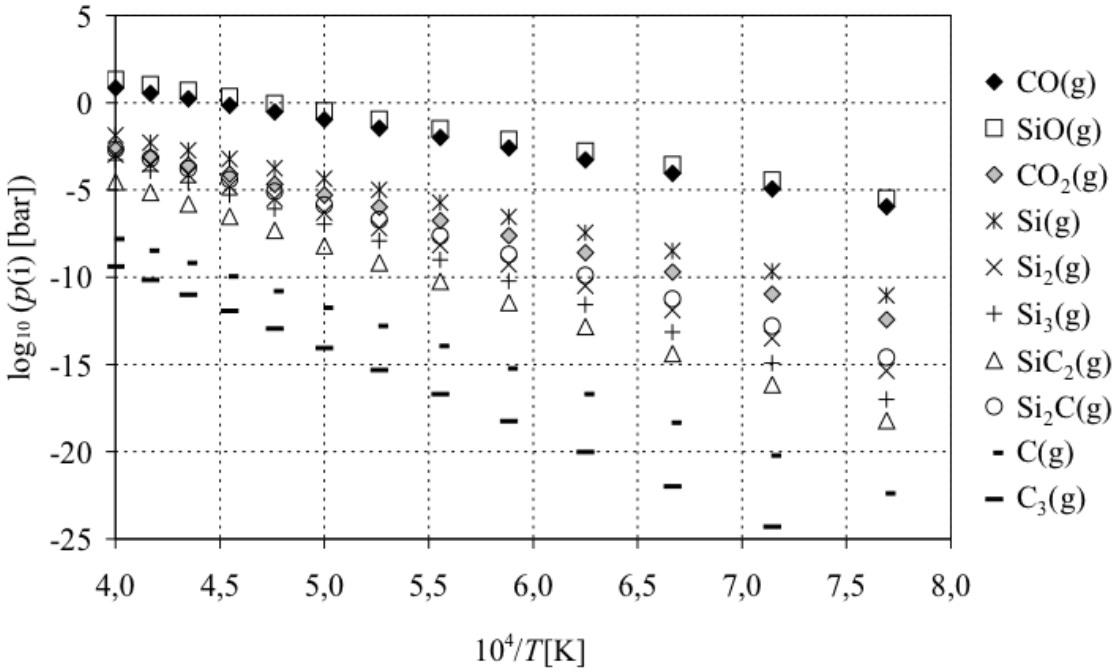

Figure 2.12: Decimal logarithmic plot of partial pressures for SiC-SiO_2 mixture for vaporization in the pseudo-binary section (congruent vaporization) as a function of the inverse of temperature.

Table 2.2: A and B coefficients for the decimal logarithmic plot of partial pressures (in bar) according to $\log p = \mathrm{A}\frac{10^4}{T} + \mathrm{B}$. For the compositions rich in Si after Si melting temperature at 1685 K the slope will change.

Mixture	**A**		**B**	
Si-SiC–SiO_2	$T < 1685\,\mathrm{K}$	$T > 1685\,\mathrm{K}$	$T < 1685\,\mathrm{K}$	$T > 1685\,\mathrm{K}$
SiO	-1,7535	-1,6234	8,3903	7,6191
CO	-2,1033	-2,4938	9,209	11,523
CO_2	-3,0137	-3,4913	9,3747	12,202
Si	-2,3117	-2,0514	7,4389	5,8965
Si_2	-2,9988	-2,4782	9,1334	6,0487
Si_3	-3,1838	-2,403	9,6291	5,0021
Si_2C	-3,0527	-2,7925	9,6261	8,0837
SiC_2	-3,8805	-4,1407	10,982	12,524
SiC-SiO_2 congruent				
SiO	-1,841		8,7143	
CO	-1,841		8,2372	
CO_2	-2,6395		7,9095	
Si	-2,4866		8,0868	
Si_2	-3,3486		10,429	
Si_3	-3,7086		11,573	
Si_2C	-3,2276		10,274	
SiC_2	-3,7055		10,334	
SiC–C-SiO_2				
SiO	-1,9403		8,5967	
CO	-1,543		8,5899	
CO_2	-2,2422		8,3798	
Si	-2,6852		7,8516	
Si_2	-3,7459		9,9589	
Si_3	-4,3044		10,867	
Si_2C	-3,4263		10,039	
SiC_2	-3,7055		10,334	

2.6.2 Composition evolution due to vaporization

The main question in calculating the erosion by vaporization of SiC compounds or their mixture, including additives of Si, C or SiO_2, is to identify those parts which can be attributed either to SiC or SiO_2 erosion. We have already shown for the binary system Si-C in the previous section that by calculation of the Si and C flows and considering some assumptions for the decomposition of the condensed phase we are able to estimate erosion of the condensed phase under conditions of equilibrium partial pressures of the gaseous species.
For the only pseudo-binary SiC-SiO_2, considering erosion according to congruent vaporization, the Si flow represents the erosion of SiC and of SiO_2 at the same time (see reaction 2.15). The origin of the C flow can be only the SiC compound. So the part of Si flow coming from SiC erosion must be equal to the C flow measured in mole per hour for the evaporating surface. The remaining Si-flow is attributed to the SiO_2 erosion.
For a SiC condensed phase rich in Si it is more difficult because the source of the Si evaporated flow can be SiO_2, SiC and Si in excess. The source of C flow can be only SiC, so the number of moles of vaporized C is equal to the erosion of SiC and to the number of Si moles which comes from SiC. The erosion of SiO_2 must be also equal to half of the oxygen flow which is also equal to the number of moles of Si that comes from SiO_2. Following, the remaining Si flow is due to erosion of excess Si.
Considering a condensed SiC phase rich in carbon, still with SiO_2 impurities (triphasic SiO_2-SiC-C), we cannot consider SiC as the only source of the C flow and following equal to its erosion. Furthermore as we used the reaction

$$SiO_2 + 3C(s) = 2CO(g) + SiC(s)$$

to calculate the CO partial pressure of the C rich compounds we see that in this case we do not erode SiC at all, but it is created detrimental to SiO_2 and free carbon. Like for the Si rich compound before, we consider that half of the oxygen flow is equal to the SiO_2 erosion. Following same quantity, i.e. moles number, of Si flow is attributed to SiO_2 erosion. The C flow is equal to the erosion/elimination of carbon in excess. More precisely, in the case of C rich compounds no SiC erosion can be observed as long as SiO_2 is present.
Figure 2.13 displays the different erosion flows due to vaporization described above. To facilitate the understanding they are displayed as decimal logarithms as a function of the inverse of temperature. This figure shows that for the congruent compositions of the pseudo-binary SiC-SiO_2, SiC like SiO_2 will be eroded continuously and uniformly when increasing temperature. The ratio of eliminated SiC and SiO_2 remains constant by increasing amount of eroded material.
In the Si rich compounds Si excess will be eroded until 1700 K at first with the same amount as SiO_2 according to reaction (2.27), above the Si_{Si} flow becomes lower than that coming from SiC and above 2000 K the Si excess would not be eroded at all. At the same time the erosion of SiC which was at the beginning lower than the erosion of Si and SiO_2 increases until it is the same as SiO_2 for 2000 to 2100 K and higher than SiO_2 above 2200 K.
For the C rich SiC-SiO_2 mixtures we observe a constant ratio of erosion for C and SiO_2 with a slightly higher erosion flow from the C in excess and no erosion of SiC. This behavior is due to the considered main chemical reaction in this section, but also during the experiments and for the manufacturing process of SiC, a SiC crystal growth is generally observed on carbon surfaces such as linings or furnace kiln in graphite.

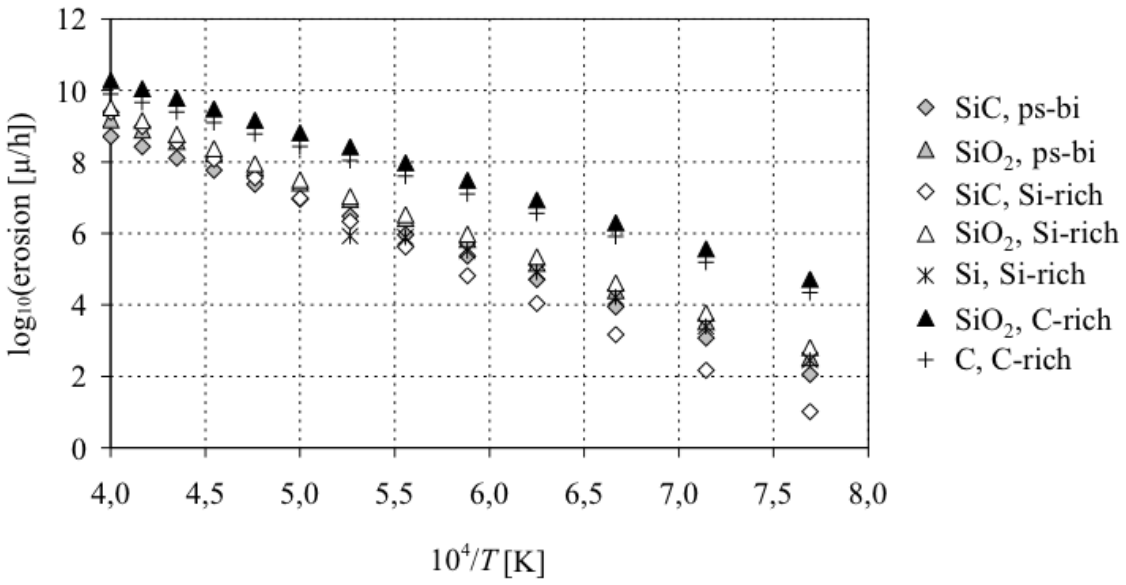

Figure 2.13: Decimal logarithmic plot of erosion flows of SiC, SiO_2, Si and C for the pseudo-binary (ps-bi), the Si rich and the C rich compounds of the three-phases Si-O-C system in micron of eroded material per hour as a function of the inverse of temperature.

The present described behavior shows that the impurities, such as Si or C in excess in SiC, are eliminated at first from the compounds as it was already shown experimentally by S. Baud et al. [58] using mass spectrometry.
It is not possible to calculate as for SiC binary the "time to change the stoechiometry" of SiC in contact with SiO_2. As long as SiO_2 is available no change in SiC stoechiometry takes place. When all SiO_2 is eliminated by vaporization the SiC behaves like binary Si-C with further C(s) precipitation [38].

Table 2.3: The coefficients A, B for the decimal logarithmic plot of the erosion flows ψ in the congruent pseudo-binary SiC-SiO_2 and in the Si-rich and C-rich three-phases domains as a function of the inverse of temperature, $\log \psi = \mathrm{A}\frac{10^4}{T} + \mathrm{B}$ with ψ measured in μm/h and T in Kelvin.

Compound eroded component	**A**	**B**
congruent		
SiO_2	-1,8025	16,4220
SiC	-1,8024	15,9610
Si-rich		
SiO_2	-1,7957	16,5720
SiC	-2,2893	18,4590
Si ($T < 1685\,\mathrm{K}$)	-1,6935	15,4910
Si ($1685\,\mathrm{K} < T < 2000\,\mathrm{K}$)	-0,6805	9,5640
C-rich		
SiO_2	-1,5066	16,345
SiC	no erosion	
C	-1,5044	15,9440

2.7 Oxidation of SiC

SiC, being a Si compound, is relatively stable in oxidizing atmospheres because of the formation of a SiO_2 layer on its surface. As reported, certain oxidative conditions are necessary to form this layer that corresponds to passive oxidation [42]. If these conditions are not established, this layer will be eliminated by vaporization of SiO(g) and CO(g) in vacuum at first. The SiC, presenting then "bare surface", will be eroded according to the main reaction:

$$SiC(s) + O_2(g) = SiO(g) + CO(g) \tag{2.37}$$

In this case the oxidation is called active. Note that according to reaction 2.37 the Si/C ratio of evaporating gases is equal to 1 (i.e. SiC composition). The transition point from passive to active oxidation is depending on the oxygen flow arriving at the surface and temperature.

2.7.1 Limits of active oxidation of SiC

Considering molecular regime or Knudsen effusion as the predominant vaporization process and elementary reactions between the solid components for gases creation, we can calculate the limits of oxygen partial pressure at the reacting surface. The reacting surface in our case is pure SiC, which can precipitate either carbon or begin to form a SiO_2-film. We are looking for the limits of oxygen partial pressure at the SiC surface, which allows to keep the surface of SiC "clean", i.e. without any precipitation. Following we have to consider two transition limits.

For the calculation of oxygen partial pressure at the limit of carbon precipitation we calculate first the silicon activity corresponding to carbon activity = 1 at the phase limit SiC-C. By varying $p(O_2)$ at the surface the flows ratio of Si and C is compared until to be equal to 1. Beginning from the maximum $p(O_2)$ which corresponds to three-phases domain SiO_2-SiC-C this ratio is checked. For this three phases system it is < 1. The $p(O_2)$ value is then decreased until the ratio $\frac{\phi(Si)}{\phi(C)} = 1$ is found. We proceed this calculation for each temperature in the concerning temperature range.

The congruent vaporization of SiC-SiO_2 is a particular case of SiC/SiO_2 interface reaction with consumption of SiO_2 and SiC. The partial pressures ratio of SiO(g) to CO(g) is equal to 3 or 3,76 according to the main vaporization reaction 2.15. We must emphasize that the calculation of congruent vaporization corresponds to vaporization under vacuum and does not consider any diffusion phenomena, either in gas or in solid phases. From experiments it is known that diffusion cuts down the vaporization and following modifies the SiO(g)/CO(g) ratio. The congruent vaporization in fact corresponds to a particular chemical state of the interface SiC/SiO_2 and does not necessary correspond to the other limits described above, that is the onset of SiO_2 precipitation. This limit is located at different $p(O_2)$ and a(Si) since the chemical conditions when starting from a bare SiC surface are different for the interface SiO_2-SiC.

Trying to find the limit of SiO_2 precipitation we made an attempt starting at very low $p(O_2)$ which corresponds to the limit SiC-C and with different a(Si) corresponding to SiC existence. Increasing oxygen pressure and looking for $p(O_2)$ which would produce SiO/CO=1 according to:

$$SiC(s) + O_2(g) = SiO(g) + CO(g) \qquad \text{with} \qquad K_p = p(SiO) \cdot p(CO).$$

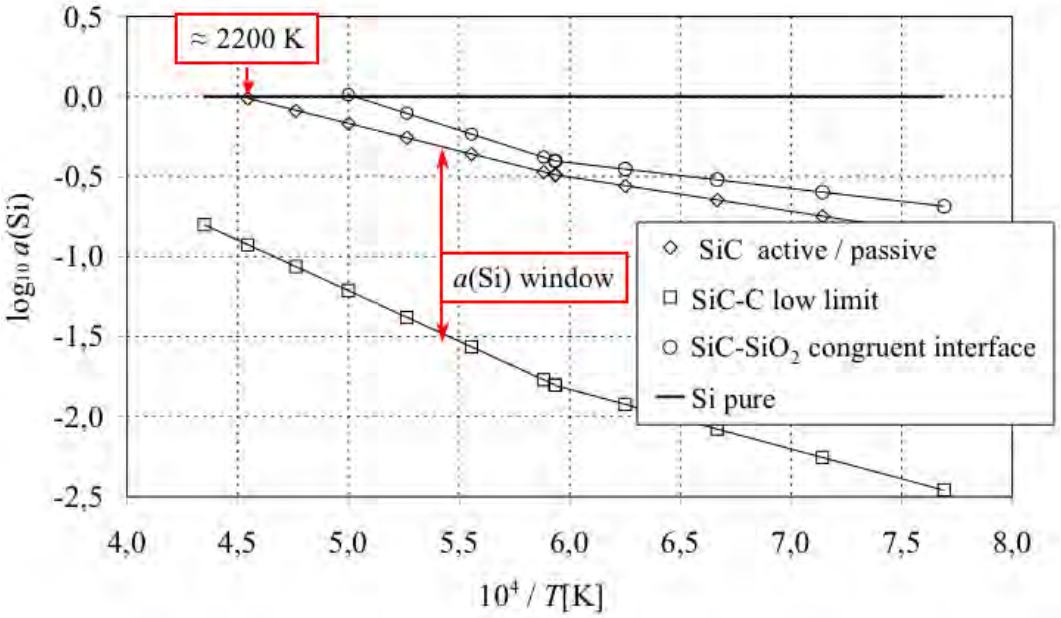

Figure 2.14: Decimal logarithm of silicon activity limit for the active oxidation of SiC-C (without carbon precipitation) as a function of the inverse of temperature compared to the silicon activity limit for active to passive transition and for congruent vaporization.

For a(Si) close to 1 we could not find any solution because at the limit to Si and SiO_2 creation (three-phases Si-SiO_2-SiC) the SiO(g) partial pressure is always much higher than p(CO) [38].
The solution was found beginning at the opposite limit for a(Si) step by step and looking for the maximum $p(O_2)$ corresponding to SiO_2 on SiC formation:

$$\mathrm{Si(s,s)} + \mathrm{O_2} = \mathrm{SiO_2(s)} \qquad \text{with} \qquad K_p = \frac{a(\mathrm{SiO_2})}{p(\mathrm{O_2}) \cdot a(\mathrm{Si})}$$

The SiO_2 activity is 1. The $p(O_2)$ is depending on the silicon activity which is then $\leqslant 1$ in the SiC. This oxygen pressure is the active oxidation limit at the silica layer creation for certain silicon activity. For each a(Si), from 1 to minimum at SiC-C, at constant temperature we look for an oxygen partial pressure which corresponds to $\phi(Si)/\phi(C) = 1$. For the phase limit Si-SiC (a(Si) = 1) this ratio is always > 1. It decreases as a function of a(Si). As soon as $\phi(Si)/\phi(C) = 1$ for a certain a(Si) we obtain the condition of active oxidation we are looking for. Furthermore we have found at the same time the silicon activity and oxygen pressure which correspond to creation of SiO_2 because the oxygen pressure is calculated from a(Si).
Figure 2.14 displays the active oxidation "window" of SiC in terms of silicon activity as a function of the inverse of temperature. We can see the reference change, solid-liquid, at the Si melting. This window shows that in the SiC existence range only a certain SiC composition range can support active oxidation. With increasing temperature pure silicon is produced at 2200 K. This Si(liq) can also be oxidized in active manner with SiO(g) evaporation or passive manner creating a SiO_2 layer. This domain is interesting for silicon

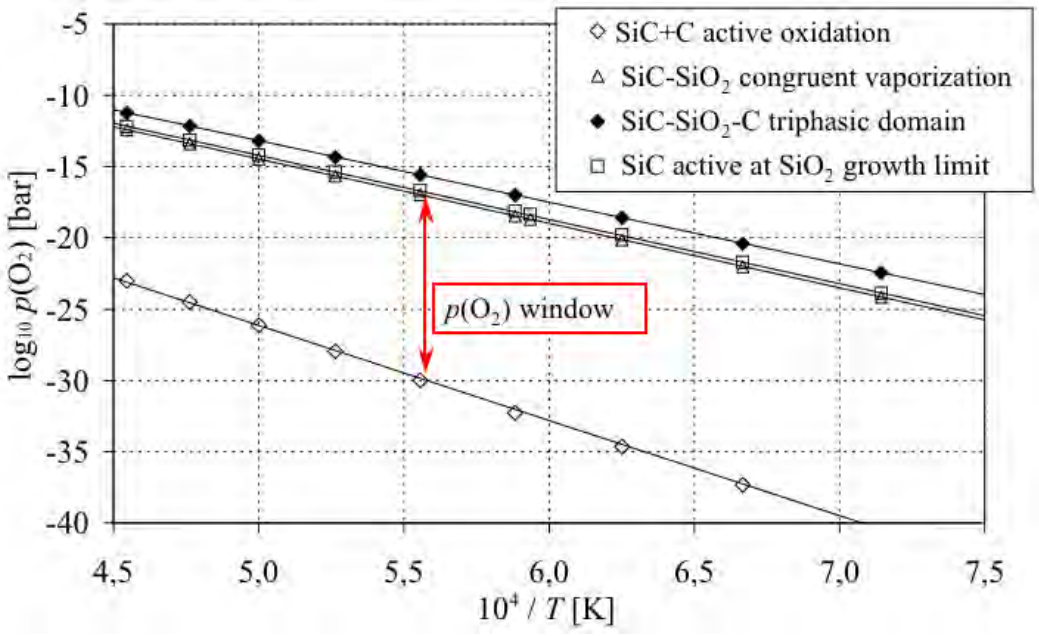

Figure 2.15: Decimal logarithm of oxygen partial pressure limit for the active oxidation of SiC-C (without carbon precipitation) as a function of the inverse of temperature compared to the oxygen partial pressure limit for active to passive oxidation and for congruent reaction. All pressures are SiC surface pressures.

production. In SiC manufacturing, this domain can be reached either using too high O_2 background pressure or with remaining excess of SiO_2.
Figure 2.15 displays the SiC active oxidation "window" in terms of surface oxygen pressure as a function of the inverse of temperature. The high oxygen pressure limit is slightly different from the values for congruent evaporation. The oxygen partial pressure at SiC surface must be slightly higher than at the SiC-SiO_2 congruent interface because the relation imposed to the Si-C-O system at variance equal 1 to become 0 is not the same: relation 2.24 for congruent vaporization and $p(\mathrm{SiO}) = p(\mathrm{CO})$ according to relation 2.37 for active oxidation.
Concluding, the upper limit represents active-passive transition and is different from the condition of congruent vaporization. During de-oxidation the oxygen pressure and silicon activity correspond to congruent vaporization of the SiC-SiO_2 interface and we obtain the passive to active transition. In the opposite with increasing surface oxygen pressure (external addition of oxygen) this transition moves to the limit of SiO_2 formation with slightly higher oxygen pressure and lower silicon activity. Independently of the experimental and characterization parameters, the observed transition does correspond to an oxygen range values domain rather than to a fixed line when oxidizing or de-oxidizing.

2.7.2 SiC composition under active oxidation

Contrarily to the binary Si-C and ternary Si-C-O, the composition of solid phase does not change when exposed to surface oxygen partial pressure value within the shown limits in the figure 2.15 because $\frac{\phi(Si)}{\phi(C)} = 1$. It vaporizes SiO(g), CO(g), Si(g), Si_2C(g), SiC_2(g) etc.

with partial pressures as calculated for active oxidation in the oxygen pressure or silicon activity windows as defined in fig.2.14 and 2.15.
The A and B coefficients for decimal logarithmic plots of these partial pressures are displayed in table 2.4. It was observed that even at the carbon rich limit the plots of partial pressures change their slopes for temperatures higher than the silicon melting temperature, 1685 K (change of reference state for pure Si).

Table 2.4: A and B coefficients for the decimal logarithmic plot of partial pressures according to $\log p = \mathrm{A}\frac{10^4}{T} + \mathrm{B}$ during active oxidation of SiC. With Si melting temperature at 1685 K the slope will change.

Limit	**A**		**B**	
SiC–SiO_2	$T < 1685\,\mathrm{K}$	$T > 1685\,\mathrm{K}$	$T < 1685\,\mathrm{K}$	$T > 1685\,\mathrm{K}$
SiO	-1,8359	-1,8979	8,5323	8,9016
CO	-1,8359	-1,9090	8,4342	8,8647
CO_2	-2,6552	-2,6663	8,3707	8,4319
Si	-2,4512	-2,5752	7,5918	8,3303
Si_2C	-3,1238	-3,5068	7,9985	10,2750
SiC_2	-3,6004	-3,9946	9,6138	11,9520
SiC-C				
SiO	-2,9363	-3,4220	6,6359	9,5122
CO	-2,6143	-2,8466	7,2506	8,6295
CO_2	-4,3701	-4,8348	5,6268	8,3844
Si	-2,6150	-2,8684	7,2557	8,7532
Si_2C	-3,2932	-3,8001	7,7028	10,698
SiC_2	-3,4478	-3,7013	10,0310	11,5290

With the flows of Si and C coming from different gaseous species we calculate the SiC erosion for each limit of oxidation. Figure 2.16 displays this. As we can see the SiC loses much less matter close to carbon precipitation limit than near the passive oxidation transition.

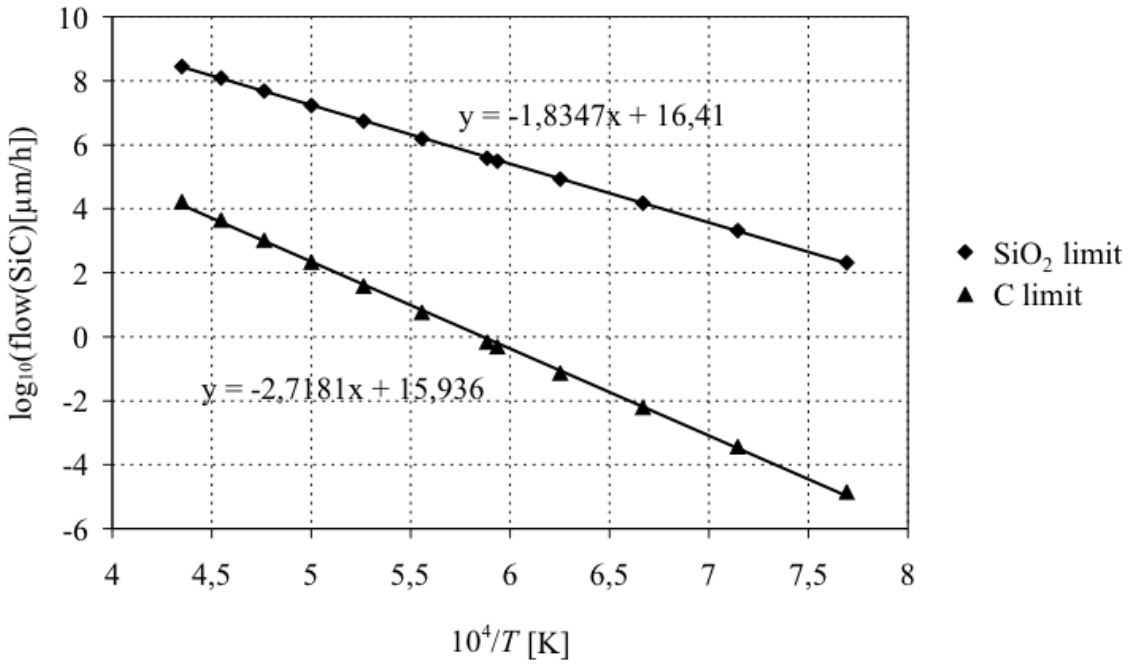

Figure 2.16: Erosion rate of SiC in μm/h as function of the inverse of temperature for the two limits of active oxidation: transition to passive oxidation with SiO_2 precipitation (SiO_2 limit) and beginning of carbon precipitation due to matter loss (C limit).

2.8 SiC erosion and deposition

2.8.1 SiC erosion

Summarizing the results from flow calculation we can compare the total flows of Si and C coming from the only $SiC_{1\pm x}$ or from SiC-SiO_2 due to vaporization at equilibrium conditions to the SiC departure as a result of active oxidation.
Figure 2.17 displays the SiC erosion flows as decimal logarithms as a function of the inverse of temperature. We can separate two groups of erosion rates with a factor of 10^4 - 10^8 difference between them. The SiC erosion rates of two-phases Si-SiC and SiC-C at equilibrium conditions and active oxidation of SiC at oxygen pressure close to carbon creation limit are close and are much lower compared to the other three. The SiC erosion rates for the congruent pseudo-binary SiC-SiO_2 and for the Si-SiC-SiO_2 triphasic compositions are similar to the erosion rate of SiC due to active oxidation with the oxygen pressures close to SiO_2 creation limit. For the later the erosion rate is maximal.
Table 2.5 summarizes the A and B coefficients of decimal logarithmic plots of calculated SiC erosion rates according to $\log \psi = \mathrm{A}\frac{10^4}{T} + \mathrm{B}$ approximation.
In the case of mixtures with SiO_2 the vaporization takes place in presence of silica which serves as an oxygen supply for the system. The presence of this silica protects the SiC from oxygen attack and following the erosion rate is lower than with bare SiC surface exposed to oxygen.

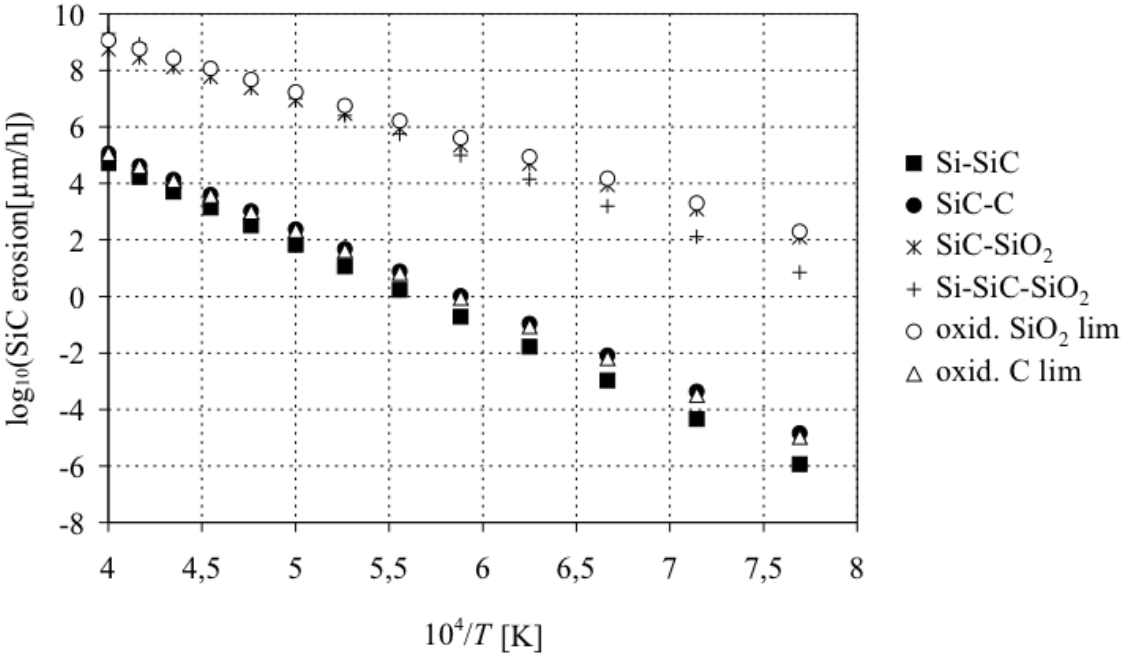

Figure 2.17: Decimal logarithms of SiC erosion rates, for the congruent pseudo-binary (SiC-SiO_2), for SiC+SiO_2 with Si excess (Si-SiC-SiO_2) compositions, for the SiC erosion due to active oxidation at the limit of SiO_2(oxid. SiO_2 lim) and C (oxid. C lim) creation. The Si rich and C rich SiC erosion are displayed. All values are in μm of SiC per hour.

Table 2.5: The coefficients A, B for the decimal logarithmic plot of the SiC erosion rates for the pseudo-binary congruent and Si-rich compounds, for two phases SiC Si- and C-rich compounds, compared to the SiC erosion with active oxidation under calculated oxygen pressure limits for C creation limit and SiO_2 creation limit as a function of the inverse of temperature: $\log \psi = \mathrm{A}\frac{10^4}{T} + \mathrm{B}$ with ψ in μm/h and temperature in Kelvin.

Compound	**A**	**B**
active oxidation:		
SiO_2-limit	-1,8347	16,4100
C-limit	-2,7181	15,936
diphasic:		
Si-rich	-2,8821	16,242
C-rich	-2,6807	15,791
pseudo-binary:		
congruent	-1,8024	15,961
Si-rich	-2,2893	18,459
C-rich	no erosion	

For the other side, at the limit of creation of carbon, two facts can be quoted. First, the erosion rate of SiC is generally lower than at SiO_2 limit, already because the oxygen pressure is much lower. Second, it is close to SiC erosion due to the equilibrium vaporization of SiC-C. The relative lowest erosion rate for the Si rich SiC compared to other compounds displayed in figure 2.17, is due to the saturation of gaseous phase in Si gas which competes with the erosion of SiC untill the elimination of Si in excess.

2.8.2 SiC deposition

We have calculated in the previous part the evaporated Si- and C-flows from the SiC and obtained general erosion rates during the vaporization experiment. We didn't pay attention to the fact that some of these flows can recombine on the surface of solid SiC to new SiC crystals.

Assuming that the gaseous species, which contains oxygen, do not recombine to solid SiC reacting with each other under mentioned conditions, only the Si- and C-flows from oxygen free gaseous species, such as Si(g), SiC_2(g), Si_2C(g) etc. are able to be re-precipitated as SiC. Minimum SiC precipitation is coming from the reaction of silicon with carbon in the gaseous phase. It is equal to the carbon flow resulting from: Si_2C, SiC_2, SiC, C and C_3.

Furthermore, due to the known Si-excess in the gaseous phase, different reactions can produce SiC(s) as for instance the main one:

$$2\mathrm{Si(g)} + \mathrm{CO(g)} \rightarrow \mathrm{SiC(s)} + \mathrm{SiO(g)} \tag{2.38}$$

Following 1/2 of Si-flow, which did not react with carbon in gaseous phase, is considered to be consumed for SiC deposition due to the CO(g)-pressure as a background component of the carrier gas. The SiC resulting from this reaction together with SiC resulting from reaction with carbon gaseous flow is the maximum possible precipitation of SiC.

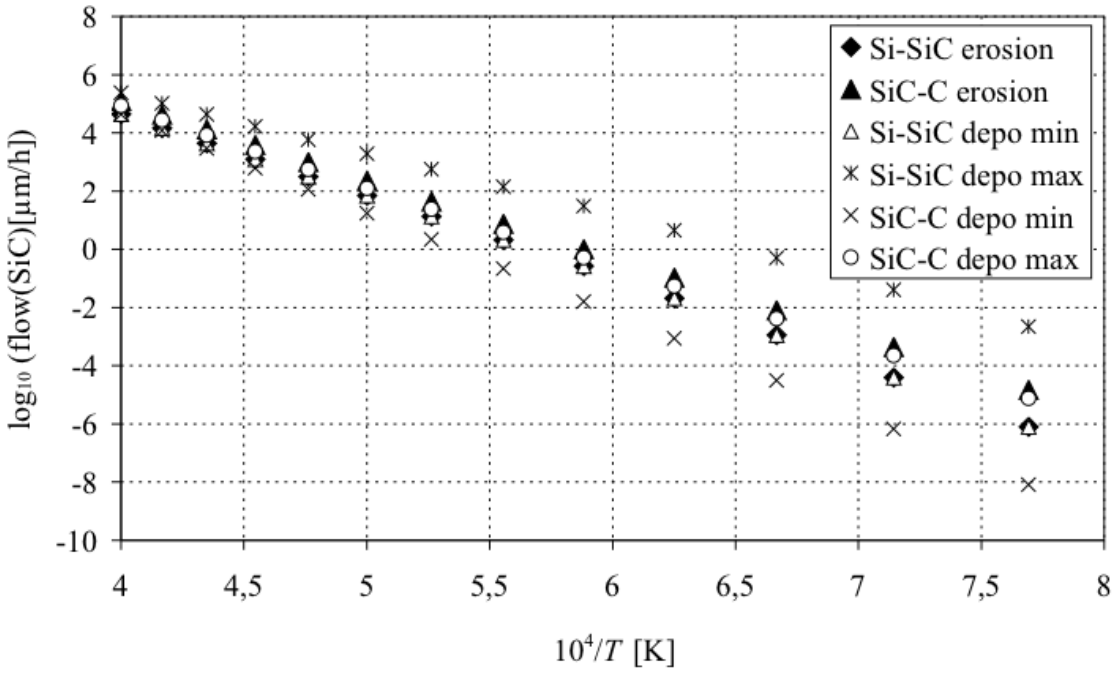

Figure 2.18: Decimal logarithms of SiC deposition rate in the diphasic Si-SiC and SiC-C in comparison to SiC erosion rate. All values are in μm of SiC per hour. For the maximum possible depositions a presence of CO(g) is indispensable.

Figure 2.18 displays the possible SiC deposition rates from the Si and C flows of diphasic SiC compounds. Additionally the SiC erosion flows for the same Si-C system are displayed. For the diphasic composition Si-SiC the minimum SiC deposition amount is strictly equal to its erosion, since the same set of gaseous species (Si_2C, SiC_2, SiC, C...) participates in the two flows based on C and the excess of silicon is coming from the pure Si phase. For the diphasic SiC-C, the erosion flow is larger than the deposition flow, since the excess of silicon in the vapor phase comes from SiC (erosion of SiC). The gain to obtain the maximum flows for the two diphasics is mainly related to Si(g) pressures which are predominant (our calculations of flows take into account the total Si excess) and maximum for Si rich compositions. The deposition yield when using CO(g) background pressure vary from 100 to 10 times when temperature increases. As the partial pressure differences decrease with temperature, all conditions for deposition merge to the quite same values at 2500 K, values which are as large as 10^5 μm/h.
Figure 2.19 displays the possible SiC deposition of the pseudo-binary composition mixtures. All SiC deposition flows are lower than the erosion rates in the pseudo-binary displayed in figure 2.17, except for C rich composition, where no SiC erosion could be found. The order for the SiC deposition of different pseudo-binary compositions is following: the highest for Si-rich compositions following by congruent compositions and minimal for C rich compositions. The SiC deposition for Si-rich and congruent composition are close to each other. As it was quoted for the diphasic compositions all values tend finally to 10^5 μm/h at 2500 K.
Figure 2.20 displays the maximum and minimum possible SiC deposition in the SiC under active oxidation with certain oxygen pressures. Comparing to the SiC erosion rate for the active oxidation displayed in figure 2.17 the possible SiC deposition rates are lower than

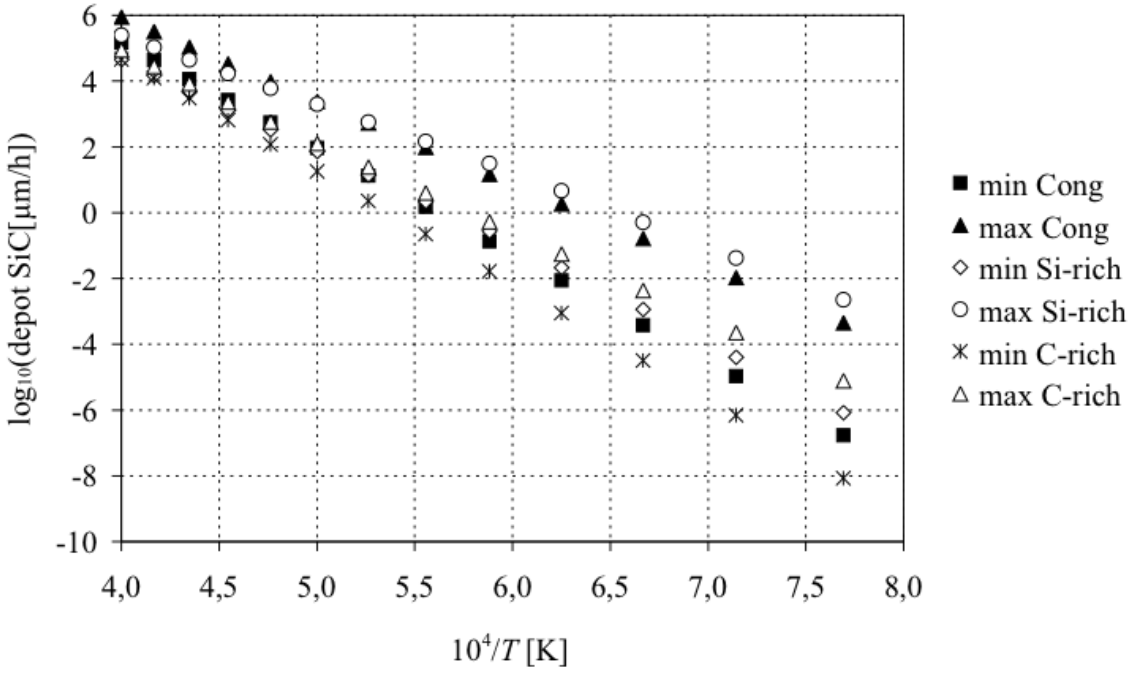

Figure 2.19: Decimal logarithms of SiC deposition rates of the congruent pseudo-binary, SiC-SiO_2 with Si excess (Si-SiC-SiO_2) and with C excess (SiC-C-SiO_2). All values are in μm of SiC per hour.

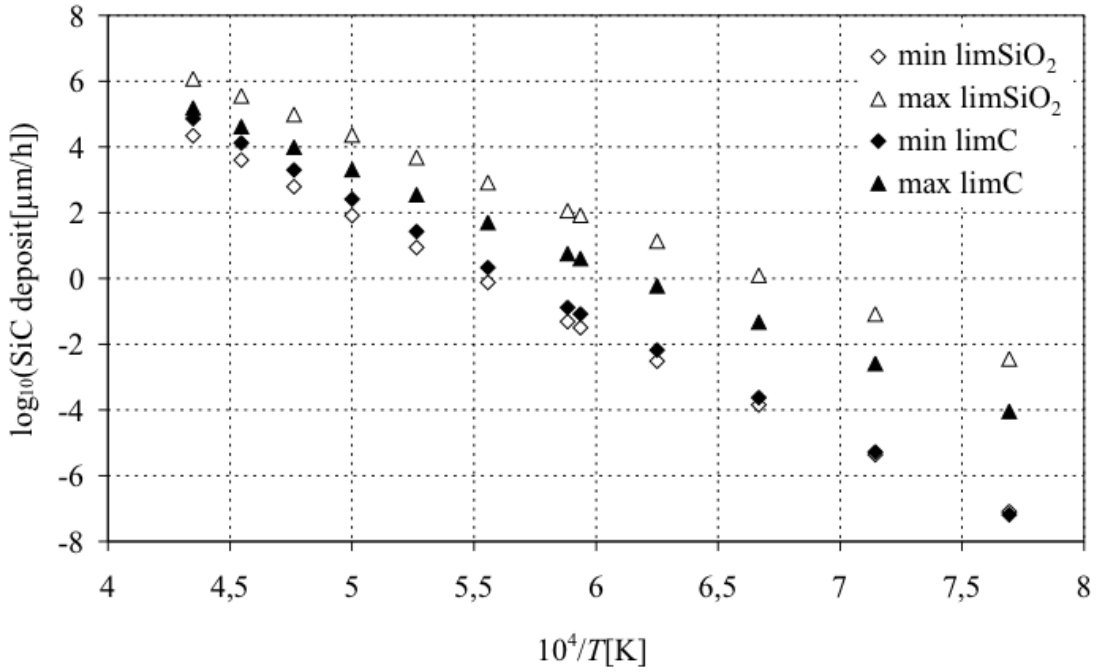

Figure 2.20: Decimal logarithms of SiC deposition during active oxidation at the limits of SiO_2 and C creation. All values are in μm of SiC per hour.

the SiC erosion rate at SiO_2 creation limit, but higher than the erosion rate at C creation limit. The maximum and minimum SiC deposition rates at C creation limit are included in the maximum and minimum deposition for SiO_2 creation limit. The tendency is also here towards the same value at high temperature, but higher than $10^5\,\mu$m/h like for the equilibrium vaporization.

Table 2.6 lists the obtained A and B coefficients of decimal logarithmic plots approximation according to $\log\psi = \mathrm{A}\frac{10^4}{T} + \mathrm{B}$ of the SiC deposition rates for different solid compositions.

Table 2.6: The coefficients A, B for the decimal logarithmic plot of the possible SiC deposition flows for the three-phases SiC-SiO_2 compounds, for two phases SiC compounds, and possible SiC deposition under calculated oxygen pressure limits for active oxidation at C creation limit and SiO_2 creation limit as a function of the inverse of temperature: $\log\psi = \mathrm{A}\frac{10^4}{T} + \mathrm{B}$ with ψ in μm/h and temperature in Kelvin.

Compound		**A**	**B**
diphasic:			
Si-SiC	max	-2,1566	14,0550
	min	-2,8821	16,2420
SiC-C	max	-2,7124	15,702
	min	-3,4465	18,462
pseudo-binary:			
congruent	max	-2,5099	15,9540
	min	-3,2311	18,1180
Si-SiC-SiO_2	max	-2,1566	14,0680
	min	-2,8821	16,2550
SiC-C-SiO_2	max	-2,7124	157150
	min	-3,4465	18,4750
active oxidation:			
SiO_2-limit	max	-2,5531	17,1370
	min	-3,4318	19,0720
C-limit	max	-2,7680	17,1450
	min	-3,6112	20,4670

Generally the SiC deposition rates in all analyzed compositions and under different conditions are in the same ranges, but the limits are included within a factor 10^4 to 10^2 from low to high temperature. Only the deposition rate in pure SiC phase during active oxidation at temperatures higher than 1800 K becomes a factor 10 higher. Furthermore for the different cases the composition rich in Si is always the one which produces maximum SiC deposition and for active oxidation it is at the SiO_2 creation limit oxygen pressure. Despite, only for the diphasic Si-SiC, for the C rich pseudo-binary composition and for active oxidation at oxygen pressure at C creation limit, the SiC erosion rate is lower than the SiC deposition rate. Following only when a certain composition attains one of the compositions just mentioned above due to material loss by vaporization, the SiC deposit dominates the SiC erosion.

2.9 Conclusion

We described the vaporization behavior of Si-C and Si-O-C systems. We observed that for the Si-C system increasing in temperature vaporization conditions involve always Si loss whatever is the SiC compound, silicon rich or carbon rich. It follows that SiC at high temperature under vaporization conditions turns in carbon rich composition then carbon precipitates at rate of Si loss and finally tends to become pure carbon. Evaluation of vaporization rates on thermodynamic basis, compared to reasonable estimates of the stoichiometric composition range of the compound SiC, shows that the precipitation of C becomes very important and rapid with temperature increase as soon as attaining 1500 K (several μm/h). In any manufacturing process, the present calculated times show that it is impossible to prevent carbon precipitation when applying any physical parameter, as for instance the total pressure applied to the system, neutral gas use or working in a strictly closed vessel.

Ternary system Si-O-C behaves differently because of formation of SiO and CO gaseous species as by far the main species. In this case the precipitation of carbon is not possible due to CO(g) formation. Partial pressures of oxygen-free species (Si, Si_2, $Si_2C\ldots$) behave the same as for the binary Si-C system as long as no solid solutions are known between different compounds. It was shown that the partial pressure of single species is different for the Knudsen flow conditions (vacuum) and for the flows under inert gas atmosphere because in one case we have to take into account the flow compositions and in other case the molar fractions in the gaseous phase. For our study the Knudsen flow conditions corresponding to vacuum conditions were used for the most of the calculations in order to further help in the understanding of Knudsen cell mass spectrometric experiment results.

Making equilibrium assumptions for these flows of different components, Si, C, O, we could calculate and distinguish the origin of the erosion (vaporization) flows for SiC or SiO_2. The original powder mixtures being very often enriched with Si, or C like impurities, these flows show the quasi-immediate possibilities of purification in the early stage of the heat treatment. Moreover, the departure of oxygen (from silica) is calculated and the evolution of the system at that time would be towards pure SiC (within its stoichiometric domain) as a stage before going to SiC-C precipitation.

We could see that if we impose a certain oxygen pressure we can control the precipitation of SiO_2 or carbon at the surface of SiC. The optimal oxygen partial pressure limits were calculated under which the homogenous erosion of SiC would be achieved at different temperatures. We defined a “window” in terms of oxygen partial pressures at the SiC surface in relation with silicon activity in the SiC compound for the so-called “active oxidation” of SiC. This kind of “window ” becomes smaller at higher temperatures and the limit to the SiO_2 precipitation tends to be closer to the oxygen partial pressure for the case of congruent reaction of SiC with SiO_2. The present existence of a window in oxygen partial pressure is related to a “clean” or bare SiC surface that may be an important condition for the SiC crystal growth. Calculations of the present window show that only part of the stoichiometric SiC composition domain can be reached for these conditions.

Figure 2.21 summarizes presented analysis of the SiC oxidation by enlarging the area of SiC stoichiometric domain. We showed with calculations of erosion of SiC that there is a certain interval where the active oxidation takes place. Because the calculations were performed using the silicon activity as basic parameter we took it also as basic parameter for this summarizing figure. Beginning by silicon activity equal to 1, which corresponds to

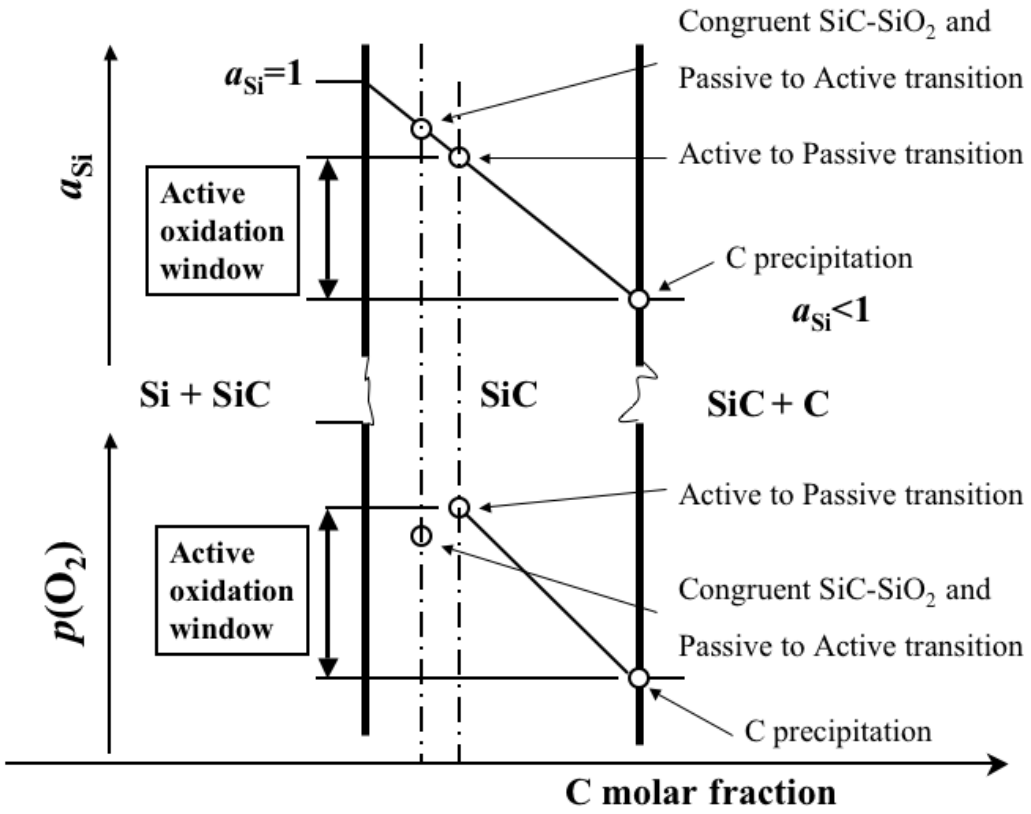

Figure 2.21: Isothermal SiC active oxidation range depending on the local surface oxygen pressure or silicon activity as a result of our calculations.

the silicon rich SiC compound, and following the diagonal line in the SiC stoichiometric domain, we arrive at the point of silicon activity for the congruent vaporization reaction of the SiC-SiO_2 pseudo-binary, built because of previous oxidation of SiC. Further two points correspond to the transition points between active to passive oxidation, depending on the oxidation reaction (first SiO_2 crystals forming) or reduction (last crystals remaining). Then at decreasing silicon activity, we are in the domain where the surface of SiC is free of SiO_2, i.e. the domain of active oxidation. This area corresponds to a range of very low oxygen pressures. The limit of low silicon activity and carbon apparition builds the end of this active oxidation domain and of the stoichiometric domain of SiC. The presented calculations will help to explain some experimental results achieved while measuring the partial pressures in SMHT and with a new reactor furnace fitted with capillary sampling and a mass spectrometer.

3 Experimental study of vaporization phenomena of Si-C and Si-C-O systems

In the first part we describe the experimental devices and choice of characterization methods. This description shows the measurement methods and make clear the difficulties of obtaining clear results. The second part lists the experiments performed in the high temperature mass spectrometer (HTMS) coupled with multiple Knudsen cell device with sample choice and parameters like temperature and material of the sample containers. The characterization results are also described. The same structure is kept for the third part which describes and discusses the results from the experiments with the capillary sampling quadrupole mass spectrometer.

3.1 Experimental instrumentation and characterization methods

The study of SiC powders was performed with vaporization analysis methods using mass spectrometry coupled with Knudsen effusion cell or capillary sampling.

High Temperature Mass Spectrometer helps to identify single components of a gaseous phase built by a sample as an effect of high vacuum and increasing temperature in a Knudsen cell. Furthermore calibrations can be performed and partial pressures can be determined. It is a unique device for thermodynamic measurements.

Quadrupole Mass Spectrometer with capillary sampling measures continuously the ionic intensities produced from single components of non-condensable gaseous phase built by a heated sample. Here a high vacuum can be applied or a protective gas atmosphere on the sample since higher pressures can be monitored than in HTMS.

After the heat treatment during which the gaseous phase characterization was performed, the samples were analyzed applying Raman spectroscopy, grain size measurement and imaging with SEM. This kind of approach allows to obtain informations about the changes in the solid phase caused by rising temperature and mass losses. We looked mainly for correlations between the obtained structures and the analyzed gaseous phase.

The Raman spectroscopy measurements were performed to show structural changes like grain to grain connections formation by the level of fluorescence. The polytypes that compose the sample could also be detected. The grain size measurements have to show the size changes of the powder grains, particularly changes in the fraction compositions of the samples composed of powders with different grain sizes. With the SEM/FEG changes were observed by imaging and local analyses with ECS device were made. Explanations of these observations are made as a function of the gaseous phase evolution as observed with High Temperature Mass Spectrometer and with capillary sampling Mass Spectrometer.

3.1.1 High Temperature Mass Spectrometer (HTMS) coupled with Knudsen effusion cells

The coupling of a Knudsen effusion cell with a mass spectrometer is the only method that allows direct observations of partial pressures, i.e. vapors in the high temperature vaporization processes.

3.1.1.1 Measurement principle with HTMS

A thermo-chemical reactor which provides the mass spectrometer with a characteristic molecular beam, includes a furnace with an effusion cell, effusing under vacuum, also called Knudsen cell. This cell is a source of a molecular beam that is then collimated by two apertures before introduction in the ionization chamber. After ionization of the selected beam of molecules by a perpendicular crossing electron beam the obtained ion beam is focused in view of mass analyzer. The simplest process of ionization is adiabatic and is described by :

$$A + e^- \rightarrow A^+ + 2e^-$$

or

$$AB + e^- \rightarrow AB^+ + 2e^-$$

The formed ions are separated according to their mass to charge ratio by a magnetic prism, a high frequency electric field or according to their time of flight in a long vacuum tube. The detection is performed by a Faraday cup or by a secondary electron multiplier which can be monitored by analogue or digital mode, i.e. pulse counting.
The identification of the gaseous molecules is made from the mass of collected ions, their isotopic abundance, ionization potential and variation of ionization efficiency which is a function of the electrons ionization energy.
Between the effusion orifice and an ion source is located a movable shutter. It serves to separate the same molecules or molecules with non resolved similar mass to charge ratio coming either from the collimated molecular beam or residual atmosphere in the source housing chamber.
The partial pressures p_i can be derived from measured ionic intensities I_i^+ according to the relation [86, 87]:

$$p_i = \frac{I_i^+ \, T}{S_i} \tag{3.1}$$

where T and S_i are the temperature of the cell and the sensitivity of the mass spectrometer for the species i respectively. This sensitivity can be written as:

$$S_i = I_e^- \cdot G \cdot \eta_i \cdot \sigma_i(E) \cdot \gamma_i \cdot f_i \tag{3.2}$$

relation in which:

η_i	transmission of the spectrometer
$\sigma_i(E)$	effective ionization cross-section at ionization energy E
γ_i	detection yield
f_i	isotopic abundance
I_e^-	intensity of the ionization electron beam
G	geometric factor independent of analyzed species

The calibration is made always experimentally because it is not possible to evaluate in advance certain of these factors. The product $I_e^- \cdot G \cdot \eta_i$ in this relation can be maintained constant for all species during one experiment depending on the kind of mass spectrometer. Figure 3.1 shows schematics of the spectrometer used for the present experiments.

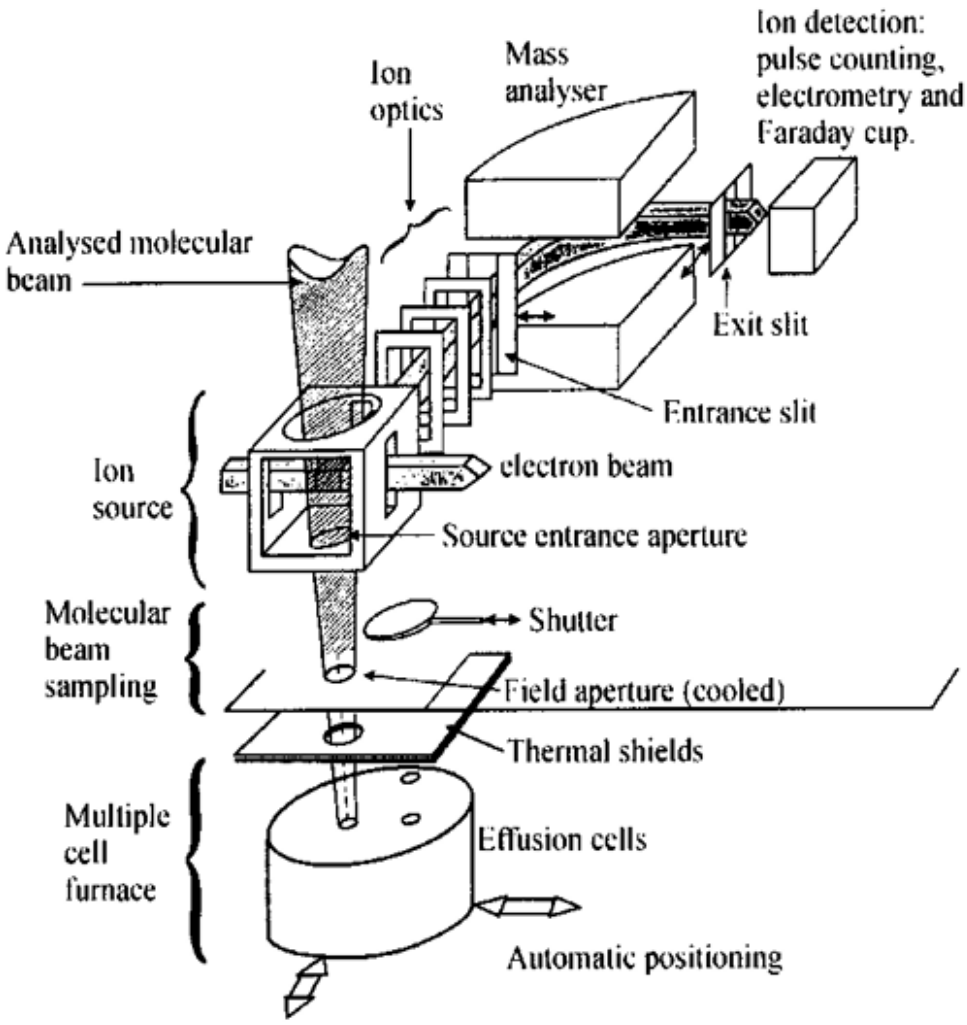

Figure 3.1: Principle of the High Temperature Mass Spectrometer at the SIMAP laboratory. A gas sample is introduced in the ionization chamber as molecular beam from an effusion cell (multiple cell). Ions formed by electron beam impact are then accelerated by an electric field. They are separated as a function of their mass to charge ratio by a magnetic prism before collecting.

3.1.1.2 Principle of the Knudsen effusion cell

The effusion cell is a crucible with a cover fitted with a small orifice (figure 3.2) working under high vacuum. The orifice cross section s must be small comparing to the surface S of the sample located in the crucible. Generally a ratio of $s/S \leq 10^{-2}$ is applied. The molecular or atomic flow vaporized from a surface s is the same as rarefied gas flow from a

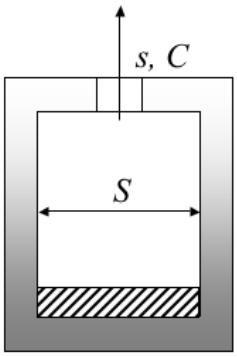

Figure 3.2: Effusion cell. S is the cell cross section or the sample cross section, s is the orifice cross section and C is the Clausing factor [89].

large vessel (isotropic conditions) through an orifice with infinitely thin edges and with the same effusion area size s. Most important point is that the mean free path of the molecules in the gas is superior to the orifice diameter ($1\,\mathrm{mm} \leftrightarrow 10^{-4}\,\mathrm{bar}$) that guarantees nearly collision-free trajectories with particle distribution easily calculable from kinetic theory of gases [86, 88].

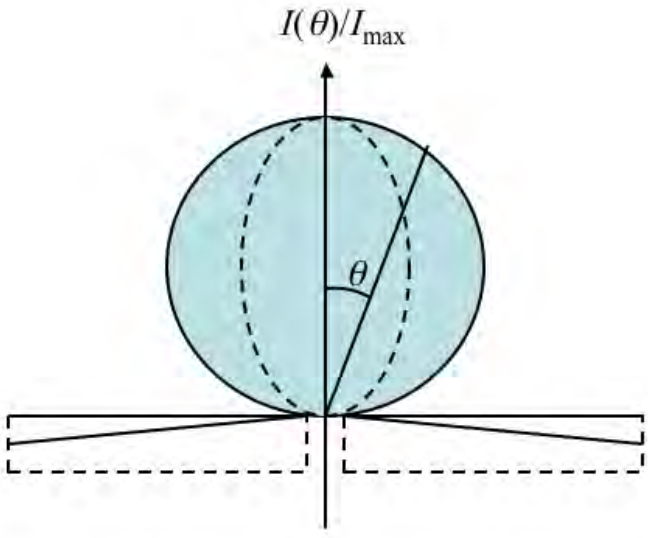

Figure 3.3: Scheme of normalized distribution (to axial value) of effusion flow from an "ideal" and from a cylindrical orifice. In the case of ideal thin edges orifice (full lines) the intensity distribution obeys the cosine law $I = I_0 \cos\theta$, that follows from the kinetic theory of gases. In the case of the cylindric form of the orifice (dashed lines) the angular distribution of the intensity confines itself around the axis of the orifice. The total probability of transmission comparing to the infinitely thin edge orifice and the angular distribution were firstly calculated by Clausing [89].

The Hertz-Knudsen relation (3.3) [88, 90] allows to calculate the total effused flow by integration over the half of the surface above the orifice. dN/dt is the molecular flow in moles per unit time that pass through the orifice of surface s:

$$\frac{dN}{dt} = \frac{ps}{\sqrt{2\pi MRT}} \tag{3.3}$$

p is the pressure in the cell, s the orifice area, M the molar mass of the effused species, R the gas constant and T the absolute temperature. This relation is to apply for the orifice with ideal thin walls. Clausing [89] introduced a coefficient C to apply it to the cylindrical non- "ideal orifices" (fig. 3.3) and Santeler [91] improved the calculation of this coefficient. The relation becomes:

$$\frac{dN}{dt} = \frac{psC}{\sqrt{2\pi MRT}} \tag{3.4}$$

The application of the molecular effusion method requires an established equilibrium inside the crucible which is closely achieved if the vaporization process is fast enough. Further limiting factors for the application of this method are:

- slow vaporization reactions,
- not inert vessel material, i.e. slow adsorption reactions with vessel walls,
- diffusion in the bulk sample for non-congruent vaporizations,
- sample surface pollution, for example a differently composed layer on the sample surface.

If one of these factors occurs during the experiment one observes partial pressures decrease. For all these cases introduction of vaporization coefficient $\alpha < 1$ is necessary. An approach for its calculation was made by Motzfeldt [92] with the equation

$$p_{\mathrm{eq}} = \left[1 + f\left(\frac{1}{\alpha} + \frac{1}{C} - 2\right)\right] p_{\mathrm{m}}, \tag{3.5}$$

with p_{eq} equilibrium partial pressure; p_{m} measured partial pressure; $f = sC/S$ the ratio of the effective orifice area to S the crucible cross section. For orthocylindrical cell, $1/C - 2$ is equal 0, that simplifies the relation (3.5) to:

$$p_{\mathrm{eq}} = \left(1 + \frac{f}{\alpha}\right) p_{\mathrm{m}}. \tag{3.6}$$

Equation (3.5), known as Motzfeldt equation, has two disadvantages mentioned by Rosenblatt [93]:

- α without subscript represents at the same time vaporization and/or condensation coefficients, which are assumed equal
- and the effective vaporizing area of a porous solid or a powder with a low vaporization coefficient will be greater than S, the cross-sectional area of the cell.

Summarizing Rosenblatt has found that for every kind of evaporating surface, which is not the same as the cell cross section, a set of appropriate assumptions must be found to approach at best the real effective evaporating surface.
Heyrman et. al.[94] separated evaporation (α) and condensation (β) coefficients and have shown how to measure them using a multiple cell device with two effusion cells with different orifices. Applying independent evaporation and condensation coefficients leads to some different equation than proposed by Motzfeldt:

$$p_{\mathrm{eq}} \frac{\alpha}{\beta} = \left(1 + \frac{f}{\beta}\right) p_{\mathrm{m}}, \tag{3.7}$$

with a condensation coefficient β, which can be calculated directly from measurements as follows:

$$\beta = \frac{f_{\mathrm{ref}} - f_i \dfrac{I_i}{I_{\mathrm{ref}}}}{\dfrac{I_i}{I_{\mathrm{ref}}} - 1}. \tag{3.8}$$

using intensities for the same sample placed in two effusion cells (i, ref) with different orifices (f_i, f_{ref} factors), which are measured during a multiple cell experiment. The obtained condensation coefficient β is then used to calculate evaporation coefficient α applying relation (3.7) and known equilibrium pressures.
In the present study two different orifices (diameter × length) were used: $f(2\times2) = 0,00965$ and $f(3,1 \times 3) = 0,0235$.

3.1.1.3 Measurement method with HTMS coupled with multiple effusion cell

We saw in the preceding sections the principles of HTMS and Knudsen effusion cell. To be able to perform credible measurements by coupling these two devices we must pay attention to some important points and limitations.

- The pressures in the cell must be within the limit of detection of HTMS ($\geqslant 10^{-11}$ bar for our spectrometer) and the limit of validity of molecular flow from a millimetric orifice ($\leqslant 10^{-4}$ bar).
- The cell material must be inert to the analyzed samples.
- By use of effusion method the calibration of mass spectrometer is performed using the sample mass loss Δm during the experiment. Combining relations 3.1 and 3.4 we obtain the sensitivity of the spectrometer:

$$S = \frac{sC\sqrt{M}}{\Delta m\sqrt{2\pi R}} \sum_{i=1}^{n} \left(I\sqrt{T}\right)_i \delta t_i \tag{3.9}$$

  The term $I\sqrt{T}\delta t$ is obtained by integration of spectrometric observation during the whole experiment.
  If more than one gaseous species are present, relation 3.9 becomes:

$$S_1 = \frac{sC\sqrt{M}}{\Delta m\sqrt{2\pi R}} \sum_{j=1}^{p} \left(\sum_{i=1}^{n} \frac{S_1}{S_j} \sqrt{\frac{M_j}{M_1}} \left(I_j\sqrt{T}\right)_i \delta t_i \right) \tag{3.10}$$

Here $i = 1$ to n corresponds to the different temperature stages during the experiment, j is the number of gaseous molecules. For the use of this last formula the ratio $\frac{S_1}{S_j}$ of sensitivities must be known or estimated and be reported to one reference sensitivity S_1. A spectrometric construction with reduced number of experimental parameters is of high interest in order to avoid accumulation of uncertainties. In the best case only the ratio of effective ionization cross sections is to estimate, like in our case.

- Temperature measurement is performed by use of a thermocouple or optical pyrometer (IR-filament). Usually the effusion orifice or long holes in the cell envelope are used as black bodies for pyrometric viewing. In these cases the transparency of the viewport have to be surveyed since molecular beam deposition can occur even by use of movable interception devices like a shutter.

- To study more than one composition in one experiment a device called multiple effusion cell was developed by Chatillon and coworkers and recently improved [95]. It allows to compare different samples with a reference directly during the same experiment. It is then possible to measure small differences in vapor pressures. This feature increases the precision in the thermodynamic analysis of chemical systems. Applying the main mass spectrometric equation the ratio becomes then:

$$\frac{p_i(j)\, S_i(j)}{p_{\mathrm{ref}}(j)\, S_{\mathrm{ref}}(j)} = \frac{I_i(j)\, T_i}{I_{\mathrm{ref}}(j)\, T_{\mathrm{ref}}}. \tag{3.11}$$

The sensitivity S for the same species j is depending on the mass spectrometer and not on the cell, following it is equal for all cells. The temperature is also the same in each cell for the multiple cell device is thermally homogeneous. The pressures ratio becomes equal to the intensity ratio:

$$\frac{p_i(j)}{p_{\mathrm{ref}}(j)} = \frac{I_i(j)}{I_{\mathrm{ref}}(j)}. \tag{3.12}$$

3.1.1.4 Instrumentation description

- Figure 3.4 shows the **multiple cell** device for four sample containers which served for the vapor pressure measurements in our experiments. The outer envelope is made from tantalum. If not mentioned the cell (crucible and lid) material was tantalum. Some runs were made with quartz and graphite cells in order to observe the interactions of the sample with the crucible material.

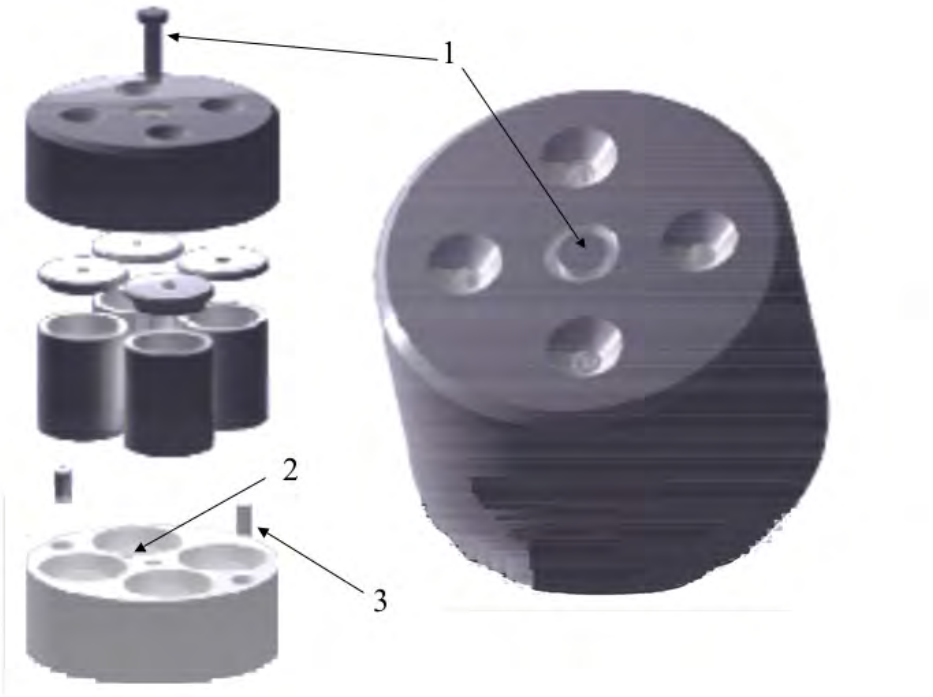

Figure 3.4: Multiple cell device. 1: Pin used for black body of the axial hole. The pyrometric viewing is done from the bottom. 2: Bottom hole for thermocouple going into the upper envelope. 3: Tungsten tips for correct assembling of the upper and bottom envelops of the multiple cell.

- **Heating of the multiple cell** was done by radiation. Figure 3.5 shows the furnace with details. The multiple cell envelope(3) made from tantalum is heated by a tungsten (W) resistor(1), which is hold by 5 tungsten rods(2). The envelop itself is hold by 3 tungsten rods(4). 10 thin laser machined tungsten shields(5) separate the stainless steel water cooled holder(6) from the heating zone. Molybdenum connection cubes(7) serve for the current arrival. 5 copper radiators(8) serve at the same time as resistor support rods(2) guides. The furnace support(10) and resistor supports guiding(9) is assured with two separated ceramic plates. For standard sheathed thermocouple there are two thermocoax passages(11) of 1 mm diameter and for four nude thermocouples two glass/metal passages(12). The pyrometer viewing is transmitted by the mirror(13). For thermocoax thermocouple there is a compensation electric slot(14). The current arrivals(15) are two for 0-250 A. Cooling is realized with water through tubing(16). The shutter of the pyrometer viewport is commanded with a double effect

pneumatic jack(17).

- **Temperature measurements** were performed with thermocouple and/or with pyrometer. The pyrometer was calibrated by NBS (now National Institute of Standards and Technology, NIST) with 12 melting points. The positioning of thermocouple in the multiple cell and the hole for pyrometric measurement are shown on the figure 3.4. We prefer to view in a long cylindrical hole drilled in the bottom of the cell in place of effusion orifices. The only problem in this case can be the adsorption by the viewport material. To avoid errors in the temperature measurement a calibration diagram was established. This diagram is necessary because above 1680°C only pyrometer can be used for temperature measurements.

- The molecular beam sampling was done by a **'restricted collimation"** device, which means adding of a "field" orifice with small diameter in the water cooled jacket which separates the furnace housing from the ionization chamber. Associated to the entrance aperture of the ionization chamber these two orifices define the molecular beam which is useful for the measurement. "Restricted collimation" means that the size of the source and field apertures limits the size of the molecular beam which is then totally included in the effusion orifice area. At the effusion orifice entrance level it means that penumbra zone with the diameter D_p (figure 3.6) is smaller than the cell orifice. The optimization of this restricted collimation device as a function of different possible diameters of the source and field apertures and their distances on the spectrometer is necessary to obtain the best transmission of molecular beam [96].

- A free floating **shutter** placed in the half-way between the furnace and the source allows to separate the useful molecular flow from the parasitic flows due to possible re-evaporations in the source housing or not-separated residuals like N_2 which interferes with Si or CO at mass 28 and CO_2 with SiO at mass 44. The spectrometer, when closing and opening the shutter, measures the contribution of gaseous species from the source housing.

  Thanks to the combination of **"restricted collimation"** and **shutter** we are able to measure the permanent gases like CO or H_2 etc. These two allow to obtain very precise measurements of partial pressures of gases coming from the cell only. The "restricted collimation" restricts the gas transfer between the furnace and source housing. The shutter closes only the cell flow, it does not change the gases flow between the furnace and source housing and it does not close the background [96].

- The **ion source** is of Nier type, that means it is made only with electrodes which induce the electric fields without magnet for electrons focalization. The electron energy can be varied continuously from 4 to 80 eV. Two filaments working altogether are used. The formed ions are accelerated by an electric field of 5000 V and focussed on the entrance slit of the magnetic analyzer with the help of a three elements electrostatic zoom lens. An exit slit is able to be adjusted continuously, in order to set up the resolution.

  Parasitic evaporation of very volatile elements in the source was radically eliminated or greatly diminished by condensation in and on the ionization box. Cooling of the latter is obtained by machining it at the bottom of a dewar containing liquid nitrogen. The liquid nitrogen is in direct contact with the ionization box made of special

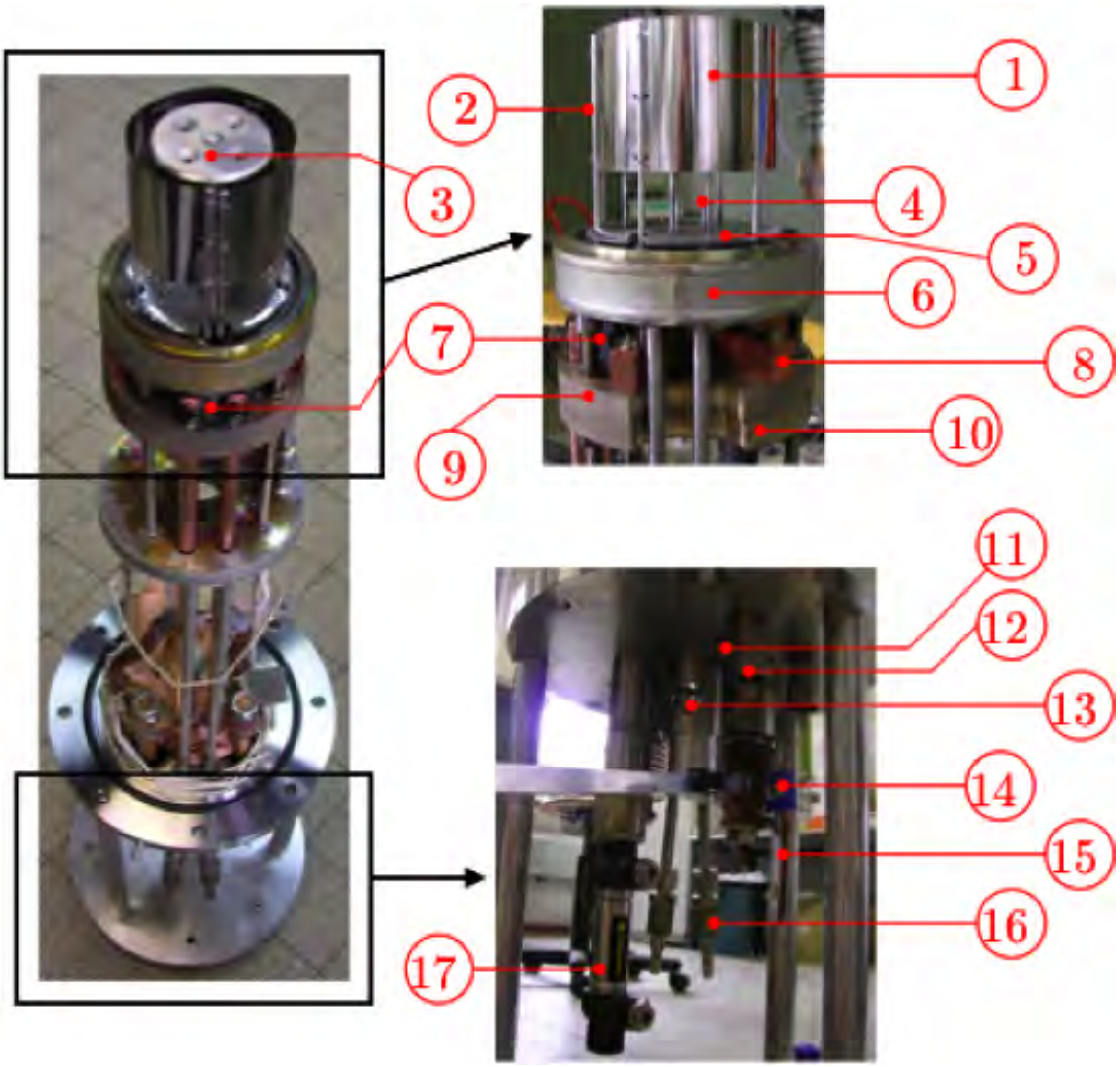

Figure 3.5: Multiple cell furnace. 1: Tungsten(W) resistor, thickness of foil 25μm. 2: Five W resistor support rods with diameter of 2 or 3 mm. 3: Multiple cell device from Tantalum. 4: Three multiple cell support rods in W with 2 or 3 mm diameter. 5: Ten packed laser machined thermal shields in W, 50 μm thickness. 6: Holder in stainless steel, water cooled. 7: Molybdenum connection cubes for current arrivals. 8: Five copper radiators and resistor support rods guides at the same time. 9: Ceramic (Al_2O_3) plate for resistor supports guiding. 10: Ceramic support plate (Al_2O_3). 11: Two thermocoax passages for thermocouple standard sheathed with 1 mm diameter. 12: Two glass/metal passages for four nude thermocouples. 13: Mirror for transmission of pyrometer viewing. 14: Compensation electric slot of "thermocoax" thermocouple. 15: Two current arrivals for 0-250 A. 16: Cooling water tubing. 17: Pneumatic jack with double effect to command the shutter of the pyrometer viewport.

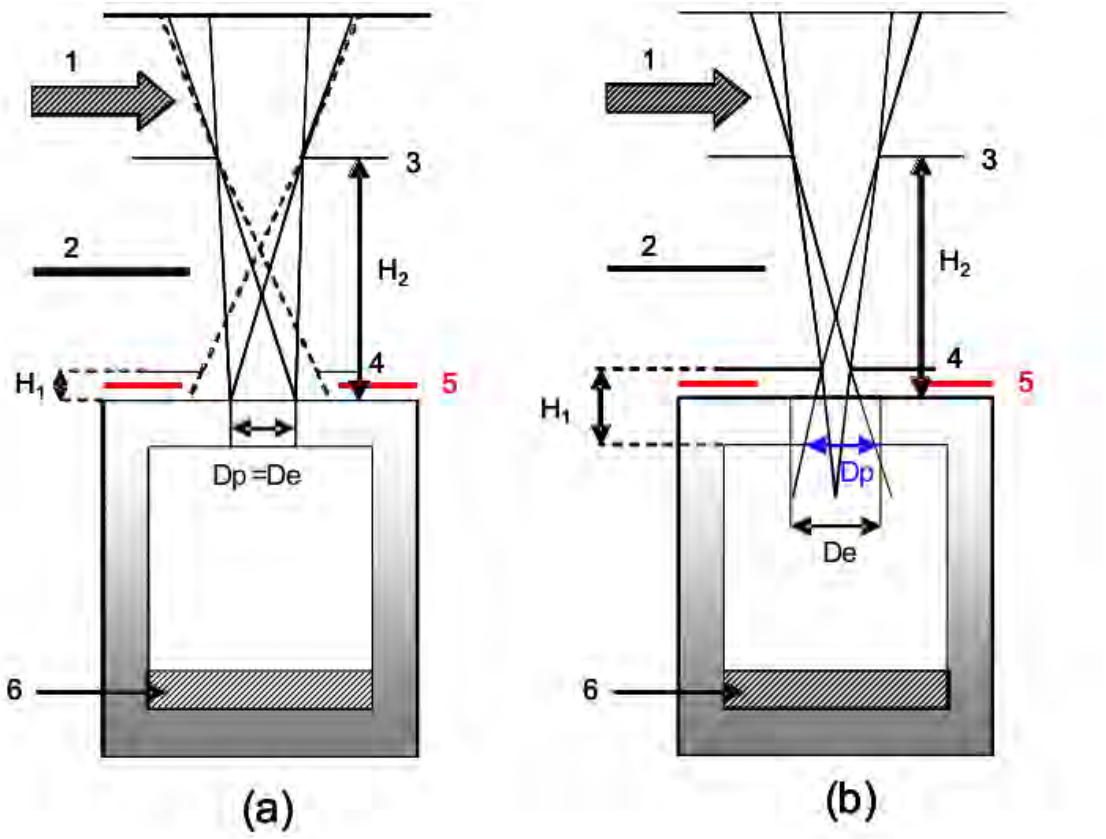

Figure 3.6: Conventional collimation (a) and restricted collimation (b) of molecular flow from effusion cell with different sampling apertures. 1: Electron beam. 2: Movable free shutter. 3: Source aperture. 4: Field aperture water cooled. 5: Furnace thermal shields. 6: Sample. D_p is the penumbra diameter and D_e is the effusion orifice diameter. [96]

amagnetic Inconel. The dewar filled with nitrogen assures electric insulation of the ionization box maintained at 4000 V [97].

- **Ion separation:** The formed ions are separated according to their mass to charge ratio by a magnetic prism. The magnetic sector has 90° and 30,5 cm curve radius. The magnetic field range is 0 to 1 Tesla. A magnetometer with a Hall sensor measures the variations of magnetic field with 10^{-5} Tesla accuracy. The magnetic field is controlled by a low voltage supply stabilized at $2{\cdot}10^{-5}$ Tesla equipped with interface IEEE and connected to a calculator that allows the mass preselection.

  The resolution of a mass spectrometer is a measure of its ability to separate and identify ions of slightly different masses and depends on the capacities of the magnetic prism. It is usually defined in terms of largest mass at which a preselected criterion is respected. Our criterion is the "valley" definition. It expresses the resolution in terms of the highest mass at which two adjacent peaks of equal height, differing in mass by one unit, have a valley between them not greater than a certain percentage, such as 10%, of the peak height [98]. For our spectrometer the resolution is at least 800 with

quite fully open mass spectrometer entrance slit at 0 % valley height.

- **Ion detection** is performed either with a Faraday cup equipped with an electrometer which allows to detect ion currents as low as $5 \cdot 10^{-15}$ A, or with a secondary electrons multiplier made for counting pulses that reduces transit time and pulses in the 2-3 ns range. The background noise is lower than 0,1 pulse/s for a yield of 10^7 to 10^8 electrons per ion entrance and corresponds to about 10^{-19} A. The signal is formated by a preamplifier. Two chains of pulse counting are available. These two chains have entrance voltage threshold discrimination to separate the pulses emitted from electronic background from those coming from ions. The background pulses have very low tension amplitude ($< 0,15$ mV at the preamplifier exit) but they are very numerous, meanwhile the pulses from ions correspond to amplitudes in the range of 0,8 to 1 V. There is a band without any pulse (nor noise) when ions arrival is stopped (darkness) It is thus possible to separate completely ions from the background by a voltage threshold.

  The secondary electron multiplier is packed in three metal boxes to prevent interferences with signals from outside. There are from outside beginning:

  - iron ARMCO for absorption of residual magnetic fields,
  - copper OFHC against HF currents,
  - μ-metal (Inconel) to discard magnetic fields.

  Even using this protection configuration sometimes parasitic pulses between 0 and 1 counts/s are observed, probably from cosmic radiation or electric interferences from power supply even using an insulation transformer. For this reason measurements are reliable from the measured currents (ion) on the scale of some 10^{-18} A (*approx* 10 ions/s).

3.1.2 Quadrupole mass spectrometer with capillary tubing

For the partial pressures higher than 10^{-4} bar collisions occur in the molecular beam and the Knudsen cell method is no longer available. In the case of our experiments with SiC beyond the condensation of SiO vapors it is still possible to observe CO gas as a permanent gas by introducing the flow of evaporated gas in a spectrometer with the help of a capillary. For this reason the quadrupole mass spectrometer with capillary tubing was used to be able to attain higher meassurement temperatures than using an effusion method. The intention was to follow the departure of CO(g) during a temperature ramp. Furthermore the measurements with a quadrupole mass spectrometer are faster and give the possibility to follow continuously a vaporization process, where the gas exhaust is more important with faster mass loss compared to the device described in the precedent part.

3.1.2.1 Instrumentation description

The experimental device contains the reactor in stainless steel with inductive heating coil for the crucible, HF generator, primary vacuum pump for the reactor and a Pfeiffer quadrupole mass spectrometer with its own pumping station. The reactor and mass spectrometer are connected by a stainless steel capillary. The pressure between capillary and mass spectrometer is regulated with a gas dosing valve.
Figure 3.7 shows the experimental arrangement and figure 3.8 shows the arrangement inside the reactor.

- The **crucible**, crucible cover and capillary connecting parts are made from graphite (Carbon Lorraine 2192). To prevent diameter reducing or clogging of the capillary, due to condensable evaporated species (like SiO(g)), the crucible cover is machined as a cone. This cone is always cooler than other crucibles zones because of the temperature gradient. The capillary is connected to the tip of the cone cover. The groove in the bottom of the crucible helps to place it in the center of the susceptor and to stabilize it on the holder plate. To assure that every individual experiment is comparable with other experiments a new crucible arrangement was used in every experiment.

  The sample is placed in a graphite crucible inside the reactor and heated applying primary vacuum or protective gas (Ar) atmosphere. Depending on chosen temperature ramp a characteristic gaseous phase is established in the crucible by condensed sample vaporization. This gaseous phase is sampled with capillary.

- The **heating** of the samples was performed by inductive heating. The work coil couples with the graphite susceptor that radiates the heat over the crucible to the sample. The power supply is obtained by HF generator (12 kW).

- The **temperature** is measured pyrometrically by sighting through a porthole directly on the cone through a small split machined in the insulation. A preliminary calibration of this pyrometer was performed to obtain the difference between the established temperature inside the crucible and the temperature measured during the experiments sighting on the cone. An experiment with SiC powder and a second pyrometer was performed. Replacing the capillary a second pyrometer was sighting directly inside the crucible on its bottom surface. A $T_{\text{cone}} + 38°$ was found for the temperature inside the crucible in the $1150 - 1650$ K temperature range.

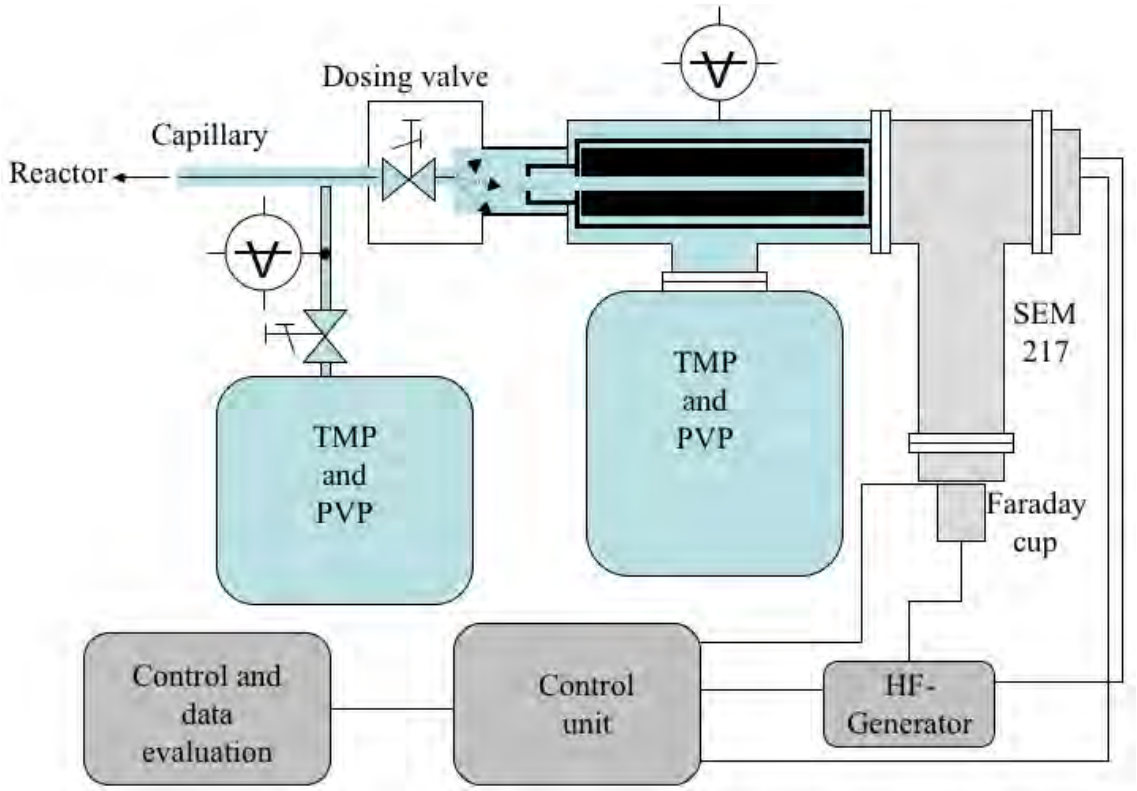

a)

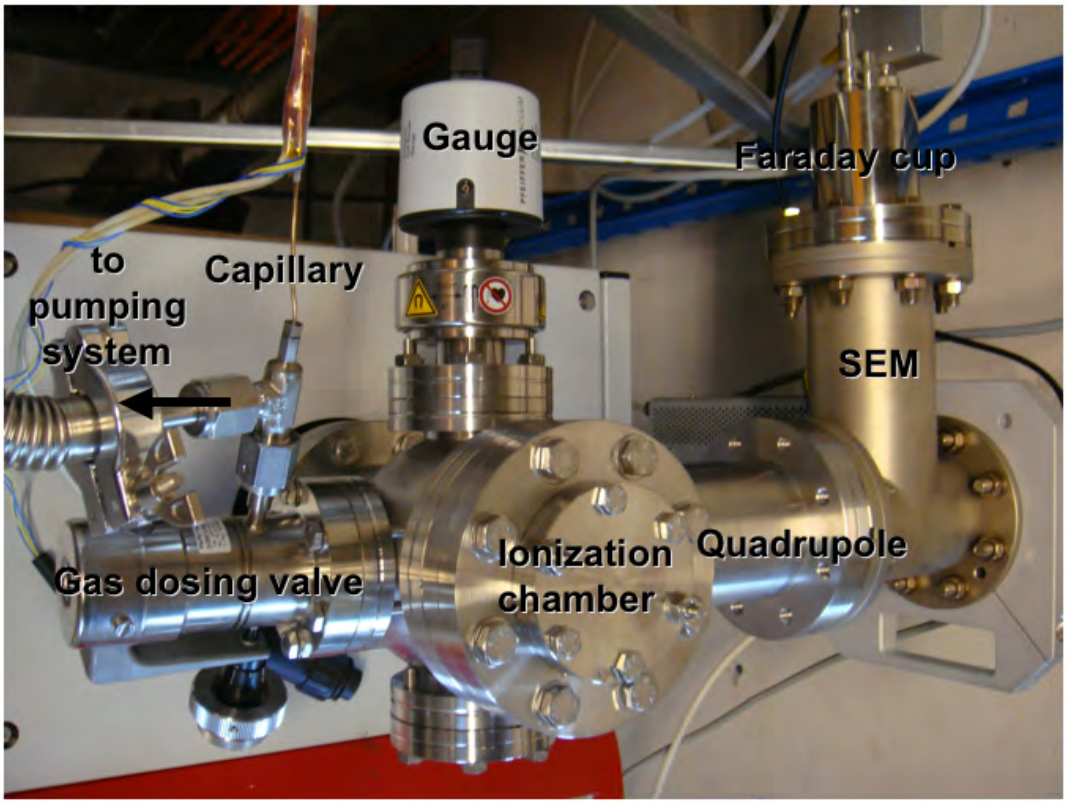

b)

Figure 3.7: Experimental arrangement with quadrupole mass spectrometer and capillary tubing: a) arrangement order of single components and b) a photograph to display orthogonal arrivings.

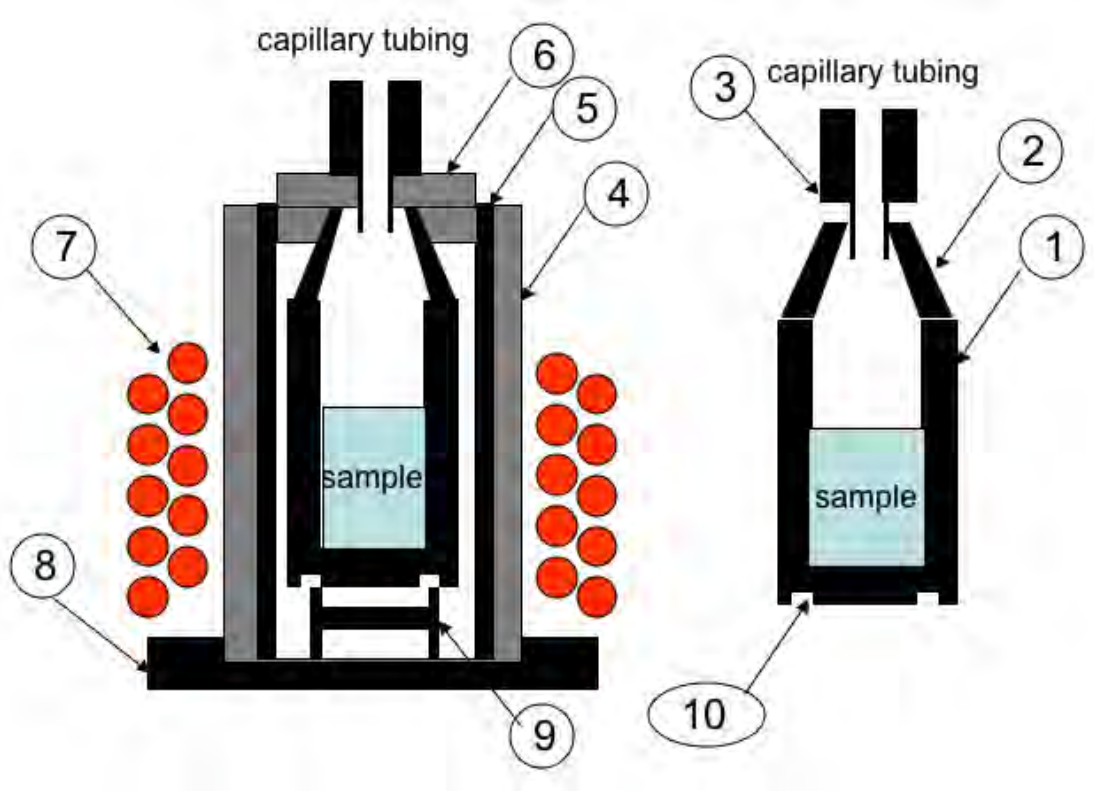

Figure 3.8: A section view through crucible with heating and insulation for the capillary reactor. 1: Graphite crucible with the sample. 2: Graphite cone for collecting of gases and condensable species before introducing non condensable species into the capillary. 3: Connecting part for the cone with capillary valve. 4: Outer graphite foam crucible insulation. 5: Dense graphite susceptor. 6: Two graphite felt pieces for cone insulation. A small split is cut in these parts for the pyrometer sighting on the cone. 7: Inductive heating coil. 8: Dense graphite holder plate. 9: Crucible holder for the exact positioning at the center of the plate and susceptor. 10: Groove in the crucible for stabilization on the positioning piece.

- The gases from the reactor arrive in the ionization chamber through 1 m long **capillary** with 0,15 mm inner diameter. The allowed inlet pressure is of 100 to 1200 mbar. The vacuum pump of the reactor assures a primary vacuum. The pressure is continuously reduced in the capillary until about 1 mbar at the entrance of the gas dosing valve. The gas flow coming from the furnace via the capillary is pumped downward by an independent pumping system. The main part of this flow is so eliminated from the mass spectrometer detection.

  Flow rate of the capillary is ≈ 2 sccm (standard cubic cm per minute) for 1 bar input gases and the transit time about 0,3 to 1 s depending on the gas viscosity.

  In order to compare experiments between each other, the total conductance must be the same. For this reason the gas dosing valve was completely open in every experiment.

- Mass spectrometer is a commercially available complete package proposed by Pfeiffer vacuum systems.

  - **ion source** is gas tight cross-beam ion source with two W filaments working separately (the second filament is mounted as a supply part). Here the molecular beam, the electron beam and ion extraction are mutually orthogonal (see fig. 3.7 a)). The condensation of the vapors or adsorption of gases on the mass spectrometer ion source electrodes is prevented by the special construction (thin sheet metal) with low heat loss and rapid heating: the interior of the source heats-up to 200°C. The filaments are located outside of the formation space of ions that discard any direct reactions of analyzed gases with the hot filament surfaces.

    The present gas tight version is particularly suitable for analyzing gases fed under high pressure directly in the ionization chamber via orifices or gas dosing valves. Typical application fields are trace analysis of ultra pure gases, respiration analysis in human medicine and isotope analysis because of low gas consumption, low background pressure in the rest of the analyzed vacuum chamber and a very short time constant of the ion source. But it must be kept in mind that the danger of possible coating of the inner surfaces of the ion source increases due to lower effective pumping capacity of the vacuum system. [99]

    In the cross-beam source the background gases which are coming from the capillary tubing and transport tube in the mass spectrometer housings are analyzed.

  - The **ion separation** is performed according to their mass/charge ratio in a high frequency quadrupole field. It is produced with four Molybdenum cylindrical rods of 6 mm diameter and 100 mm length. The coupled analyzer is of mass range of $1 - 100$ amu. This kind of mass spectrometer work as a mass filter. The resolution can be varied electrically by changing the U/V ratio for adapting to different tasks. Furthermore the quality of the mass filter is influenced by the rod diameter and their length. It increases by increase of diameter and length because it is easier to improve the relative mechanical allowance during fabrication. But an other important criteria for the size is the mass discrimination. The greater the diameter and the length of the rod system the lower is the mass discrimination [99]. For this kind of mass spectrometer the resolution corresponds to the mass range, i.e. 100. Thus masses 99 and 100 can be separated with $\approx 0\%$ valley.

  - For **ion detection** 90° off axis SEM 217 and Faraday detector were chosen. This choice is based on the required detection sensitivity and detection speed. The most important advantage of Faraday detector is that the Faraday signal is not affected by degradation or mass discrimination effects at the detector. The simplest case, but also with the least systematic errors, is if the ions hit the Faraday collector (Faraday cup). It is used alternately in combination with a discrete dynode SEM (secondary electron multiplier) detector. Mostly the Faraday cup is used alternately in combination with a SEM detector. SEM 217 is a discrete dynode SEM, which is used in the case of very low ion currents and requirement of very high measuring speed. The ions leaving the rod system are reaccelerated to several KeV (the H.V. of the SEM, ≈ 3000 V) and are then

detected when they hit the first dynode of the SEM. They eject here a number of electrons which are then multiplied in a series of further dynodes (16 in SEM 217). In order to minimize the contribution of impacting photons, soft X-rays or fast neutral particles, which can also come from the rod system, the SEM is off line by 90° from the axis of the rod system. The ions are deflected by an electrostatic field that does not have any influence on uncharged particles. The highest possible signal-to-noise ratio will be obtained in this manner. Current amplifications up to 10^8 can be reached. SEM 217 can be operated in the analogic mode (electrometer) as well as in a pulse counting mode (depending on the electronics).

Present configuration is particularly suitable for residual gas analysis and fast processes. Detection limits are $4 \cdot 10^{-11} - 1 \cdot 10^{-4}$ mbar using Faraday cup and $1 \cdot 10^{-14} - 1 \cdot 10^{-5}$ mbar for SEM 127 use.

3.1.3 Samples characterization methods

3.1.3.1 Grain size measurement

Measuring grain size before and after the experiments is a simple method to verify grain growth or elimination of a grain size fraction due to the temperature treatment.
The measurements were performed with a CILAS 1064 particle size analyzer that offers a wide range of particle size measurements, from 0,04 to 500 μm. The fine particles are measured by capturing the diffraction pattern, and applying Fraunhofer or Mie theory. The coarse particles are measured using a real time Fast Fourier Transform of the image obtained with a CCD camera equipped with a digital processing unit (DSP). The principle is shown at figure 3.9. Sample powder is put into the liquid bath section where the most of agglomerates are destroyed by ultrasonic waves. The liquid is pure water or water with addition of a dispersant agent.

3.1.3.2 Raman spectroscopy

Raman spectroscopy is a non-contact optical characterization method. It is based on the Raman effect that is the name for the emission of light from with monochromatic light illuminated sample. This emitted light has different frequencies than the diffused light. The intensity of this emitted light spectrum is very low and difficult to observe together with the diffused light. This effect is caused by the interaction of monochromatic light phonons with the atomic structure of the analyzed material. The resulted observed frequencies from a solid are functions of the masses of atoms and their bonding forces. The number of observed peaks depends on the number of atoms in the primitive cell and of its symmetry. The more is the cell simple and symmetric, the less is the number of peaks. The form of these peaks (width, asymmetry, etc.) indicates the quality of the analyzed crystal like structure faults, impurities or doping elements presence.
Raman spectroscopy is particularly suitable for the measurements on the SiC crystals, to determine the kind of SiC polytypes. Every polytype has its specific peaks number and theirs positions are well determined. The increasing period length of 4H-, 15R- and 6H SiC-polytypes lets move characteristic peaks to shorter Raman-displacements.

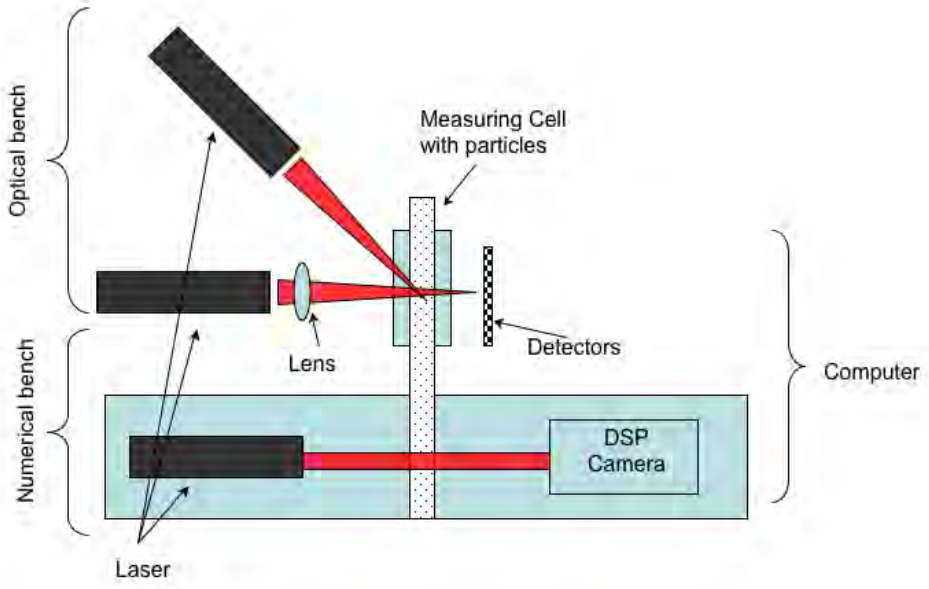

Figure 3.9: Grain size measurement principle of the CILAS 1064.

By measurements on a powder sample the shifted level of the background is another indication for the quality connections between the single grains. The fluorescence causes the raise of the whole spectrum with higher frequencies. This fluorescence comes from the phonons, which are emitted to eliminate the energy received from the excitation light. In a solid sample this energy can be transmitted through its atom network in the sample holder. When the powder grains build connections during a heat treatment, this background raise decreases because the received energy can be evacuated through the sample material itself. The measurement bench is composed of:

- laser as an excitation source,
- optic microscope to focus and to collect electromagnetic waves,
- monochromator as dispersion system for the collected light,
- CCD camera for detection of diffused light, which is focused on it.

The sample is located on a movable platform (x,y). The electromagnetic wave from the laser is focused by a microscope on the surface of the sample. The wave diffused by the sample is also collected by the objective of the microscope and turned from the way of entering wave by half-reflecting optics. The diffused wave is finally focused on the pinhole, an aperture with the possibility to change the size of the entrance slit. The Raman diffusion is really weak compared to the Rayleigh radiation, that must be eliminated by a monochromator or a Notch filter. For this reason the diffused wave enter in a monochromator before the photons dispersed in the monochromator are finally collected by a detector CCD (Charge-Coupled-Devices)
The performed measurements were done with a spectrometer, equipped with a triple-monochromator (600, 1800 or 2400 rot/mm), and a CCD camera cooled with liquid nitrogen. An argon laser was used as an excitation source with 514 nm light wave length in

the visible and 488 nm (with double frequency usable also as 244 nm) and 363 nm in the UV range. Figure 3.10 shows a scheme of the Raman spectrometer.

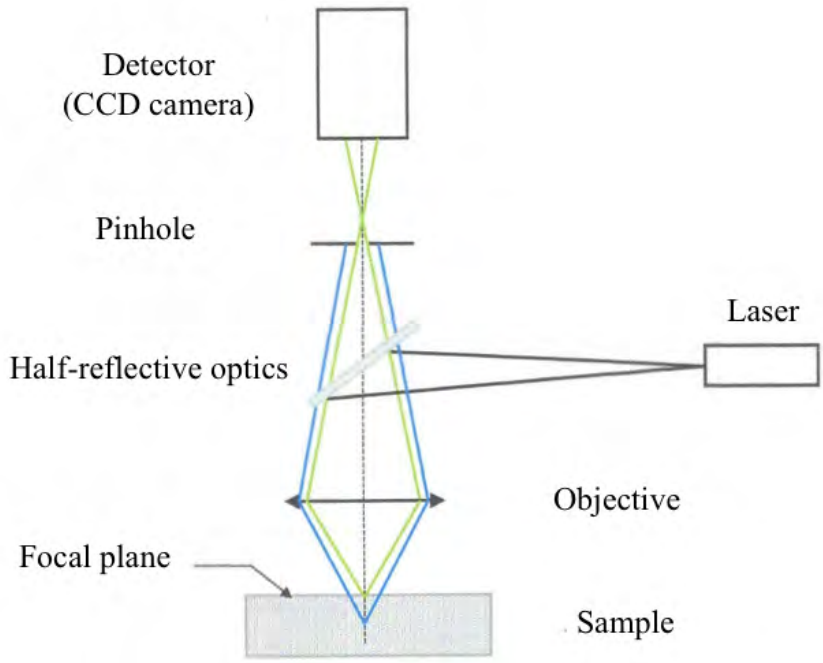

Figure 3.10: Raman spetrometer.

3.1.3.3 Imaging with Scanning Electron Microscopy (SEM)

Imaging with a SEM is a well known technic for already more than 50 years. It is based on the interaction between the sample surface and an electron beam. The sample must be an electric conductor or a semi-conductor. In the case of insulator there is a possibility to cover the sample with a thin (some atoms) layer of gold or graphite.
The first equipment used was a LEO XL30 SEM to show details of the SiC powders in the micrometer range. SiC is a semi-conductor material but the powders can also act as insulator. For better quality of the images sometimes a fine graphite layer was put on with the BALZERS CED 030 sputter.
ZEISS Ultra 55 Field Emission Gun (FEG)-SEM equipped for Electron Backscatter Diffraction(EBSD) and with TexSEM Laboratories (TSL) software was used. The features of this device allow ultra high resolution for surface information and to present compositional information. Resolutions of 1 nm can be attained. The function of this imaging device is based on the Shottky effect in the case of thermal field emission (TFE) and on the tunnel effect for cold field emission (CFE). An electric field in the range of 10^7 V/m for TFE and 10^9 V/m for CFE is applied. Ultra high vacuum ($< 10^{-8}$ Pa) is necessary for the function of a FEG-SEM.
With FEG-SEM we could obtain pictures of formed necks between the single SiC grains.

3.2 Vaporization in quasi equilibrium state: Experiments in High Temperature Mass Spectrometer

Experiments with pure SiC powders and with addition of SiO_2 were performed in high temperature mass spectrometer. The design of effusion cells allows to measure partial pressures in quasi equilibrium state. The addition of SiO_2 was performed in form of a powder or by oxidizing of SiC powder in a humid atmosphere. The influence of different amounts of SiO_2 on the developed gaseous phase was examined. Furthermore the influence of grain size of sample powders and their mixtures was studied.
The samples after experiments were analyzed in view of changes in the macro- and microstructure: grain growth, change of the grain appearance comparing to the powders before and growth of new SiC polytypes.

3.2.1 Measurement conditions

Every experiment began with a set up of the mass spectrometer followed by its calibration. A little amount of thin silver foil (5 mg) was placed in every cell of the multiple cell device. Silver begins to evaporate a detectable amount already at 750°C until 900°C so one can make the necessary calibrations before the samples begin to emit large amounts of molecules and undergo changes due to raising temperature. Before the beginning of the measurements, silver is already completely evaporated (< 1100°C) and one can study the gaseous phase established by the sample only with set upped mass spectrometer.
The first step of set up is the detection of mass 28 which is a mass of numerous gases present in the background. As soon the peak 28 is found one can set up the electronic devices coupled with mass spectrometer. After the set up of electronics, like repeller analysis, is accomplished, the current position of a cell must be checked [95].

3.2.1.1 Ionization

For the estimation of the sensitivity of mass spectrometer the ionization cross sections σ of the molecules must be estimated. They depend on the ionization energy at which the mass spectrometric measurements are performed. For the calibration of the measurements ionization efficiency curves for each measured molecule, if possible, were established.

3.2.1.2 Mass spectrum and resolution

Before the beginning of measurement of a certain molecule a mass scan must be established. It shows if the mass of a molecule was shifted. Furthermore same molecules and molecules with the same or similar mass, which come from the background are separated by the shutter (for example: N_2 from Si(g) or CO(g); SiO(g), CO_2 and $C_nH_{2(n+1)}$) and sometimes different ionizing energies are necessary to help the resolution. Using the shutter we are able to keep higher sensitivity for molecular beam detection compared to reducing the entrance and exit slits.

3.2.1.3 Cells centering

Further step to obtain reliable measurements is the positioning of a cell precisely in front of the field aperture. This position assures the function of the restricted collimation, i.e. direct

"viewing" inside the cell on the sample surface. Specific improvements necessary for the accuracy of positioning system were done by the present team and are described in [95].

3.2.2 Si-C vaporization behavior

The grains of any SiC powders are covered with a silicon oxide layer due to passive oxidation of SiC as soon as exposed to oxygen containing atmosphere. This behavior is common for all Si containing compounds. The amount of this SiO_2 is not the same for all SiC powders. It depends on the manufacturing history of each powder. Some kinds of milling favor the oxidation at air. If during milling process the Si-C bonds are split and mostly open Si bonds are located on the surface this encourage more building of the oxide layer than open C bonds close to grain surface.

3.2.2.1 Choice of the powders

For the study of Si-C vaporization behavior the most possible pure SiC powders were necessary. As the grain size have also an influence on the vaporization behavior, the grain size distribution has to be as narrow as possible too. We couldn't find this kind of powders, so a commercial sufficiently pure powders were sieved to obtain several powder samples with different narrow grain size distributions. Further advantage of using the same SiC powder is that every sample has the same origin and by the study of the vaporization behavior of different grain size fractions the SiC origin would not interfere with the measurements. We analyzed samples with grain sizes of 0,5, 5, 10 and 20 μm. Table 3.1 lists impurities and trace elements from the chemical analysis for quality certificate.

Table 3.1: Impurities and trace elements in the original SiC powder used for the study of Si-C vaporization behavior.

Trace element	ppm	Chemical analysis	wt%
Al	52	Free C	0,03
Fe	12	Free Si	0,08
Ti	9	Tot O	0,03
Ca, V	8		
Cu	2		
Mg, Cr, Ni, Zr	1		

In preliminary experiments SiC powders of different origins were used. Short description of these powders is given in table 3.2. The A-HP and B-HP (High Purity) powders are used in electronics, and the C-abr and D-abr powders generally for the abrasive applications. The latter have very narrow grain size distribution, but they are not as pure as the HP powders.
The experiments for the Si-C vaporization study were performed with the multiple cell device. The samples were placed in tantalum cells, which are the most inert to SiC in the

Table 3.2: Impurities and grain size (d50) in the preliminary used SiC powders for different industrial applications.

	A-HP	B-HP	C-abr	D-abr
d 50 [μm]	0,23	1,84	16,80	0,70
Free C [wt%]	0,26	0,22	0,06	0,32
Free SiO_2 [wt%]	1,48	-	0,13	1,93
Free Si [wt%]	0,03	0,03	0,04	0,05
Fe_2O_3 [wt%]	-	-	0,009	0,037
SiC [wt%]	-	-	99,76	98,65

concerned temperature range, until 1800°C, with 14,6 mm diameter for the evaporation cross section. Covers with orifices of 2 mm diameter and 2 mm thickness were used.

3.2.2.2 Performed experiments

Table 3.3 gives a brief description of experiments performed for the Si-C vaporization study.

Table 3.3: Multiple cell experiments performed for Si-C vaporization study in high temperature mass spectrometer. Multiple cell contains 4 cells.

Experiment label	Sample powder	d50 [μm]	T_{max} [K]	Observed gaseous molecules
SiC-02m	A-HP B-HP C-abr D-abr	0,23 1,84 16,80 0,70	1760	Al, Fe, SiO, CO, Si, Si_2, Si_2C
SiC-05m	sieved SiC powders	0,5 5 10 20	1900	SiO, CO, Si, Si_2C SiC_2
SiC-07m	sieved SiC powders	0,5μm+5μm mix (3:7) 0,5μm+10μm mix (3:7) 0,5μm+graphite (1:1)	1925	SiO CO Si

3.2.2.3 Experimental results

In this part we will see the results from the multiple cell experiments performed to study the vaporization behavior of the SiC powders. The departure of the native SiO_2 layer from the grains was observed measuring SiO(g) and CO(g) partial pressures. Further the vaporization of Si(g), Si_2C(g) and SiC_2 was observed when obtained pure SiC. It was also examined which SiC composition was obtained after the elimination of native oxygen, stoechimetric pure SiC or one rich in Si or C.

3.2.2.3.1 Powders for different industrial use The measurement of SiO(g) and CO(g) partial pressures in the experiment to confirm SiO_2 presence in the original powders were performed. p(CO) and p(SiO) decreases with increasing temperature due to SiO_2 elimination by vaporization were observed.
Figures 3.11 and 3.12 display decimal logarithm of SiO(g) and CO(g) partial pressures respectively as functions of the inverse of temperature for powders for different industrial applications.
The first observation to make is that measured SiO(g) and CO(g) partial pressures are much—at least 100 to 1000 times—lower than calculated for equilibrium of pseudo-binary system SiC-SiO_2. Contrarily to thermodynamic evolution with increasing temperature, a partial pressures decrease was observed. Such vaporization behavior must be caused by change of the vaporizing composition, in particular by oxygen depletion in the powders. The ratio p(SiO)/p(CO) remains smaller than 1 and so significantly smaller than the predicted 3,76 value by thermodynamics (for the flows ratio ψ(SiO)/ψ(CO) = 3).

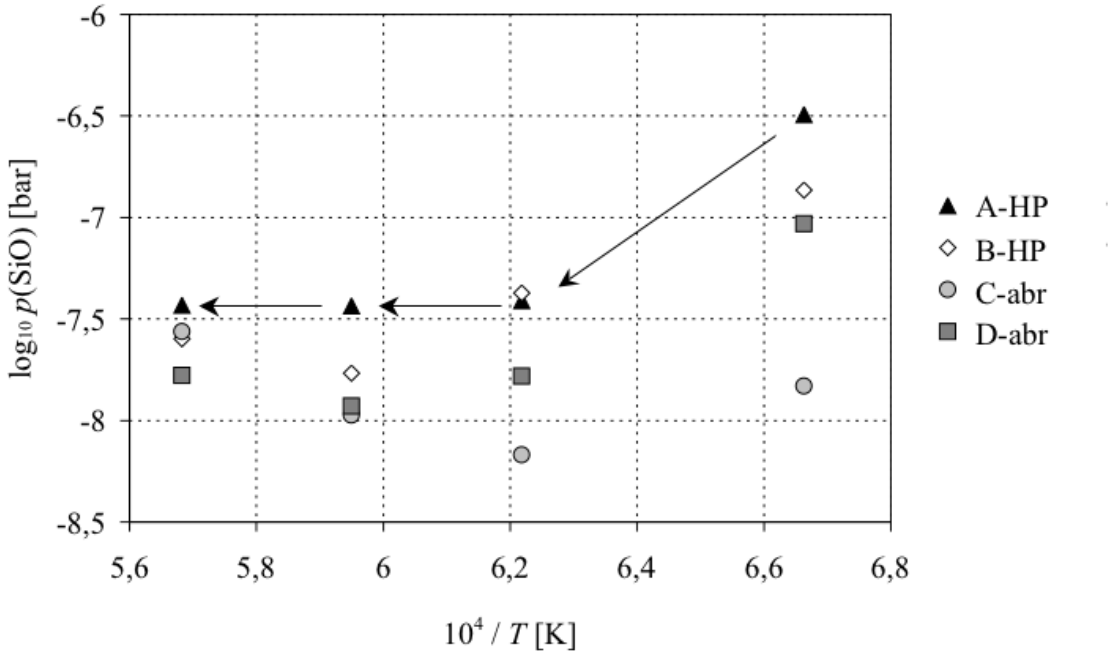

Figure 3.11: Decimal logarithm of SiO partial pressure for powders from the SiC-2m experiment as a function of the inverse of temperature. Arrows show evolution with time.

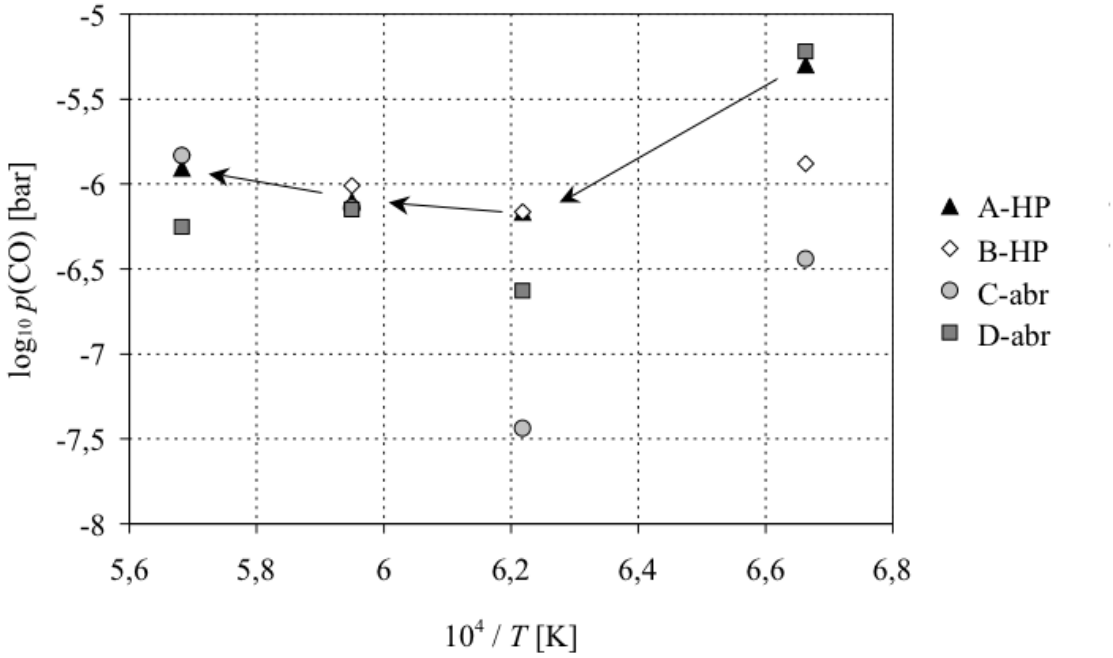

Figure 3.12: Decimal logarithm of CO partial pressure for powders from the SiC-2m experiment as a function of the inverse of temperature. Arrows show evolution with time.

We can see on both diagrams that the powders vaporize differently in the early stage of the experiment as at its end. At the beginning of the measurements at lower temperatures all powders establish different pressures in their crucibles. At high temperatures the measured partial pressure values from different powders are closer together than at low temperature.

Figure 3.13 shows the measured Si(g) partial pressures. Because of overlap with CO at the same mass, 28, the Si partial pressure could be detected only at high temperatures, where the p(Si) is much higher compared to p(CO). This is also the reason of increasing p(CO) at figure 3.12 for $T > 1640\,\mathrm{K}$ contrarily to the observation made for p(SiO) at figure 3.11. The values of p(Si) for all samples are very similar and close to pure Si(g) equilibrium value. They increase with increasing temperature as predicted by thermodynamics.

Figure 3.14 shows the measured Fe(g) partial pressures. For $T < 1700\,\mathrm{K}$ iron is not volatile, which explains its presence in the samples up to this temperature before depletion at $T > 1700\,\mathrm{K}$. It has a doping role in this case. At low temperature the Fe(g) partial pressure is significantly higher for samples originally richer in Fe.

As conclusion for this preliminary experiment with SiC industrial powders we have seen that even the powders for electronic applications contain a certain SiO_2 amount, which was shown with SiO(g) and CO(g) detection in the early vaporization stages. The partial pressures of SiO(g) and CO(g) decreased rapidly and their ratio, $p(\mathrm{SiO})/p(\mathrm{CO})$ was much smaller as predicted by thermodynamic calculations, i.e. equal 3,76. The measured partial pressure of Si(g) from $T > 1640\,\mathrm{K}$ is close to the partial pressure from pure Si(s), which is consistent with the free Si presence as impurity in the samples (see table 3.2). The iron impurity was also volatilized in the early stages of vaporization experiment and detected as Fe vapor with p(Fe) lower than from Fe(s) pure. The samples C-abr and D-abr contained

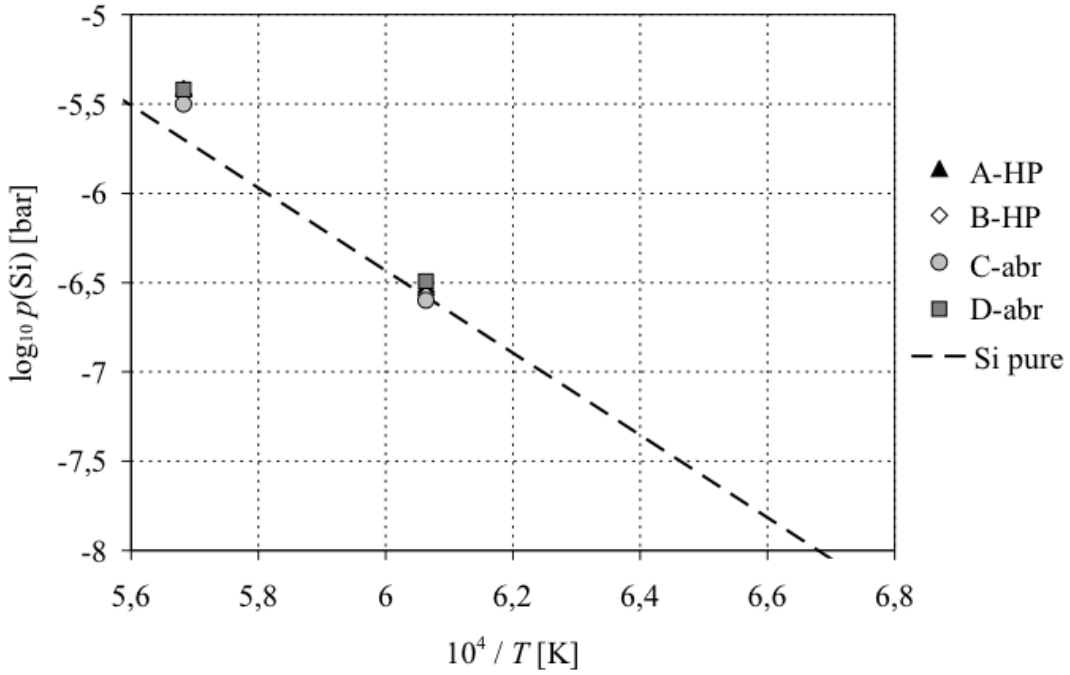

Figure 3.13: Decimal logarithm of Si partial pressures for powders from the SiC-2m experiment as a function of the inverse of temperature.

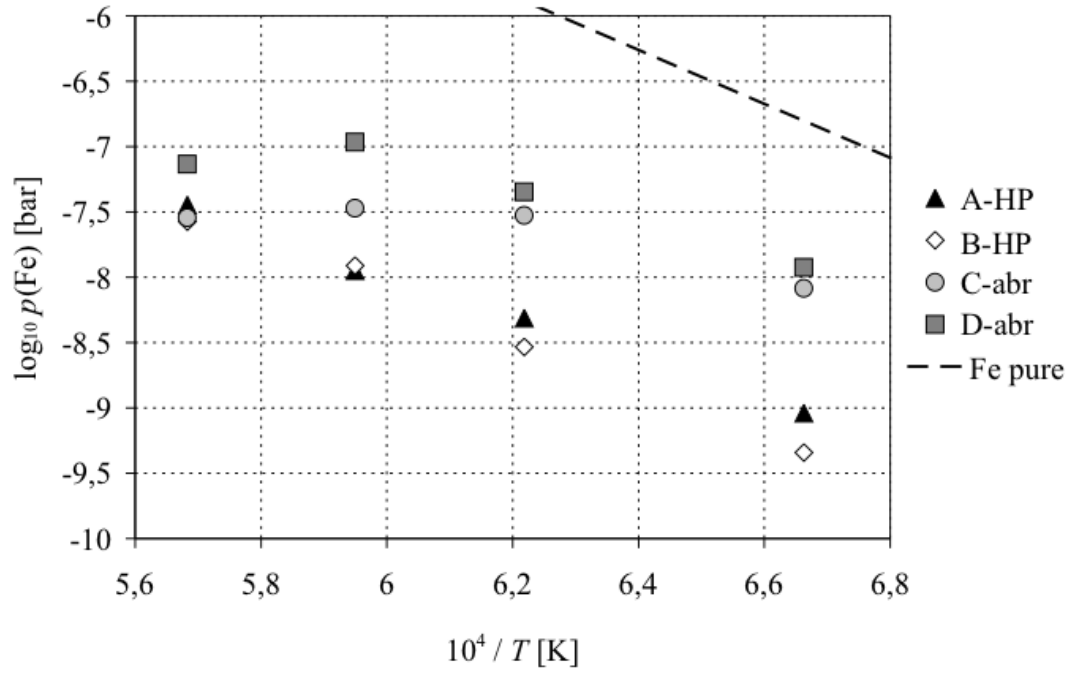

Figure 3.14: Decimal logarithm of Fe partial pressure for powders from the SiC-2m experiment as a function of the inverse of temperature.

initially Fe(s)(see table 3.2), and to the end of experiment their p(Fe) became close to p(Fe) from the iron-less A-HP and B-HP samples. Following the impurity Fe(s) is eliminated from the condensed sample in the early stages of the vaporization experiment.

3.2.2.3.2 Vaporization of different grain size SiC powders Powders used in this experiment are originally from the same batch, which was fractioned to different grain sizes by sieving. Attention was payed to load each of our cells with the same powder volume.

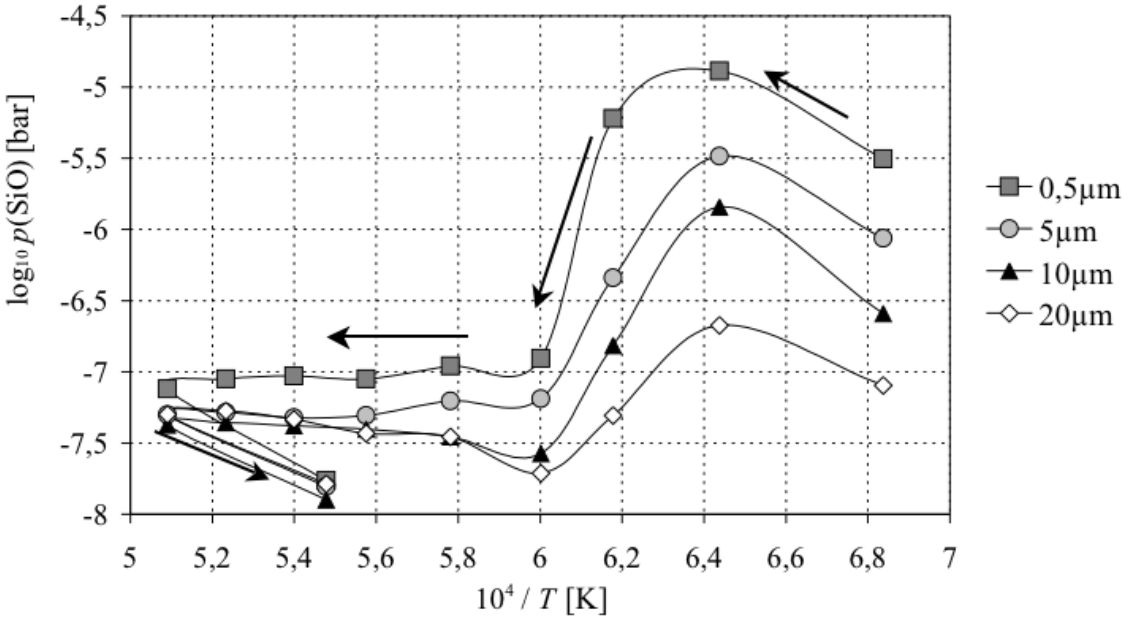

Figure 3.15: Decimal logarithm of SiO(g) partial pressure for powders from the SiC-05m experiment as a function of the inverse of temperature.

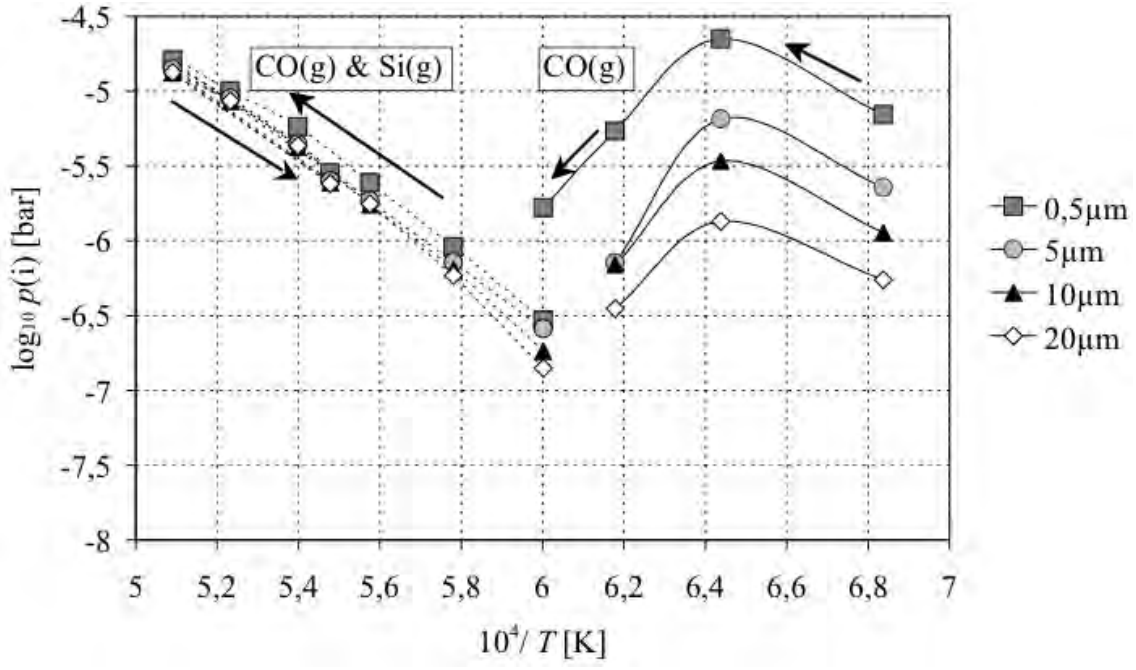

Figure 3.16: Decimal logarithm of CO(g) partial pressure for powders from the SiC-05m experiment as a function of the inverse of temperature.

Figures 3.15, 3.16 and 3.17 show the diagrams of SiO(g), CO(g) and Si(g), Si_2C(g) and SiC_2(g) partial pressures as a function of the inverse of temperature.
SiO(g) and CO(g) partial pressures at figures 3.15 and 3.16 show same behavior in low temperature region. Increasing partial pressures are in agreement with thermodynamic predictions, but the following decrease indicates composition variation due to vaporization losses. This partial pressure decrease shows the de-oxidation of sample powders, i.e. elimination of the native SiO_2 layer on the grain surfaces. After this de-oxidation the SiO(g) remains constant with increasing temperature, but CO(g) seems to increase. This increase is due to Si(g) apparition, which cannot be separated completely during the measurements. So the real CO(g) behavior can only be estimated as with constant partial pressure values after sample de-oxidation, because it is the same as SiO(g).
Further remarkable feature is the difference in measured SiO(g) and CO(g) partial pressures for different samples. According to thermodynamics, samples of same compositions must evaporate in the same manner. Here only the grain diameters are different which lead to different evaporating surfaces even if the cell cross section remains the same. Smaller grains sample have larger evaporation surface, that results in higher SiO(g) and CO(g) partial pressures due to the presence of an evaporation coefficient. Indeed, the evaporation coefficient is connected with evaporating surface of a sample to produce a kinetic steady-state in the cell [92].
We can see at figure 3.15 that SiO(g) was still detected after de-oxidation and has constant values for partial pressures. The necessary oxygen to maintain these pressure values is coming from the Ta cell which is able to dissolve large quantities of oxygen and carbon.
After de-oxidation step oxygen free species were detected: the partial pressures are shown for Si(g) in figure 3.16 and in figure 3.17 also for Si_2C(g) and SiC_2(g). For all samples similar partial pressures were measured. This indicates firstly quite same composition of analyzed samples and secondly the absence of evaporation coefficient for pure SiC. Comparing the present measured values for these species to thermodynamic calculations shows that p(Si), $p(Si_2C)$ and $p(SiC_2)$, are located between the two diphasics, SiC rich in Si and SiC rich in C. For Si(g) the two diphasic domains are presented in fig. 3.17. This result confirms that the samples are pure stoichiometric SiC after de-oxidation. The pressures evolution with time shows clearly a composition evolution in the SiC non-stoechiometric domain towards the SiC-C diphasic domain.
As conclusion to the presented results from the vaporization experiment with SiC powders from the same batch with different grain sizes we have seen:

- The SiO(g) and CO(g) partial pressures are different due to the different evaporating surfaces in the case of different grain sizes. Indeed the samples with small grain size and following larger evaporating surface for the same load volume had higher partial pressures compared to samples with large grain sizes. Vaporization of SiO(g) and CO(g) is kinetically limited and is not at equilibrium. Partial pressure ratio of SiO to CO is much lower than expected 3,67.

- The Si(g), Si_2C(g) and SiC_2 are not influenced by the different grain sizes and following by the evaporating surface differences. The vaporization of these gaseous species is not kinetically limited.

- The composition of condensed phase evolve finally towards SiC-C, which is monitored with Si(g) partial pressure evolution towards the one in the diphasic SiC-C domain.

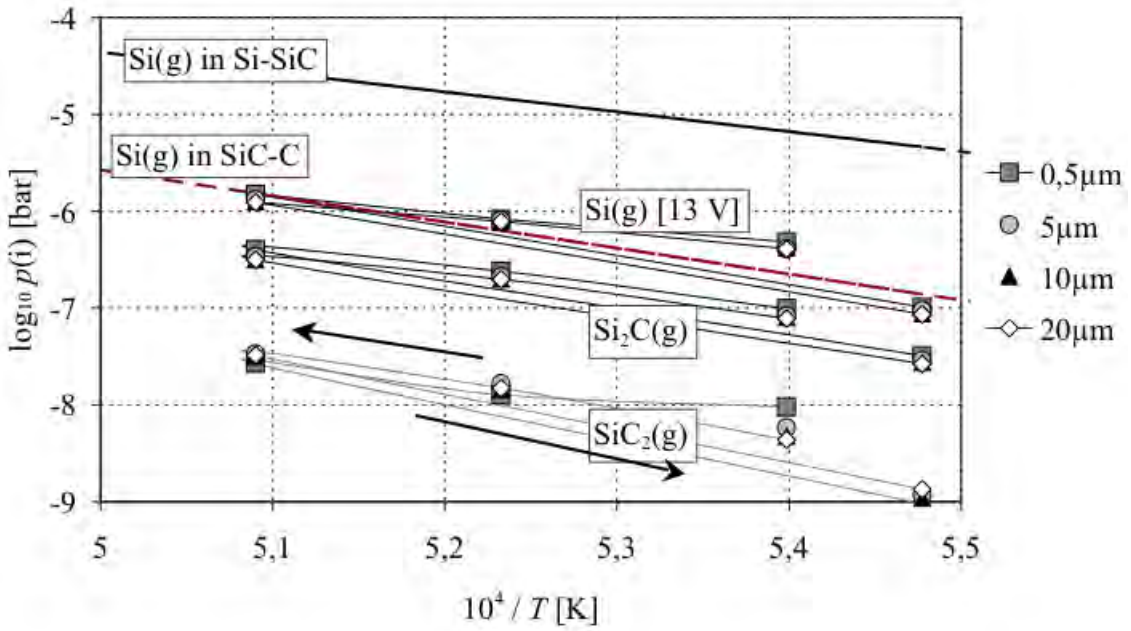

Figure 3.17: Decimal logarithm of Si, Si_2C and SiC_2 partial pressures for powders from the SiC-05m experiment as functions of the inverse of temperature. Arrows show the evolution with time.

3.2.2.3.3 Vaporization of mixtures of different grain sizes SiC powders In this experiment vaporization behavior of SiC powders of different grain sizes mixed together was observed. Two mixtures (3:7) of same SiC powders described before were analyzed, 0,5+5 μm and 0,5+10 μm. They were compared to a reference, a 1:1 mol SiC : graphite mixture in a graphite cell. This kind of reference was chosen to check if one of the analyzed samples approaches to or become a diphasic SiC-C.
Due to some calibration difficulties the partial pressures were not obtained, but yet we can still compare the obtained results by observing the products of intensity and temperature, which are directly proportional to partial pressures.

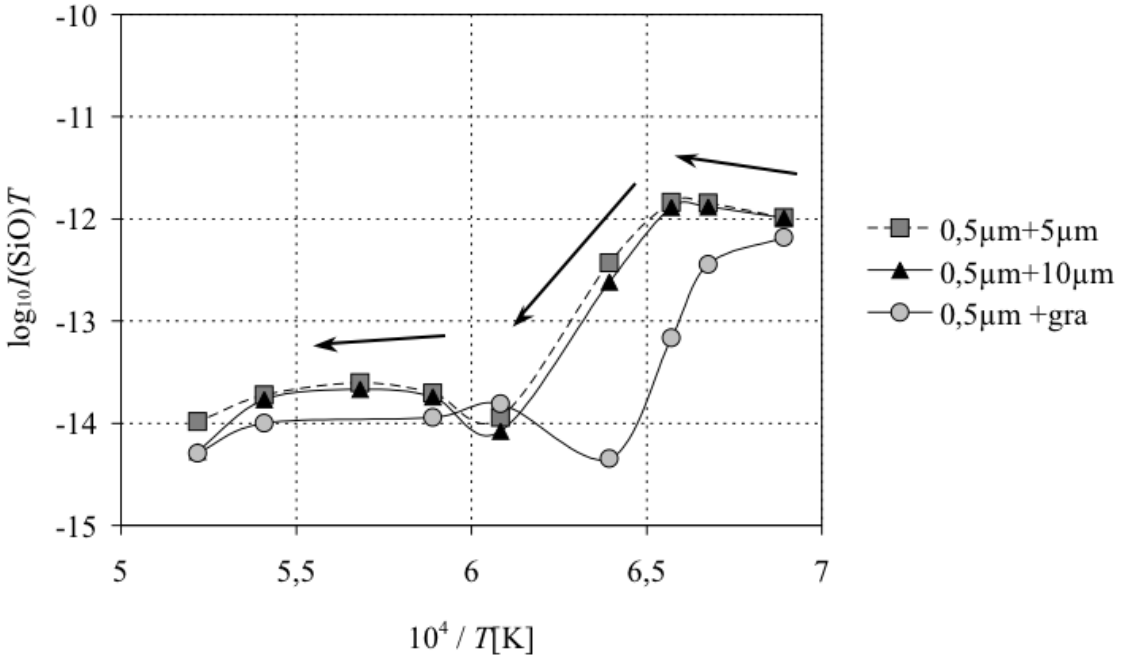

Figure 3.18: Logarithm of $I \cdot T$ products for SiO(g) as a function of the inverse of temperature from different grain sizes mixtures. Arrows show the evolution with time.

Figures 3.18 and 3.19 show the logarithm of $I \cdot T$ products for SiO(g) and CO(g) respectively as a function of the inverse of temperature. Very small difference was observed between the 0,5+5 μm and 0,5+10 μm samples. The reference powder with graphite has a similar trend but it lose earlier the oxygen via CO(g). Indeed, the partial pressure of CO(g) is the largest above the reference SiC-C. The increase of CO(g) at higher temperatures ($> 1650\,\mathrm{K}$) indicates the Si(g) apparition, the samples themselves don't contain any more oxygen as we can see at figure 3.18 observing SiO(g).
The ratio of p(SiO) to p(CO) remains always lower than 1.
Figure 3.20 shows the Si(g) pressure ratios of different grain size mixtures to the reference powder as a function of temperature after the first de-oxidation step ($T \approx 1650\,\mathrm{K}$). The p(Si) of the reference SiC-C is much lower than the p(Si) of the mixture samples, until 3 times lower. The reason is the composition of SiC powders which has remained within the limits of the stoechiometric SiC after the first de-oxidation. This result is consistent with thermodynamic calculations: partial pressure decrease with increasing temperature

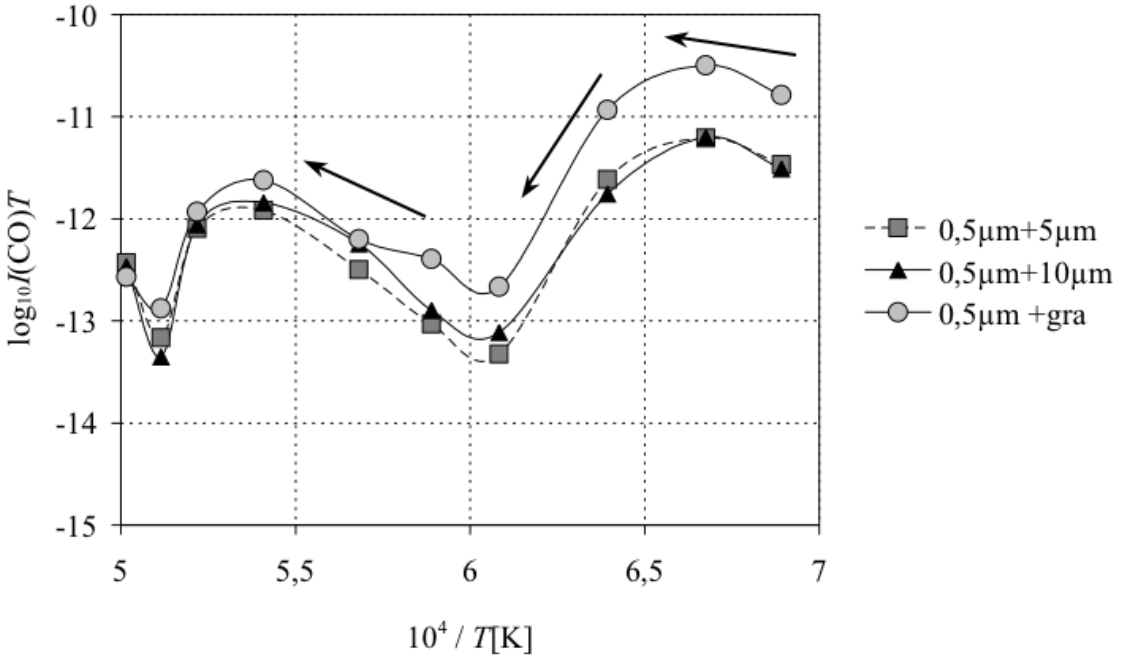

Figure 3.19: Logarithm of $I \cdot T$ products for CO(g) as a function of the inverse of temperature from different grain sizes mixtures. Arrows show the evolution with time.

is in agreement with compositions evolution towards the limit of diphasic SiC-C. But the pressure decrease is reduced, because the oxygen stored in the tantalum walls causes partially active oxidation of the sample powders. This active oxidation has no effect on Si(g) pressure for the reference sample with excess of C. For all the cells the active oxidation is attested by the existence of the SiO(g) pressure whatever is the temperature.
As conclusion of the experiment with mixtures of different grain sizes SiC powder we have seen that both mixtures show similar behavior. The only difference was in the coarse grains size fraction. Following the partial pressure is mainly influenced with the vaporization surface developed by fine fraction powder, i.e. 0,5 μm. The reference with carbon in excess had lower SiO(g) and higher CO(g) partial pressures compared to the SiC mixture samples, as it was expected. Furthermore the SiO(g) partial pressure of the reference powder decreased earlier than by the SiC mixture samples, which means that the de-oxidation was achieved earlier in the reference. The Si(g) pressures for the SiC mixture samples are until 3 times higher than for the reference with C excess.

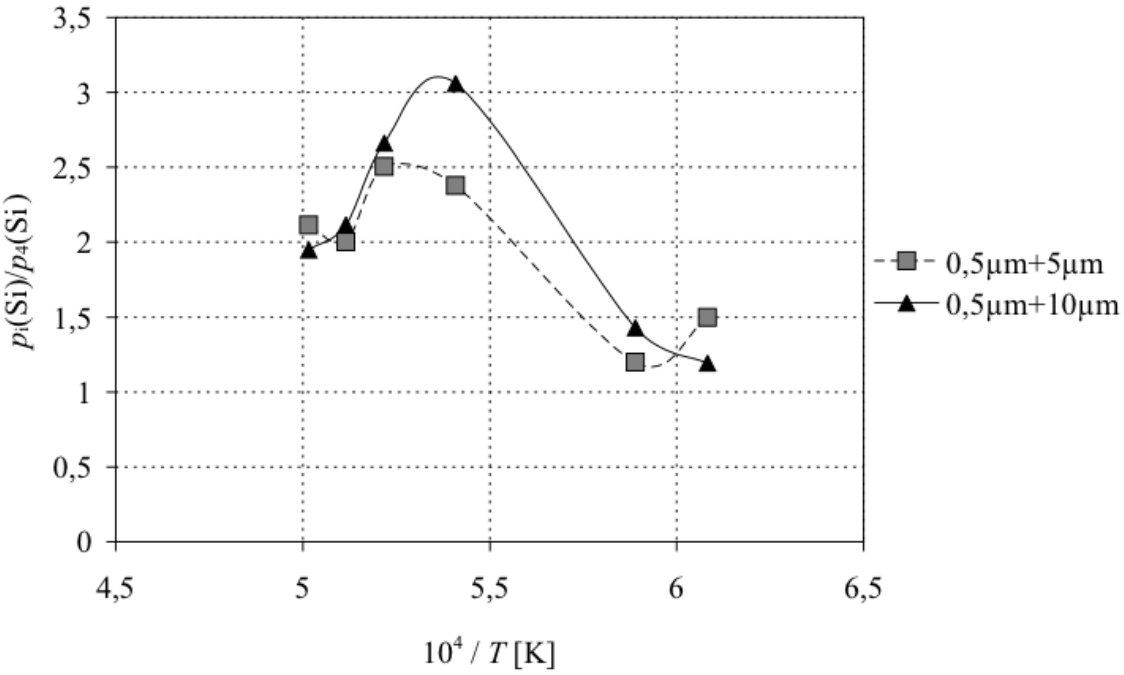

Figure 3.20: Si(g) vapor pressure ratio (reference 1:1 mol SiC-C mixture) as a function of temperature from different grain sizes mixtures in the high temperature range after the first de-oxidation step ($T > 1650\,\mathrm{K}$).

3.2.2.4 Characterization results

The powder samples obtained after vaporization experiments were analyzed for agglomeration, grain growth and interconnection of grains. Furthermore it was looked for the presence of silica in the treated samples.

3.2.2.4.1 Powders for different industrial use

Grain size measurement Table 3.4 lists the results of the grain size distribution measurements of initial powders. The d50 values were measured larger than listed in table 3.2 (p. 78) from the measurements performed after manufacturing. It can be explained by formed agglomerates from the fine powder grains, which was also seen by SEM imaging. Furthermore for powder B-HP a bimodal grain size distribution was observed.

Table 3.4: Measured distribution of grain size as d50, d90 and d10 of the different initial SiC powders used for the SiC-02m experiment.

Sample	d50 / μm	d90 / μm	d10 / μm
A-HP	0,66	16,2358	0,075
B-HP	1,24	9,67	0,22
C-abr	19,28	33,06	9,1341
D-abr	1,14	16,809	0,33

Raman spectroscopy Figures 3.21 and 3.22 show Raman spectra of powder samples B-HP and D-abr before and after the vaporization treatment. The upwards shifted initial spectrum of B-HP samples compared to its spectrum after the treatment is an indication of a better heat conduction in the sample after the vaporization experiment. The single grains must have built some conductive bridges due to the heat treatment. Indeed, the received energy from laser could then be evacuated through the sample material and not by Raman light emission like it is the case before the treatment.
The shift of initial D-abr spectrum (fig. 3.22) is low. Its good heat conduction before the vaporization treatment is quite surprising. From the table 3.2, which lists the impurities and trace elements in the sample powders, we can see that the D-abr powder has iron oxide impurity. This is the reason for its better energy conduction already before the treatment. Differences in the peak shapes show changes of the SiC polytypes due to the heat treatment. Furthermore carbon peaks are observed at 1500 and 1700 cm^{-1}.

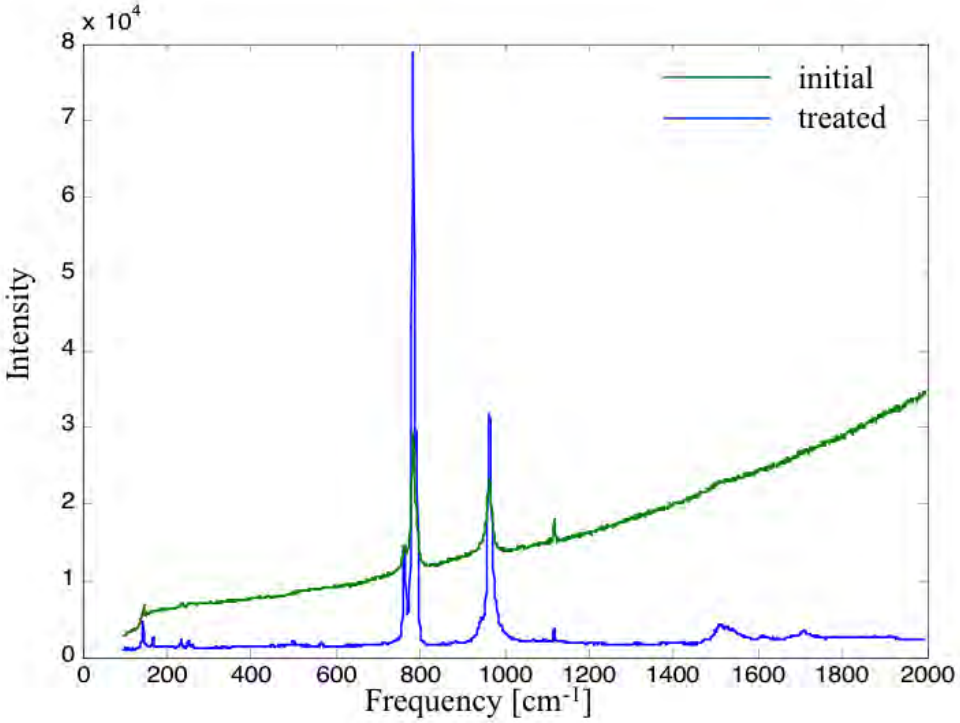

Figure 3.21: Raman spectra of B-HP initial sample powder before and after the vaporization up to 1760 K and heat treatment during the SiC-02m experiment.

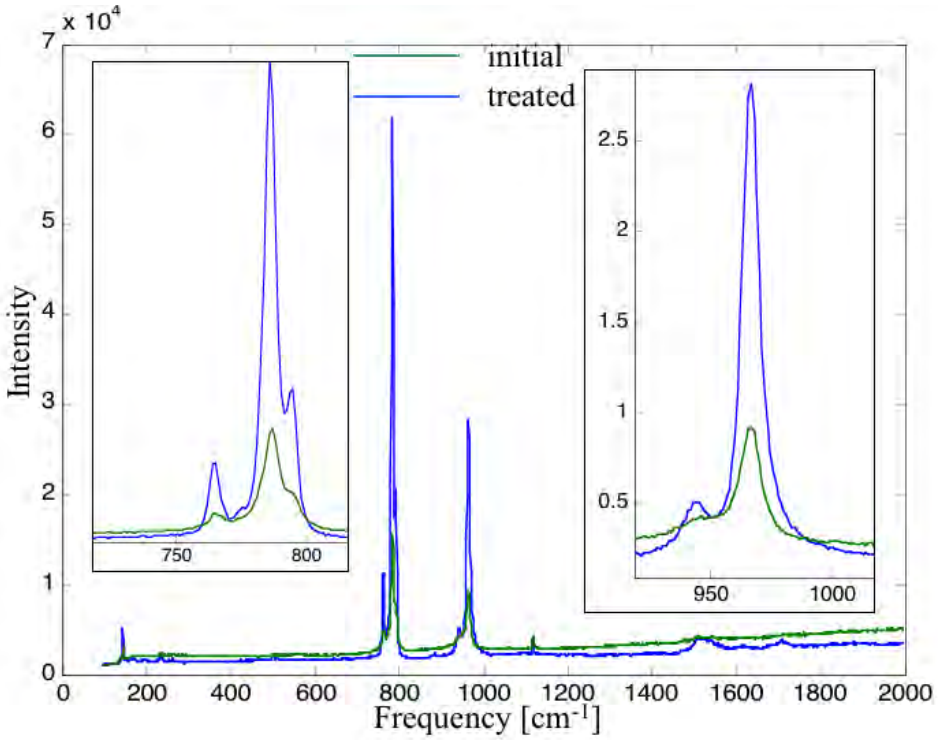

Figure 3.22: Raman spectra of D-abr initial sample powder before and after the vaporization up to 1760 K and heat treatment during the SiC-02m experiment.

SEM/FEG imaging Figure 3.23 shows the SEM images of A-HP, B-HP, C-abr and D-abr powders samples before and after the experiment. On the left side we can see the initial sample powders and on the right the same powders after the vaporization and heat treatment. We can see that the grains of all samples became at least rounded, the sharp edges disappeared. Very fine fractions have also disappeared and the next fine grains seem interconnected. After maximum temperature of 1700 K no more SiO_2 was observed in the high temperature mass spectrometer.
The B-HP sample, which has a bimodal grain size distribution as it was observed by grain size measurement, show several formed connections between clearly rounded grains after heat treatment (image d) of fig. 3.23).
D-abr sample had originally most Fe impurities. This powder has good thermal conduction already before the treatment as observed with Raman spectrometry. The SEM image g) of figure 3.23 show that the initial powder was also agglomerated. After the heat treatment (image h) fig. 3.23) the agglomerates can be still observed, but interconnections between the grains are also to observe.

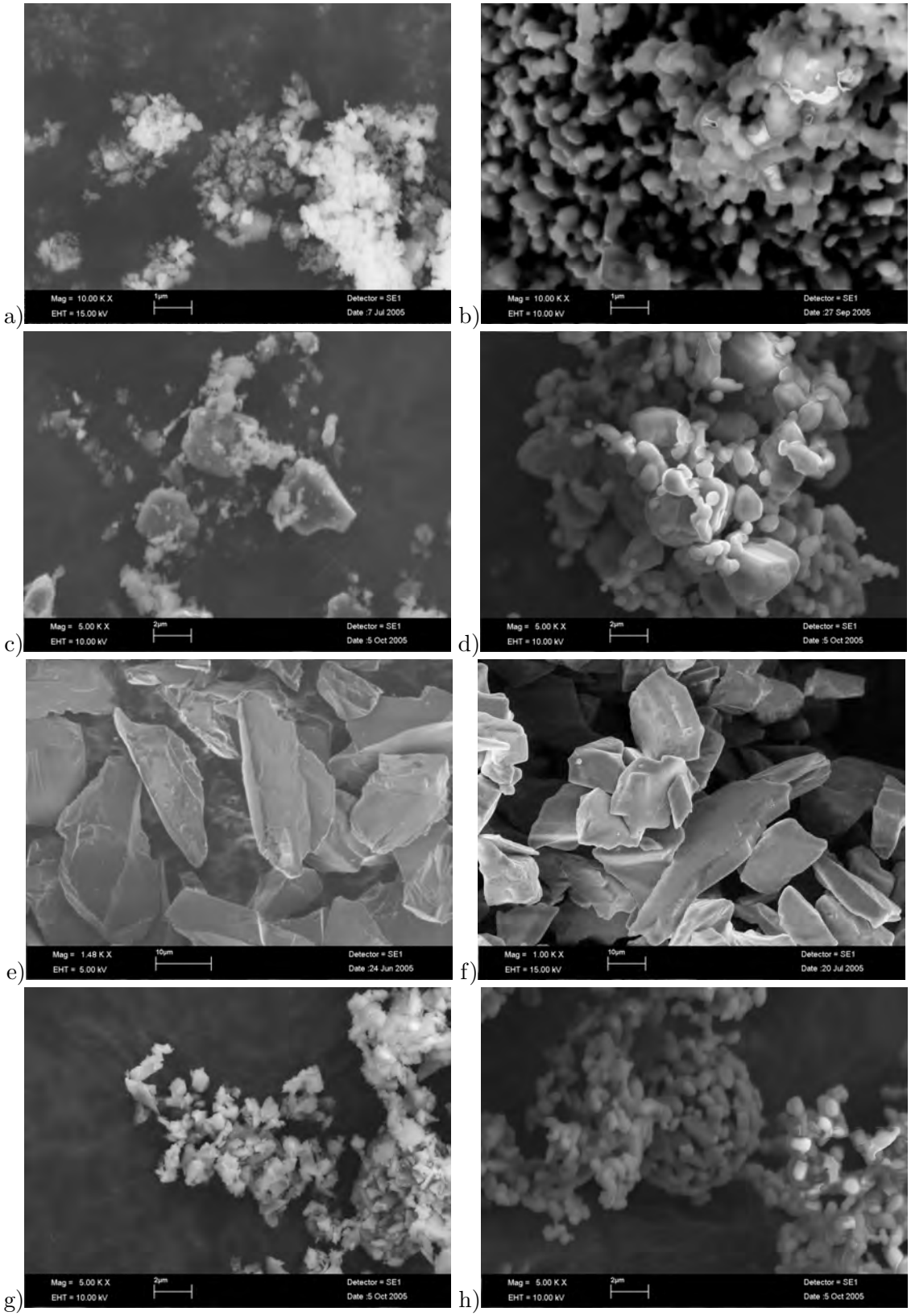

Figure 3.23: SEM images of sample powders for SiC-02m experiment. a) A-HP initial powder; b) A-HP after experiment; c) B-HP initial powder; d) B-HP after experiment; e) C-abr initial powder; f) C-abr after experiment; g) D-abr initial powder; h) D-abr after experiment

Summary The finer grained powders, A-HP, B-HP and D-abr have undergone most changes in the structure as shown at best by SEM imaging. The agglomerates, present in these powders already before the heat treatment, were not destroyed. The iron, present as impurity, improved the heat conduction through the powder already before the vaporization experiment. The grains of all samples became rounded due to the heat treatment and got visibly interconnected except from the most coarse sample C-abr ($d50 = 19,28\,\mu m$).

3.2.2.4.2 Different grain size SiC powders

Grain size measurement Figure 3.24 shows the grain size distribution of 0,5 μm powder sample obtained by sieving of an industrial SiC powder batch. Table 3.5 lists the measured values of d50, d90 and d10 of the different samples.
The measured value for the d50 on the 0,5 μm powder is clearly higher than it was intended to obtain by sieving the powders. The SEM image (fig. 3.25 a)) shows a lot of agglomerates of 10-13 μm size which is often the case for wet separation methods. It explains the grain size distribution diagram displayed in figure 3.24 where we can observe that the most of the grains were measured with 13 μm diameter. Usual granulometric measurement methods don't measure correctly the grain size of such fine grained powders. Only the SEM imaging can show the true grain size in these particular cases.

Table 3.5: Measured values for d50, d90 and d10 of the different grain sizes of initial SiC powder used for the SiC-05m experiment, measured with particle size analyzer CILAS 1064.

Sample label	d50 [μm]	d90 [μm]	d10 [μm]
0,5 μm	9,87	17,7	2,42
5 μm	3,55	6,97	0,71
10 μm	8,57	12,44	4,9
20 μm	19,46	27,52	12,75

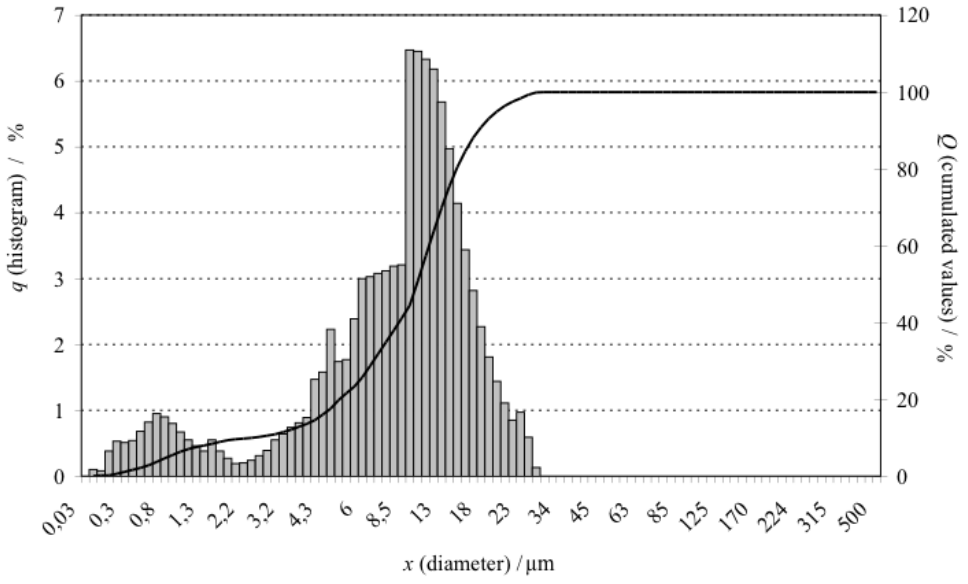

Figure 3.24: Granulometric grain size distribution of initial 0,5 μm powder.

SEM/FEG imaging Figure 3.25 shows the different grain size powders before and after the treatment. The maximum temperature reached during the experiment was 1900 K. No more SiO_2 departure was observed at this experiment state. The grains of all samples rounded. The initial samples 0,5 μm and 5 μm show a kind of poly-modal distributions, fine and coarse grain fractions can be observed. After the experiment the finest fraction of 0,5 μm sample disappeared, next small size grains have got interconnected and seem to include/inclose coarser grains in such formed network. Facets are observed on the coarse grains of the sample 5 μm, image d). The coarse grains are clearly connected to the fine grains. The coarsest powder sample lost only its sharp edges due to the heat treatment during experiment, images f) and h), and interconnections are not observed.

Summary All powders had reach the same stage of vaporization to the end of the high temperature mass spectrometer experiment. The agglomerates present already in the powders before the heat treatment remain and were not destroyed during vaporization experiment. In the most coarse powder with d50 = 20 μm no necks were observed contrarily to the samples with lower d50.
The question of the bridges formation is persisting. Assuming the interconnection formation only via vaporized Si(g) and Si_xC_y(g) we must consider, that the differences in the connections growth can come only from the grain size or morphology since the same partial pressure values of oxygen free species for all powders were measured.

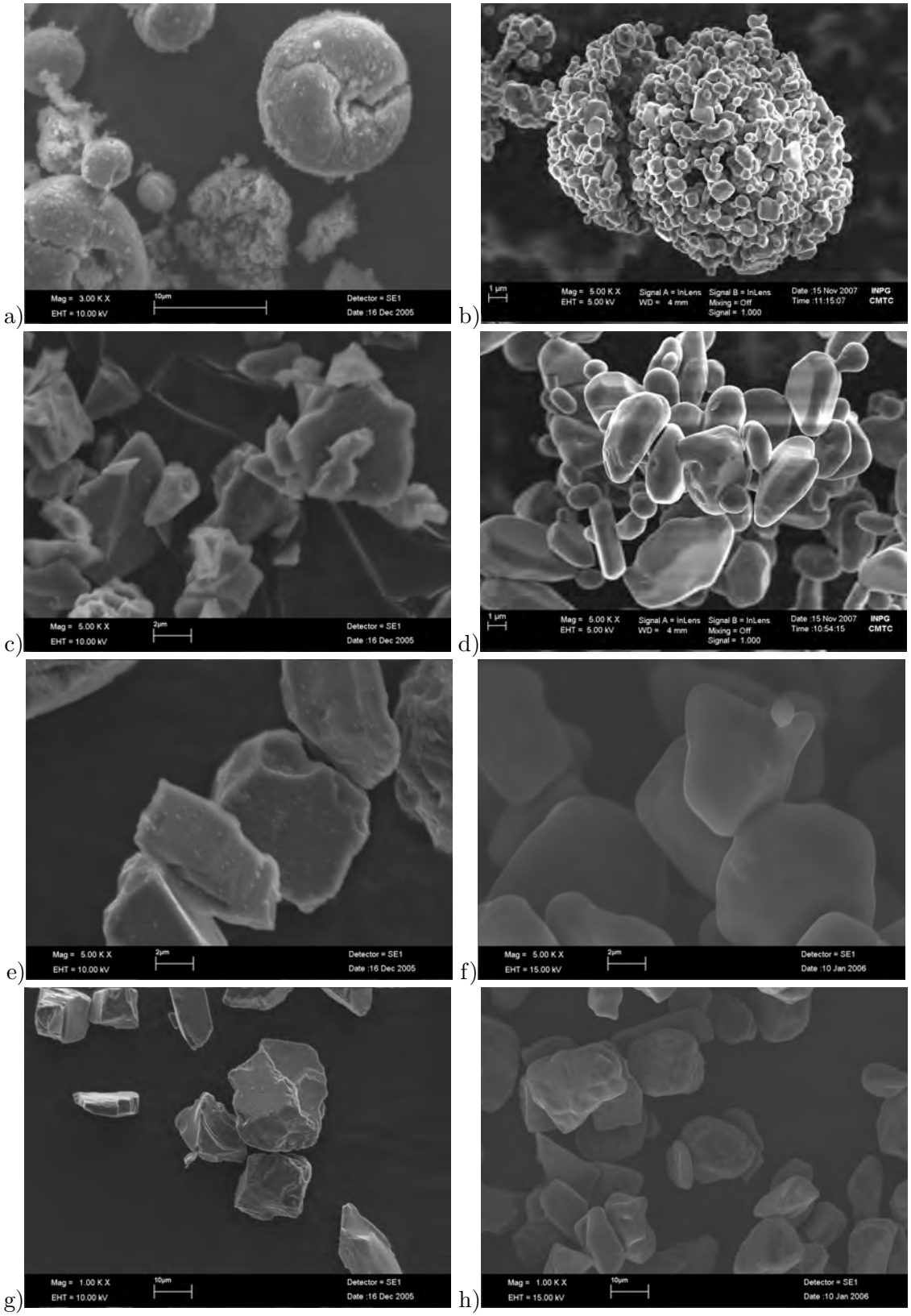

Figure 3.25: SEM images of the different grain sizes of SiC powder before and after the heat treatment in the HTMS: a) 0,5 μm initial powder; b) FEG image of 0,5 μm powder after experiment; c) 5 μm initial powder; d) FEG image of 5 μm powder after the SMHT; e) 10 μm initial powder; f) 10 μm powder after experiment; g) 20 μm initial powder; h) 20 μm powder after experiment.

3.2.2.4.3 Mixtures of different grain sizes SiC powder

Grain size measurement Grain size distributions of 0,5+5 μm and 0,5+10 μm bimodal SiC powder mixture samples were measured before and after vaporization experiment in the high temperature mass spectrometer.
Table 3.6 summarizes the results for measured d50, d90 and d10. As we can see initially different measured values got quite close after the heat treatment. The two samples became similar in view of grain size distributions.

Table 3.6: In laser particle size analyzer measured values for d50, d90 and d10 of the mixtures of 0,5+5 μm and 0,5+10 μm grain sizes of sieved SiC powder.

Sample		d50 [μm]	d90 [μm]	d10 [μm]
0,5+5 μm	initial	4,56	12,94	1,07
	treated	20,41	34,61	8,15
0,5+5 μm	initial	8,82	15	2
	treated	23,34	39,34	9,64

Figure 3.26 displays for instance the grain size distributions of 0,5+5 μm SiC powder mixtures. Image a) shows the grain size distribution of the samples before and b) after experiment. Initial grain size distributions of both mixtures, 0,5+5 μm and 0,5+10 μm were different and correspond to each coarse grain size initial mixture, but after experiment they become similar. The large initial grain size distribution of the 0,5+5 μm mixture become closer and the median grain size shifts to coarser size. Apparently the single grains have formed agglomerates/bridges.

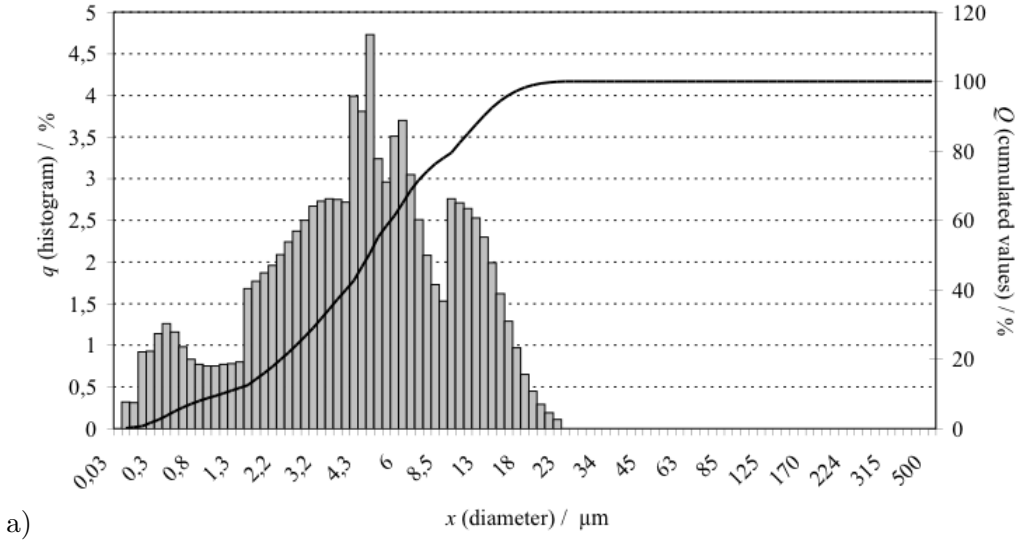

a)

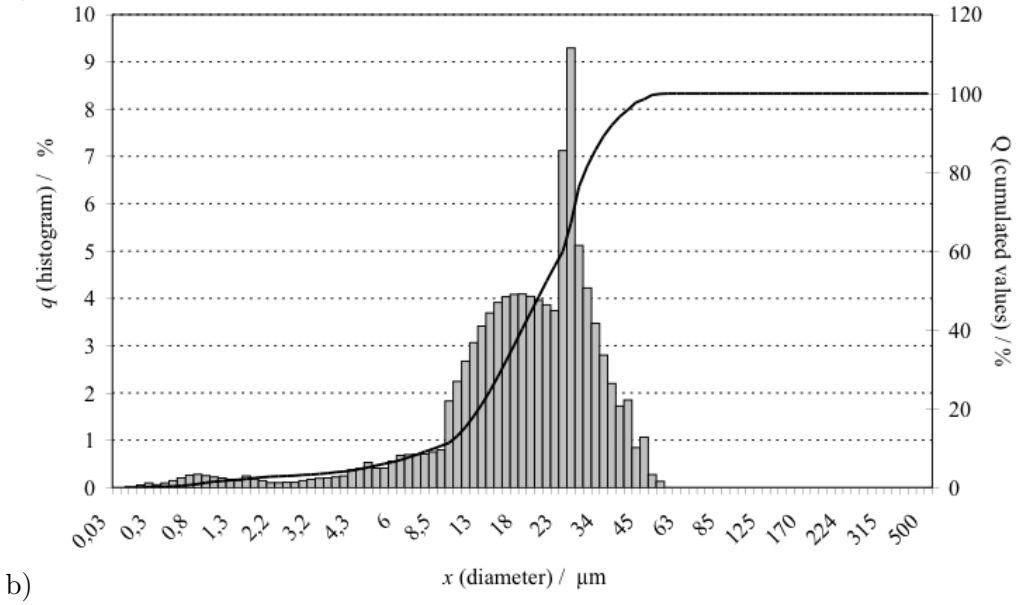

b)

Figure 3.26: Measured grain size distribution of the SiC powder 0,5+5 μm mixture a) before the vaporization experiment and b) after the vaporization experiment.

SEM/FEG imaging Figure 3.27, which displays FEG images of SiC mixtures and the reference mixture of SiC powder and graphite, confirms the formation of connections in both mixtures. Image a) shows the 0,5+5 μm mixture after the vaporization treatment and b) the 0,5+10 μm sample.
The images c) and d) show the reference powder, SiC mixed with graphite. SiC grains build clearly connections between them, although with graphite presence. These connections are different compared to the precedent images from the only SiC powders connections. They seem to be more compact, the grains being packed closer together compared to precedent images where a loose network of grains can be observed. This effect must be due to earlier de-oxidation of the SiC grains in the case of graphite presence. It means that bare SiC surfaces began earlier with vaporization of oxygen free species and created thicker connections compared to pure SiC powder mixtures. The whole necks formation process seems to have reached farther stage than observed for all other samples with only SiC powders initial mixtures.

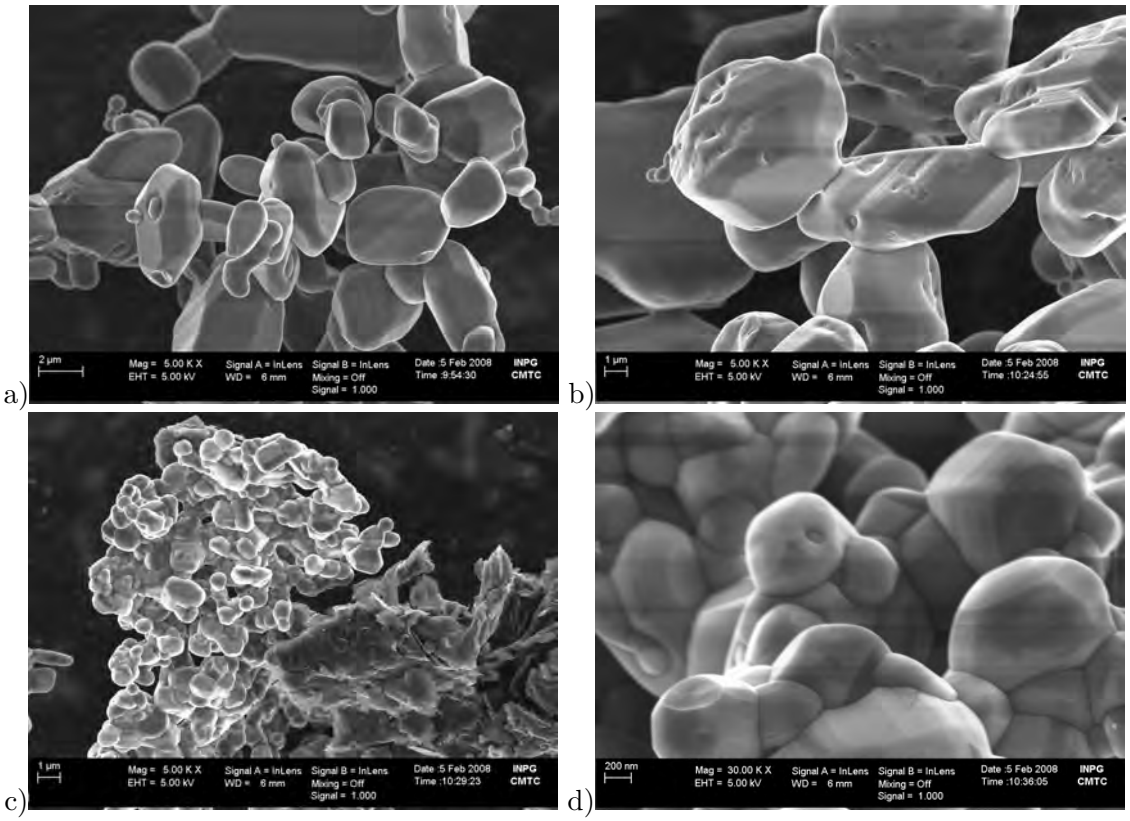

Figure 3.27: SEM images of different grain sizes powder mixtures after a vaporization experiment in the HTMS: a) 0,5+5 μm SiC mixture; b) 0,5+10 μm SiC mixture; c) 0,5 μm SiC and graphite mixture (reference); d) zoom onto SiC agglomerate of the reference powder.

Summary Two bimodal mixtures of SiC powders contain 70 mass% of coarse and 30 mass% of fine powder. The coarse powders are 5 μm and 10 μm and 0,5 μm grain size is the fine powder. These mixtures behaved similar during vaporization experiment, i.e. the emitted gaseous species had close partial pressure values. Their grain size distributions being different before the experiment became similar after the experiment. In both cases necks formation was observed.
The reference powder contained 50 mol% SiC powder of 0,5 μm and 50 mol% of graphite powder. In this reference powder the single SiC grains were also interconnected with larger connecting surfaces than for all other samples consisted of SiC powders only. The earlier de-oxidation has allowed the graphite containing sample to reach farther stage of necks formation.

3.2.2.5 Conclusion

First conclusions after in this part presented experiments are concerning vaporization in the diphasic system Si-C. We observed SiO(g) and CO(g) species for every SiC sample powder. This is an indicator for SiO_2 presence in all used SiC sample powders. Observed partial pressures of SiO(g) and CO(g) are always lower than calculated for thermodynamic equilibrium conditions for the triphasic Si-O-C. Following their vaporization must be kinetically limited. If we presume that the SiC powder grains are covered with a SiO_2 layer, the diffusion from the SiC-SiO_2 interface through this layer to the SiO_2 surface must be the above mentioned limiting factor. It is not clear yet if C^+ and O^- or CO are the diffusing species.
At certain moment the elimination of oxygen containing species (de-oxidation) was observed for all analyzed powders.
Experiment with different grain size SiC powders has shown differences in SiO(g) and CO(g) partial pressures: for smaller grain diameters higher partial pressures were observed. The reason is the difference in the evaporating surface which is larger for smaller grains compared to the same volume of grains with larger diameters.
The observations during the experiment with powder mixtures of different grain sizes have shown small difference in SiO(g) and CO(g) partial pressures. Both mixtures were made with 30 mass% of the fine 0,5 μm SiC powder. The partial pressure of oxygen containing species for the both samples is therefore controlled by this fine powder until the moment of oxygen elimination. For the graphite containing reference powder mixture with 50 mol% of graphite and 50 mol% of fine grained SiC powder this moment of de-oxidation was observed earlier than for the pure SiC powder samples. Indeed, graphite accelerated the oxygen departure from the sample producing more CO(g).
The presence of SiO(g) due to active oxidation of SiC with oxygen was observed after de-oxidation of samples. This oxygen was stored in the crucible walls and was released at $1600-1700$ K. Meanwhile SiO(g) remains constant, CO(g) is hidden by Si(g) vaporization. As it is known that CO(g) behaves in the same manner as SiO(g) it must remain also constant due to oxidation with oxygen stored in the sample surroundings.
After the departure of oxygen containing species the samples attain pure stoechiometric SiC domain. The measured pressures of Si(g), Si_2C(g) and SiC_2(g) are higher than calculated for the diphasic SiC-C, so we are sure that we didn't attain directly the diphasic SiC-C domain. Usually, these partial pressures decrease, because the carbon content increases in the solid phase due to not-congruent vaporization of Si. At that time, the partial pressures of

Si(g), Si_2C(g) and SiC_2(g) are the same for all SiC powder samples. Their vaporization does not depend on the vaporization surface, indirectly on the grain size, and the evaporation coefficient α is equal to 1.
Rocabois et al. [100] measured an evaporation coefficient for diphasic domain SiC-C equal to 0,05 because of a carbon layer, which make necessary the diffusion of Si gaseous molecules. With above observations for the other diphasic domain, Si-SiC, we can consider a similar mechanism: building of a silica layer on the SiC grains which retards vaporization of oxygen free gases because of necessity of diffusion. This phenomenon leads to lower partial pressures of Si(g), Si_2C(g) and SiC_2(g).
Concerning the moment when the SiC grains get bridges, partially we can say that this moment is surely not before the SiO_2 layer elimination. The surface of the SiC grains must be free of SiO_2 precipitation. Graphitization, meaning occurring of carbon on the SiC grain surface, stops the process of interconnection. But the presence of carbon in the samples, not located on the grain surfaces, seems not to disturb the necks building process, like it was observed in the experiment with graphite containing powder sample (reference). The graphite presence seem to favor the departure of silica scale from the grains and to prepare bare SiC surfaces earlier for the connections formation.
All initial powders contain different grain sizes within the allowed limits of distribution. We observed for all performed experiments with SiC powders that coarser grain fractions rounded, the fine grain fraction disappeared. The building of bridges was also observed but it is not clear on which stage of experiments it took place.
The powder with Fe_2O_3 impurity has shown a better thermal conduction before treatment (observed by Raman spectrometry) and built more interconnections after the heat treatment.

3.2.3 Si-C-O vaporization behavior

We have seen in the previous section that SiC exists always as pseudo-binary SiC-SiO_2. SiC, being a Si containing compound, build always a layer of SiO_2 at its surface. Addition of shaping agents and calcination steps in industrial processes can be another source of the SiO_2 which forces us to analyze also the ternary Si-C-O system to complete the silicon carbide study.
Vaporization behavior of SiC powder mixed with different amounts of SiO_2 powder, from 66 to 0,5 mol%, was analyzed. Furthermore the influence of SiO_2 as added powder and as added oxidation layer was compared. Also the influence of the container material was tested.

3.2.3.1 Choice of the samples

For the study of vaporization behavior of Si-C-O, more exactly SiC-SiO_2 pseudobinary, we mixed SiC and SiO_2 powders. We used the finest (d50 $= 0,5\,\mu$m) SiC powder already described, with impurities and trace elements given in table 3.1 (p. 77). The SiO_2 powder is the Degussa Sipernat 350. Table 3.7 lists its characteristics. As it is seen from table 3.7 the principal impurity of this SiO_2 powder is Na_2O. It means that this impurity will lead to Na(g) vaporization. As it vaporizes at lower temperatures and is the only isotope at mass 23 we used it for the initial set up of the mass spectrometric experiments.

Table 3.7: Degussa Sipernat 350 characteristics.

d50 [μm]	Na_2O [%]	Fe_2O_3 [%]	SO_3 [%]
4,5	0,8	0,03	0,2

Any SiO_2 powder is known to keep crystallized water in its structure. To remove this water the SiO_2 powder was heated until 900°C within 1,5 hours and treated during 10 hours. After such treatment the powder was kept in a desiccator.
For the experiments performed with powder mixtures the necessary amounts of SiO_2 and SiC powders were lightly mixed and put in a tubula rotator for minimum 3 hours. Bigger agglomerates were broken in a mortar.
In order to observe some difference of vaporization behavior for added SiO_2 either as powder or as an oxidation layer on the SiC grains, an experiment with the sieved SiC 0,5 μm powder previously oxidized for different times at 900°C in presence of water vapor was performed.

3.2.3.2 Performed experiments

Table 3.8 lists performed experiments for the vaporization of SiC-SiO_2 mixtures.
Experiments were also performed to investigate influence of the sample container material on the vaporization behavior. For this reason we used dense graphite and quartz cellss with the same geometry as shown in figure 3.2 (p. 60). As reference we used tantalum cell. In the same series of experiments a forth cell (made from tantalum) with 3,1 mm orifice diameter was used in order to measure the evaporation coefficient.
Table 3.9 lists the performed experiments with different crucible materials and different orifices for evaporation coefficient measurement.

Table 3.8: Multiple cell experiments performed for Si-O-C vaporization. Different SiO_2 content in Ta Knudsen cells with 2 mm diameter orifice.

Experiment label	SiO_2 amount	T_{max} [K]	Gaseous molecules observed
SiC-SiO_2-06m	15, 30, 45 and 66 mol%	1658	Na, SiO and CO
SiC-SiO_2-07m	2, 5, 10 and 15 mol%	1702	Na, SiO and CO
SiC-SiO_2-17m	Au reference 2, 1 and 0,5 mol%	1624	SiO and CO
SiC-SiO_2-08m	SiC oxidized for 3, 10 and 30h and 15 mol%	1576	SiO and CO

Table 3.9: Multiple cell experiments performed for Si-O-C vaporization with different crucibles.

Experiment label	SiO_2 amount	Crucibles material and orifice diameters	T_{max} [K]	Gaseous molecules observed
SiC-SiO_2-09m	15 mol%	Ta, Quartz or Graphite (2 mm) and Ta (3,1 mm)	1626	Na, SiO and CO
SiC-SiO_2-10m	5 mol%		1708	
SiC-SiO_2-11m	66 mol%		1626	
SiC-SiO_2-13m	45 mol%		1663	

3.2.3.3 Experimental results

Partial pressures of SiO(g) and CO(g) were measured with increasing temperature. In order to prevent field aperture orifice clogging with the products of vaporization the temperature increase was limited and several data points were taken with decreasing temperature. Only SiO(g) and CO(g) partial pressures were measured. Partial pressures of oxygen free silicon based gaseous species are too low in the concerning temperature range to be detected with high temperature mass spectrometer.

3.2.3.3.1 Different SiC-SiO_2 mixtures Vaporization behavior of SiC-SiO_2 mixtures with different contents of SiO_2 powder, from 0,5 mol% to 66 mol%, were analyzed.
Figures 3.28 and 3.29 show decimal logarithms of partial pressures of SiO(g) and CO(g) for samples with 15, 30, 45 and 66 mol% of SiO_2 as a function of the inverse of temperature. The last three values taken with decreasing temperature are located on a trendline parallel to those of earlier values, measured with increasing temperature. This can have two reasons: the diameter of the field aperture (see fig. 3.1 p. 59) had decreased because of deposited vapor products, or the sample powders were depleted in the vapor species supply. The

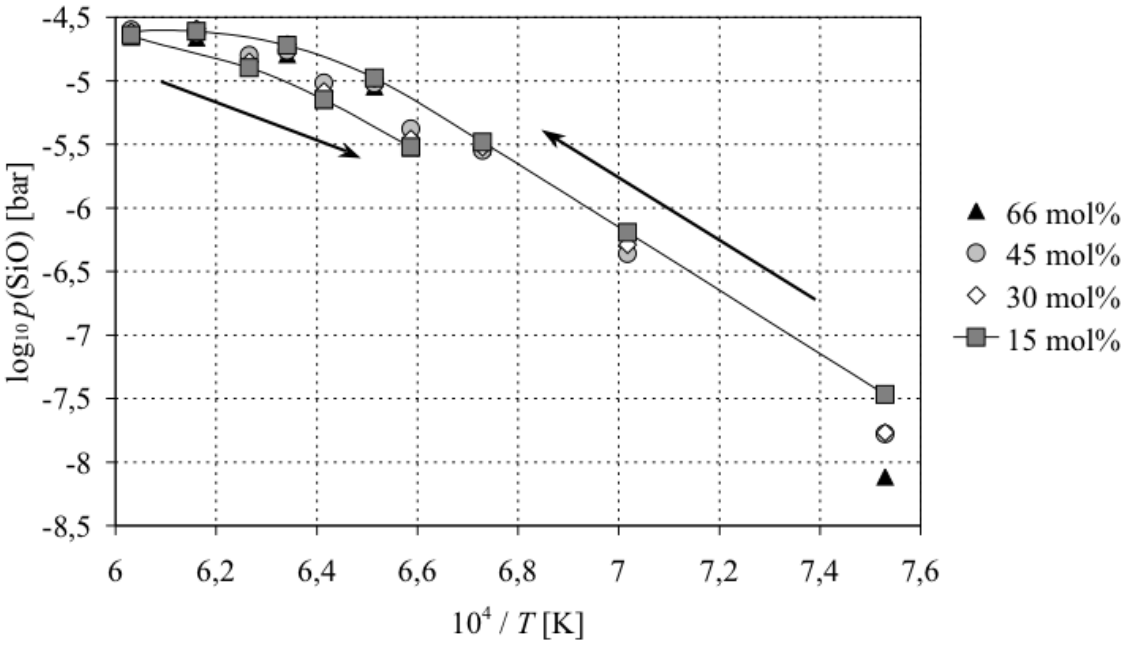

Figure 3.28: Decimal logarithm evolution of SiO partial pressures for SiC-SiO_2 mixtures with high SiO_2 content as a function of the inverse of temperature. Arrows show the evolution with time.

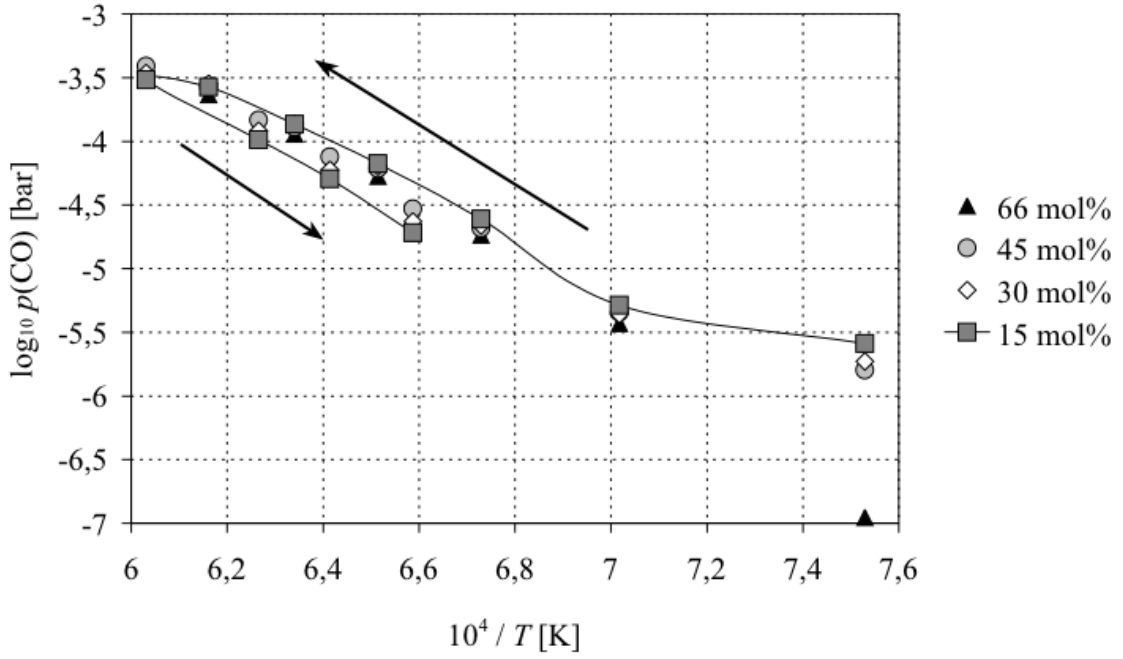

Figure 3.29: Decimal logarithm evolution of CO partial pressures for SiC-SiO_2 mixtures with high SiO_2 content as a function of the inverse of temperature.

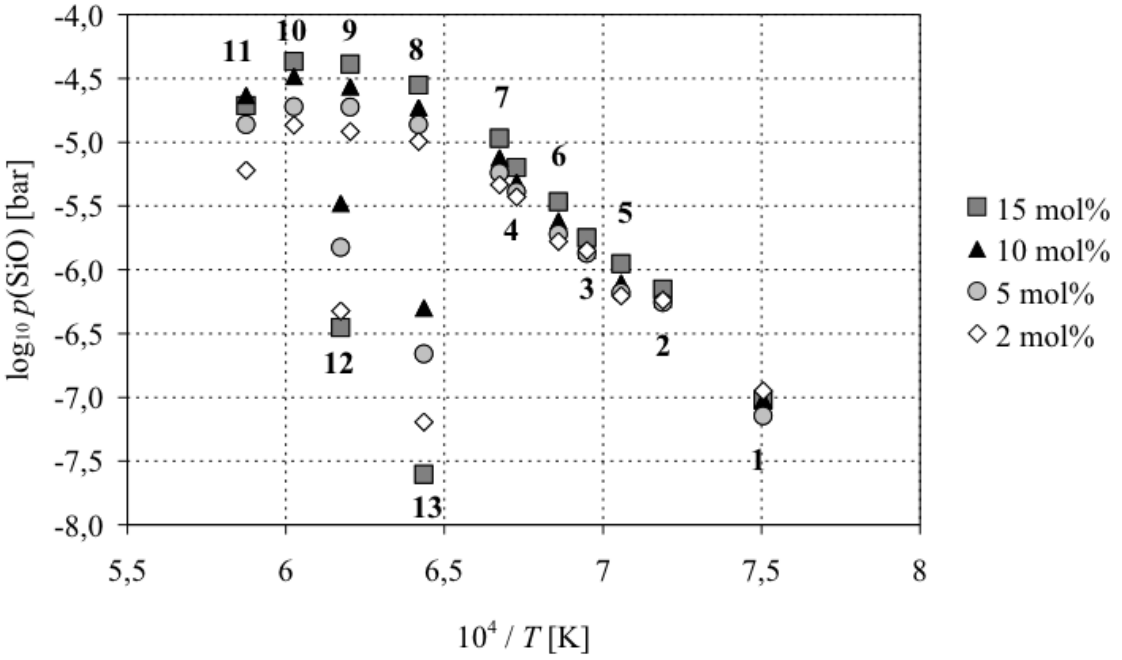

Figure 3.30: Decimal logarithm evolution of SiO partial pressures for SiC-SiO_2 mixtures with low SiO_2 content as a function of the inverse of temperature.

second case we have called powder aging. Checking powder aging is only possible with a stable reference like gold or platinum in one of the cells of multiple cell device. For pseudo-binary compositions between 15 and 66 mol%, both graphs for p(SiO) and p(CO) have very similar forms. The p(CO) is higher than p(SiO) and there are no significant pressure differences for different samples as predicted for thermodynamics. Figures 3.30 and 3.31 show logarithms of partial pressures of SiO(g) and CO(g) of the samples with SiO_2 contents from 2 to 15 mol%. Like for the higher SiO_2 loaded samples the evolution differences in the graphs for SiO(g) and CO(g) partial pressures is small. The CO(g) partial pressure values are still higher than the SiO(g) one's.
First monitored values 1 to 4 at figure 3.31 seem to follow a different evolution than the values 5 to 8 for p(CO) and this is an indicator for a change in the samples. The temperature range for these data is the same as for the impurities elimination like Na_2O as we can see in figure 3.32. The Na(g) partial pressure decreases visibly until the temperature of 1540 K ($= 6,5 \cdot 10^{-4}\,\mathrm{K}^{-1}$). This Na(g) vaporization must interfere with the CO(g) vaporization according to the main vaporization reaction:

$$\mathrm{Na_2O(s.\,s.\ in\ SiO_2)} = 2\,\mathrm{Na(g)} + 1/2\,\mathrm{O_2(g)} \tag{3.13}$$

with

$$\mathrm{O_2(g)} + 2\,\mathrm{C(s.\,s.\ in\ SiC)} \longrightarrow \mathrm{CO(g)} \tag{3.14}$$

and finally

$$\mathrm{Na_2O(s.\,s.)} + \mathrm{C(s.\,s.)} = \mathrm{CO(g)} + 2\mathrm{Na(g)}. \tag{3.15}$$

The Na_2O vaporization does not seem to have a significant influence on the SiO(g) vaporization as seen in fig. 3.30.

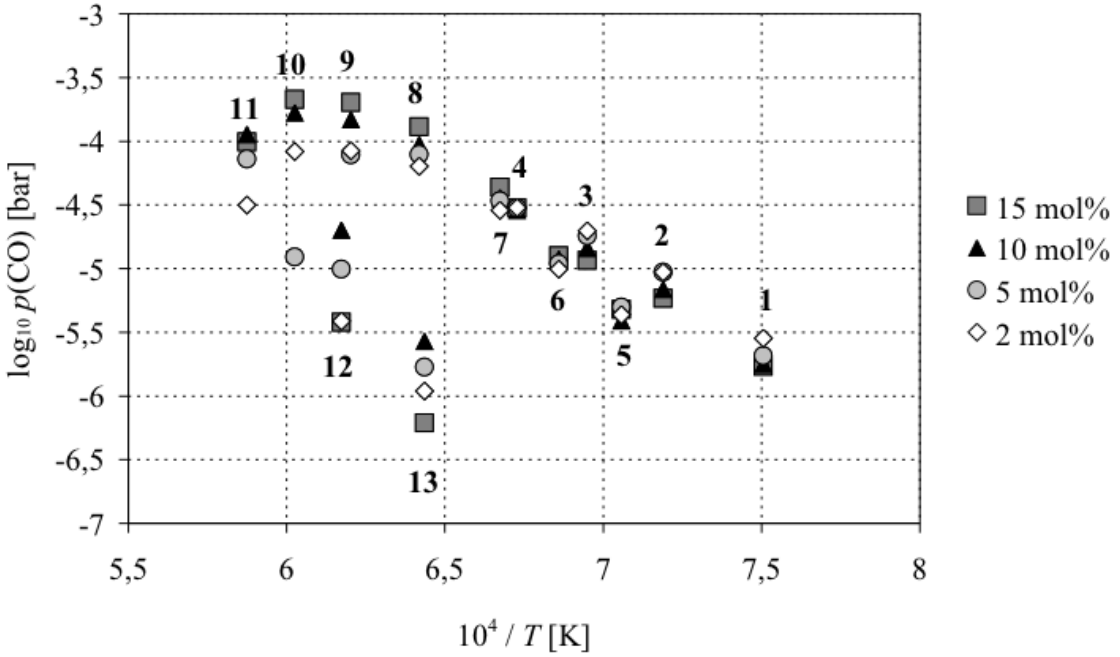

Figure 3.31: Decimal logarithm evolution of CO partial pressures for SiC-SiO_2 mixtures with low SiO_2 content as a function of the inverse of temperature.

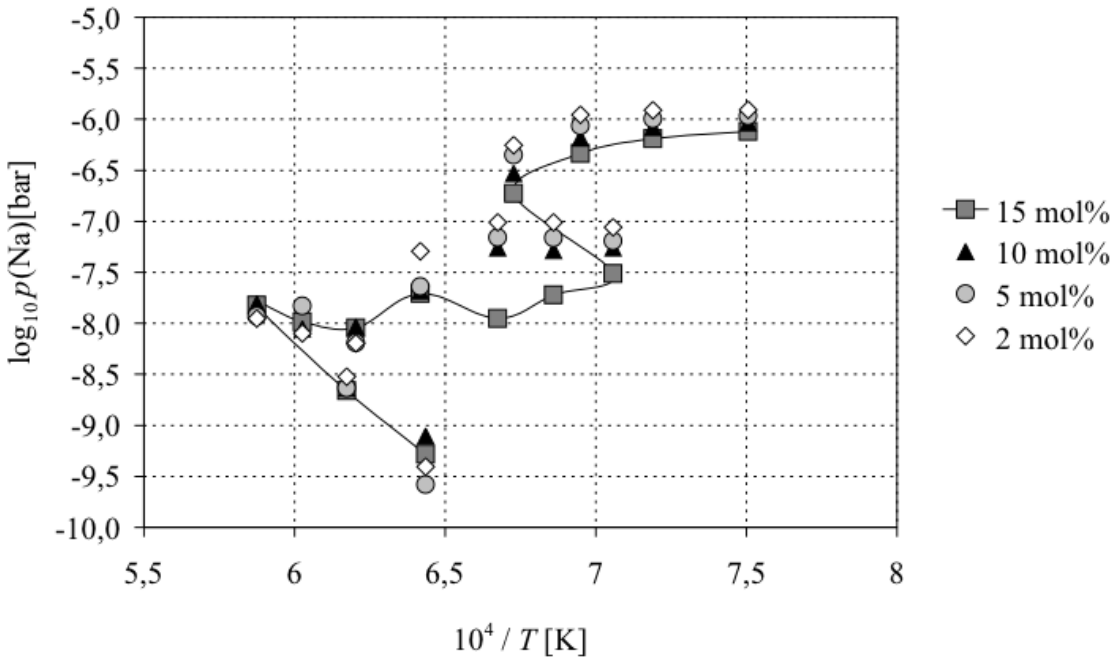

Figure 3.32: Evolution of the decimal logarithm of Na(g) partial pressures for SiC-SiO_2 mixtures with low SiO_2 content, 15, 10, 5 and 2 mol%, as a function of the inverse of temperature.

Comparing to higher SiO_2 loaded samples there is more difference in partial pressure values for samples with low SiO_2 content. At high temperature, each sample produces different amount of SiO(g) and CO(g). This behavior does not agree with thermodynamics. The generally lower values in the last sequence, when temperature decrease, seem to be caused by the powder aging and the composition with 15 mol% seems to undergo most change.
Some difficulties occurred in mass spectrometer set up during the experiment for very low SiO_2 contents—2 to 0,5 mol%—and determination of the absolute values of partial pressures of SiO(g) and CO(g) was not possible. Gold in a graphite cell served as reference. With this reference we checked if the lowering of partial pressures at the end of experiments when decreasing temperature is due to clogging of the field aperture orifice or to aging of the powders. It was found that powder aging was responsible for lower partial pressure values at the end of experiments. Figures 3.33 and 3.34 show the logarithm of intensity-temperature

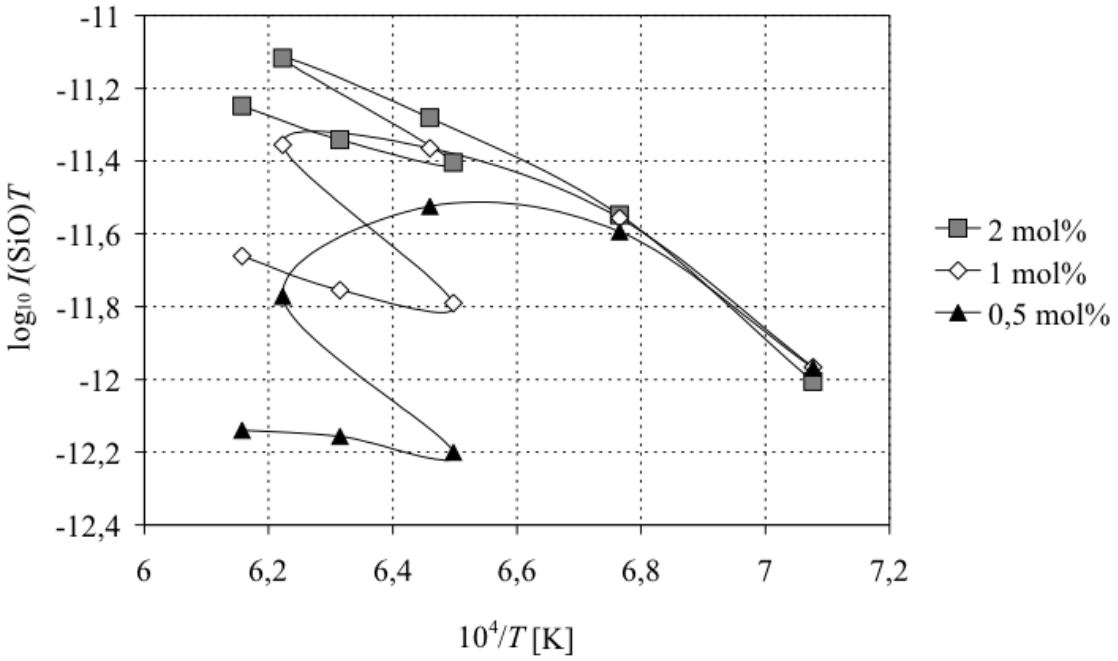

Figure 3.33: Evolution of the decimal logarithm of $I(\mathrm{SiO}) \cdot T$ for SiC-SiO_2 mixtures with 2, 1 and 0,5 mol% SiO_2 content as a function of the inverse of temperature.

products ($\sim$ partial pressures) as a function of the inverse of temperature. The values were corrected for mass spectrometric sensitivity evolution with the help of gold reference. The product is proportional to partial pressure of the measured species, so we can compare the samples between each other and speak about partial pressures.
The SiO(g) values (figure 3.33) are not very different for different samples until 1481 K ($6,75 \cdot 10^{-4}\,\mathrm{K}^{-1}$). In the last stages of the experiment the sample with less SiO_2 content undergoes most changes.
The CO(g) partial pressures behave a few differently than SiO(g) one's (fig. 3.34). In the last stage when temperature decreases the pressure values increase again when increasing temperature. This is due to the beginning of Si(g) vaporization.
The ratio $p(\mathrm{CO})/p(\mathrm{SiO})$ is still smaller than 1, $p(\mathrm{CO})$ being higher than $p(\mathrm{SiO})$.
The aging of samples is proportional to SiO_2 content. It is most pronounced with small

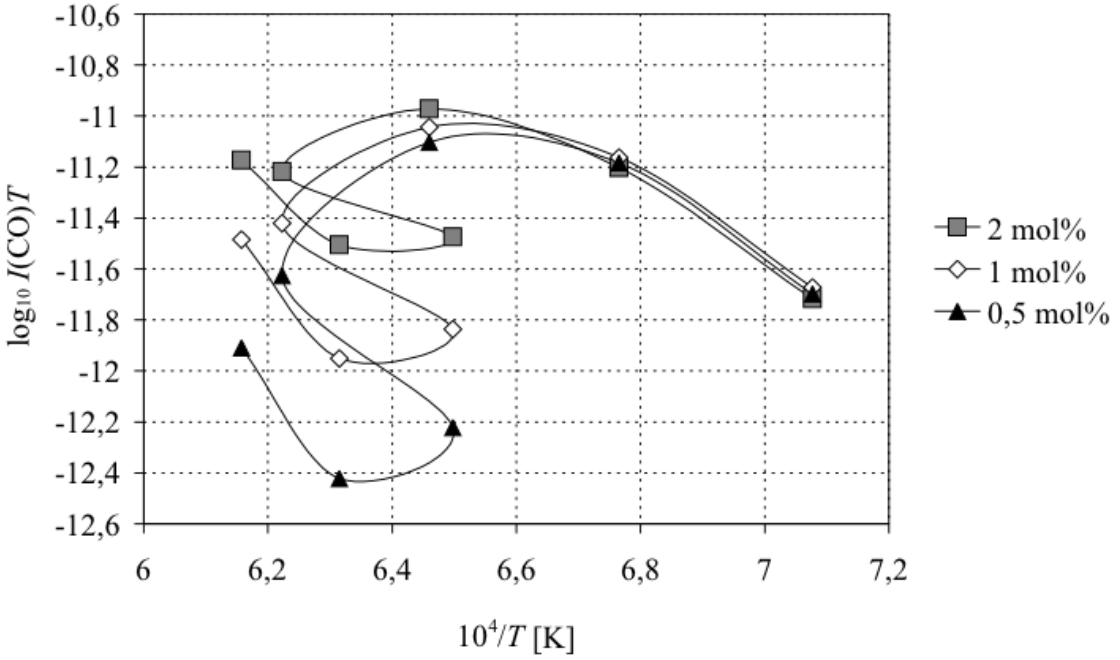

Figure 3.34: Evolution of the decimal logarithm of $I(\mathrm{CO}) \cdot T$ for SiC-SiO_2 mixtures with 2, 1 and 0,5 mol% SiO_2 content as a function of the inverse of temperature.

amounts of SiO_2 and only little or not at all for high SiO_2 contents in SiC powders. The aging can be caused by decrease of specific surface due to elimination of fine grain fraction and rounding of coarser grains. Another possible and more likely reason is the SiO_2 depletion in the sample powder bed.
Figure 3.35 is a result from experiments with powder mixtures of SiC and SiO_2. It shows the ratios of SiO(g) and CO(g) partial pressures referenced to 15 mol% sample as a function of SiO_2 amount in the samples. The graph is isotherm with $T = 1625\,\mathrm{K}$. From the 66 mol% until the reference value of 15 mol% both gaseous species show similar trend, the partial pressure or intensity ratios are situated in 0,9 to 1,1. The maximum is located within the composition range of 30-45 mol%. From 15 mol% only SiO(g) ratios have a regular trend. The CO(g) pressure ratios seem to freeze at 0,3 for mixtures with SiO_2 amount lower than 5 mol%. When the initial SiO_2 amount is low the Si(g) interferes with the CO(g) measurements (same mass 28 for CO(g), N_2 and Si(g)) at higher temperatures. The SiO(g) the partial pressure ratio decreases with decrease of SiO_2 amount in the samples.
The existence of a maximum in the figure 3.35 does not agree with the thermodynamics. For the congruent vaporization according to reaction:

$$\mathrm{SiC(s)} + 2\mathrm{SiO_2(s)} = 3\mathrm{SiO(g)} + \mathrm{CO(s)},$$

a gaseous phase of constant composition and pressure is predicted for a fixed constant temperature, independent of the composition of condensed phase. This irregularity may come from the influence of kinetic limitations, such as diffusion phenomena, between the reacting SiC and SiO_2 powder grains on the vaporization rate.
Summarizing the experiments with different SiC-SiO_2 sample compositions, the partial pressures of SiO(g) and CO(g) depend on the samples composition with maximum for

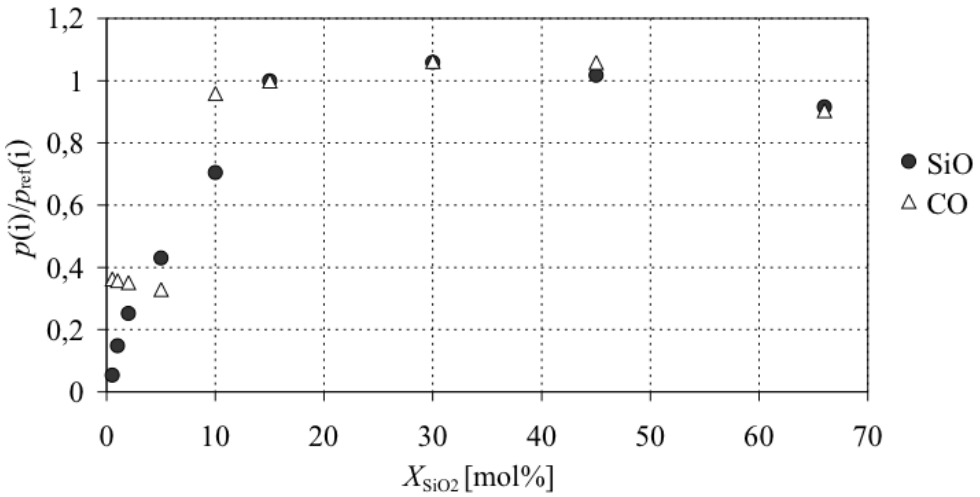

Figure 3.35: Relative partial pressures of SiO(g) and CO(g) as a function of powder composition of different samples referenced to 15 mol% at 1625 K.

SiO_2-contents between 30 and 45 mol%. The SiO(g) and CO(g) partial pressures are lower than the calculated equilibrium values for pseudo-binary SiC-SiO_2 system. The pressures ratio of SiO(g) to CO(g) is always lower than 1.

3.2.3.3.2 Oxidized SiC powders In this paragraph the results from the experiment with oxidized powders are described. Sample with mixed 15 mol% SiO_2 and SiC was taken as reference. Powders oxidized during different times are presumed to have different SiO_2 layer thickness. We looked for difference in vaporization behavior compared to powder mixtures and for its relation to scale thickness.

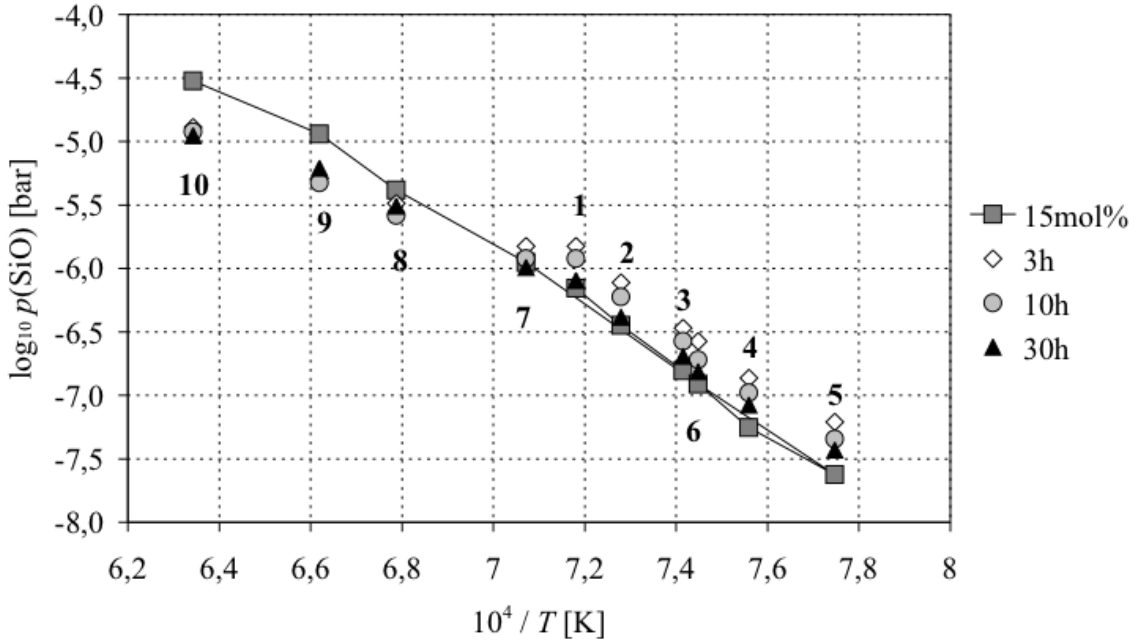

Figure 3.36: Evolution of decimal logarithm of SiO(g) partial pressures as a function of the inverse of temperature for oxidized SiC powders during the experiment.

Figures 3.36 and 3.37 show measured SiO(g) and CO(g) partial pressures decimal logarithm respectively as a function of the inverse of temperature. Looking on the graphs we can distinguish two temperature regions. The slope of the SiO(g) and CO(g) partial pressures changes at $T \approx 1350\,\mathrm{K}$. It is an indication for a structural change and concerning the SiO_2 layer a transition from high quartz to high cristobalite fits to the temperature region ($1079 \pm 250\,\mathrm{K}$ [5]).
In the low temperature region ($T < 1400\,\mathrm{K}$) every sample show different SiO(g) and less different CO(g) partial pressures. For $T > 1400\,\mathrm{K}$ there are no more differences in SiO(g) and in CO(g) partial pressures.
The reference sample, SiC with 15 mol% SiO_2 powder mixture, does not attain the state of powder aging at the final temperature. Furthermore it does not show any slope changes. It is confirmed as good reference.
The partial pressures of SiO(g) and CO(g) are still lower than the calculated ones for the pseudo-binary SiC-SiO_2 section according to the main vaporization reaction:

$$\mathrm{SiC(s)} + 2\mathrm{SiO_2(s)} = 3\mathrm{SiO(g)} + \mathrm{CO(s)}.$$

This behavior is due to the net evaporation coefficients α(SiO) and α(CO), which are equal 1 at equilibrium and lower than 1 when the vaporization process is kinetically hindered, and which depend on the temperature. The diffusion process through the formed SiO_2 layer on the SiC grains caused retarded vaporization.

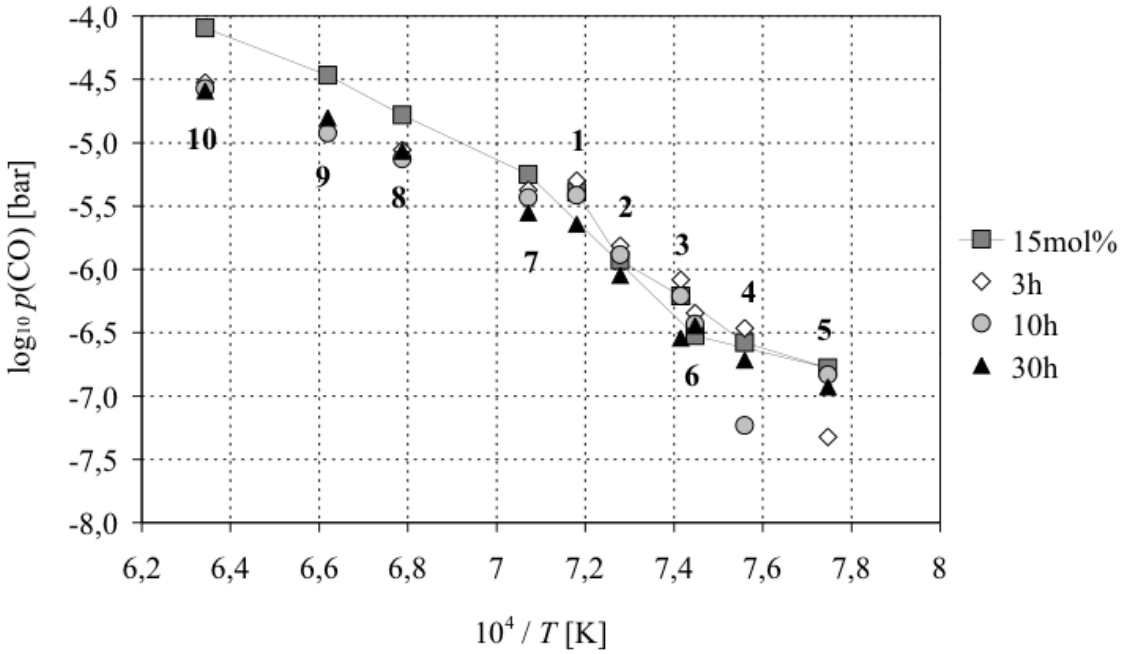

Figure 3.37: Evolution of decimal logarithm of CO(g) partial pressures as a function of the inverse of temperature for oxidized SiC powders during the experiment.

The ratio of p(SiO) to p(CO) is still much lower than 3 and the vaporization appears not congruent, like we have already seen for the powder mixtures (ratio $\leqslant 1$).

3.2.3.3.3 Different crucible materials In this part the results from the experiment series aimed to study the influence of different crucible material on the measured SiO(g) and CO(g) partial pressures are presented. Moreover the evaporation coefficients of SiO(g) and CO(g) were measured.
Four experiments were performed with samples of 5, 15, 45 and 66 mol% SiO_2 content. Powder samples of same composition were placed in three standard cells, made from dense graphite, quartz and tantalum (as reference), with orifice dimensions of 2×2 mm (diameter $\times$ height) for direct comparison of partial pressures from each cell. The fourth cell, loaded with same sample like the other three, had orifice dimensions of $3,1 \times 3$ mm and was made from tantalum. It served to measure the evaporation coefficient.

Partial pressures Figures 3.38 and 3.39 show the logarithms of SiO(g) and CO(g) partial pressures respectively as a function of the inverse of temperature for different SiO_2-SiC powders mixtures.
Tantalum and quartz containers seem quite neutral in the vaporization of SiO(g) and CO(g). Quartz container shows the same behavior as tantalum whatever is the sample composition. The CO(g) does not react with the quartz vessel.
The graphite container increase CO(g) partial pressure for all compositions. It appears detrimental to SiO(g) partial pressure for composition with low SiO_2 content (5 mol%). When the SiO_2 content is more important, the reaction of SiO(g) with C does not have any effect on the SiO(g) partial pressure.

Evaporation coefficient In the preliminary experiments we observed that the measured partial pressures never attain the calculated equilibrium values. This means vaporization is controlled by kinetics. Evaporation coefficient is an expression for kinetic vaporization limitation. For this reason two cells with the same sample and from the same material with different orifices, 2×2 and $3,1 \times 3$ mm (diameter $\times$ height) were used to measure this coefficient according to the method developed by Heyrman [94]. Table 3.10 lists obtained sets of condensation and evaporation coefficients. The values of the evaporation coefficients show that some kinetic limitations occur during the vaporization reaction, but they don't say anything about the mechanism of these kinetic limitations.

Table 3.10: Evaporation coefficients of SiO(g) and CO(g) of samples with different amount of SiO_2.

SiO_2 amount [mol%]	T range [K]	α(SiO)	α(CO)
5	1317–1708	$(4,73 \pm 2,9) \cdot 10^{-4}$	$(3,52 \pm 3,75) \cdot 10^{-2}$
15	1309–1626	$(1,56 \pm 0,38) \cdot 10^{-3}$	$(1,19 \pm 1,34) \cdot 10^{-1}$
45	1447–1612	$(2,4 \pm 0,68) \cdot 10^{-3}$	$(1,75 \pm 5,1) \cdot 10^{-1}$
66	1369–1626	$(7,61 \pm 24,6) \cdot 10^{-1}$	$(-1,06 \pm 0,81) \cdot 10^{-1*}$

*these values are not meaningful and correspond probably to large uncertainties in individual measurements

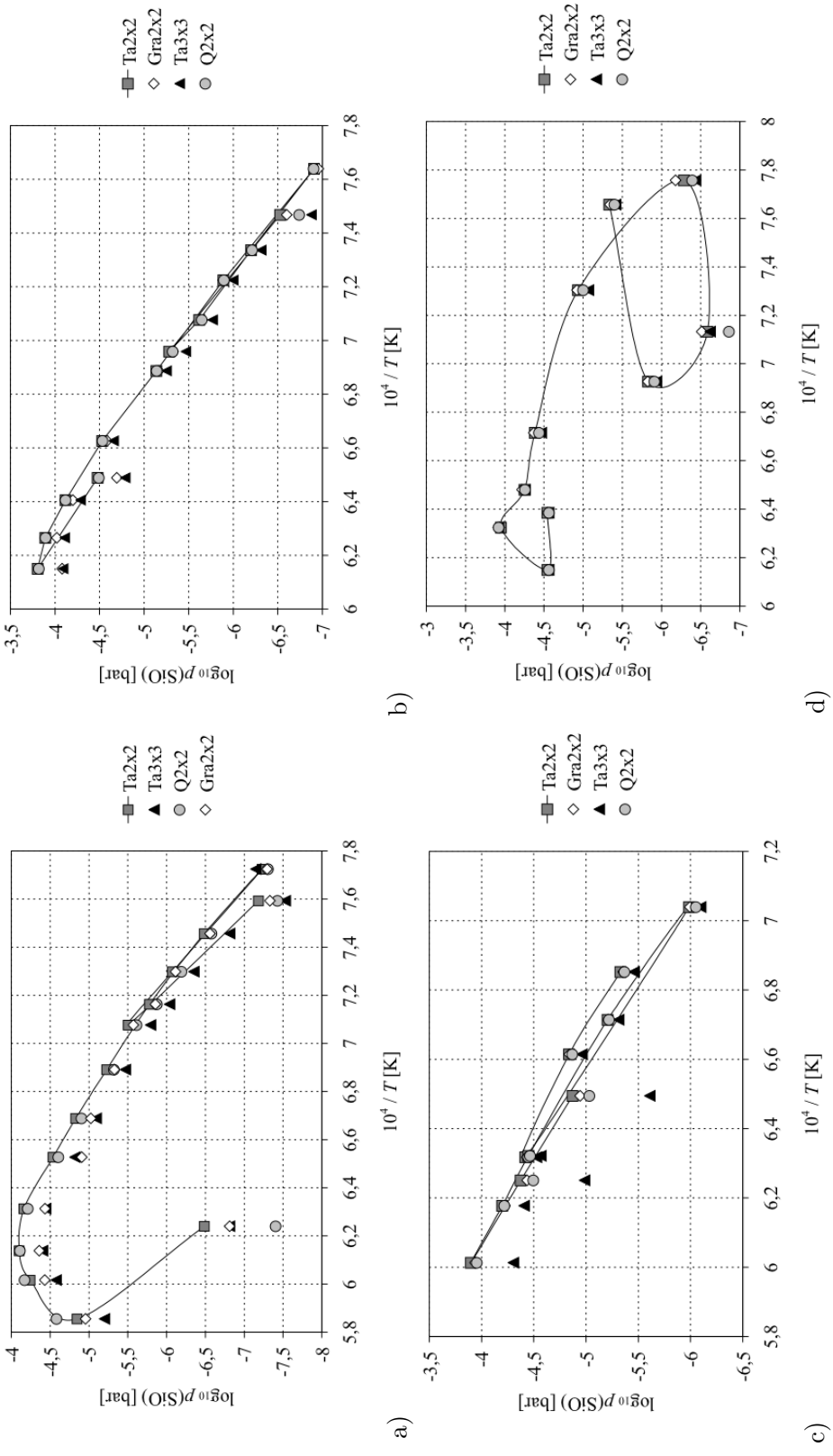

Figure 3.38: Evolution of decimal logarithm of $p(\mathrm{SiO})$ as a function of the inverse of temperature for SiC-SiO_2 powder mixtures placed in cells made from tantalum (Ta), quartz (Q), graphite(G): a) 5 mol%; b) 15 mol%; c) 45 mol%; d) 66 mol%.

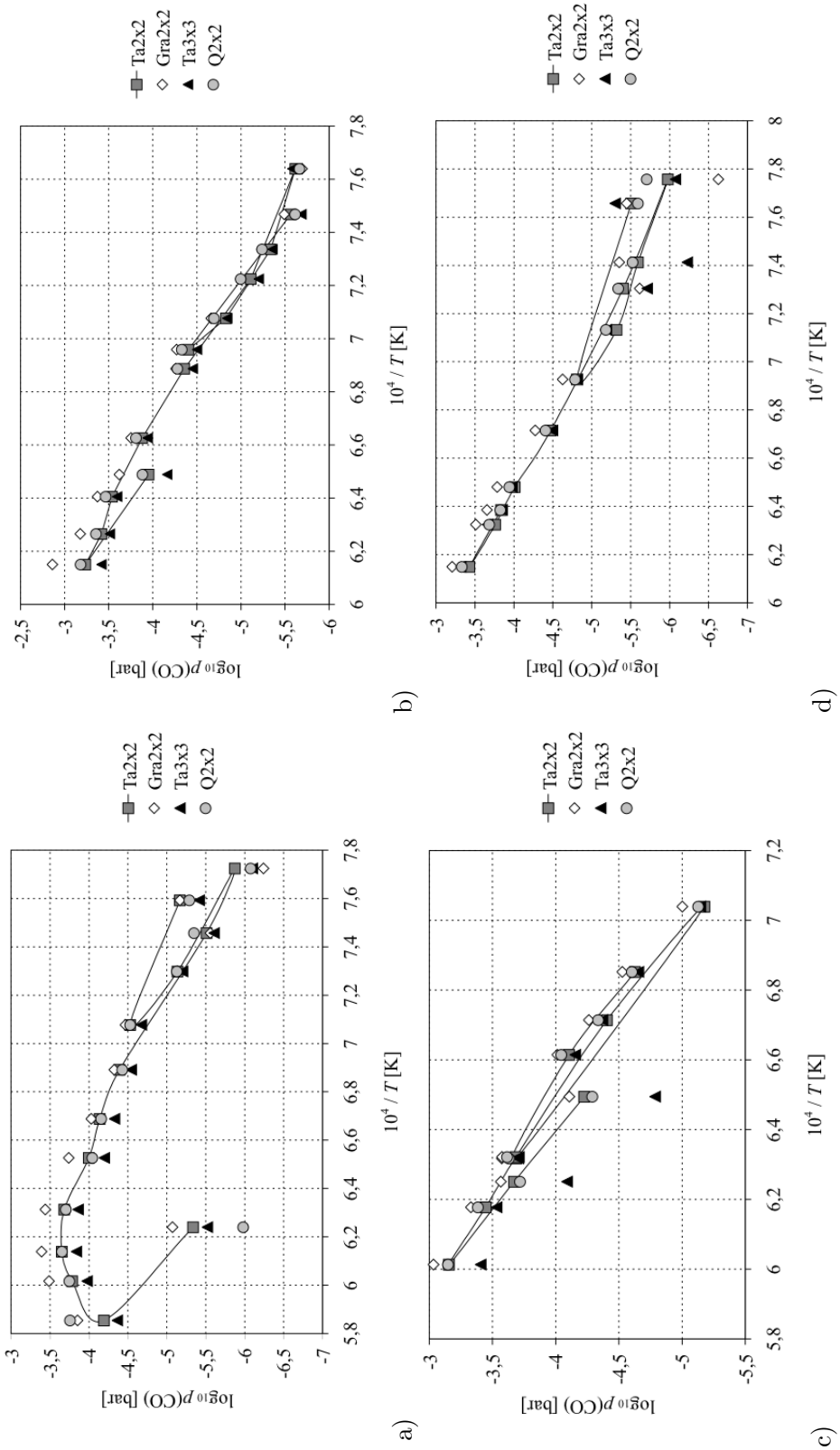

Figure 3.39: Evolution of decimal logarithm of $p(\mathrm{CO})$ as a function of the inverse of temperature for SiC-SiO_2 powder mixtures placed in cells made from tantalum (Ta), quartz (Q), graphite(G): a) 5 mol%; b) 15 mol%; c) 45 mol%; d) 66 mol%.

3.2.3.3.4 Conclusion The experiments performed in the high temperature mass spectrometer with the different SiC-SiO_2 sample compositions have shown that the SiO(g) and CO(g) vaporization is not congruent and not at equilibrium. The measured partial pressures were lower than equilibrium partial pressures calculated for the pseudo-binary section SiC-SiO_2. Their ratio, $p(SiO)/p(CO)$ is always lower than 1. The vaporization of SiO(g) and CO(g) is hindered.

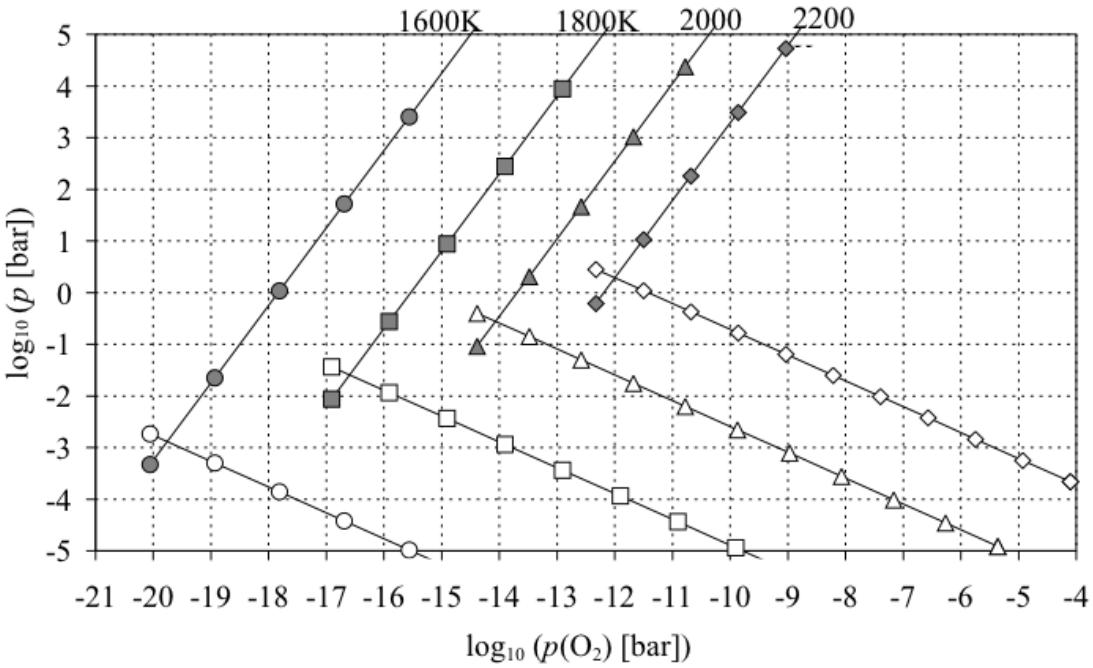

Figure 3.40: Decimal logarithm of calculated SiO(g) (white symbols) and CO(g) (dark symbols) partial pressures plotted as a function of decimal logarithm of oxygen pressure at the SiC grains surface which is varied from its minimum for a congruent reaction between SiO_2 and SiC (interface of SiO_2 and SiC) and its maximum for congruent vaporization of only SiO_2 grains at 1600, 1800, 2000 and 2200 K.

The non-equilibrium situation may be related to the tendency to independent vaporization behavior of two condensed systems: SiO_2 + SiC pseudo-binary and SiO_2 pure. These two systems vaporize at different oxygen potentials and a steady-state situation is reached in the effusion cell that is measured with the mass spectrometer. In order to understand the SiO(g) and CO(g) partial pressures evolution they are displayed in fig. 3.40 as a function of oxygen potential. With increasing oxygen potential, starting from the SiC + SiO_2 pseudo-binary, i.e. the congruent interface SiC/SiO2, we observe that CO(g) equilibrium partial pressure increases and SiO(g) decreases for equilibrium reaction

$$SiC(s) + 2SiO_2(s) = 3SiO(g) + CO(s).$$

After their cross-point, at different $p(O_2)$ for different temperatures, we obtain $p(CO)$ higher than $p(SiO)$, exactly the observed situation during the HTMS experiments with SiC and SiO_2 powders.

3.2.3.4 Characterization results

The samples of SiC-SiO_2 powder mixtures and of oxidized SiC powders after vaporization experiments were analyzed. Grain size measurement characterizes the building of agglomerates and grain growth. Raman spectroscopy shows the ability of energy conduction through sample material and makes evident changes in the structure due to the vaporization/heat treatment. X-ray diffraction shows the presence of SiO_2 in the samples and finally electron microscopy visualizes described effects, particularly the built grain connections.

3.2.3.4.1 SiC-SiO_2 mixtures

Grain size measurement For the mixtures with different SiO_2 content the grain size distributions were measured before and after experiment. As all the mixtures are constituted from the same powders the diagrams of initial grain size distributions do not change much from one sample to an other. Figure 3.41 displays the grain size distribution of 30 mol% initial sample and serves as an example for all SiC-SiO_2 mixture samples. The main peak is due to the agglomerates of fine grain fraction.

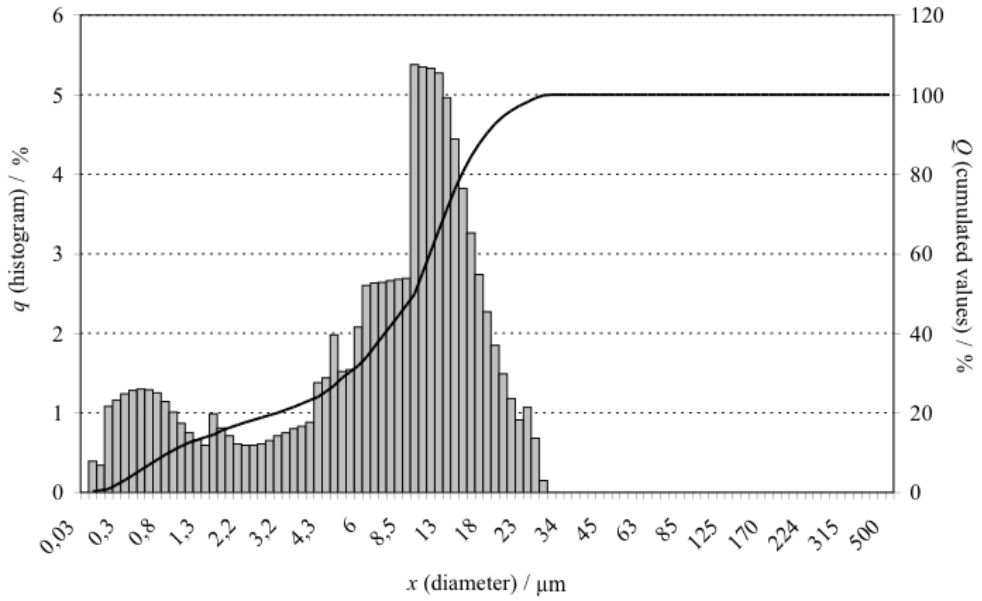

Figure 3.41: Grain size distribution of initial mixture of SiC with 30 mol% SiO_2. As it does not change significantly for different SiO_2 content, this figure serves also to display all other initial grain size distributions.

Table 3.11 lists the d50, d10 and d90 resulting from grain size measurement of different initial SiC–SiO_2 mixtures and the same after vaporization/heat treatment.
Figure 3.42 displays the distributions of mixtures with 0,5 and 30 mol% SiO_2 after the experiment as examples of two different kind of grain size distribution diagrams. Grain size distributions of samples with SiO_2 amount lower or equal to 10 mol% did not change much. Only the first peak for diameters of 0,3-1,3 μm got lower with decreasing amount of SiO_2 in the samples. The maximum grain/agglomerates size remains constant by 35 μm like

Table 3.11: Measured values for d50, d90 and d10 of different SiC–SiO_2 mixtures before and after heat treatment during HTMS experiments.

Sample		d50 [μm]	d90 [μm]	d10 [μm]
0,5 mol%	initial	10,22	18,72	2,85
	treated	10,99	18,9	4,43
1 mol%	initial	10,17	19,22	1,85
	treated	11,14	19,302	4,54
2 mol%	initial	6,2	15,48	0,48
	treated	10,55	18,68	2,4
5 mol%	initial	9,86	19,55	1,11
	treated	10,11	18,39	2,2
10 mol%	initial	10,04	27,6	0,8
	treated	10,92	18,21	2,04
15 mol%	initial	10,62	15,48	0,48
	treated	6,11	21,68	0,67
30 mol%	initial	9,03	17,85	0,84
	treated	6,36	32,21	0,61
45 mol%	initial	9,52	40,04	0,41
	treated	14,27	74,43	0,41
66 mol%	initial	9,35	16,33	1,11
	treated	53,72	136,79	2

displayed in fig. 3.42 a). This result confirm the powder aging found during vaporization experiment.
From 15 mol% SiO_2 amount in samples the grain size distribution changes much more compared to initial distribution. The proportion of fine fraction does not decrease and the agglomerate size increases until 315 μm for 66 mol% (see fig 3.42 b)).

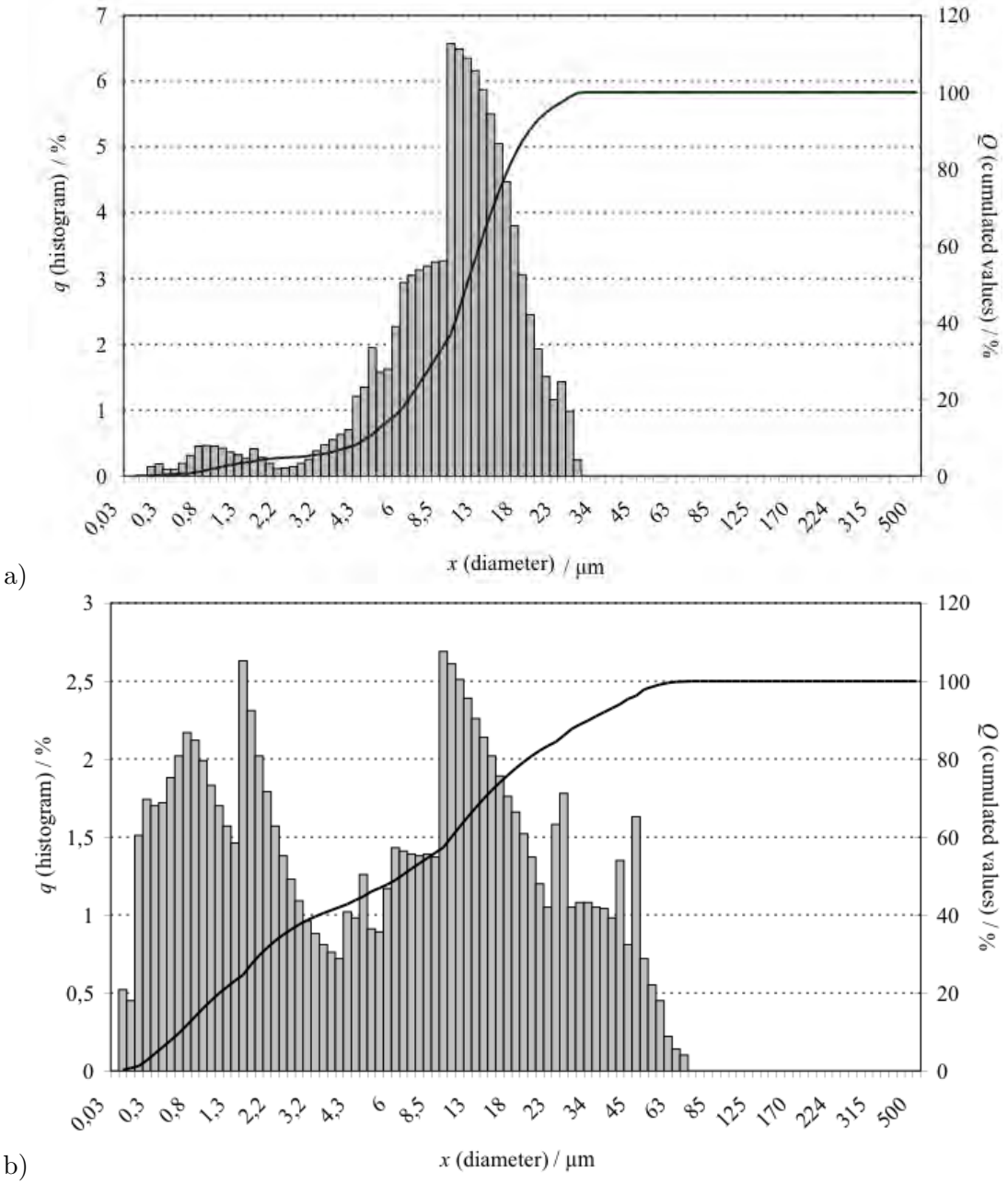

Figure 3.42: Grain size distribution after heating in SMHT experiment of a) 0,5 mol% and b) 30 mol% samples.

Raman spectroscopy Figure 3.43 shows Raman spectra measured for SiO_2 containing samples after experiment in high temperature mass spectrometer. As we can see the level of fluorescence is proportional to the SiO_2 content, the higher was the amount of silica in the sample the higher is the level of fluorescence. This is observed until 15 mol% SiO_2 content in the samples. For lower SiO_2 loaded samples no more fluorescence was observed. As mentioned before the fluorescence is an indicator for low heat conduction capacity. In the powders with SiO_2 content higher than 15 mol% not enough connections between the single SiC grains were formed to make them able to eliminate the received laser energy through the bulk material. The lower loaded samples, contrarily, could eliminate most energy. The excess of SiO_2 in the samples with more than 15 mol% prevented the elimination of the silica layer on the SiC grains, the de-oxidation.

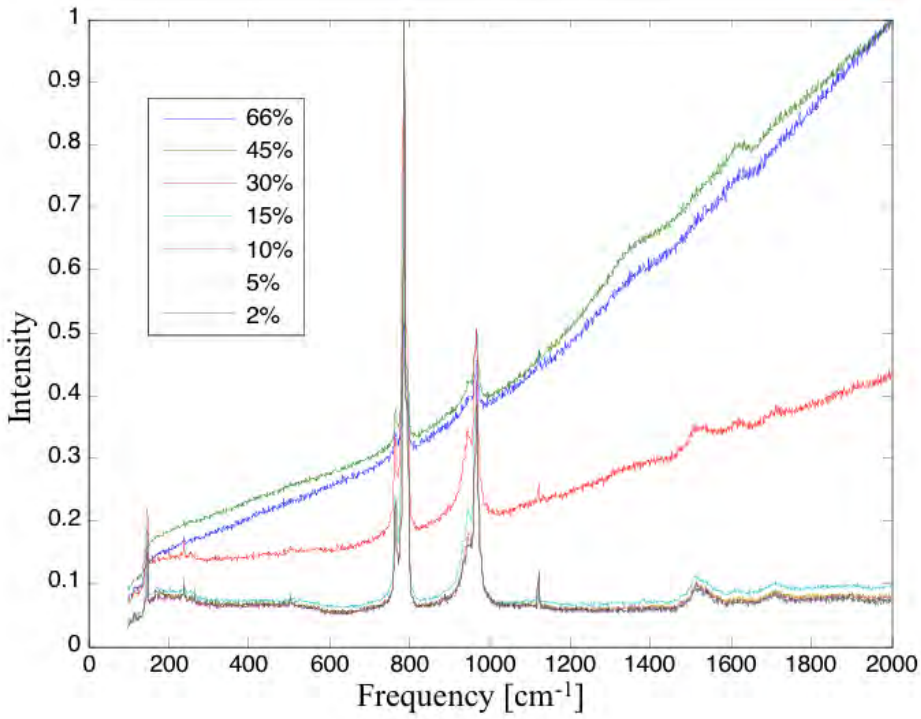

Figure 3.43: Raman spectra of SiC-SiO_2 mixtures with SiO_2 content from 2 to 66 mol% after SMHT experiment.

With decreasing fluorescence the single peaks get more pronounced. Carbon peak is clearly observed only for samples with less than 30 mol% of SiO_2. Above it is hidden by fluorescence, but can still be observed. Following the samples contain carbon after the experiment. It shows, that there is no possibility to prevent Si loss in excess from the SiC and following to prevent local carbon precipitation.

X-ray diffraction measurement Figure 3.44 shows X-Ray diffraction spectra of SiC-SiO_2 mixtures after vaporization experiment. It displays the SiO_2 peak close to (2 theta) = 22° and peaks for 4H and 6H SiC-polytypes. The SiO_2 peak is well pronounced for samples with more SiO_2 than 30 mol%. Further we can observe that each sample shows differences in 4H and 6H peaks, the measured intensities are different. With SiO_2 amount decrease in the initial samples the peaks got finer.

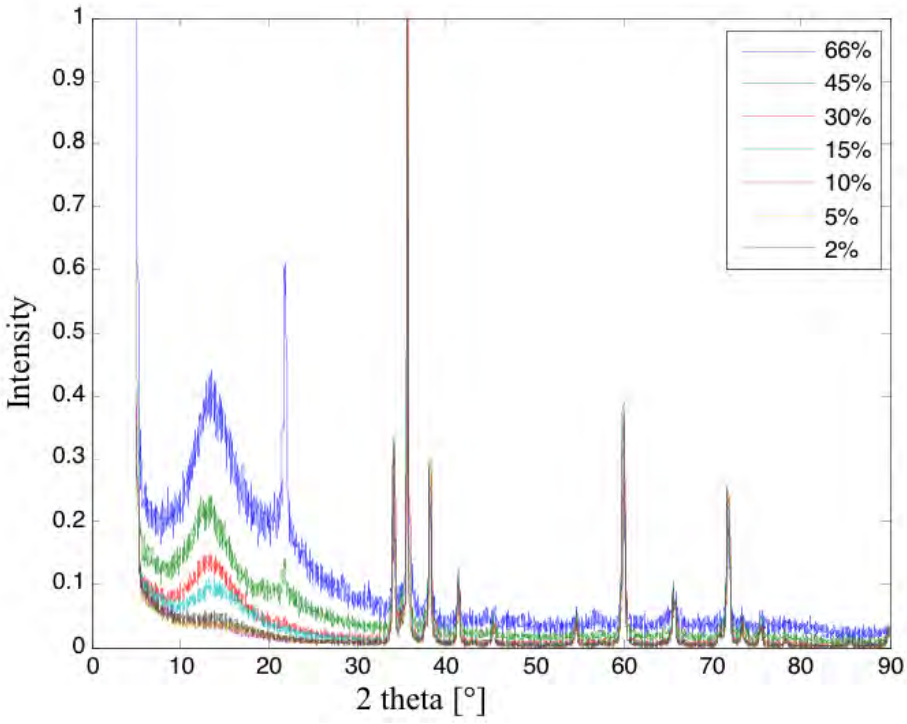

Figure 3.44: X-Ray diffraction spectra of SiC-SiO_2 mixtures with SiO_2 content from 2 to 66 mol% after SMHT experiment.

SEM/FEG imaging Figures 3.45 and 3.46 show FEG images of SiC-SiO_2 mixtures after heating in high temperature mass spectrometer. For comparison a 2 mol% initial mixture is displayed at image a) of figure 3.45. The sample with 66 mol% SiO_2 does not show much evolution. From 45 mol% the grains of the powder mixtures rounded more and more with decreasing SiO_2 content, some plain surfaces, facets, with hexagonal shapes are visible. Furthermore from 15 mol% grains connections are clearly observed on the SEM images. For the powders with lowest SiO_2 contents, from 5 mol% to 0,5 mol% (fig. 3.46) more coarse grains interconnection can be distinguished than for 15 and 10 mol% powder mixtures. Following with decreased SiO(g) pressure and observed higher powder aging for these samples the coarse grains could form connections.

Summary The vaporization experiment was stopped for all samples before the elimination of SiO_2. The powder samples have formed agglomerates observed with grain size measurement method. Fluorescence in Raman spectra results from low heat conductivity of samples with originally more than 15 mol% SiO_2 and a SiO_2 peak was observed with XRD for samples with SiO_2 content above 30 mol%. This SiO_2 content prevented the elimination of native layer on the SiC grains and has build a barrier to grain-to-grain connections formation. Several connections were observed with FEG in the samples with from 45 mol% SiO_2 content, but compared to lower initial SiO_2 contents they are not sufficient to eliminate the received energy during Raman spectra measurement.

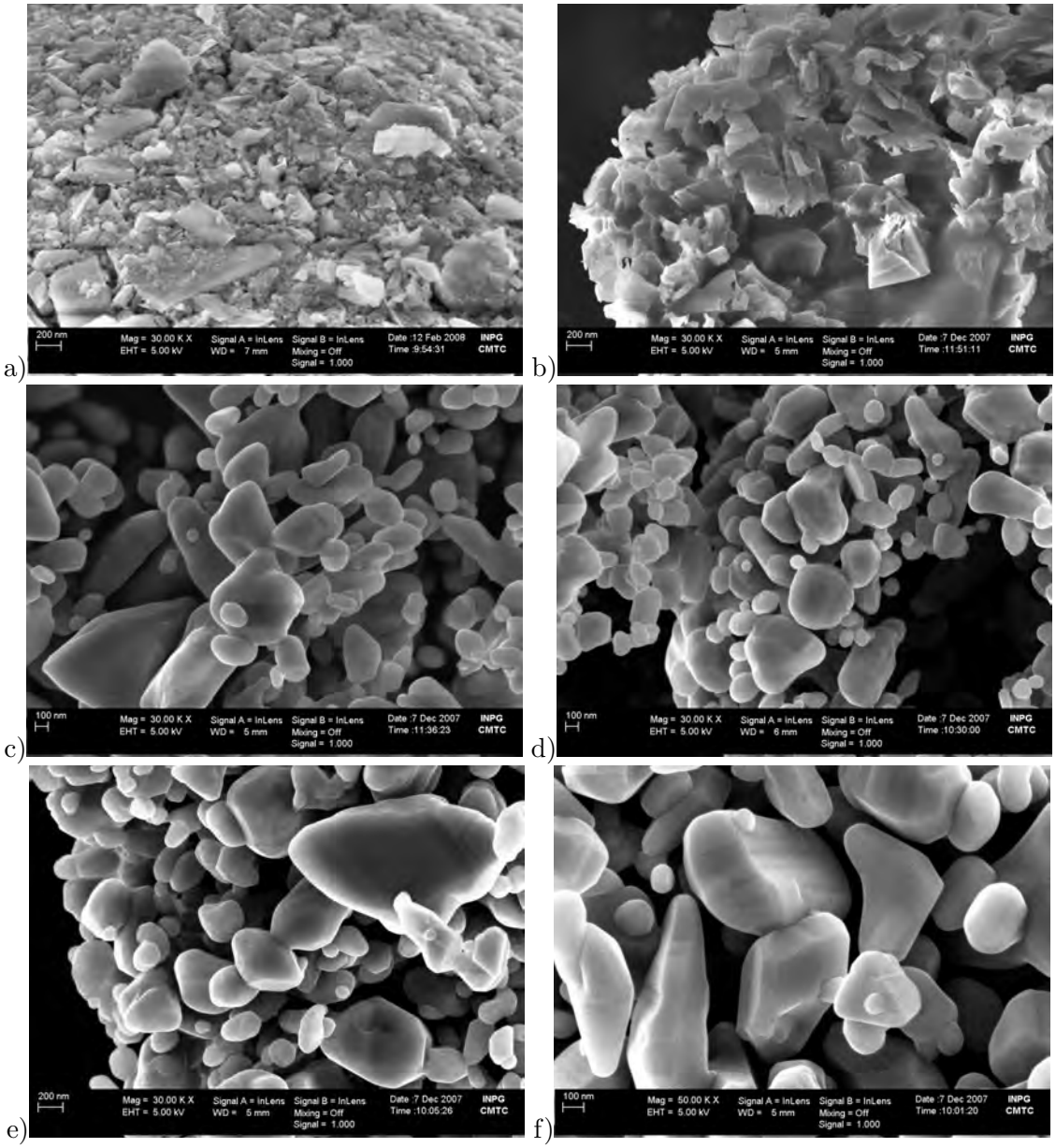

Figure 3.45: FEG images of SiC-SiO_2 mixtures with SiO_2 content from 10 to 66 mol% after SMHT experiment and 2 mol% before SMHT experiment. a) 2 mol% initial powder; b) 66 mol%; c) 45 mol%; d) 30 mol%; e) 15 mol%; f) 10 mol%.

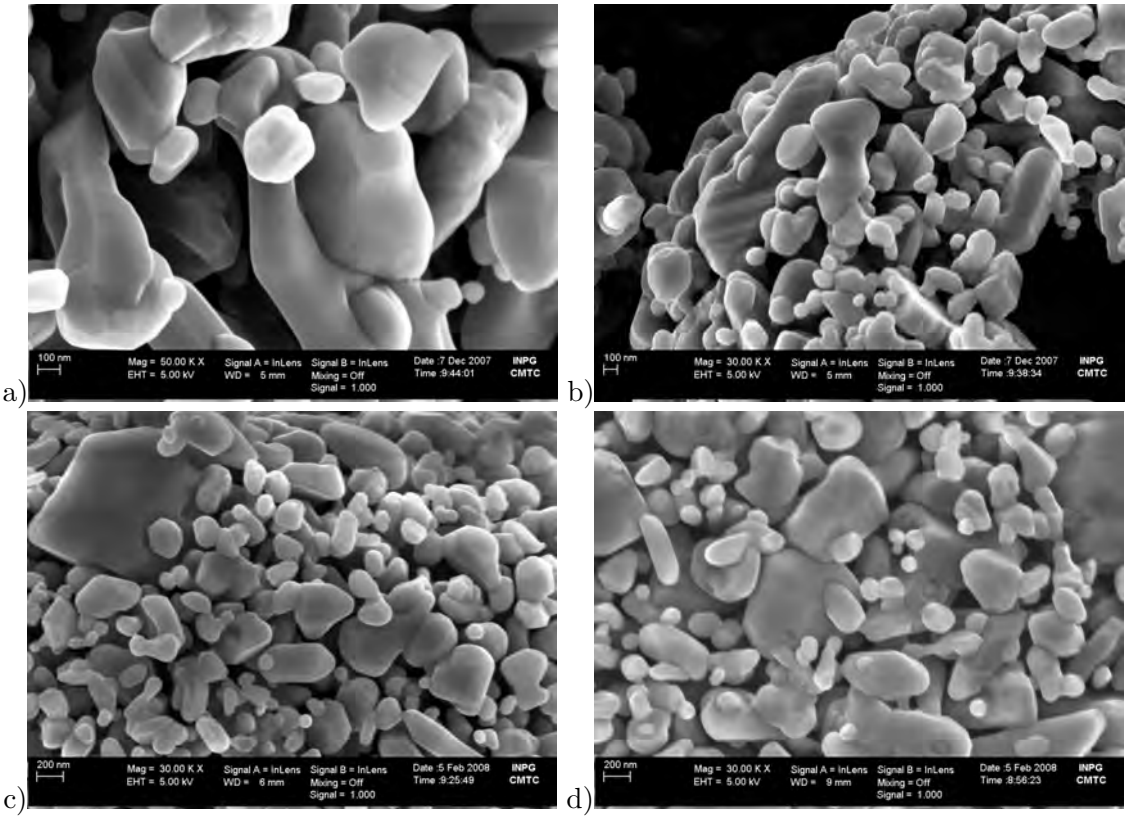

Figure 3.46: FEG images of SiC-SiO_2 mixtures with SiO_2 content from 0,5 to 5 mol% after SMHT experiment. a) 5 mol%; b) 2 mol%; c) 1 mol%; d) 0,5 mol%.

3.2.3.4.2 Oxidized powders

Raman spectroscopy Figure 3.47 displays Raman spectra of initially oxidized SiC powders after heating in the high temperature mass spectrometer. The level of fluorescence is higher for the shorter time oxidized powder. The 10 and 30 hours oxidized powders have clearly lower fluorescence shift. The difference between the 10 and 30 hours oxidized powders is much smaller than for each of them compared to 3 hours oxidized. It means the 10 and 30 hours oxidized SiC powders must have built a kind of bridges from SiO_2 to eliminate the received energy from laser better than the 3 hours oxidized powder. Some SiC polytype variation is observed. At 910 cm^{-1} a new peak occurred which we could not identify. Local carbon formation is shown with the peaks at 1400 and 1600 cm^{-1}.

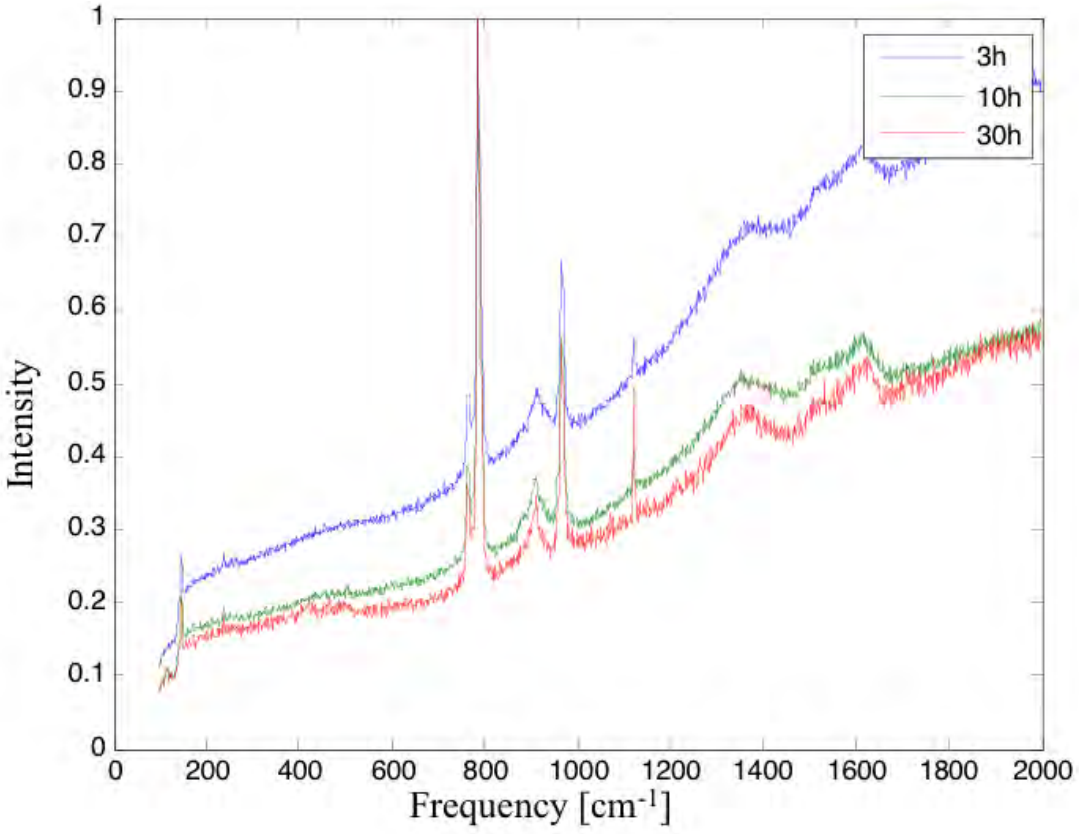

Figure 3.47: Raman spectra of 3, 10 and 30 hours oxidized SiC powders after vaporization experiment in SMHT.

XRD measurement Figure 3.48 shows the X-Ray diffraction spectra of the 3, 10 and 30 hours oxidized SiC powders after vaporization heat treatment. Image a) zooms on the SiO_2 peak and b) on the SiC polytypes peaks from 2 theta = 32 to 42°. The zoom on the SiO_2 peak displays the differences in SiO_2 content of the powders after vaporization experiment compared to the non-oxidized SiC powder. The figure displays that the 30 hours oxidized powder shows the highest SiO_2 peak intensity and for pure SiC powder no SiO_2-peak is observed.
Figure 3.48 b) makes a zoom on the SiC polytypes peaks from 2 theta = 32 to 42°. The non-oxidized reference SiC powder shows the highest peaks, the one from 3 hours oxidized sample is lower lower. The lowest peaks we can observe for 30 hours oxidized powder, caused by thicker SiO_2 layer that covers the SiC grains.

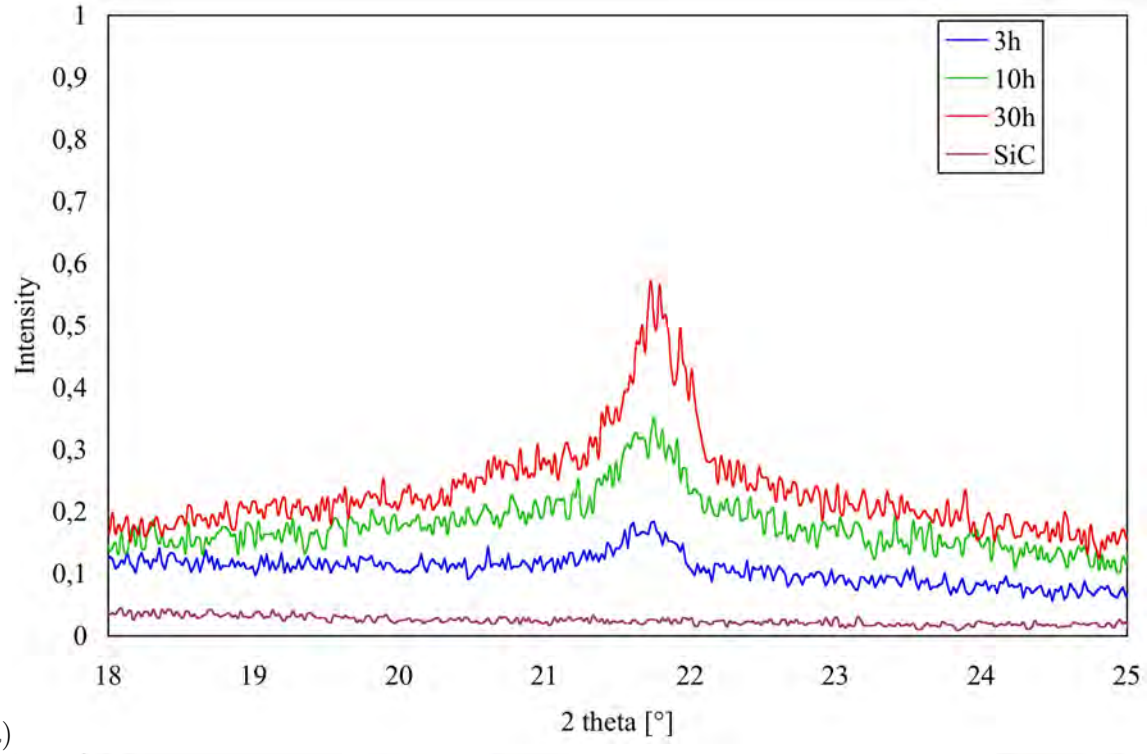

a)

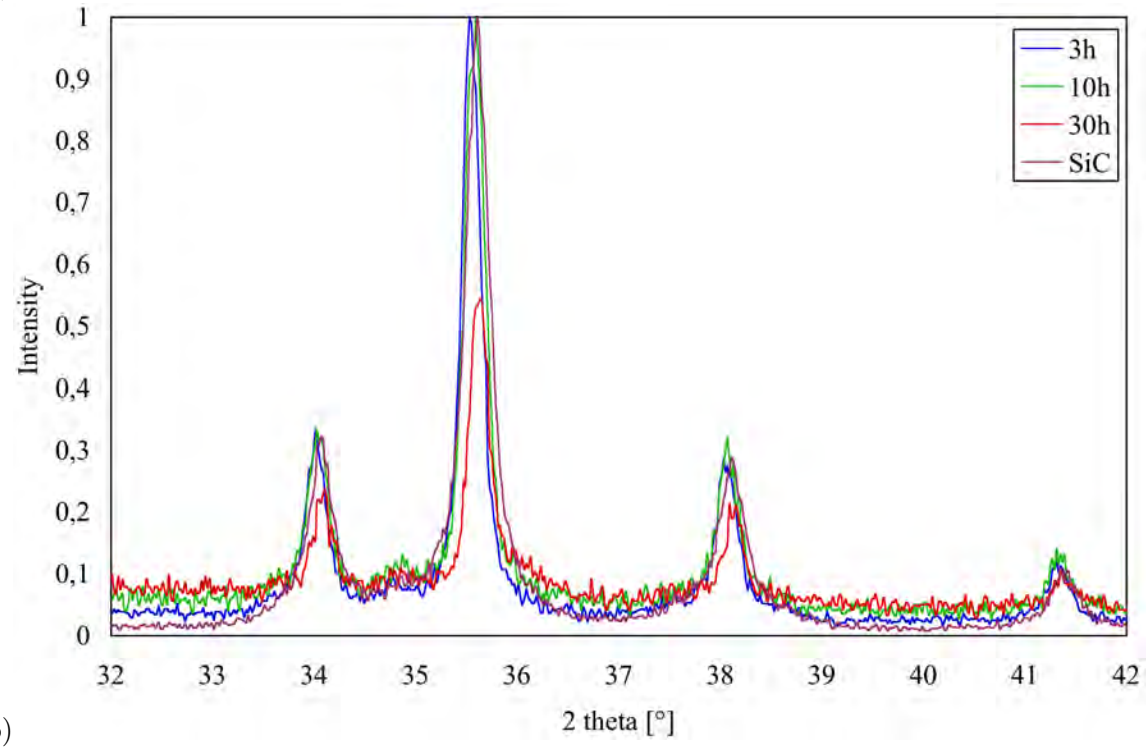

b)

Figure 3.48: XRD spectra of 3, 10 and 30 hours oxidized SiC powders after vaporization experiment in SMHT. Zoom on a) SiO_2 peak and b) 4H/6H SiC-polytypes peaks.

SEM/FEG imaging Figure 3.49 displays images obtained from EDX analysis in SEM for oxidized powders before the heat treatment. Silicon was detected only on the grains. Oxygen on the grains and also near the grains on the carbon tape. Carbon was only detected on the tape. Oxygen is found associated to silicon from the SiC which means that SiO_2 covers entirely the SiC grains.

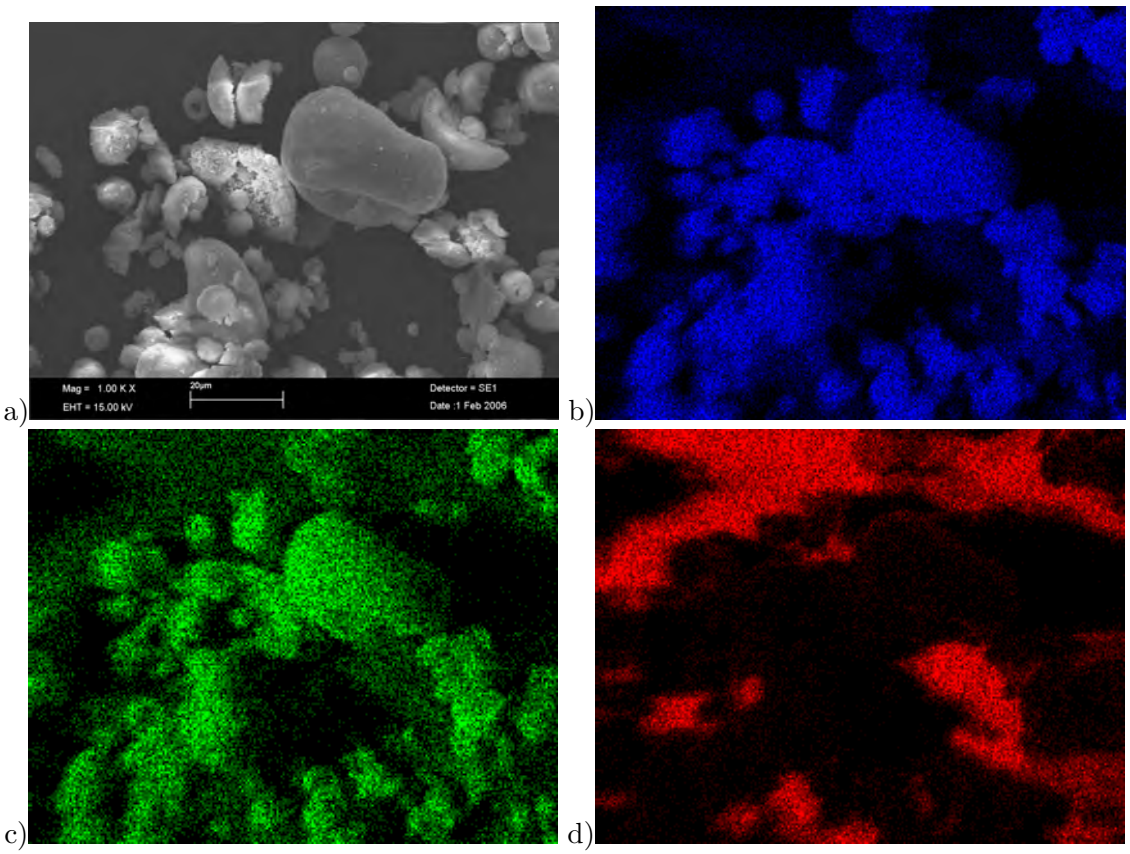

Figure 3.49: SEM images of EDX analysis for 30 hours oxidized SiC powder: a) Image of analyzed surface; b) silicon distribution on the surface; c) oxygen distribution d) carbon distribution.

The SEM images of oxidized SiC powders before and after heating in the high temperature mass spectrometer experiment have shown large agglomerates of 10-20 μm diameter. The temperature treatment did not have any effect on the powders and their agglomerates, at least it was not observed with SEM imaging method.

Summary With any characterization method a certain SiO_2 content was still observed after the treatment in SMHT for all SiC-SiO_2 mixture sample. SiC polytype variation for the different times oxidized samples was observed after the experiment. Local carbon precipitation was detected with Raman spectroscope. The oxide layer covered completely the SiC grains before experiment, as it was observed in the SEM. Agglomerates did not allow to observe with SEM any changes in the sample structures after the vaporization experiment.

3.2.3.4.3 Different crucible materials With the SiC-SiO_2 mixtures we have always excess of SiO_2. The SiO(g) and CO(g) partial pressures were still observed at the end of vaporization experiment at 1600 K.

SEM/FEG imaging Figure 3.50 shows the SEM images of obtained samples with 5 and 66 mol% initial SiO_2 content. The fine grains remained agglomerated after vaporization treatment. It is not clear if any bridges were created whatever is the cell material, which had influenced the SiO(g) and CO(g) partial pressures.

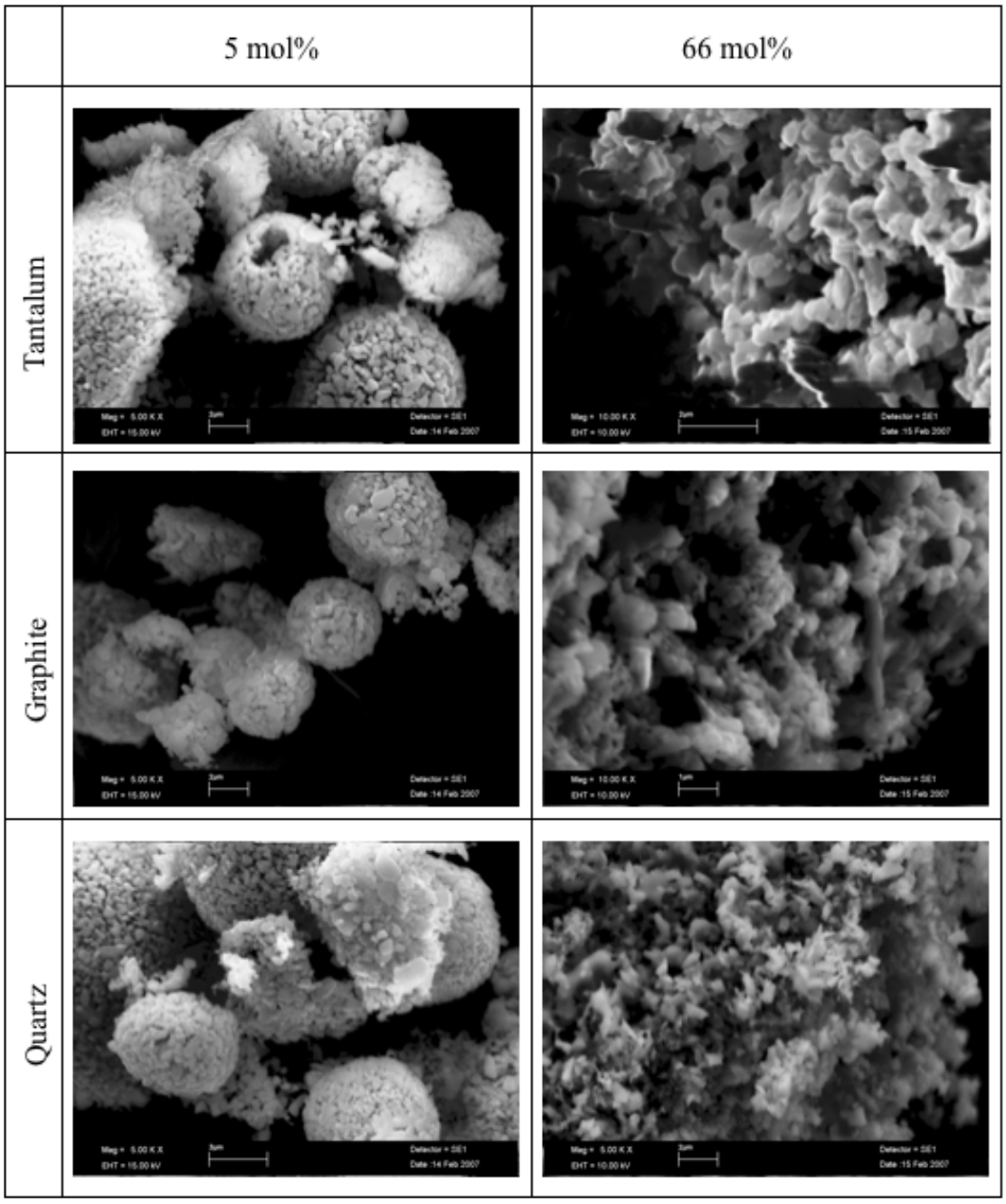

Figure 3.50: SEM images of SiC-SiO_2 mixtures with 5 and 66 mol% SiO_2 content after SMHT experiment in different crucibles.

3.2.3.5 Conclusion

Vaporization experiments with SiC and added SiO_2 as powder or oxidation layer on the SiC grains served to study the influence of the latter on the SiC grain connections creation and SiC grain growth.
The addition of SiO_2 in form of powder bring Na_2O as impurity into the samples. This is a most common impurity in the SiO_2 powders. In the temperature range of $1300 - 1500\,K$ it acts as oxygen supplier which causes CO(g) excess formation detrimental to SiO(g) formation. The mixtures purifies vaporizing Na(g).
The vaporization experiments of the SiC with 0,5 to 66 mol% SiO_2 powder mixtures in the temperature range of $1300 - 1700\,K$ have shown that the evaporation process does not attain its equilibrium. The SiO(g) and CO(g) partial pressures are:

- always lower than calculated following thermodynamics,
- dependent on the composition contrarily to theoretically invariant behavior
- and the ratio SiO/CO is always inferior to 3 (or 3,76) predicted by thermodynamics for congruent vaporization.

These observations indicate kinetically limited vaporization, the responsible phenomena is to look for.
The evaporation coefficient measurements have shown that the oxygen / SiO_2 elimination is cut down by the factor 10 to 1000 compared to thermodynamic calculations. Furthermore they decrease with decreasing SiO_2 content in the samples: 10^{-1} to 10^{-4} for SiO(g) and 10^{-1} to 10^{-2} for CO(g).
The SiO(g) and CO(g) partial pressures do not vary much for SiO_2 contents of 66 to 15 mol%. Contrarily, for low SiO_2 contents of 15 to 0,5 mol% they decrease by a factor 30. More significant powder aging was observed only for samples with low SiO_2 amounts (< 15 mol%) and seemed accelerated above 1650 K with SiO_2 departure.
After Raman spectroscopy and SEM/FEG analysis following observations were made:

- no modifications for sample with initially 66 mol% SiO_2;
- for samples with initially 15–45 mol% SiO_2 in moderate temperature range the SiC grains became rounded but the inter-connection of them was not clearly observed;
- for initial amounts lower than 15 mol% SiO_2 powder aging was observed; finer grains disappear and grain growth for coarser grains was observed; connections formation was also observed.

The experiments with oxidized powders were performed with change of added silica nature and Na_2O impurity absence. Furthermore it was assumed that the SiO_2 covers entirely the SiC grains. Transformation of SiO_2 layer was observed at $\approx 1400\,K$ from amorphous to crystallized (cristobalite). Different SiO(g) and CO(g) partial pressures for different times oxidized samples were observed below the mentioned temperature of transformation contrarily to similar values above. SiO(g) and CO(g) were observed until the end of experiment. No formed grain-grain connections or any structural changes of powder samples were observed.
Use of different crucible materials—tantalum, graphite and quartz—has shown that quartz and tantalum have very small effect on the partial pressures, but graphite increases CO(g)

partial pressure detrimental to SiO(g). This accelerates the departure of oxygen, that is SiO_2. The formation of bridges and SiC grain growth was accelerated in graphite crucible and also for samples with low SiO_2 contents.

3.3 Vaporization in non-equilibrium state: Experiments with Quadrupole Mass Spectrometer and capillary sampling

Quadrupole mass spectrometer with sampling via capillary tubing is suitable for continuous gas phase identification in non-equilibrium state, i.e. under flow conditions which correspond to more important flows than applying the Knudsen flow method. Furthermore, the analyzed sample mass is more important.
Vaporization behavior of SiC powder mixtures was analyzed observing the CO(g) release from different samples under different conditions and with increasing temperature. The changes in the samples structures—grain rounding, necks formation between the grains etc.—as a result from the heat treatment during the mass spectrometric measurements were analyzed by Raman spectroscopy and observed with SEM/FEG imaging.
SiC powder, SiC-2 mol% SiO_2 powder mixture and oxidized SiC powder bimodal mixture samples were compared between each other. Differences in their vaporization behavior, i.e. changes of the observed CO(g) peaks, were related to the total SiO_2 content, its nature and mono- or bimodal grain size distribution in the initial samples. Furthermore, we examined the influence of the heat treatment duration, different heating rates and attained maximum temperature on the final sample's structure.

3.3.1 Measurement conditions

For every experiment a new graphite crucible was used with all the connections to the capillary made from graphite. This prerequisite was applied to guarantee same conditions for each experiment.
Measurements of CO(g) intensity were performed for samples heated until 1740 K for several hours. The choice of temperature increase rate and maximum temperature was adjusted differently to each sample, except in the experiments with fixed temperature ramps.

3.3.2 Experiments

3.3.2.1 Samples

We used 0,5 μm SiC powder obtained by sieving of same SiC powder batch and Degussa Sipernat 350 SiO_2 already described in precedent chapter. The oxidized SiC powder bimodal mixture is a SiC powder mixture composed from ~33 mass% 0,5 μm and ~67 mass% 10 μm grain sizes. This mixture was heated up to 500°C under oxidative conditions (air).

3.3.2.2 Performed experiments

Table 3.12 summarizes the experiments performed with the capillary sampling mass spectrometer.
For experiments with fixed temperature ramps until 1373 K the heating process was almost the same for all samples:

- from room temperature to 1053 K 0,5h;
- from 1053 to 1273 K 1h;
- from 1273 to 1373 K 1h, except the "200" sample.

Table 3.12: Performed mass spectrometric experiments with capillary sampling.

Experiment label	Sample	T_{hold} or T_{max} [K]	holding time or end condition
16-10	0,5 μm SiC powder	1600	1h
19-10	mixture of 0,5 μm SiC and 2 mol% SiO_2 powders	1700	1h10
26-10		1500 and 1690	2,5h and 1,5h
06-11		1500 and 1740	1,5h and 2h
08-11		1500	no CO(g) observed, 40 min
06-12		1650	p(CO) maximal
23-10	oxidized SiC bimodal powder mixture	1500 and 1600	1,5h and 1,5h
13-11		1529	no CO(g) observed, 45 min
28-11		1560	p(CO) maximal
25		1473	25 K/h for $1373 < T < 1473$ K
50		1473	50 K/h for $1373 < T < 1473$ K
100		1473	100 K/h for $1373 < T < 1473$ K
200		1473	200 K/h for $1273 < T < 1473$ K

We can be sure to observe only CO(g) at the mass of 28 because Si(g) intensity is still too weak in the temperature range of performed experiment and any vapor like SiO(g), Si(g), Si_2C(g) etc. condenses before entering the capillary tubing. If not the capillary tubing would be quickly clogged.

3.3.2.3 Experiment results

During the experiments the same part of the total gas flow through the capillary tubing was monitored due to the same conductance for sampling. The intensity of the CO peak was observed with increasing temperature. Figure 3.51 displays the resulting CO(g) intensity diagram from the experiment 06-11 as an example. From the temperature of ≈ 1300 K the CO(g) intensity can be observed because the CO(g) partial pressure became sufficiently high to be added to the spectrometer background. The CO(g) intensity continues to increase with increasing temperature and also if the temperature is kept constant like in figure 3.51 at 1500 K. After a maximum (peak CO(g) intensity) it begins to decrease if the temperature is still kept constant. At the last step, with a new temperature increase a new CO(g) peak can be observed but smaller and the decrease is steeper than for the first peak. The CO(g) intensity decrease to a minimum until the end of the experiment when the temperature is kept constant. With a new increase of temperature the CO(g) rose for a short period and then decreased rapidly. This behavior of the CO(g) intensity was noticed for all analyzed samples.
Increase of the CO intensity as a function of increasing temperature resulted in total ion current increase. At high temperatures, up to 1300 K, the gaseous phase contained more than 50% of CO(g).
The emission of CO(g) from the samples comes from the SiO_2 presence in every sample, even in only SiC powder sample. As already explained in the precedent chapter, the SiC material build a SiO_2 layer on every surface exposed to oxygen containing atmosphere, which is

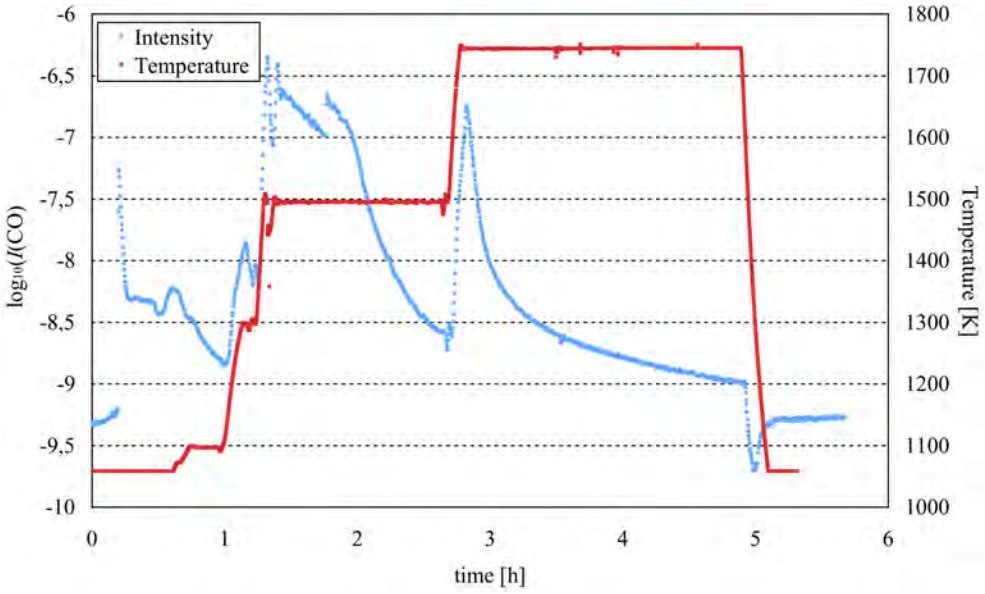

Figure 3.51: Decimal logarithm of as measured CO(g) intensity data with corresponding temperature increase rate from 06-11 experiment with SiC-2 mol% SiO_2 powder mixture sample as a function of experiment duration.

always the case at air. At high temperature in vacuum this layer is volatilized building SiO(g) and CO(g) flows. The SiO(g) is condensed in the cone into SiO_2-SiC mixtures as it was analyzed. The cone builds a cold trap due to the intentional temperature gradient. When CO(g) arrived at its minimum it means that the heated zone of the sample is depleted in SiO_2. The new short raise of CO(g) intensity with new increase of temperature is due to expansion of the heat zone on the new sample regions (closer to the central symmetry axe and in the upper crucible parts), which still contain some SiO_2 (original or condensed) until this zone will also loose it by vaporization of SiO(g) and CO(g). Following the observation of CO(g) intensity peak is directly related to SiO_2 loss of the heated sample.

3.3.2.3.1 Results of experiments with manually adjusted temperature increase Figure 3.52 displays CO(g) intensities of SiC pure, SiC-SiO_2 2 mol% mixture and oxidized bimodal SiC powder mixture measured by capillary mass spectrometer. The diagrams are corrected with sensibility factor calculated from nitrogen intensity measured before heating begins. The shape and size of the peaks from the different samples are different. The peak of SiC powder sample is very low compared to other two samples. The peak from the oxidized bimodal SiC powder mixture is the largest and highest one. The SiC with 2 mol% SiO_2 mixture sample needs most time to get its CO(g) intensity at minimum.
The CO(g) intensity peak is related to the loss of SiO_2 by the sample as found above, and following is an indicator for the general SiO_2 amount in the initial sample. It means that the smallest peak from the SiC powder sample is due to its very low SiO_2 content which comes from the native surface oxidation of the single SiC grains at air. It is obvious that the amount of the native surface SiO_2 is lower than in the other two samples. The oxidized bimodal SiC powder mixture sample contained most SiO_2 before the temperature treatment because its peak is the largest and highest one. So apparently the amount of

SiO_2 brought by oxidation on the grains exceeded the equivalent of 2 mol% of SiO_2 which was added in the SiC-2 mol% SiO_2 mixture sample.
The slower release of CO(g) is remarkable for the SiC–2 mol% SiO_2 mixture indicating that the added grains of SiO_2 serve as an oxidation reserve for the SiC grains. Because of these SiO_2 grains a certain oxygen level inside the crucible is maintained longer. It provokes active oxidation of bare SiC grains, which have already lost their protective SiO_2 layer (CO peak), with SiO(g) and CO(g) formation, contrarily to the SiC powder and the oxidized bimodal SiC mixture samples. They have lost all their SiO_2 content when loosing their oxidation layer.

3.3.2.3.2 Results from fixed temperature ramps experiments Figure 3.53 shows the CO(g) intensity peaks of the samples from experiments with different temperature ramps between 1373 and 1473 K. The shapes from the CO(g) peaks of different samples are different, particularly in the temperature range where the different ramps were applied. Table 3.13 lists the observed temperature fix points for each sample.
A sufficient amount of CO(g) to be detected from the mass spectrometer was emitted from all samples 1,5 h after the begin of heat treatment and corresponds to $T > 1273$ K. The four peaks of different samples occur at different temperatures. The single peak occurs at higher temperature when the heating rate is slower. The decrease of CO(g) intensity depends also on the temperature increase rate: the emission of CO(g) became earlier not

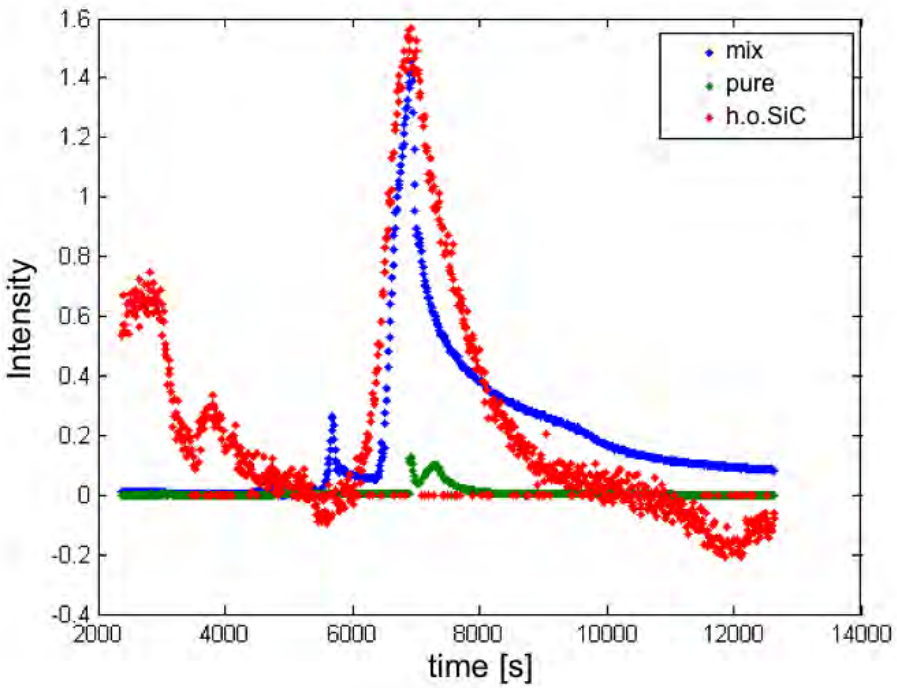

Figure 3.52: Intensities of CO ions during vaporization of SiC powder (green), SiC with 2 mol% SiO_2 mixture (blue) and oxidized bimodal SiC powder mixture (red) as functions of time. The intensities are corrected applying a sensitivity factor from nitrogen intensity.

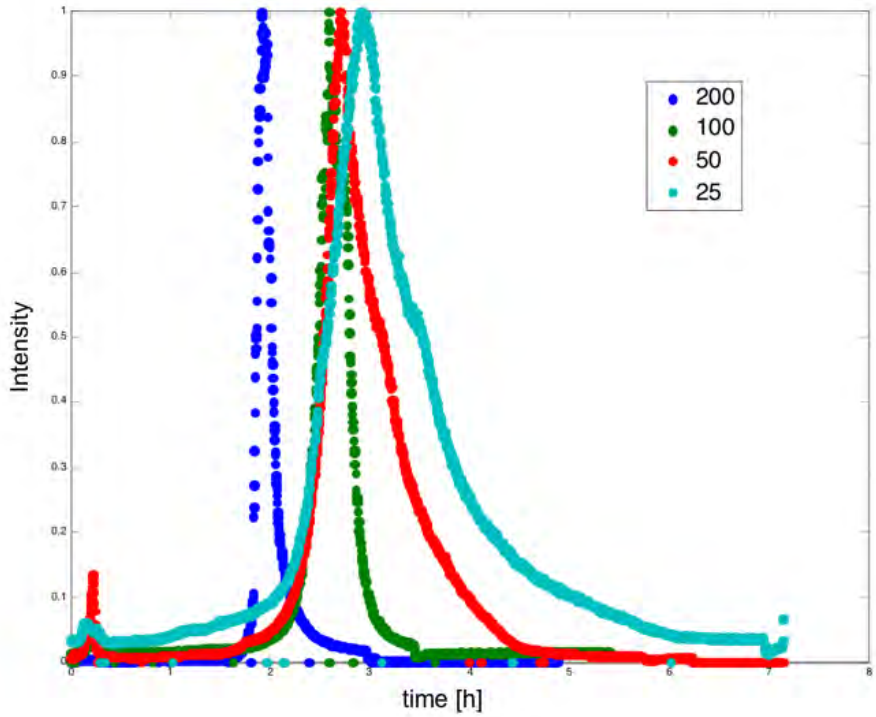

a)

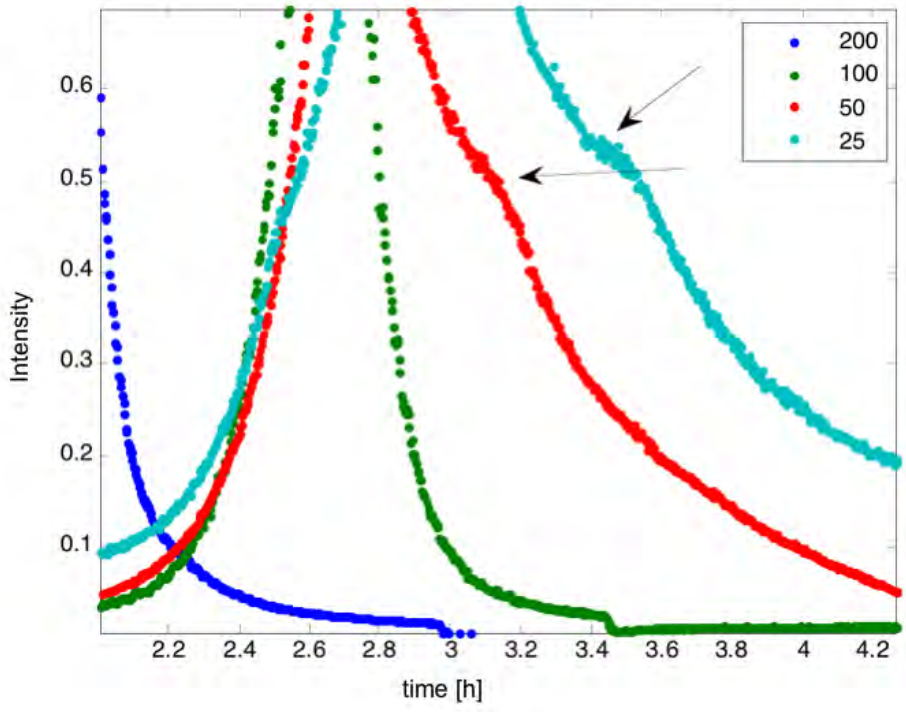

b)

Figure 3.53: a) Diagrams of CO(g) intensity normalized to their maxima as a function of the heating time with different temperature ramps from 1273 K up to 1473 K; b) Zoom on the occurred shoulder for slow temperature ramps.

Table 3.13: Observed temperature fix points for CO(g) intensity during capillary mass spectrometric experiments applying different ramps between 1273 and 1473 K.

Temperature of: Sample	emission begin [K]	maximal emission [K]	emission end [K]	shoulder [K]
200	1273	1347	1446	1367
100	1273	1361	1461	1367
50	1273	1410	1473	1430
25	1273	1422	1473	1450

detectable of the samples with fast temperature increase rate compared to samples from slower temperature increase, but all samples ended the CO(g) emission as soon as attaining 1473 K. Following the CO(g) emission for all samples ended before the stabilization begin at 1473 K (or got lower than the detection limit of mass spectrometer), or, to say differently, when the temperature increase was stopped.
The influence of the ramps on the vaporization behavior of the samples is caused by the heat zone expansion and temperature distribution inside the sample. With slow ramps the heat zone is moving slowly to the core of the sample in the crucible, the temperature gap zone between the crucible walls and its core is smaller than in the case of rapid ramps. Once attaining the necessary temperature each grain evaporates its SiO_2 surface layer. If the heating is performed more homogeneously, the depletion is more uniform and complete, but slow, which is the case for slow ramps.
In the last column of table 3.13 the temperature for the occurring shoulders, displayed at figure 3.53 b), are listed. Figure 3.53 b) zooms in a region of figure a) and displays these shoulders for the 50 and 25 K/h heating rate samples. They are observed clearly only for slow ramps. For the samples heated 200 and 100 K/h they occur too close to the main peak and are finally covered with the total CO(g) emission.
These shoulders may be due to the bimodal constitution of the powder samples. There are several effects:

- different vaporization rate for different powder grain size (as observed in the high temperature mass spectrometer experiments),
- radial temperature gradient,
- vertical temperature gradient and re-condensation.

These effects make altogether a difference, the coarse grains attain the same vaporization stage like the small grains when they attain the corresponding temperature in the heated sample region, with some delay, and the emitted CO(g) intensity is lower than from the fine grains, which lead to building of a “bump” in the CO(g) intensity curve. The figure 3.54 is an approximation of an experimentally obtained graph with a sum curve of three peaks. As discussed above, the two main peaks can be attributed to the fine and coarse grains contribution to the sum peak. The lower third peak must be considered from the asymmetric shape of the experimental diagram. The crucible and graphite insulations emit at high temperature some CO and contribute to the total CO-gas flow measured with mass spectrometer.

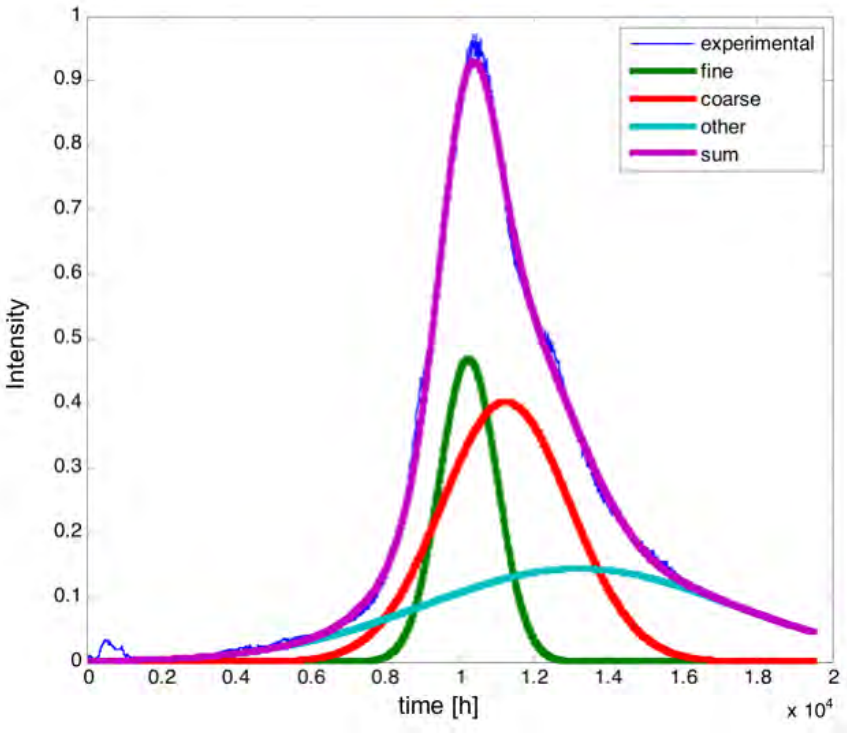

Figure 3.54: Approximation to experimentally obtained CO(g) intensity diagram as a sum of several intensity peaks due to different vaporization behavior of different sample components.

3.3.2.4 Summary of experimental results

Summarizing the results we have seen that the observed CO(g) intensity is directly related to the SiO_2 depletion of the samples. The CO(g) intensity can be observed as soon as the sample attains 1273 K. It increases with increasing temperature until a maximum and decreases then continually due to SiO_2 depletion in the heated zone of a sample.
The gradual temperature increase has shown different effects:

- The CO(g) pressure made a peak with every temperature increase step in the beginnings.
- Every temperature increase step mobilized the SiO_2 reserve either remained in the still not heated sample regions or in the higher container regions, where it has remained or was re-crystallized because of intentioned temperature gradient.
- The last temperature increase did not mobilize any SiO_2 if CO(g) intensity was decreasing.
- The remaining oxygen participate on the active oxidation of the SiC grains.
- The time is also an important factor, for the outgoing total flow is determining for the SiO_2 elimination.

The shape of the CO(g) intensity peak and its decrease depend on the sample and temperature increase rate. In the case of SiC and SiO_2 powder mixtures, active oxidation of bare

SiC grains, which have already lost their protective layer, maintain a certain CO(g) partial pressure resulting in slower decrease of CO(g) intensity than for other samples, with SiO_2 in form of a surface layer only.
Because of the bimodal grain size distribution in the corresponding samples double peaks or shoulders in the CO(g) intensity graph occur due to different SiO_2 depletion rate of different grain sizes. The slower heating rates shift the CO(g) intensity peaks and the end of CO(g) detection to higher temperatures due to more homogeneous temperature distribution in the sample and container.

3.3.3 Characterization results

3.3.3.1 Manually adjusted temperature increase

3.3.3.1.1 Raman spectrometry The powder samples after experiment in capillary mass spectrometer were analyzed by Raman spectroscopy. Figure 3.55 displays the Raman spectra from SiC powder, SiC–2 mol% SiO_2 powder mixture and oxidized bimodal SiC powder mixture samples with zooms in the frequency regions between 100-600 and 700-1050 cm^{-1}. Different observations lead to following conclusions:

- The background level of the oxidized bimodal SiC powder mixture sample in the low frequencies region, 100-300 cm^{-1}, is higher than from other two samples. This is an indication for remained amorphous structures like SiO_2.

- No fluorescence is observed for SiC–2 mol% SiO_2 powder mixture sample, but SiC powder and oxidized bimodal SiC powder mixture sample show also only a low fluorescence level. In the case of SiC–2 mol% SiO_2 powder mixture sample the received energy during Raman spectra measurement was eliminated at best, so the quality and/or quantity of grain interconnections must be also the best for this sample.

- All samples show a carbon presence with the peaks at high frequencies between 1500 and 1700 cm^{-1}. The heating process was performed beyond the active oxidation limit until carbon precipitation for all experiments from these samples.

- At the zoom insert in the low frequency region we can see that the shape of the peaks is similar for SiC powder and SiC–2 mol% SiO_2 powder mixture. They correspond to the 6H SiC polytype except the small peak at 256 cm^{-1} corresponds to 15R. Furthermore the oxidized bimodal SiC powder mixture sample has a 4H peak at 195 cm^{-1}. Zoom at the peaks in higher frequencies shows further differences between the samples. The shoulder at 789 cm^{-1} is present only for the SiC–2 mol% SiO_2 mixture sample. This frequency corresponds theoretically to 6H SiC-polytype, but in this frequency region peaks from different SiC-polytypes are located too close to each other or occur even altogether at same frequencies. Following it is not possible to separate them properly in different SiC polytypes. The lack of a shoulder at 938 cm^{-1} for SiC–2 mol% SiO_2 mixture sample should be also mentioned. A peak at 938 cm^{-1} would correspond to 15R polytype. In low frequencies zoom the 15R peak is very small for SiC–2 mol% SiO_2 mixture and it is hardly to separate from the background. It confirms the lack of 15R SiC polytype in SiC–2 mol% SiO_2 mixture sample.

According to W.F. Knippenberg [67], different SiC polytypes during heat treatments are formed at different corresponding temperatures when the Si/C ration in the corresponding gaseous phase is equilibrated.

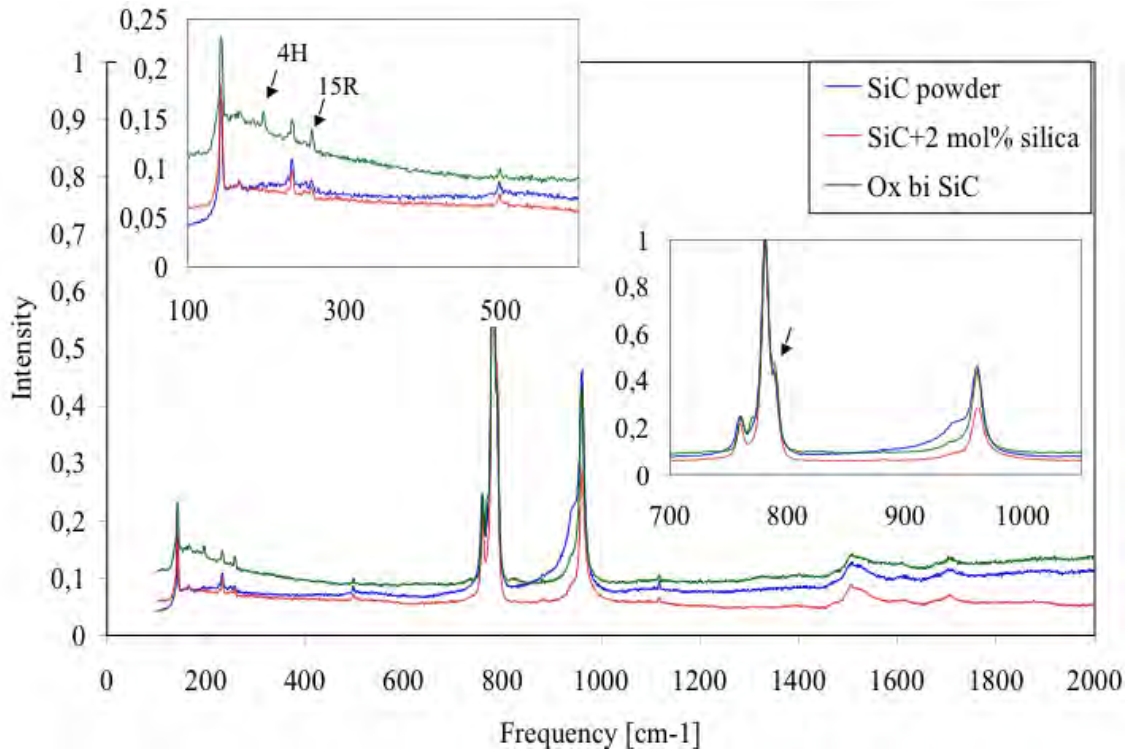

Figure 3.55: Raman spectra of SiC powder (16-10), SiC–2 mol% SiO_2 powder mixture (26-10) and oxidized bimodal SiC powder mixture (23-10) samples characterized after capillary mass spectrometer experiments.

3.3.3.1.2 SEM/FEG observations SEM/FEG images displayed at figure 3.56 give further informations about SiC powder, SiC–2 mol% SiO_2 powder mixture and oxidized bimodal SiC powder mixture samples which correspond to the Raman spectra discussed above. The agglomerates of SiC powder sample at image a) were already observed in the images of initial powder. No grain to grain connections can be observed. It confirms observed fluorescence at the corresponding Raman spectrum. The heat treatment at 1600 K for 1h was not sufficient for neck formation for this powder sample.
Best connections formation is observed for the SiC–2 mol% SiO_2 powder mixture sample after 26-10 experiment, fig. 3.56 b), which confirms the observed lack of fluorescence for this sample in the Raman spectra at fig. 3.55. This sample was heated at 1500 K for 2,5h and at 1690 K for 1,5h. Besides the connections between the grains we can observe several plain surfaces on the grains, facets. This occur via surface diffusion at high temperatures due to surface energy minimization. The necks between the grains have formed during the first plateau at 1500 K for 2,5h, we will see in later discussed results that this temperature is sufficient. The slow departure of SiO_2 content, as observed via CO(g) release in capillary mass spectrometer, results in active oxidation of SiC grains and still bare surfaces (no

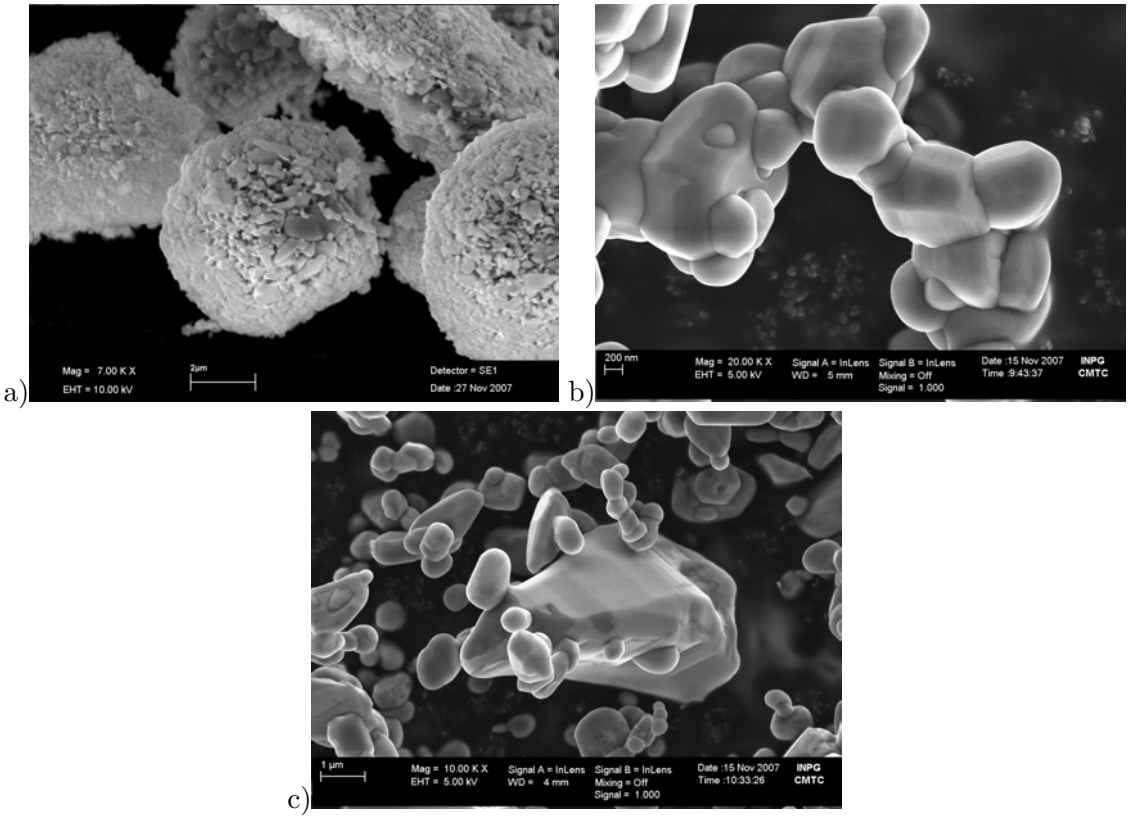

Figure 3.56: SEM/FEG images of a) SiC powder sample after 16-10 experiment ($T_{\max} = 1599\,\mathrm{K}$), b) SiC–2 mol% SiO_2 powder mixture sample after 26-10 experiment ($T_{\max} = 1700\,\mathrm{K}$) and c) oxidized bimodal SiC powder mixture sample after 23-10 experiment ($T_{\max} = 1600\,\mathrm{K}$).

carbon precipitation) at high temperature. It is the main reason for the observed SiC grain to grain connections quality. The surface diffusion occurred during the second plateau at 1690 K.

At image 3.56 c) only some grain interconnections are observed. The fine grain fraction of the bimodal mixture is still present. There are the fine grains which become rounded and built connections between each other and to the coarse grains. The treatment of this sample was similar to the one of SiC–2 mol% SiO_2 powder mixture: two plateaux of 1500 K and 1600 K each for 1,5h (experiment 23-10). The few connections are insufficient to eliminate the energy received from laser during Raman spectrum measurement. The result is the shifted level of fluorescence. In this sample the whole amount of SiO_2 was superior to the one in SiC–2 mol% SiO_2 mixture sample as observed during capillary mass spectrometer experiment. But in this case the nature of SiO_2 is different, it is a layer on the SiC grains. Bare SiC surfaces are only present when all SiO_2 is gone. Thus there is no more sufficient oxygen to keep them bare when the Si begins to vaporize in excess to carbon.

Figure 3.57 a) shows the SiC–2 mol% SiO_2 mixture after heating up to 1500 K for 40 min. and oxidized bimodal SiC mixture sample after $T_{\max} = 1529\,\mathrm{K}$ during 45 min. The grains of SiC–2 mol% SiO_2 mixture sample have clearly build up necks between each over. Furthermore they got facets which proves surface diffusion to minimize surface energy.

a) 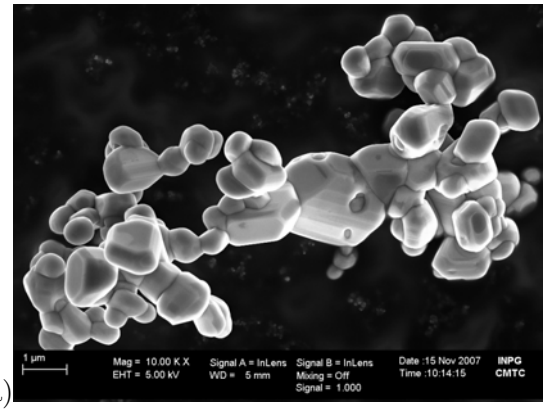

b) 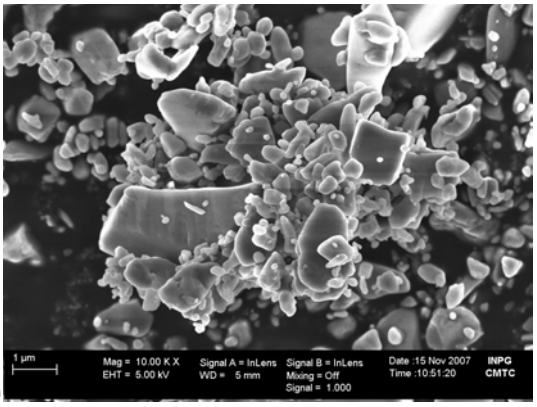

Figure 3.57: SEM/FEG images of a) SiC–2 mol% SiO_2 mixture sample after 08-11 experiment ($T_{max} = 1500\,K$ during 40 min) and of b) oxidized bimodal SiC mixture sample after 13-11 experiment ($T_{max} = 1529\,K$ during 45 min).

a) 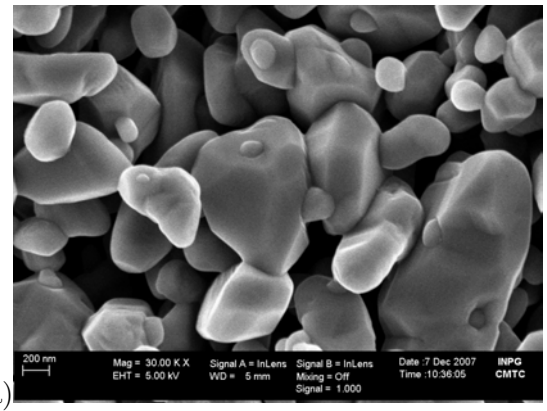

b) 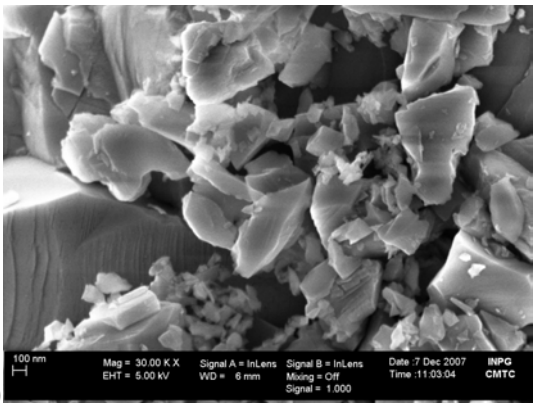

Figure 3.58: FEG images of a) SiC–2 mol% SiO_2 mixture after 06-12 experiment ($T_{max} = 1650\,K$) and b) oxidized SiC bimodal powder mixture after 28-11 experiment ($T_{max} = 1560\,K$).

The grains from oxidized bimodal SiC mixture sample at the same figure in image b) got rounded. No facets are observed in this case.
These two different samples got similar heat treatment in the capillary mass spectrometer. The samples were heated until no more CO(g) was observed at $\approx 1500\,K$. The reasons for the observed difference in the obtained structures can be only the nature of present SiO_2 in the initial powders and SiC grain size distribution. In the case of oxidized SiC bimodal mixture only the grains which have got bare surfaces in the concerning temperature region have built necks between each other. It is the fine grain fraction. Coarser grains have kept a little layer of SiO_2. SiC grains of certain size need higher temperature treatment to lose their SiO_2 layer. The observed necks between coarse and fine grains are due to locally bare surface on the coarse grains because the kept SiO_2 layer does not cover the whole surface of the grain, it has got gaps due to the temperature treatment.
Figure 3.58 shows the FEG images of the SiC–2 mol% SiO_2 mixture after 06-12 experiment and oxidized bimodal SiC mixture sample after 28-11 experiment. Each experiment was stopped just when the CO(g) peak began to decrease for the first time. It was the case

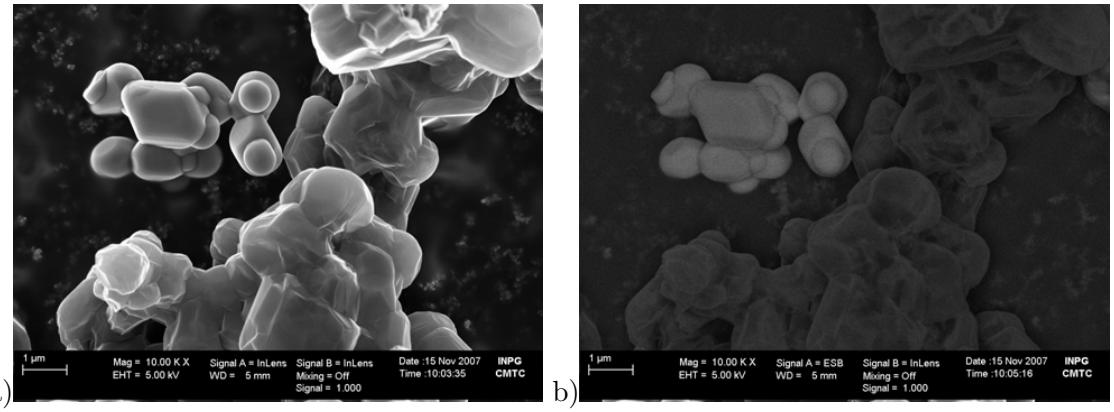

Figure 3.59: FEG images of SiC–2 mol% SiO_2 mixture after 06-11 experiment (T_{hold} = 1500 and 1740 K during 1,5 and 2h): a) normal imaging mode; b) back scattered electron detection imaging mode makes visible the graphite layer on the surface of the right grain group.

at 1650 K for the SiC–2 mol% SiO_2 mixture sample and already at 1560 K for oxidized bimodal SiC mixture sample. The mixture with SiO_2 shows necks and facets, when the oxidized bimodal SiC powder sample does not show any significant difference to the initial powder. One reason may be the different maximum temperature, which is 90 K higher for SiC-SiO_2 powder mixture. But according to mass spectrometric measurements both samples have reached the same reaction state—partial pressure of CO(g) began to decrease. The main reasons are the bimodal grain size distribution and the more important thickness of the oxidation layer on the grains of the oxidized bimodal SiC mixture sample. At given temperature only fine grain size has lost its SiO_2 layer by vaporization. For the vaporization from the coarser grains higher temperature was necessary. CO(g) partial pressure began to decrease and no necks could be formed because the temperature decreased immediately. Contrarily, in the sample of SiC–2 mol% SiO_2 mixture there is no large gap between the grain sizes, the CO(g) release is made continuously. When the thin oxidation layer is gone there is still the added SiO_2 powder which has kept the CO(g) partial pressure level. It begins to decrease at clearly higher temperature. The bare surfaces were present before the temperature was decreased, following necks and facets could be formed.

Figure 3.59 shows the sample after 06-11 experiment (T_{hold} = 1500 and 1740 K during 1,5 and 2h). The maximum temperature was hold during 2 hours. We can see in the middle of image a) a group of interconnected powder grains. Comparing to the group on the left side we can see that the connections between the grains are different. Image b), obtained with ESB detection, shows that the grain group in the middle is covered with a graphite layer contrarily to the group on the left side. This can occur only when the connections have formed at different times. The grain group covered with graphite was formed much earlier, during the holding time at 1500 K. We can even observe facets under the graphite layer. This group began already to lose Si(g) in excess because of non-congruent vaporization of SiC observed by different authors [19, 20, 101] and proved with calculations based on collected free energy data [5]. There was locally not enough oxygen to remove the remained carbon. Besides in the concerning temperature region no more CO(g) was observed, so no more SiO_2 as oxygen supplier was present.

The grain group which was not covered with graphite was made later. It shows facets, it was still in the surface diffusion phase as the experiment was stopped and the temperature decreased. The location inside the crucible is a further reason for different reaction state. The group non-covered with C was located near the top of the crucible and there are two reasons for which it did not reach the same reaction state: (i) due to the temperature gradient the temperature at the crucible top was lower than at the crucible bottom, (ii) the condensed SiO_2 in the cone and top sample layers begins to evaporate and enrich the local atmosphere with oxygen. Because of the build-in temperature gradient we were able to observe different states of evolution in the same experiment.

3.3.3.1.3 Summary The presence of SiO_2 is necessary for well grain interconnection. At the same time the SiC grains must present bare surfaces when the mass transport via gaseous species is running. For this reason addition of SiO_2 in form of powder is to prefer rather than an oxidation layer on SiC grains. The re-condensed SiC forms new SiC polytype structures observed by Raman at $789\,cm^{-1}$. According to Raman observations the necks are constituted from 6H polytypes coming from 15R and 4H grains because the re-crystallization conditions, like temperature range and Si/C ratio in the gaseous phase, have favored the re-crystallization of 6H.
The SiC grains begin to reorganize their surfaces by surface diffusion and to build facets for surface energy minimization when the necks are already formed and the temperature remains still high enough. When the temperature increase continues or a next higher temperature is held during a certain time the formed grain groups begin to precipitate carbon on their surfaces.

3.3.3.2 Fixed temperature ramps

3.3.3.2.1 Raman spectrometry Raman spectra of samples after capillary mass spectrometer experiments applying different temperature ramps are displayed in figure 3.60. The only difference between the powders is the temperature increase rate in the $1273 - 1473\,K$ interval. In all samples carbon peak at $> 1500\,cm^{-1}$ frequencies was observed, figure 3.60 c). The sample after $100\,K/h$ ramp has the lowest level of fluorescence in high frequency region but generally no direct relation between the heating rate in the concerning temperature range and fluorescence level was observed (see figure 3.60 c)).
Zooming onto 100-300 cm^{-1} frequency interval at figure 3.60 a) we observe the lack of 4H SiC polytype peak at $195\,cm^{-1}$ for the sample from $25\,K/h$ ramp. There is at $776\,cm^{-1}$, figure b) zooms in this frequency interval, another characteristic peak of 4H SiC polytype. We can observe the lack of it for sample from $25\,K/h$ ramp. The $25\,K/h$ sample remained the longest time in the $1373 - 1473\,K$ temperature region. This should have influenced the gaseous phase, particularly the Si/C ratio, during this time. Following it was different compared to the other ramps and not favorable for the formation of 4H SiC polytype.

3.3.3.2.2 SEM/FEG observations In the FEG images, connections between the single grains of the fine grain size fraction and between fine and coarse grains and facets were observed. But no significant differences between the different samples were observed.
Contrarily to the experiments with adjusted increase in temperature here the heating was performed slower. The maximum temperatures in the precedent experiments varied from 1500 to $1600\,K$ for 45 min. to 1,5h. The connections of similar quality were obtained only

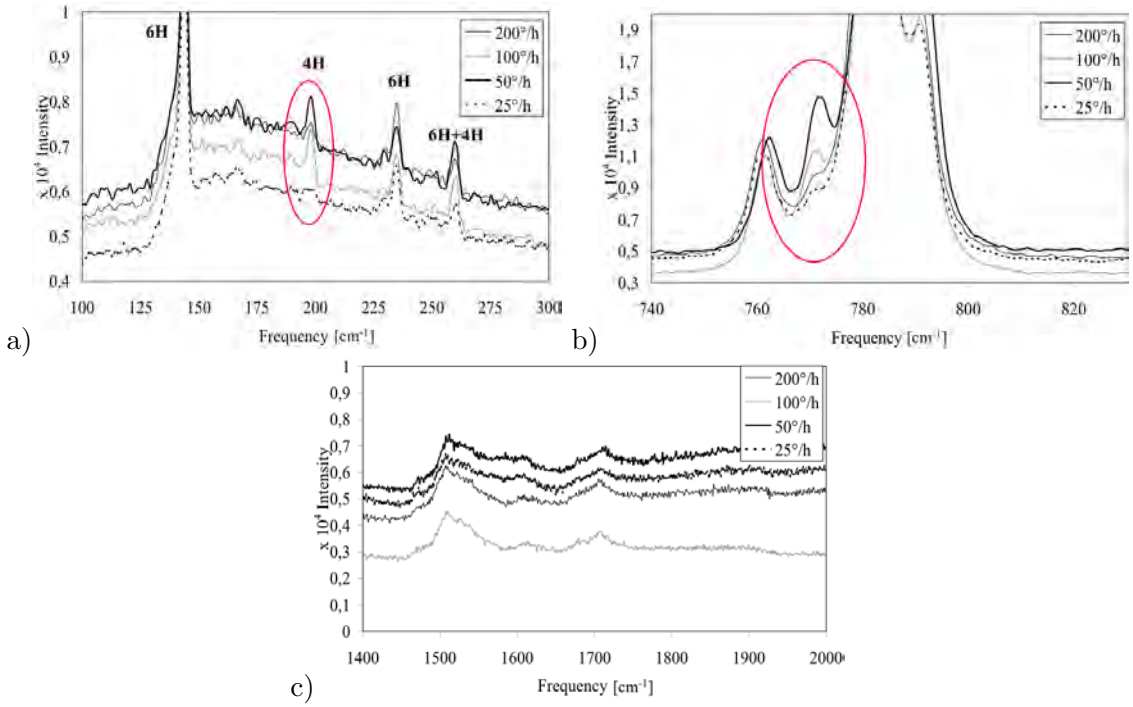

Figure 3.60: Zoom on Raman spectra of oxidized bimodal SiC powder mixture samples from experiments with different temperature ramps.

in experiment 23-10 with two holding plateaux at 1500 and 1600 K for 1,5h each. For the fixed temperature ramps experiments the maximum temperature was only 1473 K but the samples remained for 0,5 to 4 hours above 1373 K and 1h at 1473 K. This time was sufficient to get the SiC grain surfaces bare due to SiO_2 vaporization via SiO(g) and CO(g). The grains could build necks and facets. No graphite covered grain groups were observed (fig. 3.61).

3.3.3.2.3 Summary Differences in CO(g) release were observed by different heating rate apply. The reason for these differences was found to be the nature of the sample, the bimodal grain size distribution mixture. As the coarse grain size fraction vaporized slower an apparition of a shoulder was noticed for slow temperature ramps. No direct relation of temperature increase rate and fluorescence level of Raman spectra was found. Only the absence of 4H SiC peak was observed for the slowest ramp sample, 25 K/h. It means that the 25 K/h heating between 1372 and 1473 K is not favoring for the formation of 4H SiC polytype. It may mean also that mainly this polytype is consumed by vaporization process, as we have found earlier that the SiC grains are constituted from 4H polytype. Necks and facets were observed for all sample from the fixed temperature ramps experiments. No significant differences were observed in the SEM images of samples from different ramps experiments.

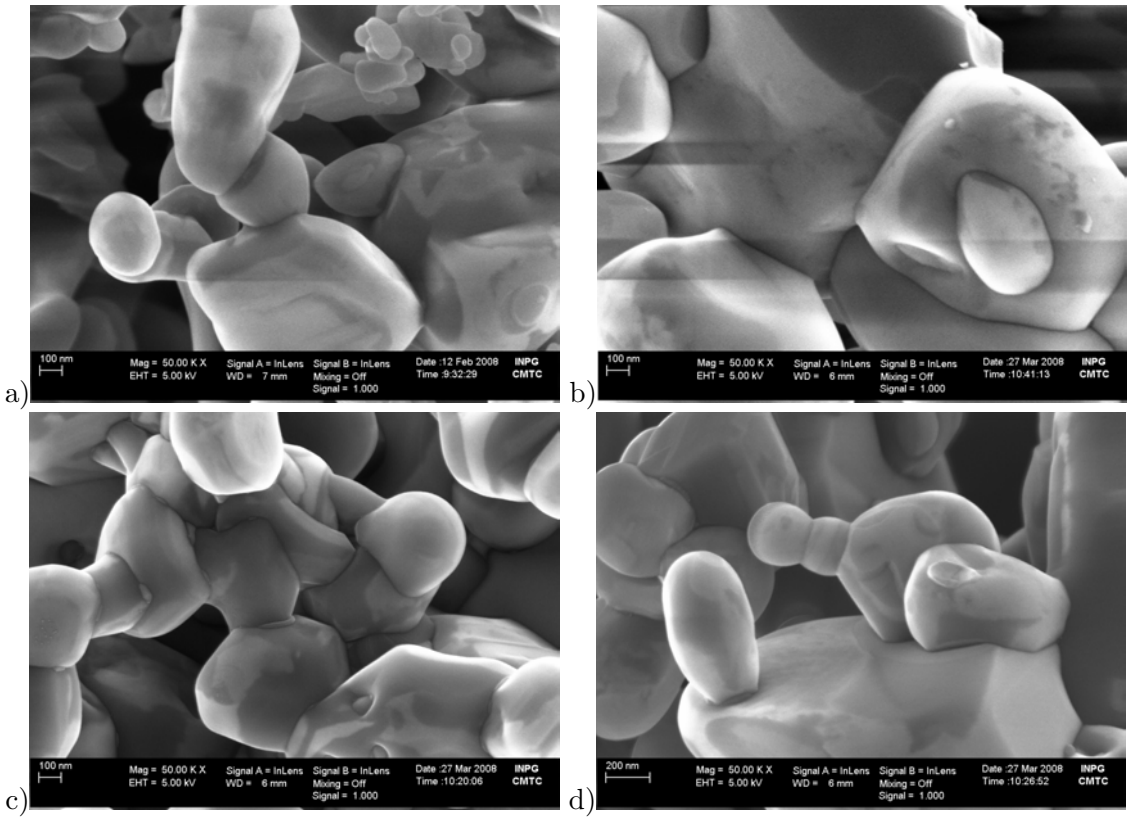

Figure 3.61: FEG images of oxidized bimodal SiC powder mixture samples from experiments with different temperature ramps a) 200 K/h, b) 100 K/h, c) 50 K/h, 25 K/h.

3.3.4 Conclusions

We have already seen in the experiments in the high temperature mass spectrometer that SiO_2 loss is obtained by vaporization via SiO(g) and CO(g). The intensity of the latter was observed here with capillary mass spectrometer. SiO(g) re-condensed in the crucible cone mainly to SiO_2 with some SiC content.
The presence of SiO_2 in the initial sample powder was found as necessary for well grain interconnection. With increasing temperature the SiC grains must present bare surfaces. It is realized via SiO(g) and CO(g) vaporization, which transport the SiO_2 and carbon from the SiC grain surfaces. For this reason addition of SiO_2 in form of powder is to prefer rather than oxidation of SiC grains, which cover their surface with SiO_2 layer. The re-condensed SiC forms new SiC polytype structures observed by Raman at $789\,cm^{-1}$. According to Knippenberg [67], modification of the heating treatment with stable equilibrium gaseous phase, particularly the Si/C ratio in the vapor, have direct influence on the grown SiC polytype. Different SiC polytypes in the treated samples were identified with Raman spectroscopy. It is possible that the necks are constituted from 6H and the initial SiC grains from 4H and 15R polytypes.
If the temperature remains relatively high for a certain time or increases the connected SiC grains begin to reorganize their surfaces by surface diffusion and to build facets to decrease the surface energy. When the temperature increase continues or a next higher temperature is held during a certain time the formed grain groups begin to precipitate carbon on their surfaces.
Oxidized powder samples made from two different SiC grain sizes got a shoulder in the CO intensity diagram due to the gap between the CO(g) partial pressure from fine grain size and from coarse grain size. Their peaks became separated due to slower CO(g) release for coarse grain sizes.
Necks can be formed already at 1473 K, only the temperature increase rate must be slow enough to obtain bare SiC surfaces at the same time with residual low oxygen pressure resulting from SiO_2 evaporation.
If the temperature is held longer, the grains become faceted due to surface diffusion. And when the temperature treatment lasts too long carbon precipitation occurs at the grain surfaces.

4 Evaporation/condensation mechanism in SiC powders

In this chapter we propose a consolidation mechanism for the fine grained SiC powders based on the results from the experiments performed in HTMS and in quadrupole mass spectrometer fitted with capillary and thermodynamic calculations. This mechanism is more complex than proposed by Kriegesmann [63, 102].

4.1 SiC and SiO_2 interactions

We have seen that the SiC compound does not vaporize congruently, the gaseous phase is always richer in Si(g) and the condensed phase becomes poor in Si(s, l). The risk to precipitate free carbon increases. Furthermore the SiC grains are always covered with a native SiO_2 layer due to earlier passive oxidation at ambient conditions (wet or dry grinding at atmospheric pressure and room temperature). Additionally this layer may become thicker due to different processing steps during industrial process of a bulk SiC material manufacturing. Attention must be payed to these points before any consideration can be made.
In the early stages of any vaporization process of SiC or during vaporization of SiC and SiO_2 containing powder samples two main points were observed:

- SiO(g) and CO(g) as vaporization products were detected with partial pressures always lower than calculated according to the main vaporization reaction:

$$\mathrm{SiC(s)} + 2\mathrm{SiO_2(s)} = 3\mathrm{SiO(g)} + \mathrm{CO(g)}. \tag{4.1}$$

- The pressure ratio $p(\mathrm{SiO})/p(\mathrm{CO})$ was always lower or equal to 1, contrarily to predicted ratio of 3 (azeotrop) or 3,76 (under vacuum) according to the congruent reaction 4.1.

This vaporization behavior was noticed for all samples, independent on the added SiO_2 amount and also for the oxidized powders, where a SiO_2 scale additionally to the native scale was built intentionally.
At the end of experiments with powder mixture samples powder aging was observed with increasing temperature. For higher SiO_2 contents less powder aging was observed.
Figure 4.1 a) displays SiO(g) partial pressures from three samples as examples for only SiC powder vaporization, mixture of SiC with SiO_2 and oxidized SiC powders. Three domains are observed:

- The vaporization in the first domain can be fitted with arrhenius equation, $\log p = \mathrm{A}\frac{10^4}{T} + \mathrm{B}$. The mass flow via the gases is still too low to change the condensed sample.

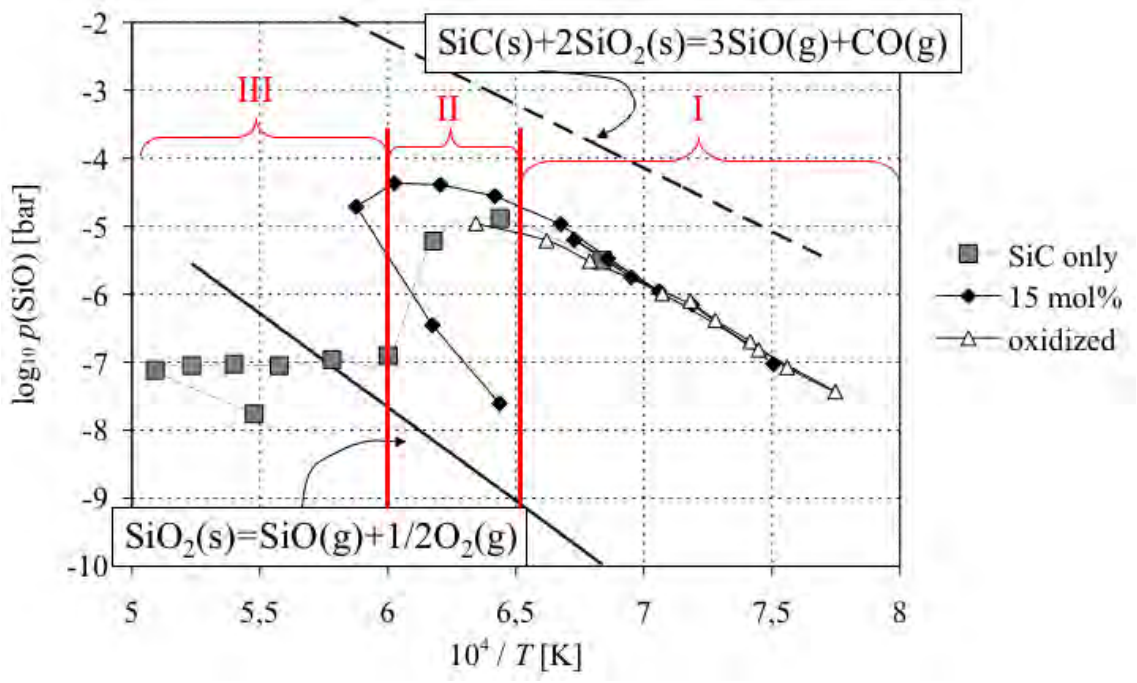

a)

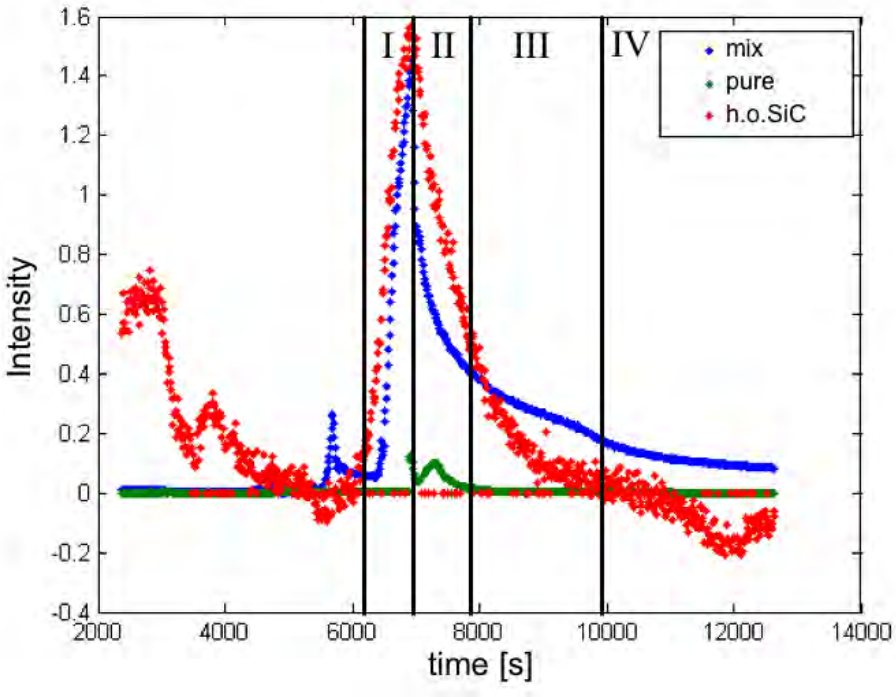

b)

Figure 4.1: Domains of Arrhenius evolution (I), powder aging and SiO_2 elimination (II), active oxidation (III) and carbon precipitation(IV) displayed on: a) SiO(g) partial pressure measured during vaporization experiments in HTMS compared to p(SiO) calculated for congruent SiO_2 pure vaporization and for SiO_2/SiC vaporization at interface. b) CO(g) intensities from experiments in mass spectrometer reactor with capillary tubing.

- Vaporization in the second domain corresponds to powder aging. Here the samples began to change their composition. In our case it is the domain where the SiO_2 loss becomes more important. There is no more enough SiO_2 in the samples to keep the pressure increase with increasing temperature.

- The third domain corresponds to complete SiO_2 loss in the solid samples, either SiO_2 powder grains or scale on SiC grains. It is also the domain of active oxidation of the SiC sample, since we have detected SiO(g) which remains constant. Only the SiC powder samples attained this state. The SiC–SiO_2 mixtures were still in "powder aging" domain when the temperature was decreased.

Figure 4.1 b) displays CO(g) intensities of three samples from experiments in mass spectrometer reactor with capillary tubing. Here we can also separate the same domains as described above. The forth domain is added to display the risk of carbon precipitation if no more oxygen is available in close vicinity of the SiC surface.

4.1.1 SiO(g) and CO(g) partial pressures

To answer the question why the SiO and CO pressures are lower than at equilibrium and their ratio smaller or equal 1, we propose a model of vaporization of SiC with SiO_2 powder mixture, which is explained below.
We have seen, that any SiC powder does never exist as just SiC but its grains are always covered with a layer of SiO_2, which is more or less thick. The result is, that mixing SiC powder with a certain amount of SiO_2 powder we would never obtain bare SiC and SiO_2 powder surfaces in contact. Regarding the surfaces there are only SiO_2 powder in front of SiO_2 scale. This explains why in the experiments with SiC-SiO_2 powder mixtures and with only oxidized SiC powder same general observations for the SiO(g) and CO(g) partial pressures were made. Figure 4.2 shows the proposed model for generation of the gases observed during HTMS experiments before aging.
A SiO_2 scale surface for an isolated SiC grain, will have the oxygen potential of the congruent SiC/SiO_2 vaporizing surface.
An isolated SiO_2 grain has the tendency to vaporize congruently according to:

$$SiO_2(s) \rightarrow SiO(g) + 1/2O_2(g) \tag{4.2}$$

$$2SiO_2(s) \rightarrow Si_2O_2(g) + O_2(g) \tag{4.3}$$

$$O_2(g) \leftrightarrow 2O(g) \tag{4.4}$$

$$SiO_2(s) \rightarrow Si(g) + O_2(g) \qquad \text{etc...} \tag{4.5}$$

The main species resulting from calculations of the congruent vaporization are SiO(g), O_2(g) and O(g). The oxygen potential created in this way is by far higher than the one at the SiC/SiO_2 interface.
As we can see SiO(g), O_2(g) and O(g) are produced. Calculated equilibrium partial pressure of SiO(g) from reaction (4.2) is a factor 10^3 to 10^4 lower than the measured SiO(g) pressures over the SiC-SiO_2 system. It means that the vaporizing sample is trying to keep the equilibrium constant $K_p(T)$ from reaction (4.2) and increases the SiO(g) partial pressure because O_2(g) is consumed or lost elsewhere. Indeed, O_2 is consumed because of diffusion of O^{2-} ions through the SiO_2 scale on the SiC powder grains, as reported in reference [47],

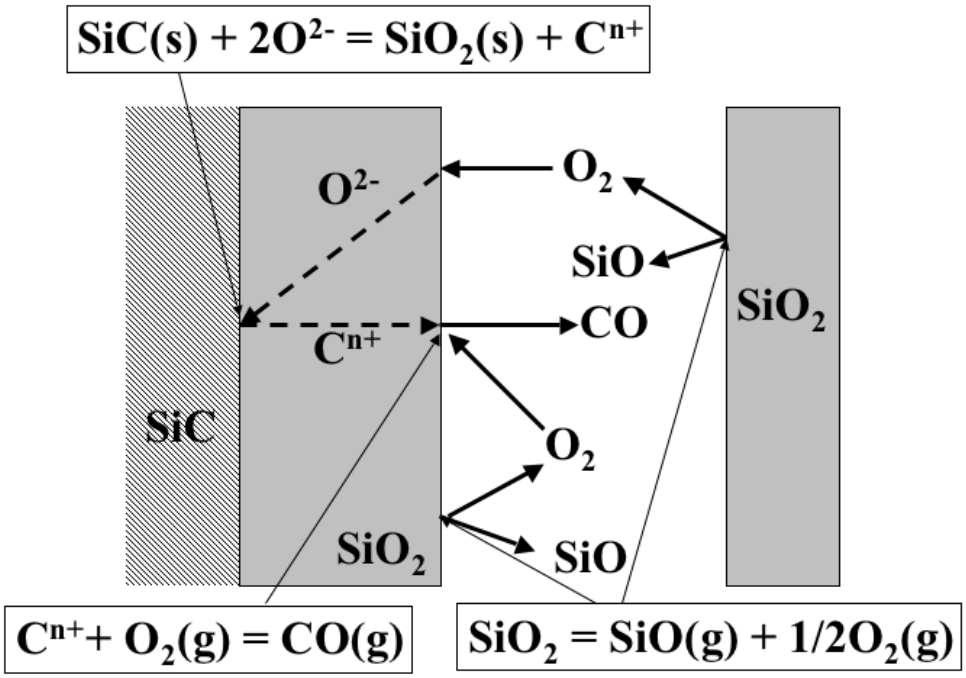

Figure 4.2: Surface of SiC grain covered with SiO_2 scale in front of SiO_2 grain surface. Diffusion through the SiO_2 scale and corresponding reactions which generate the gaseous phase.

to react with SiC according to:

$$SiC(s) + 2O^{2-} = SiO_2(s) + C^{n+}. \tag{4.6}$$

Due to this reaction the SiO_2 scale on the SiC is maintained and C^{n+} ions are created. Produced C^{n+} diffuses outwards through the SiO_2 scale (reported in reference [47]) * and reacts with oxygen at the surface to form CO(g), which we measured with HTMS. The partial pressures generated due to proposed mechanism are lower than in the case of azeotrop/congruent reaction (4.1) due to diffusion kinetics.

The oxygen potential in this system is generally very low. We have calculated the SiO(g) and CO(g) partial pressures as a function of oxygen potential, which was varying from one corresponding to the azeotrop/congruent reaction (4.1) to congruent SiO_2 vaporization, reaction (4.2). We considered all possible reactions for the oxygen production in the corresponding system. This oxygen serves for the following oxidation of SiC. The SiO(g) is calculated as coming from the SiO_2 congruent vaporization and active oxidation of SiC, the CO(g)—from SiC active oxidation only. The results are displayed in figure 4.3 for several temperatures. We can see, that the SiO(g) pressure is higher than CO(g) pressure for the azeotrop/congruent reaction and with increase of oxygen potential they reverse. Indeed, when we consider higher oxygen potential than for the reaction (4.1), the $p(\mathrm{SiO})/p(\mathrm{CO})$ ratio become equal or less 1, exactly as we have observed during the HTMS experiments.

*Zheng et al. [47] have measured the ^{13}C profile in the SiO_2 layer on the $Si^{13}C$ in the frame of SiC passive oxidation study. They concluded that the diffusion of carbonaceous species is rapid compared to oxygen. They assumed C, CO and CO_2 diffusion but finally it is not clear, which carbonaceous species is diffusing. For this reason we are using C^{n+} to describe any carbonaceous species/ion diffusion.

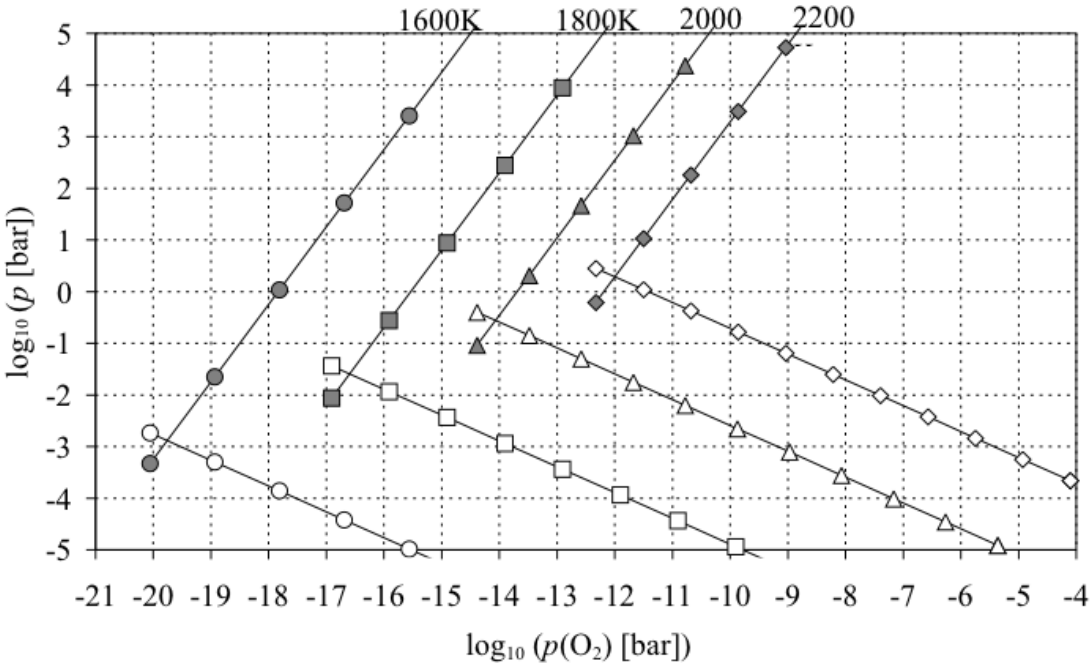

Figure 4.3: Decimal logarithm of calculated SiO(g) (white symbols) and CO(g) (dark symbols) partial pressures plotted as a function of decimal logarithm of oxygen pressure at the SiC grains surface which is varied from its minimum for a congruent reaction between SiO_2 and SiC (interface of SiO_2 and SiC) towards its maximum for congruent vaporization of only SiO_2 grains at 1600, 1800, 2000 and 2200 K.

A secondary consequence of this model is, that as long as SiO_2 grains are present in the mixture with SiC grains it is very difficult or even impossible to eliminate the SiO_2 scale on the SiC grains because of reaction according to (4.6). The presence of SiO_2 grains in the powder mixture maintains a higher oxygen potential than at congruent vaporizing SiC/SiO_2 interface, which is the limiting case of scale thickness tending towards 0.

4.1.2 SiO_2 amount and SiO(g) and CO(g) partial pressures

For vaporization according to reaction (4.1), which is azeotrop or congruent (vacuum), same partial pressures at fixed temperature are predicted for any condensed phase composition. In experiments with different amounts of SiO_2 powder we have seen that the partial pressures of SiO(g) and CO(g) depend on the SiO_2 quantity in the mixture sample (see fig. 4.4), contrarily to the above thermodynamic prediction.

Applying the model of SiC grains covered with SiO_2 scale mixed with grains of SiO_2 powder the differences in the SiO(g) and CO(g) pressures for different amount of added SiO_2 powder is explained, because no congruent or azeotrop reaction is presumed. For the SiO_2 contents higher than 30 mol%, the gaseous phase becomes saturated with emitted gases and cuts down the other gases generating process. It results in some lower partial pressures than at maximum, were a steady state between generation and effusion through the orifice was attained. For the SiO_2 contents below 30 mol% the total surface of SiC increases compared

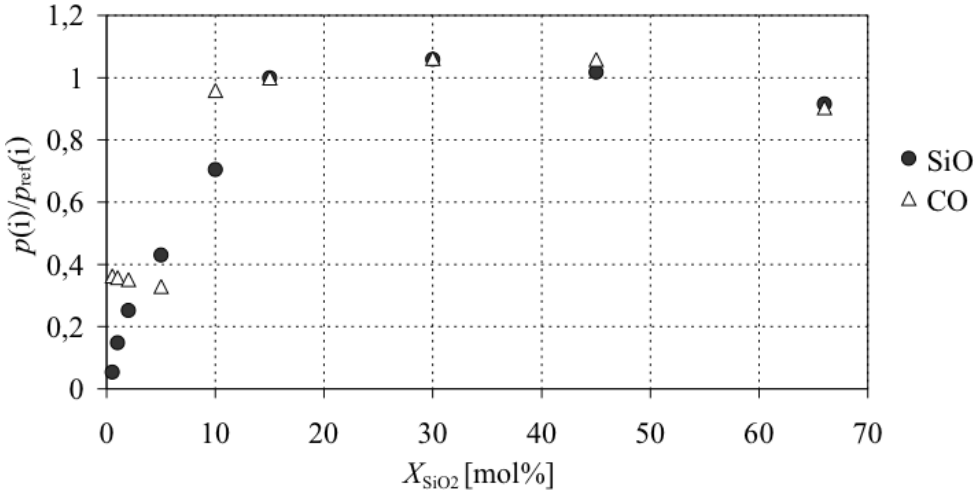

Figure 4.4: Relative measured partial pressures of SiO(g) and CO(g) as a function of powder composition of different samples referenced to 15 mol% at 1625 K. For SiO_2 contents lower than 10 mol% the CO(g) partial pressures should behave in the same manner as SiO(g): indeed, the obtained almost constant values for low SiO_2 contents were measured with Si(g) interfering in the mass spectrum 28.

to the O_2 generating SiO_2 surface. The mean oxygen potential decreases and the O^{2-} diffusion controlled process of CO generating becomes then again less important than the escape of the gases from the grain surface.

4.1.3 Powder aging

The phenomenon of powder aging describes irreversible changes in the condensed samples due to material loss by vaporization. It was particularly well observed for the powders with low SiO_2 content, but generally for all SiC-SiO_2 mixture samples. It was characterized with different SiO(g) and CO(g) partial pressures with decreasing temperature which were much lower than the pressures measured with increasing temperature. Following, these samples must have undergone more structural and/or composition changes than samples with high SiO_2 content samples. Indeed, at the SEM images of these samples (figures 3.45 and 3.46 on pages 123-124) we observed something like grain interconnections besides rounded grains shapes.

Figure 4.5 displays single steps of powder aging which result from application of our model and a SEM image of 15 mol% sample as example for observed SiO_2-neck formation as result of powder aging. Image a) shows that the SiC grains with irregular form become rounded due to reaction of SiC with diffused oxygen into SiO_2 firstly at the angles and edges. The SiC is consumed (reac. (4.6)), and transformed into SiO_2 during SiO_2 elimination at the scale surface (reac. (4.2)). At least this stage was attained by the samples with high SiO_2 content, we observed rounded grains. Image b) displays that for two grains in contact the CO departure is geometrically limited, the evaporation surface is decreased and gases cannot escape at the same rate as at the open SiO_2 scale surface. This results in thicker scale at the contact points than elsewhere (image c)) and finally, when the scale became very thin at the open surfaces, it remains thicker at the grain to grain contact points and

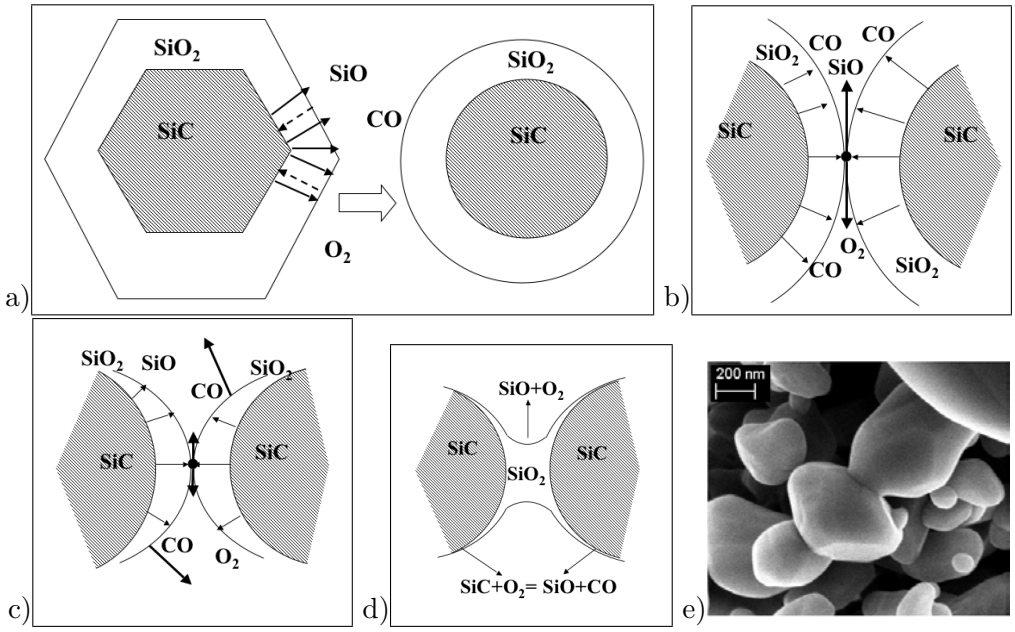

Figure 4.5: Powder aging displayed in steps. a) SiC grains rounding; b) vaporization of SiO(g) and CO(g) is cut down at grain contact points; c) irregular elimination of SiO_2 scale; d) SiO_2 necks are formed; e) necks observation with SEM for 15 mol% SiO_2 sample.

simulate a neck, observed sometimes for samples with high SiO_2 content and more often for low SiO_2 content samples.
Necks from SiO_2 are formed as a result of powder aging in the SiC-SiO_2 samples before complete elimination of silica from the sample.

4.1.4 Conclusion

Proposed model of SiC powders covered with SiO_2 scale in mixture with SiO_2 powders and keeping of this scale until complete elimination of SiO_2 powder is well confirmed with the SiO(g) and CO(g) partial pressure observations during performed experiments. Three different domains of changes in the condensed phase are found:

- domain of regular equilibrium vaporization, which can be plotted applying arrhenius law, without large changes in the condensed phase;
- domain of sample powder aging, where the changes in the vaporization samples become important due to material loss via vaporization, and decrease of SiO/CO partial pressures because of elimination of SiO_2 either from the added SiO_2 powder or from the SiC scale;
- last domain, where no more SiO_2 is present in the condensed sample; oxygen-free species become important because of high temperature and measuring of SiO(g)/CO(g) is only due to the SiC active oxidation with oxygen reserves in the sample surroundings, liberated because of high temperature.

The elimination of SiO_2 scale in the narrow space between two grains is geometrically hindered, produced vapors cannot escape freely. This lead to locally thicker scale and afterwards necks of SiO_2 between the SiC grains. These necks were observed with SEM/FEG in samples from the experiments, where the SiO_2 was not completely eliminated. It was confirmed with SMHT measurements, that the samples were still in the powder aging state. The samples with high contents of SiO_2 develop higher SiO(g)/CO(g) pressures than the samples with low SiO_2 contents. At the same time less powder aging than for low contents of SiO_2 was observed since the experiments were finished with same temperature values.

4.2 SiC bare surface

We have seen in the precedent part that the SiC powders lose their SiO_2 layer during heating process by evaporation of SiO(g) and CO(g). In the present section we will see what happens afterwards, when bare SiC grain surfaces are obtained.

4.2.1 Obtaining bare SiC surface

Obtained SiC composition just after elimination of the SiO_2 scale, according to thermodynamics, must become placed somewhere in the Si-C stoichiometric domain. At the same time the silicon activity is increasing with increasing temperature and becomes finally 1 if T exceeds 2000 K. Figure 4.6 displays the Si-O-C triphasic diagram with in-drawn possible stoichiometric composition evolution tie-lines for the pseudo-binary SiC-SiO_2 section. Composition evolution for the firstly predicted interface SiO(g)/CO(g) partial pressures ratio equal 3 is shown with dashed red line but was not confirmed with results from performed experiments. The observed ratio was rather $\leqslant 1$ displayed in fig. 4.6 with point E and evolution towards pseudo-binary SiC-SiO_2 with green line crossing the stoichiometric SiC domain. Following, according to thermodynamics, silicon rich composition would be obtained due to excess loss of carbon via CO(g). But in this approach no diffusion phenomena were considered.
Including diffusion, evolution following the in-drawn dashed pink line (fig. 4.6) must be considered. This evolution corresponds to steady state between SiC/SiO_2 interface and SiO_2 surface with SiO(g)/CO(g) $\leqslant 1$. This steady state is established due to different oxygen potentials at the interface and surface, which is finally controlled by diffusion of oxygen through the SiO_2 scale. Finally obtained SiC composition at SiO_2 departure will be less rich in silicon than predicted by thermodynamics.
In any case, the compositions obtained at the end of SiO_2 loss remain in the stoichiometric SiC domain as observed when measuring Si(g), Si_2C(g) and SiC_2(g) during vaporization experiments with different SiC powder grain sizes.

4.2.2 Maintaining SiC surface bare

As soon as the surface of SiC grains is bare the C precipitation is extremely rapid when no residual oxygen is remained. This oxygen is necessary for active oxidation and for homogeneous Si and C elimination as SiO(g) and CO(g). As long as oxygen partial pressure remains in the range of calculated active oxidation window represented in figure 4.7 (for near explanation of this calculation see page 46) no carbon can be precipitated. In fact

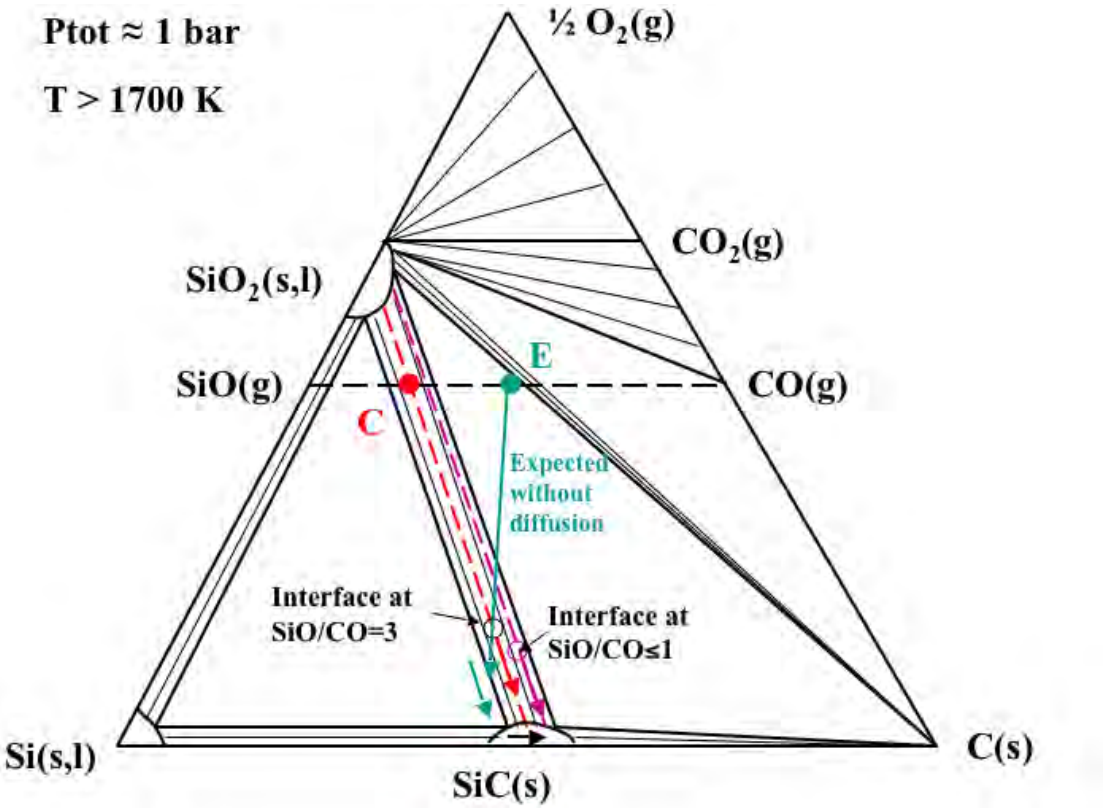

Figure 4.6: Schematic triphasic diagram of Si-O-C with SiC-SiO_2 tie-lines of composition evolution due to silica loss.

this window is more restricted, because, according to approach described above, the obtained SiC composition after SiO_2 loss is less rich in silicon than the composition predicted by thermodynamics and for which the upper limit was calculated. The real upper limit of oxygen partial pressure, which corresponds to the SiC composition after elimination of SiO_2, is much lower than displayed in figure 4.7. The oxygen reserve available then for active oxidation is lower than if the SiC composition evolution would begin from the value corresponding to the displayed SiO_2 limit. The dashed line in figure 4.7 displays this "real" upper window limit.
We know that in our experiments with SiC powders of different grain sizes in HTMS certain residual oxygen potential was maintained, because low SiO(g) and CO(g) partial pressures were detected after elimination of SiO_2 scale. So we can be sure that the surfaces of SiC single grains were maintained bare after SiO_2 elimination until the end of experiments due to the oxygen stored in the walls of the Knudsen cells. These are the experiments where most grain interconnections were observed with SEM/FEG.

4.2.3 Conclusion

The composition of SiC powders just after elimination of SiO_2 scales on their grains is less silicon rich than predicted by thermodynamics due to the diffusion phenomena during scale elimination. The presence of residual oxygen potential is absolutely necessary after scale elimination to prevent carbon precipitation. This precipitation occurs as soon as the surface

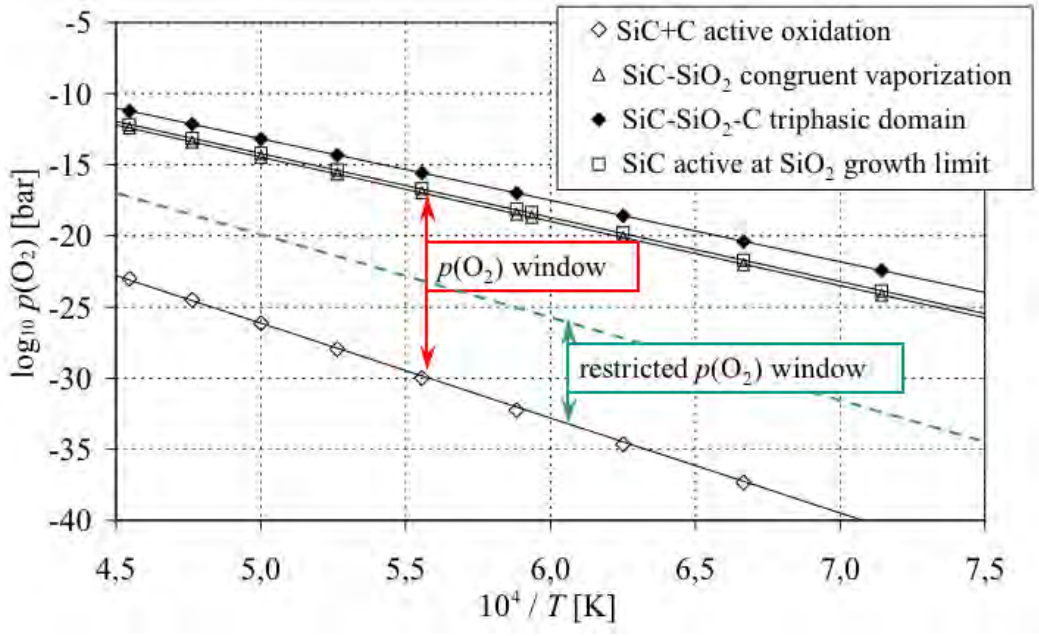

Figure 4.7: Oxygen partial pressure limit for the active oxidation of SiC (without carbon precipitation) as a function of the inverse of temperature compared to the oxygen partial pressure limit for active to passive oxidation transition and for congruent reaction. All pressures are SiC surface pressures. Dashed line displays approximative arrival location of solid SiC composition just after SiO_2 scale elimination and the real (restricted) oxygen potential window available until precipitation of carbon.

oxygen partial pressure becomes lower than for calculated SiC active oxidation carbon limit displayed in figure 4.7.

4.3 Deposition of SiC, necks formation

In the powders, where all SiO_2 were eliminated due to vaporization, grain to grain connections were observed with SEM/FEG imaging methods. These interconnections have different nature than already described for SiO_2 connections. They are constituted from pure SiC and their building mode is described.
Resulting from our experimental observations the necks formation period must occur during the active oxidation of bare SiC grain surfaces. So we can already conclude that the necks can occur only if bare SiC surface is present, free of SiO_2 scale.
The observed partial pressures of Si(g), Si_2C(g) and SiC_2(g) during experiment with SiC powders with grain sizes of 0,5 to 20 μm were the same whatever the grain size in the active oxidation domain. So the surface tension cannot be the main chemical force that increases the partial pressures in order to transfer SiC from small grains to large grains as reported by Kriegesmann [102]. Besides in the SEM/FEG images the necks formation was observed between the small and coarse grains without difference, no small grains elimination was observed (see figure 4.8). Furthermore the evaporation coefficient is equal 1, following, thermodynamic calculations can be applied without restriction for pure SiC.

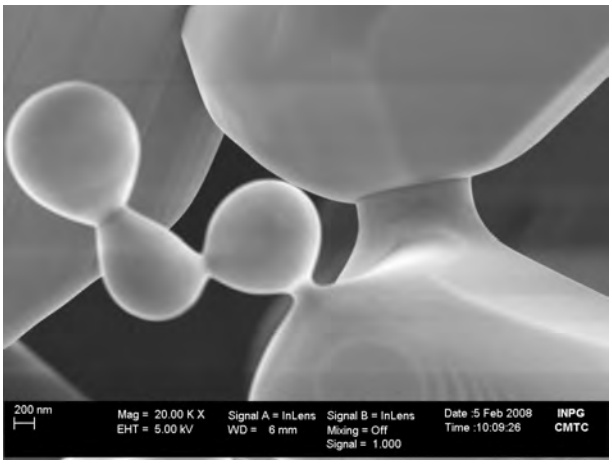

Figure 4.8: Necks formation in the sample of 0,5+10 μm grain sizes mixture after heating up to 1925 K.

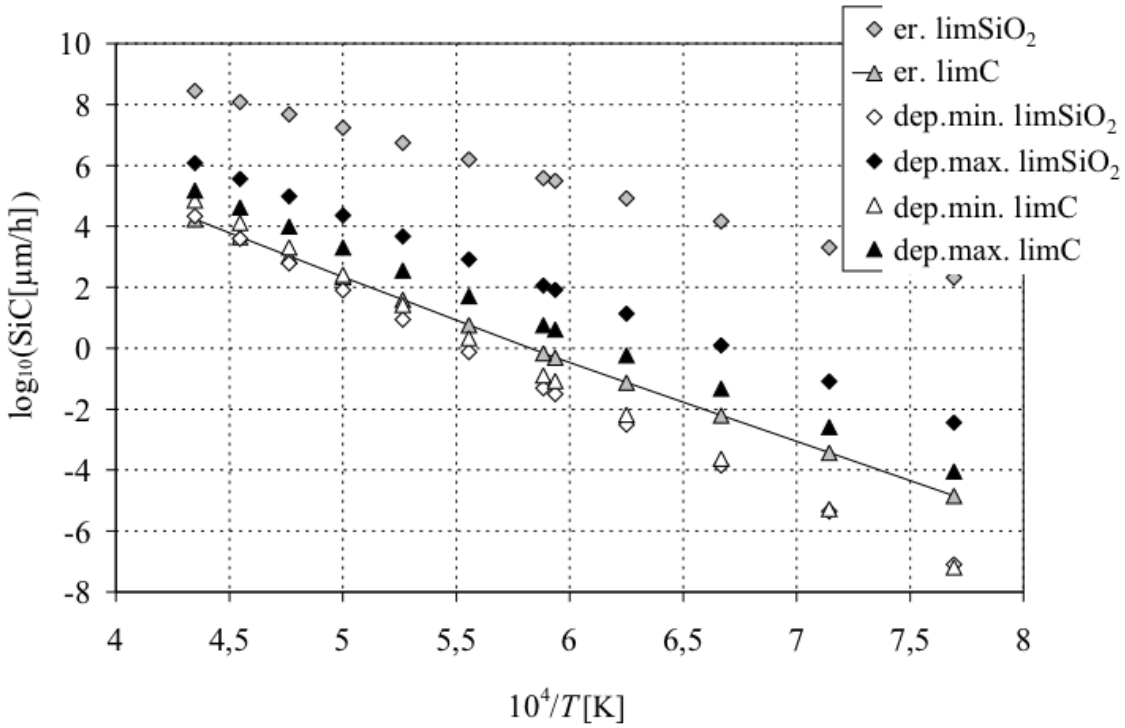

Figure 4.9: Decimal logarithm of SiC erosion (er.) or deposition (dep.) during active oxidation at limits of SiO_2 and C precipitation. All values are in μm of SiC per hour for 1 m^2 vaporizing surface.

In the theoretical approach (chapter 2) we have calculated the erosion rates of SiC under different conditions. Furthermore minimum and maximum possible SiC material depositions were calculated assuming in the first case only re-condensation of oxygen free Si and/or C containing vapors and for the maximum deposition reaction of Si(g) with CO(g) according to:

$$2\mathrm{Si(g)} + \mathrm{CO(g)} \rightarrow \mathrm{SiC(s)} + \mathrm{SiO(g)}$$

The necks formation occurs during active oxidation period, so we have to compare only the results of calculations which correspond to these conditions. Figure 4.9 displays calculated possible SiC erosion and SiC minimum and maximum depositions at the active oxidation limits to the SiC-SiO_2 and SiC-C formations. As we can see the erosion of SiC with oxygen potential close to SiO_2 formation is too high, in this case no necks can be formed, because the SiC erosion is higher than SiC deposition. So only the limit close to the carbon precipitation can be considered as favorable for necks formation. Furthermore we can see that for $T < 2000\,\mathrm{K}$ the presence of an excess of CO(g) is necessary to maintain SiC deposition close to its maximum and higher than erosion. At $T > 2000\,\mathrm{K}$ the minimum SiC deposition, without CO(g) presence, is also higher than SiC erosion.

CO(g) presence is assured by active oxidation but to obtain maximum neck growth its flow must be two times higher than Si(g) flow. This is problematic close to the SiC-C limit because the CO(g) partial pressure was calculated as practically the same as Si(g) partial pressure. Only if the gaseous phase would be enriched with CO(g) more escaping Si(g) can react to SiC and maximum SiC deposition displayed in figure 4.9 can be achieved.

Comparing observed necks in the different grains SiC samples after HTMS experiments and some samples from experiments in reactor with capillary tubing we have seen that the necks size is generally smaller than expected from calculations. The answer must be the insufficiency of CO(g) comparing to escaping Si(g) during active oxidation period. In any case the number of interconnected grains is important.

4.4 Carbon precipitation

Resulting from our experiments we have seen, that the presence of carbon in SiC powder mixture does not prevent the necks formation between SiC grains. But there is certainly an exception of carbon location on the SiC grains as we have explained in the precedent part that the SiC necks are formed only on the bare SiC surface. Otherwise even an improvement of necks building could be observed in reference sample with 50 mol% added graphite powder (fig. 4.10). This improvement was assumed to be related to the early de-oxidation of the sample, but view the recently discussed importance of CO(g) presence, it was rather the role of increase of CO(g) pressure during active oxidation step since the experiment has shown a higher $p(\mathrm{CO})$ for this sample.

In the samples, which were heated too long after the active oxidation step, like during the experiment 06-11 in reactor with capillary tubing with sample of SiC with 2 mol% SiO_2 mixture heated at 1500 K for 1,5h and at 1740 K for 2h (figure 4.11) carbon was precipitated. We can see that necks of the same shape as in figure 4.10 are present which were covered with carbon. Following, the carbon precipitation takes place after the necks formation step, which occur during active oxidation.

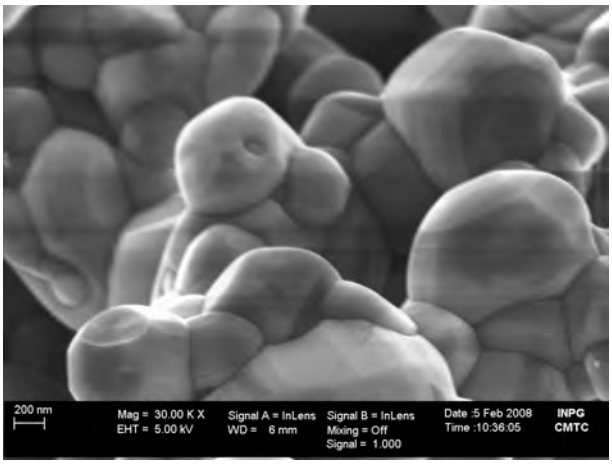

Figure 4.10: Necks formation in the sample of 0,5 μm grain size SiC with graphite mixture after heating up to 1925 K.

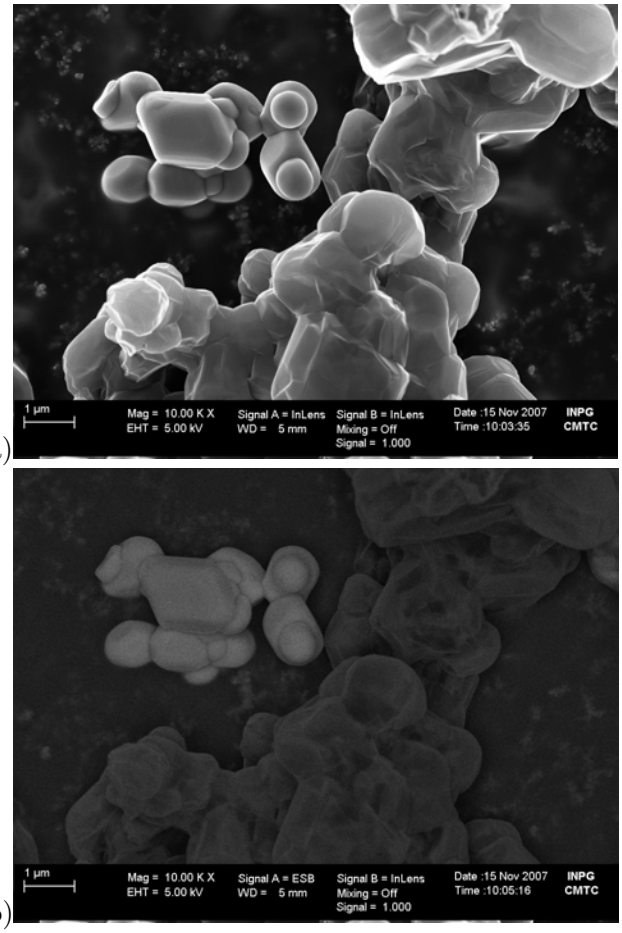

Figure 4.11: Necks formation and graphitization in sample of SiC with 2 mol% SiO_2 mixture after heating up to 1740 K for 2 hours in reactor coupled with mass spectrometer: a) SEM/FEG image; b) and back scattered electron detection imaging mode.

4.5 Conclusion

A complete SiC necks building mechanism in SiC powder samples is proposed. Different steps can be separated:

1. Elimination of added SiO_2, if present, and general purification of sample SiC powder. During this step the added components of SiC based mixture are eliminated and also volatile impurities such as CaO, Na_2O etc. Less volatile impurities like Fe_2O_3 remain longer in the powders, but it is not clear yet until which step exactly.

2. Elimination of SiO_2 scale on the SiC powder grains. SiO_2 necks can occur if the heating is stopped during this step.

3. Active oxidation maintain the SiC grain surfaces bare and at the same time SiC necks are built.

4. If the heating is not stopped after the end of active oxidation step, precipitation of carbon occurs.

During each of these steps different gaseous phase is established and the reactions and changes in the solid phase are directly related to this gaseous phase.
During the first step the SiC grains are covered with SiO_2 scale. The equilibrium gaseous phase of the interface SiC/SiO_2 can never be measured because this interface is always hidden with the scale in presence of any oxygen containing species, which can act as oxidative agent. The scale remains maintained as long as any independent SiO_2 (grains) is present in the sample.
The direct presence of carbon in the next SiC grain vicinity seems not to disturb necks building mechanism or even improve it due to enriching the gaseous phase with CO(g). But as soon as the active oxidation step is terminated with first carbon precipitation the SiC necks growth ends. Further heating would result in SiC erosion due to elimination of Si in excess.

5 General conclusions

The study of consolidation mechanism of SiC powder based samples was the subject of this study. Particularly the gaseous phase at high temperature was analyzed and related to the SiC necks formation between the grains. A mass spectrometer coupled with an effusion multiple cell device was utilized to characterize the gaseous phase developed by a condensed samples due to heating. An other mass spectrometer connected with a reactor via capillary tubing was composed during the study work. This device served for continuos vapors flow observation during heating period. The observed gaseous phase was related to the direct heat treatment of the samples. Furthermore the samples were analyzed after experiments with several characterization methods to relate the achieved transformations in the samples structure to the heat treatment and observed gaseous phase. Additionally thermodynamic calculations were performed by modeling the samples behavior as a function of temperature and oxygen potential, which exists in stationary state in vicinity of reacting surfaces.
The first important result of the study is the establishing of a mechanism model which explains the observation of systematically lower SiO(g) and CO(g) partial pressures from the SiC powders and SiC-SiO_2 powder mixtures than predicted by thermodynamic calculations. Indeed the capability of SiC powder to build a SiO_2 scale is mainly responsible for this behavior. This surface SiO_2 is maintained as long as an added quantity of SiO_2 powder remains present in the sample. The real SiC-SiO_2 interface remains hidden by the scale. The SiC grains decrease their size because of oxidation with inward diffusing oxygen producing new SiO_2 and C^{n+} which diffuses outward through the scale. The SiC-SiO_2 samples from experiments stopped during SiO_2 elimination step didn't build SiC necks but an other kind of grains connections could be observed locally, which results from the powder aging. These grain connections are constituted from SiO_2. At the end of SiO_2 scale elimination step some residual oxygen partial pressure is maintained due to SiO(g) and CO(g) molecules.
Second result is the demonstration of an active oxidation phase as long as residual oxygen is available. An active oxidation window was calculated inside of which the SiC surface remains bare, free of precipitation. The upper limit is the precipitation of SiO_2 due to passive oxidation of SiC and the low limit is the point of leaving the SiC stoichiometric domain towards precipitation of carbon. For the first time this window is defined by oxygen surface pressure and silicon activity, because both are related during active oxidation. The width of this window displays that there is a certain duration of active oxidation depending on the decrease rate of silicon activity in SiC or decrease of oxygen partial pressure in the SiC surface gaseous phase.
Third result is the quantification of competition between SiC erosion and deposition rate during active oxidation. Inside the active oxidation window the SiC erosion rate close to Si rich composition is always more important than deposition rate. Only close to the SiC stoichiometric domain rich in carbon the growth of SiC necks is possible, due to the higher SiC deposition rate than erosion. In any case the progressive oxygen elimination from the SiC surface vicinity assures the passage through the zone of SiC necks growth, independent on the starting point. The presence of CO(g) excess allow to increase the necks growth

because of reaction with escaping excess of Si(g). The absence of CO(g) excess or the SiC bare surface obtaining at oxygen pressures to close to the upper limit of active oxidation window can be interpreted in pore size increase during consolidation of SiC based ceramics. The fourth and last result concerns carbon precipitation when the active oxidation conditions are no more established. This precipitation is very fast if no residual oxygen is available. Carbon precipitation occurs always on the SiC crystal surface. Anyway the begin of this precipitation is also rather a transition zone than a frontier line the width of which depends on the oxygen decrease rate and or silicon loss via vaporization.
The main effects of heat treatment in active oxidation zone are the erosion and deposition of SiC in form of necks. Starting with SiO_2 presence in the SiC, as native grain scale or intentionally added powder, the passage through the active oxidation zone between elimination of silica and precipitation of carbon is a must. When the conditions of active oxidation are established long enough, the SiC necks growth is observed before carbon precipitation at the surface.
Regarding these results the model of SiC reaction/transformation states can be established for any heat treatment of SiC based material in view of consolidation step knowing the changes of gaseous phase composition in corresponding temperature zone.

Bibliography

[1] H. Scholze. *Die physikalischen und chemischen Grundlagen der Keramik*. Springer Verlag, Berlin, Heidelberg, New York, 1968.

[2] L. Michalowsky. *Neue keramische Werkstoffe. 1.* Dt.Verl. für Grundwerkstoffindustrie, Leipzig, 1994.

[3] H.N. Baumann. The relation of alpha and beta silicon carbide. *J.Electrochem. Soc.*, 99:109–114, 1953.

[4] M. Yarahmadi. *Gefüge und mechanische Eigenschaften von SiC-Werkstoffen*. PhD thesis, Fachbereich Werkstoffwissenschaften der Technischen Universität Berlin, 1985.

[5] M.W. Chase et al., editor. *NIST-JANAF Thermochemical Tables*, volume Monograph 9 of *Journal of Physical and Chemical Reference Data*. American Chemical Society, American Institute of Physics, N.Y., 4th edition, 1998.

[6] W. Bergmann. *Werkstofftechnik. Teil 2: Anwendung*. Carl Hanser Verlag München Wien, 1991.

[7] R.W. Olesinski and G.J. Abbaschian. The C - Si (Carbon-Silicon) System. *Bull. All. Phase Diagrams*, 5(5), 1984.

[8] R.T. Dolloff. Research Study to Determine the Phase Equilibrium Relations of selected Metal Carbides at High Temperature. Technical Report 60-143, Wright Air Dev. Div. Tech. Report, 1960.

[9] H. Kleykamp and G. Schumacher. The Constitution of the Silicon-Carbon System. *Ber. Bunsenges. Phys. Chem*, 97(6):799–805, 1993.

[10] J. Gröbner, H.L. Lukas, and F. Aldinger. Thermodynamic Calculation of the Ternary System Al-Si-C. *CALPHAD*, 20(2):247–54, 1996.

[11] Scientific Group Thermodata Europe (SGTE). C-Si (Carbon-Silicon). In W. Martienssen, editor, *Landolt-Börnstein:Thermodynamic Properties of Inorganic Material*, volume 19B of *New Series IV*. Springer-Verlag, Berlin, Heidelberg, 2004.

[12] R.I. Scace and G.A. Slack. Solubility of Carbon in Silicon and Germanium. *J. Chem. Phys.*, 30:1551–55, 1959.

[13] L. Kaufman. Coupled Phase Diagrams and Thermochemical Data for Transition Metal Binary Systems. VI. *CALPHAD*, 3:45–76, 1979.

[14] F. Durand and J.C. Duby. Carbon Solubility in Solid and Liquid Silicon – A Review with Reference to Eutectic Equilibrium. *J. of Phase Equilibria*, 20(1):61–63, August 1999.

[15] P. Rocabois, C. Chatillon, and C. Bernard. Thermodynamics of the Si-C system I. Mass spectrometric studies of the condensed phases at high temperature. *High Temperature – High Pressures*, 27/28:3–23, 1995/96.

[16] D.P. Birnie III and W.D. Kingery. The limit of non-stoichiometry in silicon carbide. *J. Mat. Sci.*, 25:2827–34, 1990.

[17] D.P. Birnie III. A model for Silicon Self-Diffusion in Silicon Carbide: Anti-site Defect Motion. *Am.Ceram.Soc.Commun.*, 69(2):c33–c35, 1986.

[18] M.G. Inghram and J. Drowart. Mass spectrometry applied to high temperature chemistry. In *High Temperature Technology*, pages 219–240. McGraw Hill, New York, 1959.

[19] J. Drowart, G. DeMaria, and M.G. Inghram. Thermodynamic Study of SiC Utilizing a Mass Spectrometer. *J. Chem. Phys.*, 29(5):1015–21, 1958.

[20] J. Drowart and G. DeMaria. Thermodynamic Study of the Binary System C-Si Using a Mass Spectrometer. In J.R. O'Connor and J. Smiltens, editors, *Silicon Carbide*, pages 16–23. Pergamon Press, New York, 1960.

[21] C. Chatillon. *Contribution à l'étude par spectrométrie de masse des phases métalliques à haute température.* PhD thesis, USMG and INPG, Grenoble, France, 1975.

[22] P. Rocabois, C. Chatillon, and C. Bernard. Thermodynamics of the Si-C system II. Mass spectrometric determination of the enthalpies of formation of molecule in the gaseous phase. *High Temperature-High Pressures*, 27/28:25–39, 1995/96.

[23] G. Meloni, R.W. Schmude Jr., and K.A. Gingerich. Knudsen-effusion mass spectrometric study of the group 14 atomic clusters. In K. Hilpert, F.W.Froben, and L. Singheiser, editors, *High Temperature Materials Chemistry*, volume 15 Part II, pages 505–508. Forschungszentrum Jülich, Germany, 2000.

[24] K.A. Gingerich, Q. Ran, and R.W. Schmude Jr. Mass spectrometric investigation of the thermodynamic properties of the Si_6 molecule. *Chem. Phys. Letters*, 256:274–278, 1996.

[25] R.W. Schmude Jr., Q. Ran, and K.A. Gingerich. Atomization enthalpy and enthalpy of formation of gaseous Si_4 from mass spectrometric equilibrium measurements. *J. Chem. Phys.*, 99(10):7998–8004, 1993.

[26] Q. Ran, R.W. Schmude Jr., M. Miller, and K.A. Gingerich. Mass spectrometric investigation of the thermodynamic properties of the Si_5 molecule. *Chem. Phys. Letters*, 230:337–42, 1994.

[27] R.W. Schmude Jr., Q. Ran, and K.A. Gingerich. Atomization enthalpy and enthalpy of formation of gaseous Si_2 and Si_3 from mass spectrometric equilibrium measurements. *J. Chem. Phys.*, 102(6):2574–79, 1995.

[28] G. Verhaegen, F.E. Stafford, and J. Drowart. Mass Spectrometric Study of the system Boron-Carbon and Boron-Carbon-Silicon. *J. Chem. Phys.*, 40:1622–28, 1964.

[29] R.W. Schmude Jr. and K.A. Gingerich. Thermodynamic Study of Small Silicon Carbide Clusters with a Mass Spectrometer. *J.Phys.Chem.*, A(101):2610–13, 1997.

[30] R.G. Behrens and G.H. Rinehart. Vaporization Thermodynamics and Kinetics of Hexagonal Silicon Carbide. In J. Hastie, editor, *Characterisation of High Temperature Vapors and Gases*, volume 1, pages 125–142. National Institute for Standards and Technology, Gaithersburg, Maryland (USA), 1979.

[31] S.G. Davis, D.F. Anthrop, and A.W. Searcy. Vapor Pressure and the Dissociation Pressure of Silicon Carbide. *J. Chem. Phys.*, 34(2):659–64, 1961.

[32] A. Ghosh and G.R. St.Pierre. Ternary Phase Diagrams for the Si-C-O System. *Trans. Met. Soc. AIME*, 245:2106–08, 1969.

[33] R. Pampuch, W. Ptak, S. Jonas, and J. Stoch. Formation of Ternary Si-O-C Phase(s) During Oxidation of SiC. *Material Science Monograph*, 6:435–48, 1980.

[34] L. Porte and A. Sartre. Evidence for a silicon oxycarbide phase in the Nicalon silicon carbide fiber. *J. Mat. Sci.*, 24:271–75, 1989.

[35] M. Nagamori, J.-A. Boivin, and A. Claveau. Thermodynamic stability of silicon oxycarbide $Si_5C_6O_2$ (Nicalon). *J. Mat. Sci.*, 30:5449–56, 1995.

[36] S.M. Johnson, R.D. Brittain, R.H. Lamoreaux, and D.J. Rowcliffe. Degradation Mechanism of Silicon Carbide Fibers. *J. Am. Ceram. Soc.*, 71(3):C132–35, 1988.

[37] P. Rocabois, C. Chatillon, and C. Bernard. Vapour pressure and evaporation coefficients of SiO(amorphous) and SiO_2(s)+Si(s) mixtures by the multiple Knudsen cell mass spectrometric method. *Rev.Int.Hautes Temper.Refract., Fr.*, 28:37–48, 1992-1993.

[38] P. Rocabois, C. Chatillon, and C. Bernard. High temperature analysis of the thermal degradation of silicon-based materials. II: Ternary Si-C-O, Si-N-O, and Si-C-N compounds. *High Temperature-High Pressures*, 31:433–454, 1999.

[39] T. Varga, A. Navrotsky, J.L. Moats, R.M. Moats, F. Poly, K. Mueller, A. Saha, and R. Raj. Thermodynamically Stable $Si_xO_yC_z$ Polymer-Like Amorphous Ceramics. *J. Am. Ceram. Soc.*, 90(10):3213–19, 2007.

[40] N.S. Jacobson and E.J. Opila. Thermodynamics of Si-C-O System. *Metallurgical Transactions A*, 24A:1212–14, May 1993.

[41] N.S. Jacobson, K.N. Lee, and D.S. Fox. Reactions of Silicon Carbide and Silicon(IV) Oxide at Elevated Temperatures. *J. Am. Ceram. Soc.*, 75(6):1603–11, 1992.

[42] W.L. Vaughn and H.G. Maas. Active-to-Passive Transition in the Oxidation of Silicon Carbide nad Silicon Nitride in Air. *J. Am. Ceram. Soc.*, 73(6):1540–43, 1990.

[43] J.W. Hinze and H.C. Graham. The Active Oxidation of Si and SiC in the Viscous Gas-Flow Regime. *J. Electrochem. Soc.*, 123(7):1066–73, 1976.

[44] T. Narushima, T. Goto, Y. Yokoyama, Y. Iguchi, and T. Hirai. High-Temperature Active Oxidation of Chemically Vapor-Deposited Silicon Carbide in CO-CO_2 Atmosphere. *J. Am. Ceram. Soc.*, 76(10):2521–24, 1993.

[45] E.J. Opila and R.E. Hann Jr. Paralinear Oxidation of CVD SiC in Water Vapor. *J. Am. Ceram. Soc.*, 80(1):197–205, 1996.

[46] W. Bremen, A. Naoumidis, and H. Nickel. Oxidationsverhalten des pyrolitisch abgeschiedenen β-SiC unter einer Atmosphäre aus CO-CO_2-Gasgemischen. *Journal of Nuclear Materials*, 71:56–64, 1977.

[47] Z. Zheng, R.E. Tressler, and K.E. Spear. Oxidation of Single-Crystal Silicon Carbide. I Experimental Studies. *J.Electrochem. Soc.*, 137(3):854–58, 1990.

[48] Z. Zheng, R.E. Tressler, and K.E. Spear. Oxidation of Single-Crystal Silicon Carbide. II Kinetic Model. *J.Electrochem. Soc.*, 137(9):2812–16, 1990.

[49] K.L. Luthra. Some New Perspectives on Oxidation of Silicon Carbide and Silicon Nitride. *J. Am. Ceram. Soc.*, 74(5):1095–1103, 1991.

[50] N.S. Jacobson. Corrosion of Silicon-Based ceramics in combustion Environments. *J. Am. Ceram. Soc.*, 76(1):3–28, 1993.

[51] E.A. Gulbransen and S.A. Jansson. The High-Temperature Oxidation, Reduction, and Volatilization Reactions of Silicon and Silicon Carbide. *Oxid. Met,*, 4(3):181–201, 1972.

[52] C. Wagner. Passivity during the Oxidation of Silicon at Elevated Temperatures. *J. Appl. Phys.*, 29(9):1295–97, 1958.

[53] B. Schneider, A. Guette, R. Naslain, M. Cataldi, and A. Costecalde. A theoretical and experimental approach to the active-to-passive transition in the oxidation of silicon carbide. *J. Mat. Sci.*, 33:535–47, 1998.

[54] K.G. Nickel, H.L. Lukas, and G. Petzow. High Temperature Corrosion of SiC in Hydrogen-Oxygen Environments. In K. Hack, editor, *The SGTE Casebook - Thermodynamics at Work*, pages 200–211. Woodhead Publishing Limited, 2008.

[55] M. Balat, G. Flamant, G. Male, and G. Pichelin. Active to Passive Transition in the Oxidation of Silicon Carbide at High Temperature and Low Pressure in Molecular and Atomic Oxygen. *J. Mat. Sci.*, 27:697–703, 1992.

[56] R.S. Sickafoose, Jr. and D.W. Readey. Active Gaseous Corrosionof Porous Silicon Carbide. *J. Am. Ceram. Soc.*, 76(2):316–324, 1993.

[57] S. Baud, F. Thévenot, A. Pisch, and C. Chatillon. High temperature sintering of SiC with oxide additives: I. Analysis in the SiC-Al_2O_3 and SiC-Al_2O_3-Y_2O_3 systems. *J. European Ceram.Soc.*, 23:1–8, 2003.

[58] S. Baud, F. Thévenot, and C. Chatillon. High temperature sintering of SiC with oxide additives: II. Vaporization processes in powder beds and gas-phase analysis by mass spectrometry. *J. of European Ceramic Society*, 23:9–18, 2003.

[59] S. Baud, F. Thévenot, and C. Chatillon. High temperature sintering of SiC with oxide additives: III. Quantitative vaporization of SiC-Al_2O_3 powder beds as revealed by mass spectrometry. *J. European Ceram.Soc.*, 23:19–27, 2003.

[60] J. Kriegesmann. Competing Sintering Mechanism in Silicon Carbide. *Interceram*, 37:27–30, 1988.

[61] J. Kriegesmann. Processing Phenomena for Recrystallized Silicon Carbide. In K. Ishizaki, K. Niihara, N. Isotani, and R. Ford, editors, *Grain Boundary Controlled Properties of Fine Ceramics*, JFCC Workshop Series: Materials Processing and Design, pages 176–188. Elsevier Applied Science, London, New York, 1992.

[62] J. Kriegesmann, M. Kraus, and A. Gros. Gefügeausbildung von rekristallisiertem SiC. *cfi/Ber. DKG*, 75(4):83–88, 1998.

[63] J. Kriegesmann and J. Jodlauk. Characterizing the Consolidation of Bimodally Distributed Fine Grained Silicon Carbide Powders. *cfi/Ber. DKG*, 79(12):37–44, 2002.

[64] G.M. Rosenblatt. Evaporation from Solids. In N.B. Hannay, editor, *Treatise on Solid-State Chemistry IV Surfaces*, chapter 3, pages 165–240. Plenum Press, 1976.

[65] J.P. Hirth and G.M. Pound. Coefficients of Evaporation and Condensation. *J. Phys. Chemistry*, 64:619–26, 1960.

[66] W.D. Kingery and M. Berg. Study on the Initial Stages of Sintering Solids by Viscous Flows, Evaporation-Condensation, and Self-Diffusion. *J. Appl. Phys.*, 26:1205–1212, 1995.

[67] W.F. Knippenberg. Growth phenomena in Silicon Carbide. In *Philips research reports*, volume 18, pages 161–274. Philips' Gloeilampenfabrieken, Eidhoven, Netherlands, 1963.

[68] J.M. Powers and G.A. Somorjai. The surface oxidation of alpha-silicon carbide by O_2. *Surface Science*, 244:39–50, 1991.

[69] S. Hara, Y. Aoyagi, M. Kawai, S. Misawa, E. Sakuma, and S. Yoshida. Si desorption from a β-SiC(001) surface by an oxygen flux. *Surface Science Letters*, 278:L141–L146, 1992.

[70] R. Berjoan, J. Rodriguez, and F. Sibieude. AES study of the SiO_2/SiC interface in the oxidation of CVD β-SiC. *Surface Science*, 271(137-243), 1992.

[71] T. Rosenqvist. *Principles of Extractive Metallurgy*, pages 377–380. McGraw Hill Book Co, New York, NY, 2nd edition, 1983.

[72] I.V. Ryabchikov. Thermodynamic Investigation of the Si-O-C system at high temperatures. *Russian Metallurgy*, 2:7–10, 1966.

[73] F. Danes, E. Saint-Aman, and L. Coudrier. The Si-C-O system. Part I: Representation of Phase Equilibria. *J. Mat. Sci.*, 28:489–495, 1993.

[74] M. Nagamori, I. Malinsky, and A. Claveau. Thermodynamics of the Si-C-O System for the Production of Silicon Carbide and Metallic Silicon. *Metallurgical Transactions B*, 17:503–14, 1986.

[75] O. Kubaschewski and C.B. Alcock. *Metallurgical Thermochemistry*, pages 221–226. Pergamom Press, Oxford, 5th edition, 1979.

[76] T. Rosenqvist and J.Kr. Tuset. Discussion of "Thermodynamics of the Si-C-O System for the Production of Silicon Carbide and Metallic Silicon". *Metallurgical Transactions B*, 18:471–72, 1987.

[77] M. Nagamori, I. Malinsky, and A. Claveau. Authors Reply: The Role of SiO(l) in the Production of Metallic Silicon. *Metallurgical Transactions B*, 18:472–77, 1987.

[78] F. Danes, E. Saint-Aman, and L. Coudrier. The Si-C-O system. Part II: Isobaric evolution of the system. *J. Mat. Sci.*, 28:6524–6530, 1993.

[79] G. Eriksson and K. Hack. 23 Production of Metallurgical Grade Silicon in an Electric Arc Furnace. In K. Hack, editor, *The SGTE Casebook - Thermodynamics at Work*, volume 621 of *Materials Modelling Series*, pages 200–208. The Institute of Materials, London, 1996.

[80] K.-G. Günther. Zur Messung von Dampfdruck und Verdampfungsgeschwindigleit an glasbildenden Substanzen. *Glastechnische Berichte*, 31(1):9–15, 1958.

[81] S.I. Schornikov and I.Yu. Archakov. High temperature study of the evaporation of silicon monoxide. In K. Hilpert, F.W. Froben, and L. Singheiser, editors, *High Temperature Materials Chemistry*, volume 15 Part II, pages 431–434. Central Library, Forschungszentrum Jülich GmbH, 52425 Jülich, Germany, 2000.

[82] S.I. Schornikov, I.Yu. Archakov, and M.M. Shultz. Mass Spectrometric Study of Vaporization and Thermodynamic Properties of Silicon Dioxide: II. Determination of Partial Vaporization Coefficients of Silicon Dioxide. *Russ. J. General Chem*, 69:187–196, 1999.

[83] N.S. Jacobson. Carbothermal Reduction of Silica in High Temperature Materials. In P. Nash and B. Sundman, editors, *Applications of Thermodynamics in the Synthesis and Processing of Materials*, pages 19–27. The Minerals, Metals and Materials Society, Warrendale, PA 15086, USA, 1995.

[84] L. Muehlhoff, W.J. Choyke, M.J. Bozack, and J.T. Yates, Jr. Comparative electron spectroscopic studies of surface segregation on SiC(0001) and SiC(000-1). *J. Appl. Phys.*, 60(8):2842–53, 1986.

[85] I. Prigogine and R. Defay. *Chemical Thermodynamics*, pages 278–283. Longman, London, 4th edition, 1967. translated by D.H. Everett.

[86] C. Chatillon, M. Alibert, and A. Pattoret. Thermodynamic and physico-chemical behavior of the interactions between Knudsen-Effusion-Cells and the system under investigation: Analysis by High Temperature Mass Spectrometry. In J. Hastie, editor, *Characterization of High Temperature Vapors and Gases*, volume 1, pages 181–210. National Institute for Standards and Technology, Gaithersburg, Maryland (USA), 1979.

[87] J. Drowart, C. Chatillon, J. Hastie, and D. Bonnell. High-Temperature Mass Spectrometry: Instrumental Techniques, Ionization Cross-Sections, Pressure Measurements, and Thermodynamic Data. *Pure Appl. Chem.*, 77(4):668–737, 2005.

[88] E.D. Cater. The Effusion Method at age 69: Current state of the Art. In J. Hastie, editor, *Characterization of High Temperature Vapors and Gases*, volume 1, pages 3–38. National Institute for Standards and Technology, Gaithersburg,, 1979.

[89] P. Clausing. The flow of highly rarefied gases through tubes of arbitrary length. *J. Vac. Sci. Technol.*, 8:636–646, 1971.

[90] K.D. Carlson. The Knudsen Effusion Method. In J.L. Margrave, editor, *The Characterization of High Temperature Vapors*, pages 115–129. J. Wiley & Sons, inc. N.Y., 1967.

[91] D.J. Santeler. New concepts in molecular gas flow. *J. Vac. Sci. Technol.*, A4(3):338–343, 1986.

[92] K. Motzfeld. The Thermal Decomposition of Sodium Carbonate by the Effusion Method. *J.Phys.Chem.*, 59(2):139–47, 1955.

[93] G.M. Rosenblatt. Interpretation of Knudsen Vapor-Pressure Measurements on Porous Solids. *J.Electrochem. Soc.*, 110(6):563–69, 1963.

[94] M. Heyrman and C. Chatillon. Evaporation / condensation coefficients as determined by the multiple Knudsen effusion cell method. *J. Phys. Chem. Solids*, 66:494–97, 2005.

[95] M. Heyrman, C. Chatillon, H. Collas, and J.-L. Chemin. Improvements and new capabilities for the multiple Knudsen cell device used in high.temperature mass spectrometry. *Rapid Commun. Mass Spectrom.*, 18:163–74, 2004.

[96] P. Morland, C. Chatillon, and P. Rocabois. High temperature mass spectroscopy using the Knudsen effusion cell. I. Optimization of sampling contraints on moleculer beam. *High Temperature and Materials science*, 37:167–187, 1997.

[97] M. Tmar and C. Chatillon. Refinement of vapor pressures in equilibrium with InP and InAs by mass spectrometry. *J. Chem. Thermodyn.*, 19:1053, 1987.

[98] J. Roboz. *Introduction to Mass Spectrometry. Instrumentation and techniques.* John Wiley and Sons, Inc., 1968.

[99] Pfeiffer Vacuum GmbH. *Mass spectrometer catalog*, June 2005.

[100] P. Rocabois, C. Chatillon, and C. Bernard. High temperature analysis of the thermal degradation of silicon-based materials. I: Binary Si-O, Si-C, and Si-N compounds. *High Temperature – High Pressures*, 31:413–432, 1999.

[101] J. Drowart. *Mass Spectrometric Studies of the Vaporization of Inorganic Substances at High Temperatures*, pages 255–310. Gordon and Breach, 1962.

[102] J. Kriegesmann. Microstructure Control During Consolidation of Fine Grained Recrystallized Silicon Carbide. In *Key Engineering Materials*, volume 264-268, pages 2199–2202. Trans Tech Publications, Switzerland, 2004.

List of Figures

List of Tables

Résume de T H E S E en français

Titre anglais :

Thermodynamic and Mass Spectrometric Study of the Behaviour of Silicon Carbide (SiC) Powders at High Temperature

Titre français :

Étude Thermodynamique et par Spectrométrie de Masse du Comportement de Poudres de Carbure de Silicium (SiC) à Haute Température

présentée et soutenue publiquement

le 23/10/2009

par

Gabriele HONSTEIN

Table de matières

Introduction

Ce travail de thèse a été entrepris afin de comprendre et de clarifier l'ensemble des phénomènes qui régissent la consolidation de pièces réalisées en carbure de silicium. Il s'agit principalement du traitement thermique haute température de mélanges de poudres de différentes tailles dans un milieu en général confiné. Ce confinement n'est jamais assuré de façon totale car le niveau des températures atteintes – jusqu'à 2300 voire 2500 K –, la présence de vapeurs de silicium ou autre molécules complexes corrosives ainsi que l'absence de matériaux de conteneurs totalement inertes fait que des transferts existent dans les fours de traitement, et ce quelque soit la structure du four.

Le carbure de silicium obtenu est qualifié de SiC recristallisé, ce terme suggérant que le procédé de chauffage a entraîné une recristallisation du carbure initial, donc au moins si l'on se réfère à la métallurgie traditionnelle un grossissement des grains. En réalité il s'agit surtout de transport de SiC pour assurer par évaporation puis condensation la croissance de ponts entre les grains, ceux là même qui vont conditionner la consolidation des pièces. Les phénomènes principaux mis en jeu sont l'évaporation, la condensation mais aussi à un moindre degré la diffusion de surface des atomes. Cette dernière fait partie du processus d'évaporation condensation pour assurer le type de croissance. Elle ne sera pas étudiée dans ce travail bien que certaines observations s'y rapportent.

Le carbure de silicium n'est jamais obtenu pur, car il possède toujours en surface une couche de silice. De plus les procédés d'obtention des poudres par broyage épaississent cette couche et dans certains procédés des additifs de silice sont utilisés. Le rôle de cette silice n'est pas compris dans le détail, et la seule information globale est que sans silice la consolidation est médiocre. Ainsi dans ce travail l'étude a non seulement porté sur le système Si-C mais aussi sur le ternaire Si-C-O et plus particulièrement sur sa section pseudobinaire SiC-SiO_2.

Pour étudier la croissance de ponts de SiC entre grains de poudre lors de différents traitements thermiques la stratégie adoptée dans ce travail est de suivre l'évolution des pressions de vapeur ou celle des flux évaporés par spectrométrie de masse et de comparer la morphologie et la structure des poudres avant et après les traitements par différents moyens de caractérisation qui sont la granulométrie, la diffraction X, la spectrométrie Raman, les observations MEB et FEG. Il sera ainsi possible de comprendre le rôle de la silice par le suivi des espèces évaporant SiO(g) et CO(g) qui vont servir à caractériser les réactions principales et les différentes phases du traitement thermique. Dans certains cas la spectrométrie permet aussi de suivre d'autres espèces vapeur comme celles propres au système binaire Si-C.

Les résultats spectrométriques seuls ne sont que des indications qualitatives si l'expérimentateur ne sait pas les relier à un contexte thermodynamique ou cinétique. Pour fixer des repères, une étude thermodynamique complète des différents processus réactionnels a été effectuée qui prend en compte les phénomènes d'évaporation et de condensation, mais aussi l'impact de flux de matière en retour sur la surface de SiC et notamment toute molécule contenant de l'oxygène. Il a été ainsi envisagé d'étudier les conditions de l'oxydation passive et active du carbure de silicium.

Afin de donner une base quantitative aux observations portant sur la croissance, les flux de matière évaporée et de matière condensable sont calculés dans différentes configurations prenant en compte ou non la présence de silice ou sa disparition avec une présence résiduelle d'oxygène assurant une oxydation active du carbure de silicium. Cette quantification a permis d'une part de faire le tri entre les hypothèses proposées dans la littérature – c'est-à-dire les réactions principales menant à la croissance – et d'autre part de proposer de nouveaux mécanismes avec leurs conditions opérationnelles.

Chapitre I

Bibliographie

Les travaux sur le carbure de silicium sont très nombreux, non pas tant ceux portant directement sur les propriétés physiques, chimiques et mécaniques fondamentales, mais surtout sur l'ensemble des processus d'élaboration et de fabrication de matériaux à base de SiC pour différentes applications. Il a fallut donc trier dans la littérature scientifique et technique les points qui pouvaient aider à la compréhension des phénomènes de croissance par la phase vapeur et ce à partir de SiC pur ou plus ou moins dopé avec de la silice. Le chapitre bibliographique est donc structuré par les différentes études déjà réalisées sur des points qui étaient susceptibles d'aider à la compréhension des phénomènes de transport et de croissance de SiC:

- Structure du composé SiC, et diagrammes de phase Si-C et Si-C-O.
- Procédés de fabrication du matériau en tant que tel, celui-là même qui sert de base à la fabrication des poudres par broyage.
- Vaporisation de SiC c'est-à-dire toute étude sur le système Si-C, et sur le système Si-C-O incluant le pseudobinaire SiC-SiO_2 avec une attention particulière sur la composition de la phase gazeuse étudiée par spectrométrie de masse.
- Conditions d'équilibre ou de « non-équilibre » dans la vaporisation et mise en évidence de limitations cinétiques.
- Vaporisation de SiC dans des environnements oxydants et mécanismes de corrosion active et passive, c'est-à-dire sans et avec couche de silice respectivement.
- Approches expérimentales et théoriques de la transition d'oxydation active / passive qui peuvent permettre de comprendre la nature de la surface des cristaux de SiC et les phénomènes de transport associés à la présence d'oxygène.
- Métallurgie du silicium, l'extraction partant de mélanges de silice et de carbone avec une étape passant par la production intermédiaire de SiC.
- Structure des interfaces SiC/SiO_2 et des surfaces de SiC par différents moyens de caractérisation à l'échelle atomique (Spectrométrie Auger, XPS, LEED, SIMS..).

Au-delà de ces points le chapitre IV fait appel à la diffusion de l'oxygène et du carbone dans la couche de silice. Ces points étant établis, il n'a pas été fait de bilan bibliographique sur les phénomènes de diffusion bien que la littérature concernée ait été consultée.

La revue bibliographique met en évidence la complexité des phénomènes régissant la surface des cristaux de SiC notamment lorsque l'oxygène intervient. Ce rôle de l'oxygène quelque soit le procédé de fabrication doit être considéré car ce dernier est toujours présent à différents degrés due à la réactivité de SiC comme c'est le cas pour tout composé à base de silicium.

Chapitre II

Approche thermodynamique des conditions de la croissance de SiC

Ce chapitre fait le point des différentes approches thermodynamiques visant à comprendre la vaporisation de SiC c'est-à-dire en fait du système binaire Si-C et du ternaire Si-C-O car le composé SiC n'existe pas sans la présence d'oxygène au moins en surface ou dans l'atmosphère environnante si ce n'est intentionnellement dans les méthodes d'élaboration comme produit d'addition. L'approche thermodynamique a été entreprise avec l'intention d'aller bien au-delà du calcul traditionnel des équilibres de phases et pour cela les échanges de matière avec l'environnement via la phase gazeuse ont été pris en compte: en effet, dans les méthodes d'élaboration de produits à base de SiC – aussi bien en laboratoire qu'en site industriel - l'aspect corrosif des vapeurs issues du ternaire Si-C-O allié à la température très élevée (> 2000°C) ne permet pas de choisir des matériaux de conteneur complètement inertes ainsi que des systèmes totalement fermés isothermes et donc sans gradients de température. Les études publiées dans la littérature ont montré d'autre part que la croissance de SiC se fait principalement via le transport en phase gazeuse – dominant par rapport à tout phénomène de diffusion en phase solide - ce qui a amené à exploiter différents bilan d'évaporation / condensation comme source de croissance, en présence ou non d'oxygène. L'un des problèmes encore non résolus étant le rôle exact de l'oxygène dans le phénomène de croissance, le comportement de SiC sous différentes conditions relatives à l'apport d'oxygène a été étudié – cet apport d'oxygène se faisant via SiO_2 principalement - notamment ce qui relève de l'oxydation dite active ou passive de SiC.

II.1.Evaporation dans le binaire Si-C

Le calcul thermodynamique des pressions de vapeur dans les deux domaines diphasés Si-SiC et SiC-C associé aux flux d'évaporation – en condition de gaz neutre (transport) ou sous vide (conditions de Knudsen) – montre que la phase vapeur ou le flux qui en est issu est systématiquement plus riche en Si que le composé SiC. En cas de perte de matière via la phase gazeuse, il s'en suit un précipité de carbone en surface de tout cristal de SiC, précipité non propice par ailleurs à la croissance de SiC (fait connu en frittage par exemple). La confrontation entre les flux d'évaporation calculés et les estimations les plus récentes du domaine de stoechiométrie de SiC montre que ce précipité apparaît extrêmement rapidement et qu'il est totalement vain d'espérer éviter la précipitation du carbone par un quelconque moyen physique comme par exemple une augmentation de la pression de gaz neutre, la fermeture des conteneurs, ou la limitation des gradients de température. Ces éléments de régulation physique sont largement employés dans les fours d'élaboration sans pour autant conduire à des résultats reproductibles et à des réglages définitifs.

Les flux ont été ensuite analysés en terme d'incidence sur les produits d'origine, c'est-à-dire par l'érosion qu'ils provoquent : érosion de SiC mais aussi des impuretés de base Si ou C qui sont toujours présentes dans les poudres de SiC de départ. Leur importance montre à l'évidence que ces impuretés sont évacuées très vite dans les premières phases du traitement thermique et ne joueront pas de rôle dans les futures étapes de croissance.

II.2.Evaporation dans le ternaire Si-C-O

Les flux de vaporisation dans ce ternaire montrent un comportement pseudo-azéotropique pour le pseudobinaire $SiC-SiO_2$ ce qui veut dire que la vaporisation de SiC en présence de silice évite la précipitation de carbone. Pour ce pseudobinaire la pression de vapeur est très largement à base des deux seules molécules SiO(g) et CO(g). Une analyse de l'origine de l'ensemble des molécules évaporées ainsi que de leur proportions permet de quantifier l'érosion de SiC, celle de la silice et ceci pour différentes compositions de poudres : le triphasé riche en Si ($Si-SiC-SiO_2$), le pseudobinaire $SiC-SiO_2$ puis le triphasé riche en C ($SiC-SiO_2-C$). Ces flux d'érosion montrent un comportement très différent de celui du SiC pur, et notamment pour le dernier triphasé qui ne présente plus d'érosion de SiC, le CO(g) permettant l'élimination du carbone en excès par réaction directe avec la silice. L'élimination des impuretés classiques telles que Si et C---la plupart du temps co-existantes avec SiC---se produira très rapidement dès le début d'une phase de traitement thermique.

II.3.Oxydation de SiC

L'oxydation de SiC sous faible pression d'oxygène (ou tout autre agent oxydant comme la vapeur d'eau, CO_2 , etc…) se produit selon une réaction du type,

$$SiC(s) + O_2(g) = SiO(g) + CO(g).$$

Comme les produits SiO(g) et CO(g) sont stables et donc produits avec des pressions élevées le flux de vaporisation de ces molécules compense facilement le flux d'oxygène arrivant en surface. Cette situation est appelée oxydation active et correspond à une érosion importante de la surface de SiC. Lorsque le flux d'oxygène incident devient trop important, la surface de SiC se couvre de silice et le phénomène d'érosion se ralentit car l'interface SiC/SiO_2 qui va générer le carbone nécessaire à l'évaporation de CO(g) à la surface externe où arrive l'oxygène devient tributaire du flux incident d'oxygène via la diffusion de ce dernier dans la couche de silice – sous forme de $O_2(g)$ ou de O^{2-}selon la nature de la silice formée et la température comme cela a été montré dans la littérature. Il y a ralentissement de l'érosion de SiC et la situation est dite d'oxydation passive.

Pour aller plus loin que les études publiées dans la littérature, l'oxydation active de SiC a été calculée sous flux de Knudsen (correspondant aux expériences spectrométriques d'observation des pressions partielles) et les limites de ce phénomène ont été pour la première fois décrites. Elles correspondent aux très basses pressions d'oxygène à la limite SiC-C, et pour des pressions d'oxygène croissantes à la création en surface de la première couche de Silice. Les hypothèses du calcul montrent que ces limites correspondent en premier à des conditions portant sur l'activité du Si dans le composé SiC, et de façon corrélée à une pression d'oxygène. Il a donc été montré que ce n'est pas tout le domaine d'existence de SiC qui peut supporter des conditions d'oxydation active mais seulement une partie de celui-ci qui s'appuie d'un coté sur l'activité minimum du Si c'est-à-dire la limite de phase SiC-C (pour $a_C=1$) et de l'autre sur une activité de Si <1 : le domaine d'oxydation active n'atteint donc jamais les compositions de SiC en équilibre avec Si pur – sauf pour la précipitation de Si vers 2200 K. La fenêtre d'oxydation active de SiC a été calculée en terme d'activité de Si et de pressions d'oxygène à la surface de SiC. Ces conditions vont déterminer toutes les autres pressions partielles dans les conditions d'élaboration de cristaux de SiC en oxydation active. Ces conditions sont particulièrement importantes car assurer une surface « nue » exempte de silice pour les cristaux de SiC va être une condition essentielle dans la croissance de SiC comme le montrera ce travail de thèse. Il faut rappeler que dans les conditions d'oxydation

active, le cristal de SiC reste stoechiométrique et donc sans précipitation de C. Selon la pression d'oxygène stationnaire en surface, le cristal de SiC va avoir différentes compositions stoechiométriques.

Dans le cas des mélanges de poudres SiC + SiO_2 le présent travail a envisagé aussi les solutions intermédiaires où SiC et SiO_2 ne sont pas intimement liés, c'est-à-dire qu'il n'y a pas que des interfaces SiC/SiO_2 (ou couche de silice sur la surface des grains de SiC) mais des grains séparés par un espace vide, celui-là même existant dans une poudre. Comme la silice se vaporise de façon congruente avec un potentiel d'oxygène supérieur à celui de l'interface SiC/SiO_2, le potentiel moyen régnant dans ces mélanges qui n'ont pas encore atteint l'équilibre va générer des pressions de SiO(g) et CO(g) différentes correspondant à un état stationnaire d'échange de matière réglé par d'autres phénomènes limitant les réactions. Cette exploration de l'influence d'un potentiel d'oxygène supérieur à l'interface SiC/SiO_2 permettra d'expliquer les expériences spectrométriques de vaporisation de mélanges SiC + SiO_2 pour lesquelles des limitations cinétiques sont apparues, ces dernières conduisant à des pressions plus faibles ainsi que des rapports SiO(g) / CO(g) différents du rapport congruent pseudobinaire (= 3 ou 3,76) attendu d'une part et ressemblant fortement à celui observé pour l'oxydation active (≈ 1).

II.4.Erosion et phénomènes de dépôt via la phase vapeur de SiC

La croissance de SiC via la phase vapeur va mettre en jeu d'un coté les sources de matière par vaporisation ou érosion de SiC ou de mélanges SiC+SiO_2 et d'un autre coté des phénomènes de condensation / croissance. Cette partie fait le bilan de ces sources et des vitesses de dépôt disponibles, sans pout autant prendre en compte les gradients thermiques qui pourraient accélérer ces condensations. L'objectif est avant tout de comprendre quelles sont les forces chimiques issues du matériau SiC et de son environnement immédiat qui vont produire la croissance dans un milieu isotherme.

Pour ces études, le raisonnement va se faire à partir de la croissance évaluée en µm/h avec pour repères 1 et 10 µm/h qui correspondent aux dimensions plus ou moins extrêmes des grains habituellement utilisés. Les différentes conditions de vaporisation – Si-C pur, Si-C-O le pseudobinaire SiC-SiO_2, les triphasés SiC-SiO_2 avec Si ou C - ainsi que le composé SiC pur sous oxydation active sont comparées en terme de vitesse d'érosion soit de Si, de C, de SiC ou de silice. Ces vitesses d'érosion/évaporation sont les sources de molécules pour un dépôt ultérieur. La condensation est ensuite analysée en tenant compte de l'environnement et notamment des excès de CO(g) car ce dernier a tendance à s'enrichir dans la phase gazeuse des réacteurs car il n'est pas condensable si on le compare à SiO(g). Le monoxyde de carbone a tendance à réagir avec l'excès de Si en phase vapeur selon la réaction principale,

2 Si(g, excès) + CO(g) =SiC(s) + SiO(g).

La réaction totale a été calculée en tenant compte de l'excès réel de silicium en phase gazeuse pour différentes phases condensées de départ : SiC riche en Si ou C, avec addition ou non de silice. Cette étude met en évidence que les flux d'érosion ou de condensation sont souvent du même ordre de grandeur et que l'intervention du CO(g) comme gaz stocké dans les processus d'élaboration permettrait d'assurer une croissance en l'absence de gradient thermique.

II.5.Conclusion

Cette étude théorique basée essentiellement sur la thermodynamique de la vaporisation et condensation de SiC avec ou sans oxygène permet de bâtir des repères utiles pour comprendre et interpréter les expériences spectrométriques qui suivent. Ils sont d'autant plus utiles que comme l'avaient montré certains travaux spectrométriques antérieurs – N.S. Jacobson et al. [40]et P. Rocabois et al [15, 22, 37, 38, 100] – les phénomènes de vaporisation de SiC ou de mélanges triphasé avec silice ne produisent pas des pressions d'équilibre. Il reste à déterminer quelle est la nature des phénomènes cinétiques limitant la pression. Ce sera un des objets de ce travail de thèse.

Chapitre III

Etude expérimentale de la vaporisation et croissance de SiC

La stratégie scientifique de base qui a guidée les choix instrumentaux ainsi que les méthodes de caractérisation utilisées pour comprendre les conditions de la croissance de SiC – c'est-à-dire l'observation de ponts crées entre les grains de poudre de départ - a été

- La détermination des pressions de vapeur ou l'observation de l'évolution de ces pressions de vapeur en fonction de différents traitements thermiques
- la caractérisation des poudres après refroidissement afin de mettre en évidence leur évolution morphologique et structurale par comparaison avec leur état initial.

Les différentes observations quantitatives et qualitatives permettent ensuite de proposer des mécanismes de vaporisation et de croissance associés à la consolidation des objets en SiC en fonction de la température et de l'environnement d'élaboration.

La détermination des pressions de vapeur ainsi que leur évolution, la composition de cette phase vapeur et ainsi la présence de l'oxygène ou sa disparition en fonction du cycle thermique imposé va être relié aux effets de croissance observés après expérience.

La détermination des pressions de vapeur in situ ne peut se faire que par spectrométrie de masse couplée à une cellule d'effusion (ou réacteur effusif) avec une limitation sur les pressions maximales observées de l'ordre de 10^{-4} bar. Pour observer des évolutions à plus haute pression un spectromètre de masse muni d'un prélèvement de gaz par capillaire a été utilisé couplé à un four à induction. Les vapeurs condensables sont éliminées en sortie de four et les gaz non condensables tel CO(g) sont observés de façon continue. Ce type de spectrométrie est donc limité dans l'observation de la phase gazeuse, et il faut donc avoir une idée des espèces autres existantes.

Les moyens de caractérisation des poudres utilisés sont la diffraction de rayons X, la diffraction/diffusion Raman, et les observations microscopiques (MEB, FEG). Les poudres sont aussi analysées par leur distribution granulométrique. Ces moyens seront utilisés avant et après expérience pour observer l'évolution des échantillons après traitement thermiques.

III.1.Description des techniques expérimentales liées aux pressions de vapeur

III.1.1.Spectrométrie de masse haute température

Cette technique de mesure des pressions de vaporisation à haute température est implantée au SIMAP depuis une quarantaine d'années et a été transformée et adaptée à des études de mesure de l'activité des constituants dans des mélanges à plusieurs constituants. La version utilisant des cellules d'effusion à plusieurs compartiments – dite cellule multiple – permet de faire directement des comparaisons fines de pressions de vapeur entre différents échantillons ainsi que de déterminer quantitativement les pressions en se basant sur la perte de masse par vaporisation des échantillons analysés. C'est cette version qui a été utilisée pour l'étude des conditions de la croissance de SiC car il fallait une méthode suffisamment précise et donnant des résultats sans ambiguïté pour aborder les phénomènes complexes et concurrents associés à la croissance de SiC dans des zones de température élevée. De plus, des études antérieures faîtes au LTPCM avaient montré que le système Si-C et le système Si-C-O (thèse Ph. Rocabois en 1993) ne se vaporisait pas à l'équilibre mais était sujet à des limitations cinétiques.

Seule la technique des cellules multiples pouvait permettre de dissocier ces phénomènes de ceux décrits à l'équilibre et éviter des confusions dans l'interprétation des flux de vapeur mesurés. La description expérimentale de cette méthode de mesure est donc particulièrement soignée ainsi que sa mise en œuvre pour cette étude car il s'agissait d'obtenir des mesures de pressions partielles et de flux de vapeur essentiellement quantitatifs. Cette présentation approfondie d'une méthode qui a plus de cinquante années d'évolution est en conséquence un peu lourde pour un non spécialiste de la technique expérimentale mais elle garde sa pertinence pour toute publication dans des journaux spécialisés.

Les limites de cette méthode sont fixées d'une part par sa sensibilité (correspondant à 10^{-10} bar dans la cellule d'effusion) et d'autre part les conditions de l'effusion à l'orifice qui dépendent de son diamètre (environ 10^{-4} bar dans notre cas). Cette méthode a l'avantage de déterminer la composition de la phase vapeur produite par la cellule d'effusion et d'en suivre son évolution due aux pertes de matière par effusion qui correspondent à des flux de vaporisation faibles en regard des masses des échantillons. Dans le cas présent non seulement les pressions partielles sont comparées entre différents échantillons mais des étalonnages adéquats ont permis aussi d'accéder aux pressions partielles. Les températures d'étude vont dépendre des pressions de vapeur des échantillons étudiés. Ainsi, en présence de mélanges SiC-SiO_2 les pressions de $SiO(g)$ et $CO(g)$ sont fortes, et la température ne dépassera pas environ 1400 -1500 K. Pour des échantillons de SiC pur, les températures d'analyse peuvent atteindre 2000 K.

III.1.2.Spectrométrie avec prélèvement capillaire

Les analyses en présence de cellules d'effusion étant limitées à des pressions relativement faibles et des températures modérées, l'analyse des processus de croissance à plus haute température et pour des flux de gaz plus importants a été entreprise avec un spectromètre quadripolaire muni d'un capillaire de transfert entre le four de traitement et la chambre d'analyse. Le capillaire permet de réduire la pression de typiquement 1 bar à 1 mbar avant d'introduire le gaz dans le spectromètre de masse. Ce type de système n'est applicable que pour des gaz non condensables ou dit « permanents » comme dans notre cas $CO(g)$. Les vapeurs condensables lors de la détente le long du capillaire – dans notre cas principalement $SiO(g)$ et peut être $Si(g)$ - doivent être éliminées avant l'entrée dans le capillaire pour éviter

tout bouchage quasi instantané, et donc un soin particulier a été apporté à l'interconnexion entre le réacteur de traitement et l'entrée du capillaire. Le four a induction et la cellule de réaction ont été construits spécifiquement pour ce travail. Le spectromètre quadripolaire et son ensemble capillaire sont fournis en standard par les Ets Pfeiffer. Il existe plusieurs versions en fonction du type d'études envisagées. La version choisie est celle pour la mesure de gaz résiduels : une partie des gaz issus du capillaire est introduite directement dans la chambre sous vide où est situé le spectromètre. L'autre partie est pompée directement en sortie de capillaire. Ce type de montage sous la version commerciale ne permet pas de déterminer les pressions existant en amont du capillaire. Afin de rendre les expériences comparables, la conductance capillaire-spectromètre a été fixée par ouverture totale de la vanne doseuse qui introduit la part du gaz à analyser dans le spectromètre.

III.2.Techniques expérimentales de caractérisation des poudres

Les techniques de caractérisation correspondent à deux groupes : - (i) celles qui vont donner une indication sur la structure cristalline des matériaux, - (ii) celles qui permettent d'étudier la morphologie des cristaux et des poudres. Certaines permettent d'atteindre des informations sur ces deux aspects.

III.2.1.Diffraction de rayons X

Cette technique est utilisée principalement pour détecter une évolution des proportions de polytypes du SiC lors de phénomènes d'agglomération et de croissance. Dans certains cas il est possible de mettre en évidence la présence de silice en surface du SiC.

III.2.2.Spectroscopie Raman

Cette technique est basée sur l'interaction entre les constituants élémentaires de la matière (molécules, atomes, ions, électrons) avec un rayonnement électromagnétique, notamment une lumière monochrome.

Les différents polytypes de SiC ont la même composition chimique, mais leur propriétés physiques sont légèrement différents dues à leur structure cristalline différente. Notamment, la signature spectrale du SiC, issue des mesures Raman, est composée de fréquences de vibrations propres à chacune de structures cristallines en plus de fréquences communes à tout les polytypes. Cette mesure ne permet en l'état actuel des connaissances de réaliser un « dosages » des différents polytypes.

Les mesures réalisées sur les poudres de SiC donnent dans certaines conditions des spectres pour lesquels le niveau de base est très important et augmente avec la fréquence.
Ce phénomène est caractéristique d'une émission par fluorescence. Ce phénomène s'explique par le fait qu'une poudre relativement « isolante » donc sans ponts entre grains (poudres de départ par exemple) ne peut évacuer uniquement par conduction thermique l'énergie reçue via le laser. Une partie de cette énergie est donc évacuée par émission de photons. Après traitement et s'il y a création de ponts dus à la croissance inter-granulaire le fond diffus diminue jusqu'à disparition.

III.2.3.MEB-FEG

La microscopie à balayage permet d'observer la morphologie des grains et leur évolution après traitements. En utilisant la technique FEG (Canon à émission de champ) la profondeur de champ augmente, et les observations du type 3D permettent une meilleure visualisation des ponts créés entre les grains. L'analyse des électrons rétrodiffusés permet en

plus de connaître la composition locale du matériau, présence de silice, de silicium ou de carbone par exemple.

III.2.4.Granulométrie

La granulométrie laser utilisée permet d'analyser des grosseurs de grains allant de 0,04 à 500 µm. Les poudres sont dispersées dans un liquide afin de limiter la présence d'agrégats. Cependant, et afin d'éviter toute ambiguïté due aux agrégats résiduels, les spectres granulométriques sont toujours complétés par des observations MEB.

III.3.Résultats expérimentaux

III.3.1.Suivi par Spectrométrie de masse haute température et caractérisations

Plusieurs aspects ont été abordés pour analyser les pressions de vaporisation par SMHT dans différentes conditions :

- Comparer des poudres de différentes origines et de différentes puretés
- Comparer des poudres de même origine mais de différentes granulométries
- Comparer des poudres avec différents mélanges granulométriques
- Comparer des poudres identiques dans des matériaux de conteneurs différents
- Comparer des mélanges de poudres de SiC – SiO_2 de différentes compositions
- Comparer des poudres oxydées par des mélanges O_2 - H_2O à 900°C suivant différent temps
- Comparer différentes poudres de SiC en cours de dé-oxydation, c'est-à-dire lors du départ de la silice.
- Comparer des poudres après dé-oxydation

L'observation des pressions partielles de Al, et Fe issu des impuretés montre comme cela avait été déjà observé par S. Baud [57, 58, 59] que ces impuretés s'éliminent assez vite et ne vont pas jouer le rôle traditionnel attribué aux dopants dans les phénomènes de frittage. Cependant, le Fer – sous forme initiale d'oxyde Fe_2O_3 – est un fournisseur d'oxygène qu'il va « distiller » au fur et à mesure de l'élévation de température, le fer possédant différents degrés d'oxydation. La réduction progressive des oxydes de fer en milieu « SiC + SiO_2» attesté par la présence de Fe(g) jusqu'à 1700 K va permettre de prolonger la phase d'oxydation active. L'échantillon le plus riche en fer a d'ailleurs montré une meilleure interconnexion des grains lorsque l'expérience est stoppée après élimination de l'oxygène.

La détermination quantitative des pressions de vapeur (SMHT) a permis de mettre en évidence que le pseudobinaire SiC-SiO_2 (c'est-à-dire le SiC en présence de silice) ne s'évapore pas en conditions d'équilibre, les pressions de SiO(g) et de CO(g) étant inférieures d'un facteur 10 à 100 à celles calculées par la thermodynamique. Ces pressions évoluent en fonction des quantités de silice ce qui traduit une vaporisation limitée par une étape cinétique.

Les rapports SiO/CO sont égaux ou inférieurs à 1, et donc inférieurs à ceux attendus pour une vaporisation congruente (3 ou 3.76 selon la nature des flux de gaz) mais pour autant la composition de l'échantillon ne « sort » pas de la section pseudobinaire vers l'un des triphasés du ternaire Si-C-O. L'interprétation de ces pressions faibles devra se faire en termes de limitation cinétique.

La vaporisation de poudres de SiC dites « pures » montre la présence systématique des vapeurs de SiO(g) et CO(g), les poudres fines qui ont une surface effective plus grande à

volume d'échantillon équivalent présentant des pressions plus élevées, non pas tant à cause de leur surface spécifique ou de la tension superficielle mais par suite du couplage entre la cinétique de vaporisation et l'effusion des vapeurs.

Au moment du départ de la silice – par vaporisation de SiO(g) et CO(g) - les pressions de Si(g), Si_2C(g) et SiC_2(g) correspondent au domaine de stoechiométrie de SiC. La sortie du système pseudobinaire vers le binaire Si-C lors de la perte de silice s'effectue bien dans le domaine monophasé pur du composé SiC comme prévu par la thermodynamique.

Les poudres de SiC de différentes grosseurs de grains ainsi dégazées de leur couche de silice montrent une vaporisation à l'équilibre. Ce fait est un fait nouveau qui distingue le comportement du composé SiC pur de son diphasé limitrophe SiC-C et des triphasés avec la silice, domaines pour lesquels P. Rocabois (Thèse en 1993 au LTPCM) avait mesuré des cinétiques de vaporisation lentes et déterminé des coefficients d'évaporation faibles (10^{-2} à 10^{-3}).

La comparaison du comportement à la vaporisation des mêmes poudres de SiC dans des conteneurs en Ta, graphite ou quartz a permis d'observer le maintien de conditions d'oxydation active – après départ de la silice « native » - pour les cellules en tantale via la persistance de la molécule SiO(g). Ce fait résulte de la solubilité de O dans Ta. Il y aussi sans doute du CO(g) mais il est masqué alors par l'apparition de Si(g) à la même masse dans le spectre. Des croissances de ponts sont observées pour les échantillons ayant été traités dans ces conditions, c'est-à-dire au-delà de la perte de l'oxygène. L'échantillon ayant subi le même traitement mais en creuset de graphite (ensuite recouvert de SiC en fin d'expérience) montre une croissance plus forte due à la présence d'une pression originale plus forte de CO(g) et un temps de maintien en conditions d'oxydation active plus prolongée. On retrouve là une des prévisions de l'étude théorique sur le rôle du CO(g).

La comparaison de mélanges de poudres fines (30 mass%) et grosses montre que les pressions partielles de SiO(g) et CO(g) sont principalement fixées par la présence des fines. Ce phénomène est du essentiellement aux cinétiques de vaporisation et aux variations de surface évaporante. Dans le mélange de poudres il y a une phase gazeuse tampon imposée par les particules les plus fines, ce qui peut permettre des transferts de matière des particules fines vers particules les plus grosses dont la pression de vaporisation est plus faible. La fin de la présence de l'oxygène ne semble pas être influencée par la présence de deux tailles de poudres car les décroissances des pressions associées à la dilution en oxygène ne manifestent pas de différences que ce soit pour des poudres pures ou des poudres en mélange.

Des poudres de SiC pur oxydées préalablement par un mélange O_2-H_2O à 900°C sous pression atmosphérique pour différentes durées présentent un comportement un peu différent de la référence « mélange à 15 mol% de silice ». Une transformation s'opère vers 1400 K qui correspond en fait à des observations de la littérature montrant que la couche d'oxydation en silice amorphe se transforme à haute température en cristobalite. Indépendamment de cette transformation, les pressions de vapeur de ces poudres oxydées ne sont pas très sensiblement différentes de celui de mélanges de SiC+SiO_2 ce qui laisse penser que le même phénomène cinétique limitant la vaporisation se produit. L'expérience a été arrêtée avant la perte totale d'oxygène et aucune formation de ponts ni changement structural n'ont été clairement observés.

III.3.2.Suivi par Spectrométrie de masse capillaire et caractérisations

Le suivi des traitements thermiques par spectrométrie de masse avec prélèvement capillaire permet d'observer la pression de CO(g) issu des poudres. Comme nous l'avons vu théoriquement et par SMHT le dégagement de CO(g) est le pendant d'une quantité équivalente de SiO(g), du moins tant que de la silice existe en mélange avec SiC. La

diminution du dégagement de CO(g) est le signe d'une diminution au moins équivalente de SiO(g), voire sa disparition lorsque CO(g) disparait.

Les poudres et mélanges analysés correspondent à trois types : - (i) une poudre de SiC dite pure, - (ii) un mélange SiC-SiO_2 à 2% en fraction molaire de silice, - (iii) une poudre SiC bimodale (33 mass% grains fins et 67 mass% gros grains en mélange) préalablement oxydée.

Les traitements thermiques sont soit des paliers successifs soit des rampes de température suivies de paliers, puis d'un refroidissement naturel rapide par coupure du chauffage à induction. Les dégagements de CO(g) durant les traitements sont enregistrés et l'arrêt de l'expérience est décidé en fonction de l'observation de ce dégagement. Deux types de traitements thermiques ont été menés qui correspondaient à des problèmes de livraison et mise au point du matériel : - (i) dans un premier temps des montées de température avec des paliers sont effectués par réglages manuels, - (ii) dans un deuxième temps une rampe est programmée électroniquement, puis un palier. Le premier mode a permis de mettre en évidence des dégagements de CO(g) à chaque montée de température avant une chute définitive à haute température. Ceci illustre d'une part le gradient thermique vertical – et peut être radial - dans l'échantillon et d'autre part les re-condensations de vapeurs (en SiO_2 plus ou moins enrichie en SiC d'après les analyses) qui se produisent en tête de réacteur. Ces condensats vont se vaporiser à nouveau à chaque montée de température créant ou faisant perdurer ainsi des conditions oxydantes alors même que les échantillons de poudres coté chaud du réacteur ne contiennent plus de silice. On est alors en régime d'oxydation active. Dans le deuxième mode, des rampes de vitesses différentes ont été utilisées : elles permettent en fait de faire varier le flux total pompé par le capillaire pour un même histogramme des températures. La zone d'oxydation active s'en trouvera plus ou moins réduite dans le temps.

Les courbes de dégagement de CO(g) présentent une croissance rapide avec la température, puis un pic, et une décroissance rapide jusqu'à disparition du CO(g) observé. Par référence aux calculs théoriques et aux observations en SMHT, la croissance rapide correspond à l'augmentation de pression sur un mélanges SiC-SiO_2, selon la thermodynamique ou une loi cinétique (loi en ln p(CO) = A/T + B loi d'Arrhénius). Au moment du pic de CO(g), la quantité de silice est devenue trop petite pour assurer les conditions quasi-réversibles d'évaporation – ce qui a été vu par SMHT pour les faibles teneurs en silice – et la pression baisse. La décroissance du pic de CO(g) en début est pour une part du à l'appauvrissement en silice, la suite est la perte des réserves de SiO(g) - encore contenues ou régénéré dans le réacteur ou les poudres - via le pompage capillaire. A ce stade le réacteur est en zone d'oxydation active. Lorsque CO(g) disparait, SiO(g) a considérablement diminué et les échantillons peuvent être encore en zone d'oxydation active, mais proche de la limite SiC-C mais la capacité à détecter cette limite dépend de la limite réelle de sensibilité de l'ensemble qui n'est pas réellement connue. Ensuite, un traitement prolongé aux températures élevées (ici 1400 à 1600 K) va permettre l'élimination complète de l'oxygène et les échantillons vont précipiter du carbone en surface à cause de la vaporisation non congruente. Selon ce qui est recherché en caractérisation, des traitements ont été arrêtés dès la disparition de CO(g), d'autres juste après le pic de CO(g), et enfin d'autres après un palier de température final prolongé.

L'observation de la croissance de ponts entre grains par Raman et MEB-FEG a révélé :

- La nécessité d'un temps de maintien en zone d'oxydation active suffisamment long pour observer de la croissance de ponts entre grains
- La précipitation de carbone en surface de grains, que ceux-ci aient été ou non l'objet de croissance (avec création de ponts entre autre), lors de maintiens prolongés à haute température en l'absence de pression de CO(g)
- L'insuffisance de croissance ou peu de croissance décelable après arrêt au pic de CO(g) en présence de silice résiduelle

• L'importance de la nature de la silice dans les poudres originales : des mélanges de grains SiC + SiO_2 induisent une croissance bien plus nette que celle observée par la présence d'une couche de silice obtenue par calcination préalable ou à celle native sur les grains de SiC.

Les caractérisations Raman ont aussi montré que la création de ponts va de pair avec certains polytypes – par exemple dans les conditions expérimentales testées le 6H constituerait le matériau privilégié des ponts par rapport au 4H et 15R des grains (il y a aussi du 6H dans les grains). Ces observations sont à relier au rapport Si/C en phase gazeuse proposé par W.F.Knippenberg [67] (un diagramme essentiellement qualitatif) et en accord avec le domaine stoechiométrique accessible aux conditions de l'oxydation active comme décrit et calculé dans l'étude théorique.

III.4. Conclusion

Guidé par les éléments d'analyse thermodynamique de la vaporisation de SiC et des mélanges SiC-SiO_2 mis en place dans le chapitre précédent, les expériences spectrométriques de suivi des traitements thermiques des échantillons de poudres complétés par des caractérisations structurales et morphologiques des échantillons avant et après traitement ont permis de montrer que la croissance de SiC ne pouvait pas se faire tant qu'une couche de silice reste en surface des grains. Une surface « nue » de SiC ne peut par ailleurs être obtenue suffisamment longtemps que grâce à la présence de l'oxygène et c'est dans cette fenêtre dite d'oxydation active que la croissance par transport gazeux va se faire. Après la perte quasi totale de l'oxygène il y a apparition de carbone en surface par un phénomène que l'on peut qualifier d'érosion. Les expériences ont montré qu'avant l'apparition de précipités de C il y a toujours une croissance liée à la présence originale (et inévitable) de silice. Il est difficile alors d'en déduire dans l'état actuel si la croissance des ponts continue à se faire. Les mécanismes qui gèrent le départ de la silice, la croissance de SiC et l'apparition du carbone seront pour partie expliqués dans le dernier chapitre.

Chapitre IV

Mécanismes d'évaporation et de condensation dans les poudres de SiC

Ce chapitre fait une synthèse des mécanismes de transport dans les poudres de SiC additionnées ou non de silice et des conditions qui vont permettre la croissance de SiC, cette croissance menant à la création de ponts entre grains. Cette synthèse remet pour une part en cause les mécanismes proposés dans la littérature et pour une autre part va plus loin à partir des mesures et observations faîtes dans ce travail. Une première partie traite du rôle même de la silice tant qu'elle existe en tant que phase condensée mélangée avec le carbure de silicium. Une deuxième partie traite des conditions de l'oxydation active résultant de la présence d'oxygène résiduel après départ de la silice condensée et des sources de croissance de SiC disponibles.

IV.1.Modèle d'interaction SiC-SiO_2 à haute température sous vaporisation

La présence de silice – soit sous forme de couche native ou intentionnellement oxydée sur les grains de SiC soit sous forme additionnelle de grains purs – conduit inévitablement à un processus de vaporisation limité par la diffusion de l'oxygène dans la couche couvrant les grains de SiC puis réaction à l'interface SiC/SiO_2 selon le mécanisme,

$$SiC(s) + 2\ O^{2-}\ (diff.) = SiO_2(s) + C^{n+}\ (diff).$$

Le carbone diffuse alors rapidement – et cela a été mesuré par Z.Zheng et coll. [47, 48] – vers la surface de la couche de silice pour produire CO(g) par réaction avec l'oxygène en excès venant de la silice libre. La diffusion de l'oxygène sous forme d'ions O^{2-} à haute température (cristobalite) est en effet l'étape limitant la diffusion selon la littérature. Ce type de modèle de diffusion n'est possible que si le potentiel d'oxygène extérieur aux grains de SiC est supérieur à celui existant dans les grains. Il apparaît dans ce travail que le potentiel moyen stationnaire d'oxygène dans la poudre est en effet fixé par l'évaporation conjointe de silice libre et de SiC recouvert d'une couche de silice. C'est ce potentiel moyen correspondant à une pression de SiO(g) qui est en effet mesuré par spectrométrie de masse. Il faut noter que ce potentiel moyen va dépendre des conditions de compétition entre le flux perdu par l'échantillon (effusion ou flux capillaire) et les mécanismes de diffusion et de surface. Cependant, les observations présentes ont montré que le rapport SiO/CO change peu est reste voisin de 1, ce qui correspond à un potentiel moyen supérieur à celui de l'interface SiC/SiO_2. Cette différence de potentiel d'oxygène montre que la présence de la couche de silice perdurera jusqu'à épuisement des grains de silice par vaporisation. Toutefois on ne peut écarter la possibilité de grains de SiC à surface « nue » donc exempte de silice lorsque le tau de silice pure devient très faible soit avant sa disparition par vaporisation et due à des effets géométriques locaux. Au moment de la disparition de la silice, la présence de SiO(g) et CO(g) résiduel permettent à l'échantillon d'entrer dans une zone d'oxydation active. Les caractérisations des poudres chauffées avec présence résiduelle de silice montrent un phénomène de vieillissement – angles arrondis notamment – qui est plus prononcé lorsque le tau de silice diminue, en relation avec le degré d'élimination de la silice par vaporisation. Pour des échantillons contenant encore de la silice et lors d'un vieillissement prononcé, il y a quelques ponts entre grains qui s'apparentent plus à un phénomène de collage qu'à une

croissance de ponts. Il s'agirait alors de ponts de silice résiduelle. Les observations faîtes dans ce travail et le mécanisme de vaporisation justifié ici montrent que la croissance de SiC via des molécules oxydées telles que SiO(g) et CO(g) par la réaction principale proposée dans la littérature,

$$SiC(s) + 2\ SiO_2(s) = 3\ SiO(g) + CO(g)$$

n'est pas celle se produisant, et n'est pas réaliste en terme de gradients de potentiels chimiques dans les poudres (conditions isothermes). Une phase de dé-oxydation correspondant à la perte de silice condensée est donc préalable à toute croissance de SiC. Cette phase de dé-oxydation fournit une atmosphère résiduelle encore assez riche en oxygène propre à assurer une phase d'oxydation active qui lui succède.

IV.2.Conditions de la croissance de SiC

Les conditions de croissance de SiC sans précipitation de carbone correspondent à une fenêtre dite d'oxydation active qui d'étend entre deux limites, la limite SiC-C et celle correspondant à la création d'une couche de silice à une activité maximale de Si dans SiC bien déterminée et dépendant de la température ($a(Si) < 1$ sauf à la précipitation de Si vers 2200 K). Dans ces limites, l'oxydation active de SiC assure une surface « nue » qui va permettre la croissance de SiC. Cependant les conditions de l'oxydation active imposent une érosion par l'oxygène de cette surface (départ de SiO et CO) qui est en compétition avec l'apport de matière SiC via les molécules gazeuses Si, Si_2C, SiC_2 etc… pour effectuer un dépôt/croissance. Le bilan de ces deux phénomènes effectué en conditions d'équilibre à partir de la thermodynamique montre que la fenêtre de dépôt est bien plus restreinte que la fenêtre d'oxydation active car l'érosion l'emporte presque toujours. La fenêtre de croissance s'appui sur la limite SiC-C pour laquelle l'érosion est minimale.

Des réserves de croissance sont nécessaires qui s'appuient sur la présence d'un excès de CO(g) réagissant avec le silicium en excès en phase gazeuse selon des réactions du type,

$$2\ Si(g) + CO(g) = SiC(s) + SiO(g).$$

Les observations expérimentales montrent effectivement que

- La présence d'une zone d'oxydation active suffisamment étendue dans le temps est nécessaire pour produire plus de ponts.
- La présence de carbone (ex. creusets en graphite) favorise à la fois une pression plus importante de CO(g) et une croissance plus prononcée.
- La précipitation de carbone se produit en surface et donc après la croissance en zone d'oxydation active.

La quantification exacte de la croissance – quantité de matière mesurée en microns/h – est difficile à faire sur les poudres car seuls les ponts peuvent être évalués. En prenant arbitrairement le diamètre des ponts comme repaire, les croissances observées sont toujours inférieures à celles attendues mais souvent voisines de la limite inférieure des estimations.

IV.3.Conclusion

La succession des mécanismes de corrosion/évaporation et croissance des poudres de SiC et SiO_2 a été élucidé, et pour une certaine part quantifié. Les conditions de la croissance correspondent bien à une certaine part du domaine d'existence de SiC en conditions d'oxydation active et se limitent à des activités de Si proches de la limite SiC-C. Les flux de croissance disponibles restent cependant faibles comparés aux flux d'érosion assurant l'oxydation active, et la création de pores reste un risque réel. Le rôle d'un excès de CO(g) est primordial pour assurer une croissance plus forte apte à contrecarrer les effets d'érosion de l'oxydation active.

Conclusion générale

L'étude des mécanismes qui régissent consolidation par croissance de ponts dans des poudres de SiC à haute température a fait l'objet de ce travail. Les moyens utilisés notamment la spectrométrie de masse sous la forme classique du couplage avec une cellule d'effusion, et moins classique en utilisant un prélèvement capillaire ont permis de suivre la phase vapeur en cours de traitement thermique afin d'associer les observations de croissance post expérimentales à l'histoire thermique et chimique des échantillons de poudres de SiC et SiC-SiO_2 soumis à des pertes de masse qui en premier lieu concernent la teneur en oxygène, par flux de vapeurs. Des moyens de caractérisation ont été utilisés pour observer après expérience les transformations morphologiques et structurales des grains de poudres. Les expériences spectrométriques sont appuyées sur des calculs thermodynamiques du comportement des poudres en fonction de la température et du potentiel d'oxygène pouvant exister à l'état stationnaire dans des poudres en cours de réaction.

Le premier et important résultat est la mise en évidence du mécanisme à l'origine de l'observation de pressions de vapeur bien plus faibles qu'attendu à l'équilibre en présence de silice: la diffusion de l'oxygène dans la couche de silice native existant sur les grains de SiC, couche qui est entretenue par la présence de grains de silice lorsque celle-ci est additionnée aux poudres initiales de SiC. Le mélange de poudres de carbure de silicium et de silice ne peut s'apparenter au système chimique pseudobinaire SiC-SiO_2 car les grains de SiC sont couverts de silice qui masque le rôle de l'interface SiC/SiO_2. Les échantillons de mélanges de poudres traités à haute température ne présentent alors pas de croissance nette dans ces conditions, mais un début de vieillissement. Quelques grains peuvent présenter en fait une sorte de collage qui a été attribué à la silice. Le départ de la silice s'accompagne de la présence d'oxygène résiduel sous forme des molécules SiO(g) et CO(g) principalement qui assure alors des conditions d'oxydation active.

Le deuxième résultat est l'existence d'une phase d'oxydation active qui va perdurer tant que l'oxygène résiduel n'est pas éliminé. Une fenêtre d'oxydation active est définie à l'intérieur de laquelle la surface de SiC reste « propre » (exempte de couche de silice) et le composé SiC reste dans les limites de son domaine stœchiométrique, c'est-à-dire sans précipité de carbone. Pour la première fois, cette fenêtre est définie à la fois par l'activité du silicium et la pression d'oxygène corrélée existant à la surface sous oxydation active car les deux éléments Si et oxygène sont liés. La largeur de cette fenêtre permet de comprendre que la séquence d'oxydation active va durer un certain temps en relation avec la vitesse à laquelle s'effectuera la décroissance de la teneur en oxygène ou diminution de la pression d'oxygène dans l'atmosphère environnant les échantillons de poudres.

Le troisième résultat est la quantification de la compétition existant entre croissance et érosion des grains de SiC en condition d'oxydation active. Dans la fenêtre d'oxydation active, l'érosion est toujours plus importante pour les compositions stœchiométriques de SiC riches en silicium ce qui va provoquer l'agrandissement de la porosité. La croissance ne peut prendre le dessus par rapport à l'érosion due à l'oxydation active que pour des compositions proches de la limite SiC-C. L'élimination progressive de l'oxygène va dans le même sens ce qui assure toujours quelque soit le procédé de fabrication un passage par cette zone de croissance. Dans les conditions de l'oxydation active, la présence d'un excès de CO(g) permet d'accroitre la croissance de SiC par réaction avec l'excès de silicium existant dans la vaporisation de SiC qui se produit en même temps. En l'absence de cet excès de CO(g) et pour des compositions plus loin de la limite SiC-C l'érosion prend plus rapidement le dessus,

et le matériau SiC présentera des pores plus grands après traitement. Cette compétition est à l'origine des difficultés rencontrées dans la densification de SiC par frittage qu'il y ait additifs ou non.

Le quatrième résultat concerne la précipitation de carbone en l'absence de conditions d'oxydation active. Cette précipitation est extrêmement rapide en l'absence de l'oxygène résiduel, mais il est permis de supposer ici aussi une transition amortie par la vitesse à laquelle s'effectue la perte d'oxygène. La précipitation survient toujours en surface ce qui indique que les cristaux ont d'abord subi une phase de croissance en condition active. Le principal effet du traitement thermique après passage par la zone d'oxydation active est d'éroder le matériau – grains et ponts - en raison de la perte de silicium par vaporisation ce qui va engendrer un grossissement des pores. A partir de la présence de silice originale – celle native sur les poudres de SiC ou celle additionnée en mélange aux poudres de SiC - la zone d'oxydation active est une étape obligée, entre départ de la silice condensée et apparition du carbone. Lorsque les conditions de la zone d'oxydation active sont établies suffisamment longtemps, la croissance est observée avant même que les cristaux précipitent du carbone en surface.

ABSTRACT

Silicon carbide (SiC) is a well known material, but there are still several aspects in its manufacturing which are not well known. The aim of this thesis is to contribute to better understanding of material flows exchange via gaseous phase during bulk SiC manufacturing. The characterization of established gaseous phase above SiC containing powder samples is performed in-situ using mass spectrometry with (i) Knudsen cell or (ii) capillary tubing sampling. The heat treated powders are then characterized using SEM imaging and Raman spectrometry to analyse their state of aggregation, especially necks building between single SiC grains. The experimental study is preceded by a thermodynamic study of the SiC-SiO_2 system and SiC passive-active oxidation transition limits computations. The influence of main parameters like oxygen pollution and heating rate on the SiO(g) and CO(g) partial pressures was observed and relied to observed structure of obtained samples.

Keywords: Silicon Carbide, Si-C-O ternary system, mass spectrometry, SiC active oxidation.

RESUME

Le carbure de silicium est un matériau bien connu à ce jour, mail il y a des aspects lors de sa fabrication qui sont mal compris. Le but de ce travail est de contribuer à la compréhension des échanges de matière via la phase gazeuse lors de la fabrication de composants en SiC. La procédure expérimentale utilisée est le suivi in situ de l'évolution des pressions de vapeur ou celle des flux évaporés par spectrométrie de masse et de comparer la morphologie et la structure des poudres avant et après les traitements par différents moyens de caractérisation dont la spectrométrie Raman et les observations MEB et FEG.. Une étude thermodynamique du système SiC-SiO_2 précède et encadre l'expérimentale et le calcul des limites de la transition de l'oxydation passive-active du SiC sont effectués. L'influence des paramètres clefs comme la pollution par l'oxygène et les rampes de température sur les pressions partielles de SiO(g) et CO(g) a été observé et relié aux structures obtenues.

Mots clés : Carbure de Silicium, Si-C-O système ternaire, spectrométrie de masse, oxydation active du SiC.